NORTHWESTERN UNIVERSITY

Peptide-Based Magnetic Resonance Imaging Probes
for Detection of Enzyme Activity

A DISSERTATION

SUBMITTED TO THE GRADUATE SCHOOL
IN PARTIAL FULFILLMENT OF THE REQUIREMENTS

for the degree

DOCTOR OF PHILOSOPHY

Field of Chemistry

By

Bradley Douglas Ulrich

EVANSTON, ILLINOIS

December 2008

Peptide-Based Magnetic Resonance Imaging Probes for Detection of Enzyme Activity

Bradley Douglas Ulrich

Magnetic Resonance Imaging is a non-invasive modality that allows for deep-tissue imaging. Contrast agents decrease image acquisition time and increase the intrinsic contrast between different types of tissue. A new family of enzyme-activated contrast agents is emerging that has the ability to report on enzymatic processes in vivo. Towards this goal, five distinct approaches to modulate the relaxivity of gadolinium(III) chelates with peptides were investigated. The agents are proposed to undergo structural changes upon cleavage of a substrate peptide by a protease, ultimately resulting in a change in relaxivity.

Contrast agents attached to the N-terminus of a peptide were used to study the effect of the N-terminal amino acid on the coordination geometry of a gadolinium(III) chelate. It was determined that the coordination geometry is independent of the identity of the N-terminal amino acid.

A novel protection strategy was used to synthesize peptide-bridged macrobicyclic structures where a contrast agent is covalently attached to the side-chains of a peptide. The linker length of the macrobicyclic agents was varied in a systematic manner to study the effects of proximity of the peptide to the macrocycle in blocking inner-sphere water access.

A self-immolative linkage was used between a DEVD peptide and a gadolinium(III) chelate to produce a contrast agent for the detection of caspase-3. The agent displays a decrease in relaxivity upon cleavage by caspase-3 due to a decreased water exchange rate for the cleaved chelate. The self-immolative agent displays high uptake with MDA-MB-231 cells.

A coordinatively saturated gadolinium(III) complex, consisting of an amide-based chelate attached to the C-terminus of a peptide, provides a novel mechanism to restrict inner-sphere water access to gadolinium(III) chelates.

The attachment of a small-molecule T_1 contrast agent to a nanoparticle T_2 contrast agent with a variable PEG spacer and a substrate peptide has the potential to provide a novel mechanism of relaxivity enhancement.

The family of peptide-based contrast agents in the present work has the potential to enable MRI to detect proteases responsible for a variety of diseases. Each approach to modulate the relaxivity of gadolinium(III) chelates represents a paradigm for future studies of enzyme-activated MRI contrast agents.

<div style="text-align:center">

_____
Thomas J. Meade
Dissertation Advisor

</div>

ACKNOWLEDGEMENTS

MacRenaris, Dave Ballweg, Emily Testa, Allison Harney, and Amanda Eckermann for constructive criticism of my thesis chapters. I must apologize to and thank the entire Meade lab for tolerating my loud music in the lab throughout the years.

For encouragement, I am forever indebted to my wife, Emily, for supporting me through the years. When research was rough, she was there to cheer me up and keep me going. I truly owe my sanity in these last few months to her. The rest of my family has given me steadfast support and love; I hope this thesis makes them proud (even though they probably won't read past this page). My sister Kristy has been my Chicago mom, and I thank her for all her support through the years.

I need to thank a number of fellow graduate students for helping me relieve stress through extracurricular activities. Chris Graves, Mark Witschi, and Matt Kern provided friendship and so many fun times that I can't remember them all. I hope my snowboarding trips with Dean Shahriari, Ian Saratovsky, and Eric Kawamoto will continue in years to come. Brandon Rodriguez helped me forget lab problems through MMA training; practicing martial arts helped me refocus my self-discipline and apply it towards this thesis.

LIST OF ABBREVIATIONS

^	site of enzymatic cleavage
1-D	one dimensional
2-D NMR	two dimensional nuclear magnetic resonance
A	alanine
$A/\hbar$	scalar coupling constant
Ac	acetyl
ala	alanine
ANOVA	analysis of variance
APMA	4-aminophenylmercuric acetate
APTES	3-aminopropyl triethoxysilane
arg	arginine
asp	aspartic acid
atm	atmosphere
Boc	butoxycarbonyl
br	broad
BSA	bovine serum albumin
^{o}C	Degrees Celcius
CA	contrast agent
CAM	ceric ammonium molybdate
CEST	chemical exchange saturation transfer
CHAPS	3-[(3-chloramidopropyl)dimethylammonio]-1-propane sulfonate
CHCA	alpha-cyano-4-hydroxycinnamic acid
cm	centimeter
COSY	correlational spectroscopy
CPK	Corey, Pauling, Koltun
CPMG	Carr-Purcell-Meiboom-Gill
cyclen	1,4,7,10-tetraazacyclododecane
D	aspartic acid
d	doublet
Dap	diaminopropionic acid
dB	decibel
DCC	dicyclohexylcarbodiimide
Dde	4,4-dimethyl-2,6-dioxocyclohex-1-ylidene)ethyl
DIPEA	N,N-diisopropylethylamine
DIS	dysprosium induced shift
DMAP	4-dimethylaminopyridine

DMF	N,N-dimethylformamide
DMSO	dimethylsulfoxide
DO3A	1,4,7,10-tetraazacyclododecane-N,N',N''-triacetic acid
DOTA	1,4,7,10-tetraazacyclododecane-N,N',N'',N'''-tetraacetic acid
DPBS	Dulbecco's phosphate buffered saline
DTPA	diethylentriamine pentaacetic acid
DTT	dithiotheitol
E	energy
E	glutamic acid
EDTA	ethylenediaminepentaacetic acid
ES	enzyme substrate complex
ESI-MS	electrospray ionization mass spectrometry
EtOH	ethanol
eV	electron volts
exp	exponent
fmoc	9-fluorenylmethylcarbonyl
FOV	field of view
G	glycine
g	gram
g	gram
g/mol	gram per mole
Gd-DO3A	gadolinium(III)1,4,7,10-tetraazacyclododecane-N,N',N''-triaceticacid
Gd-DOTA	gadolinium(III)1,4,7,10-tetraazacyclododecane-N,N',N'',N'''-tetraacetic acid
Gd-DOTA-2DMA	gadolinium(III)DOTA-bis(methylamide)
Gd-DTPA	gadolinium(III)diethylenetriaminepentaacetic acid
Gd-DTPA-BMA	gadolinium(III)DOTA-bis(methylamide)
Gd-HP-DO3A	gadolinium(III)hydroxypropylDO3A
Gd-NOTA	gadolinium(III)triethylenetriaminetriacetic acid
glu	glutamic acid
gly	glycine
h	Planck's constant
h	hour
ℏ	Dirac's constant
HSA	human serum albumin
HATU	o-(7-azabenzotriazol-1-yl)-N,N,N',N'-tetramethyluronium hexafluorophosphate
H-bonded	hydrogen bonded
HEPES	4-(2-hydroxyethyl)-1-piperazineethanesulfonic acid
HPLC	high performance liquid chromatography

HPLC-MS	high performance liquid chromatography mass spectrometry
Hz	Hertz
I	intensity
ICP-MS	inductively coupled mass spectrometry
J	J coupling constant
J	Joule
K	Kelvin
K	lysine
kB	Boltzmann constant
L	leucine
L	liter
LC-MS	(high performace) liquid chromatography mass spectometry
leu	leucine
LIS	lanthanide induced shift
Ln	lanthanide
LOD	limit of detection
log	logarithmic
lys	lysine
M	magnetization
M	methionine
m	meter
M	molar
m	multiplet
m/z	mass to charge ratio
MALDI	matrix assisted laser desorption ionization
MALDI-TOF MS	matrix assisted laser desorption ionization time of flight mass spectrometry
MeCN	acetonitrile
MEM	modified Eagle's media
MeOH	methanol
met	methionine
mg	milligram
MHz	megaHertz
min	minute
mJ	milliJoule
mL	milliliter
mM	millimolar
mm	millimeter
mmol	millimole
MMP	matrix metalloproteinase

MMP-7	matrix metalloproteinase 7
MMPI	matrix metalloproteinase inhibitor
mol	mole
MOPS	3-morpholinopropane-1-sulfonic acid
MR	magnetic resonance
MRI	magnetic resonance imaging
MS	mass spectrometry
ms	millisecond
Mtt	methyltrityl
N	number
Nd:YAG	neodymium-doped yttrium aluminum garnet
nm	nanometer
NMR	nuclear magnetic resonance
NOESY	Nuclear Overhauser spectroscopy
ns	nanosecond
P	proline
PARACEST	paramagnetic chemical exchange saturation transfer
PBS	phosphate buffered saline
Pd/C	palladium on carbon
PDA	photodiode array
PEG	poly(ethylene glycol)
PET	positron emission
Phipr	phenyl isopropyl
PMT	photomultiplier tube
pNA	*para*-nitroaniline
ppb	parts per billion
ppm	parts per million
ppt	precipitate
pro	proline
psi	pounds per square inch
PTFE	poly(tetrafluoroethylene)
q	number of inner-sphere water molecules
q	quartet
R	residual
r	distance
R	arginine
r.t.	room temperature
rb	round bottom
RF	radio frequency
R_f	retention factor

ROESY	rotational Overhauser spectroscopy
RP-HPLC	reverse phase high performance liquid chromatography
s	second
s	singlet
SAP	square antiprismatic
SN	signal-to-noise
SPE	solid phase extraction
SPPS	solid-phase peptide synthesis
SUNY	State University of New York
T	temperature
T	Tesla
t	triplet
T_1	spin-lattice relaxation time
T_{1m}	proton relaxation rate
T_2	spin-spin relaxation time
τ_m	mean water residence lifetime
τ_R	rotational correlation time
tBu	*tert*-butyl
TE	echo time
TEA	triethylamine
TEM	transmission electron microscopy
temp	temperature
tert	tertiary
TFA	trifluoroacetic acid
THF	tetrahydrofuran
TIS	triisopropylsilane
TLC	thin layer chromatography
TOCSY	total correlation spectroscopy
TOF	time of flight
TR	repetition time
tris	2-amino-2-hydroxymethylpropane-1,3-diol
trp	tryptophan
TSAP	twisted square antiprismatic
UV	ultraviolet
UV/vis	ultraviolet/visible
V	valine
V	volt
val	valine
vis	visible
VT	variable temperature

W	tryptophan
X	generic amino acid residue
XPS	X-ray photoelectron spectroscopy
XRD	X-ray diffraction
α	alpha
β	beta
δ	delta
γ	gamma
υ	frequency
Π	pi
T_{1obs}	observed spin lattice relaxtion time
μm	micrometer
μL	microliter

DEDICATION

This dissertation is dedicated to my parents: Dr. Mark and Carolyn Ulrich.

They have instilled in me a great appreciation for the value of education.

TABLE OF CONTENTS

Appendix III – Luminescence and NMR Studies of α-EGadMe and β-EGadMe
Introduction
Results and Discussion

Appendix IV – Single Crystal X-ray Diffraction Structure of a Macrocyclic Synthon

References

LIST OF FIGURES

Figure A3.1 Hypothesized conformations of α-EGadMe (left) and β-EGadMe (right) in the presence of exogenous carbonate.[18] The numbering schemes for the europium(III) and yttrium(III) complexes refer to the current work…………………………………………………308

Figure A3.2 Excitation spectrum of 0.5 mM β-EGadMe (**2**) upon titration of NaHCO$_3$. With increasing concentrations of NaHCO$_3$, the excitation maximum at 579.5 nm decreases with a concomitant increase in two new maxima at 580.0 nm and 580.3 nm………………………..310

Figure A3.3 Excitation spectrum of 0.5 mM α-EGadMe (**1**) upon titration with NaHCO$_3$. The excitation intensity increases with increasing NaHCO$_3$, however there is no shift in the excitation maximum……………………………………………………………………………………311

Figure A3.4 ^{1}H-NMR spectra of the diamagnetic Y(III) complexes of α-EGadMe (**3**, top) and β-EGadMe (**4**, bottom) in D$_2$O. The broad resonances of the cyclen and sugar protons of **4** (at 2.5-3.5 ppm) are indicative of conformational fluxionality…………………………………………..314

Figure A3.5 ^{1}H-NMR spectra of the paramagnetic Eu(III) complexes of α-EGadMe (**1**, top) and β-EGadMe (**2**, bottom) in D$_2$O. The cyclen axial protons due to the SAP isomer (at 32-43 ppm) and the TSAP isomer (at 15-27 ppm) are well-resolved for **1**. In contrast, the fluxionality of **2** results in broad proton resonances……………………………………………………………..315

Figure A3.6 Low (0 ^{o}C, top) and high (80 ^{o}C, bottom) temperature ^{1}H-NMR spectra of Eu(III)-β-EGadMe (**2**) in D$_2$O. The paramagnetically shifted cyclen protons begin to coalesce at high temperature……………………………………………………………………………………….316

Figure A3.7 Low (0 ^{o}C, top) and high (80 ^{o}C, bottom) temperature ^{1}H-NMR spectra of 240 mM **2** in D$_2$O with 24 mM Na$_2$CO$_3$ added. The presence of 0.1 equivalents of carbonate has little effect on the ^{1}H-NMR spectra (compare to spectra in Figure A3.6)…………………………...317

LIST OF SCHEMES

LIST OF TABLES

CHAPTER I

INTRODUCTION TO MAGNETIC RESONANCE IMAGING

AND CONTRAST AGENTS

Magnetic Resonance Imaging

Magnetic Resonance Imaging (MRI) is a non-invasive imaging modality that allows three-dimensional imaging of opaque organisms. This chapter will start with an explanation of the underlying physical principles of MRI followed by a brief review of contrast agents. The intention of this chapter is to provide the background necessary for understanding the ideas and principles contained in the remainder of this thesis, but is in no way intended to be an exhaustive review of the subject.

PRINCIPLES OF MAGNETIC RESONANCE

Nuclei containing an odd number of protons or neutrons possess the quantum mechanical property of spin. Although many nuclei (including ^{1}H, ^{13}C, ^{19}F, ^{17}O, ^{15}N, ^{31}P, and ^{11}B) are commonly utilized for Nuclear Magnetic Resonance (NMR) spectroscopy, of particular interest in this discussion will be ^{1}H (proton) nuclei. Due to the high natural abundance of this isotope as well as the ubiquitious nature of water protons in the human body, current MRI technology is based upon ^{1}H nuclei. Since protons are spin quantum number $I = \frac{1}{2}$ nuclei, their spin will exist in either of the $I = +\frac{1}{2}$ state (spin up) or the $I = -\frac{1}{2}$ state (spin down). The energies of spin up and spin down nuclei are degenerate, therefore the two states will be approximately equally populated. However, when the protons are placed in a magnetic field, the interaction of the nuclear spin with the external magnetic field results in the spin up nuclei being slightly lower in energy than the spin down nuclei. This results in Zeeman splitting (Figure 1.1)
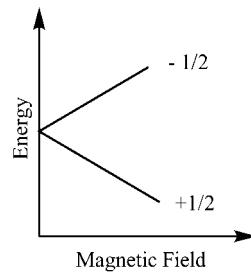
Figure 1.1 Zeeman splitting of spin ½ nuclei with applied magnetic field.

with the energy difference between spin up and spin down nuclei given by Equation 1.1:

Equation 1.1 $\Delta E = \hbar\gamma B_o$

where $\hbar$ is Dirac's constant, γ is the proton gyromagnetic ratio, and B_o is the applied magnetic field. The population of the two states, spin up (N_{up}) and spin down (N_{down}), depends upon B_o and temperature (T) and is given by Equation 1.2:

Equation 1.2 $N_{up}/N_{down} = \exp[\hbar\gamma B_o/(k_B T)]$

where k_B is the Boltzmann constant. At room temperature (300 K) and 1.5 Tesla (a common clinical magnetic field strength), the thermal distribution of proton nuclei between the two states, given by Equation 1.2, results in the spin up state being populated by approximately 0.001 % more nuclei than the spin down state. This miniscule difference in the relative amounts of spin up/spin down nuclei is the fundamental basis for developing a detectable signal in MRI yet leads to limitations in sensitivity because the scanner is essentially detecting only one out of every one

hundred thousand available nuclei. It is this small subset of the total nuclei which are

manipulated during a typical MR experiment.

The slight excess of nuclei in the spin up configuration results in a net magnetization

about the axis of the applied field. In the laboratory frame of reference, these spins process at the

Larmor frequency (equal to the frequency of the magnet). For simplicity, the following

explanation will use the rotating frame of reference in which the rotation frequency is the Larmor

frequency (Figure 1.2).
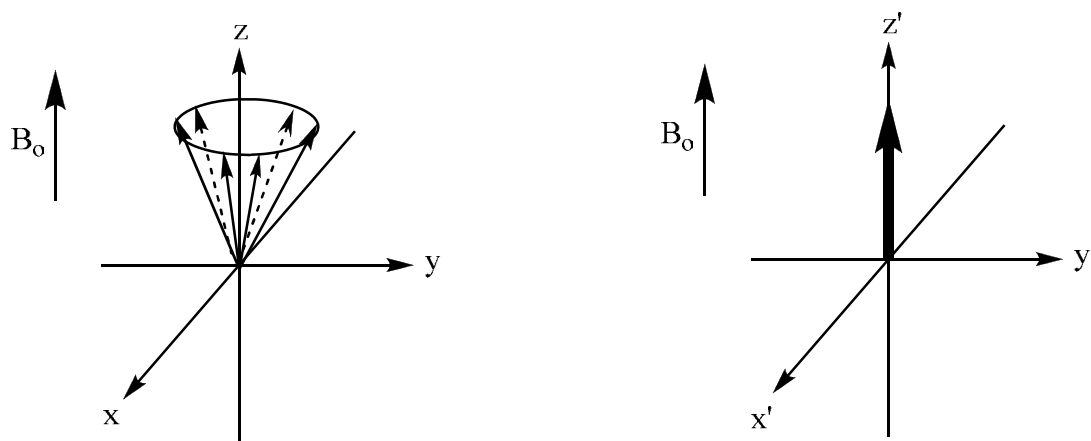
**Figure 1.2 Magnetization in the laboratory frame of reference (left) and the rotating frame
of reference (right)**

The application of electromagnetic radiation of an appropriate frequency, as dictated by Equation

1.4 (derived by rearranging Equation 1.1 and substituting Equation 1.3), causes the net

magnetization to be flipped into the x-y plane.

Equation 1.3 $E = h\upsilon$

Equation 1.4 $\upsilon = \Delta E/h = \gamma B_o/2\pi$

The frequencies (υ) used by MRI correspond to the radio frequency (RF) range of the

electromagnetic spectrum, thereby avoiding harmful ionizing radiation utilized by other imaging

modalities such as X-ray. By varying the length of the RF pulse, the degree to which the

magnetization (M) is flipped into the x'-y' plane can be varied (known as the flip angle) (Figure

1.3).
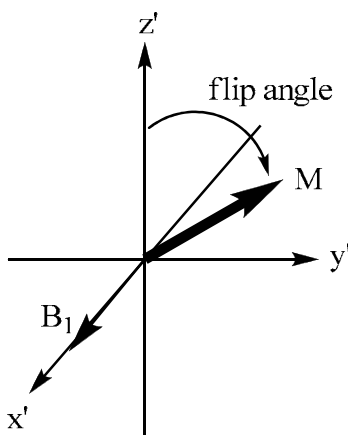
Figure 1.3 Net magnetization (M) is flipped into the x'-y' plane by application of radio frequency field (B_1)

In a typical MR scanner, the RF coils (used to induce as well as detect changes in net

magnetization) are located in the x-y plane, perpendicular to the applied magnetic field, therefore

the net magnetization of the nuclear spins about the z-axis results in zero magnetization in the x-

y plane. Application of a pulse of RF energy from the coils results in the net magnetization

being flipped into the x-y plane, which can be detected by the receiver coils. The net

magnetization does not remain in the x-y plane, however, as the nuclear spins undergo relaxation

causing the net magnetization to return to the previously established thermal equilibrium value (Figure 1.4).
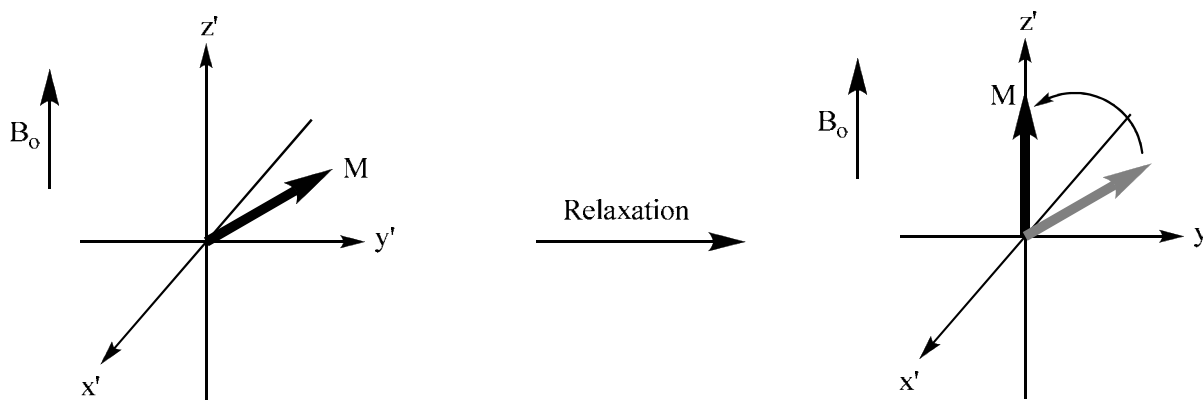
Figure 1.4 Relaxation of the net magnetization to the thermal equilibrium value

RELAXATION THEORY

Relaxation can occur through two distinct processes: spin-lattice (T_1) and spin-spin (T_2) relaxation. Spin-lattice relaxation occurs due to the nuclear spin interacting with the surrounding molecular medium (the lattice). As the molecules of the lattice move about in random fashion, their associated nuclear magnetic moments create a magnetic noise which generates a fluctuation in the local magnetic field experienced by the nuclei in study. This fluctuation in local magnetic field stimulates a transition in the nuclear spin back to the lower energy state. The spin is said to be 'relaxed' from a high energy state (induced by the RF pulse) to a low energy state (corresponding to the thermal equilibrium value given by Equation 1.2). Spin-spin relaxation occurs due to a loss of phase coherence of the nuclear spins. After the application of an RF pulse, the spins rotate coherently about the z axis and are said to be 'in phase'. The random motion of the molecules (of the nuclei in study) produces fluctuations in the angular velocity of

the nuclear spins, resulting in phase dispersion. The phases will disperse until ultimately there is total phase decoherence; at this point, the spins are said to be 'dephased' and the magnetization in the x-y plane returns to zero.

A barrage of pulse sequences have been developed as a means to accurately measure T_1 or T_2.[23] The choice of pulse sequence dictates whether the experiment is termed "T_1-weighted" or "T_2-weighted". In biological samples, T_1 and T_2 relaxation processes occur simultaneously and on the order of seconds[24].

The miniscule difference (0.001%, Equation 1.2, vida supra) in the relative amounts of spin up/spin down nuclei is the culprit for the low sensitivity of MRI. In order to overcome the problem of signal-to-noise (SN), the number of scans can be increased. The SN will grow as the square root of the number of scans. Therefore, in order to obtain a ten-fold increase in image intensity, the number of scans must be increased by one hundred-fold. Due to motion artifacts (from patient movement), there is a finite limit to the amount of scans that can be performed in a clinical setting. This is compounded by extraneous factors such as the high cost of magnet time and patient discomfort. Alternatively, the SN problem can be overcome through the use of contrast agents. Contrast agents shorten both T_1 and T_2 relaxation times into the millisecond time range to increase SN.

T_1 CONTRAST AGENTS: THEORY

T_1 contrast agents shorten T_1, thus decreasing the time required to achieve a satisfactory SN. MR image intensity (I) is proportional to $1/T_{1obs}$ (Equation 1.5).

Equation 1.5 $I \propto 1/T_{1obs}$

Equation 1.6 $1/T_{1obs} = 1/T_{1dia} + 1/T_{1para}$

Equation 1.6 shows that the observed signal (T_{1obs}) in MRI is equal to the sum of two

components: the diamagnetic contribution (T_{1dia}, intrinsic to the tissue) and the paramagnetic

contribution (T_{1para}, due to the presence of exogenous contrast agents). The paramagnetic term

can be broken down into an inner sphere component (T_1^{IS}) and an outer sphere component

(T_1^{OS}), as given by Equation 1.7.

Equation 1.7 $1/T_{1para} = 1/T_1^{IS} + 1/T_1^{OS}$

The inner sphere relaxation time is due to water molecules directly bound to the paramagnetic

metal while the outer sphere relaxation time is due to water molecules in close proximity (but not

directly bound) to the paramagnetic metal. In the case of dilute aqueous solutions (such as those

commonly employed for MRI contrast), the inner sphere term can be described by Equation 1.8

where q is the number of inner sphere water molecules, [CA] is the concentration of the contrast

agent (CA), T_{1m} is the longitudinal water proton relaxation time, and τ_m is the mean residence

lifetime of the inner sphere water molecule.

Equation 1.8 $1/T_1^{IS} = q[CA]/55.5(T_{1m} + \tau_m)$

As can be seen in Equation 1.8, T_1^{IS} is dependent on the concentration of the contrast agent,

therefore a new descriptor, relaxivity (r_1, Equation 1.9), is warranted which takes into account

the concentration of the agent.

Equation 1.9 $1/T_{1obs} = r_1[CA] + 1/T_{1dia}$

Relaxivity includes both inner sphere and outer sphere effects and is experimentally determined by the slope of $1/T_{1obs}$ vs. [CA] (Equation 1.9). Relaxivity provides a convenient metric to compare the relative efficacies of contrast agents. When comparing relaxivitiy values in the literature, it is important to denote the magnetic field strength and temperature as these parameters influence nuclear spins as given by Equation 1.2.

The relaxivitiy of a contrast agent is influenced by several physical parameters: q, τ_m, and T_{1m} (Equation 1.8). Furthermore, T_{1m} can be expressed as the sum of the dipole-dipole relaxation (T_1^{DD}) and the scalar relaxation (T_1^{SC}) as given by the Solomon-Bloembergen equations (Equations 1.10-1.12) where γ_I is the nuclear gyromagnetic ratio, g is the electron g-factor, μ_B is the Bohr magneton, r_{GdH} is the distance between the Gd^{3+} electron spin and the inner sphere water protons, ω_I is the nuclear Larmor frequency, ω_s is the electron Larmor frequency, $A/\hbar$ is the scalar coupling constant between the electrons of Gd^{3+} and the protons of the inner sphere water, and τ_{c1}, τ_{c2}, τ_{e2} are correlation times given by Equations 1.13-1.15.

Equation 1.10 $1/T_{1m} = 1/T_1^{DD} + 1/T_1^{SC}$

Equation 1.11

$$1/T_1^{DD} = (2/15)(\gamma_I^2 g^2 \mu_B^2/r_{GdH}^6)S(S+1)(\mu_0/4\Pi)^2\{[7\tau_{c2}/(1+\omega_s^2\tau_{c2}^2)]+[3\tau_{c1}/(1+\omega_I^2\tau_{c1}^2)]\}$$

Equation 1.12 $\quad 1/T_1^{SC} = [2S(S+1)/3](A/\hbar)^2[\tau_{e2}/(1+\omega_s^2\tau_{e2}^2)]$

Equation 1.13 $\quad 1/\tau_{c1} = 1/\tau_R + 1/\tau_m + 1/T_{1e}$

Equation 1.14 $\quad 1/\tau_{c2} = 1/\tau_R + 1/\tau_m + 1/T_{2e}$

Equation 1.15 $\quad 1/\tau_{e2} = 1/\tau_m + 1/T_{2e}$

In Equations 1.13-1.15 τ_R is the rotational correlation time and T_{1e} and T_{2e} are the longitudinal and transverse electron spin relaxation times of Gd^{3+}, respectively. Since Gd^{3+} forms predominantly ionic bonds and the water protons are relatively far from the paramagnetic Gd^{3+}, the scalar coupling is weak and represents only a small contribution to the overall relaxation.[24] The relationships of the variables in Equations 1.8-1.14 and how they influence relaxivity will be discussed in context with current T_1 contrast agents.

T$_1$ CONTRAST AGENTS: EXAMPLES

Clinical T_1 contrast agents are primarily based upon small-molecule Gd^{3+} chelates. While other paramagnetic metal ions (such as Mn^{2+}) may be used, Gd^{3+} is the paramagnetic ion of choice due to its highly symmetrical spherical ground state and its large magnetic moment of 63 Bohr magnetons. While it may be tempting to use the aquo ion of Gd^{3+} due to its maximum number of inner sphere water molecules (thus maximizing q, Equation 1.8), the toxicity of Gd^{3+} prohibits its use in biological samples. Being similar in size to Ca^{2+} (Gd^{3+} ionic radius is 1.07 Å while Ca^{2+} ionic radius is 1.12 Å),[25] Gd^{3+} is speculated to interfere with physiological Ca^{2+}

through transmetallation.[26] In order to lower the toxicity of Gd^{3+} to an acceptable level that can be tolerated by humans, it must be chelated. The chelate acts to sequester the ion, thereby reducing the amount of free Gd^{3+} that is available to interact with a biological system. In addition to reducing toxicity, chelates can be used to alter the pharmacokinetics of a contrast agent.[27] Two chelation moieties, 1,4,7,10-tetraazacyclododecane N, N', N'', N'''-tetraacetic acid (DOTA) and diethylenetriaminepentaacetic acid (DTPA), have emerged as common motifs upon which a great number of derivatives have been developed. Figure 1.5 shows the structures of the Gd^{3+} complexes of DOTA and DTPA with commercial names Dotarem and Magnevist, respectively.

$[Gd(DOTA)(H_2O)]^-$
Dotarem

$[Gd(DTPA)(H_2O)]^{2-}$
Magnevist
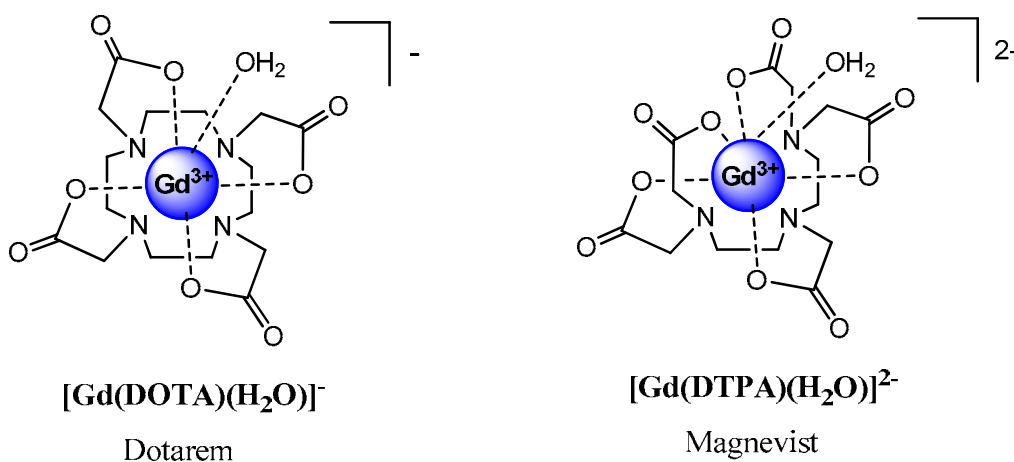
Figure 1.5 Structures of Gd-DOTA (Dotarem) and Gd-DTPA (Magnevist)

Key features of DOTA and DTPA include extremely high Gd^{3+} thermodynamic formation constants, log K_{GdL}= 25.3 and 22.46 respectively, as well as an open coordination site for an inner sphere water molecule.[28,29] In order to confer additional pharmacokinetic properties,

there have been a myriad of contrast agents developed with structures consisting of variations

of DOTA and DTPA. Among these, Gd-HP-DO3A (ProHance) and Gd-DTPA-BMA

(Omniscan) are the most clinically relevant due to their FDA approval (Figure 1.6).

Gd(HP-DO3A)(H₂O)

ProHance

Gd(DTPA-BMA)(H₂O)
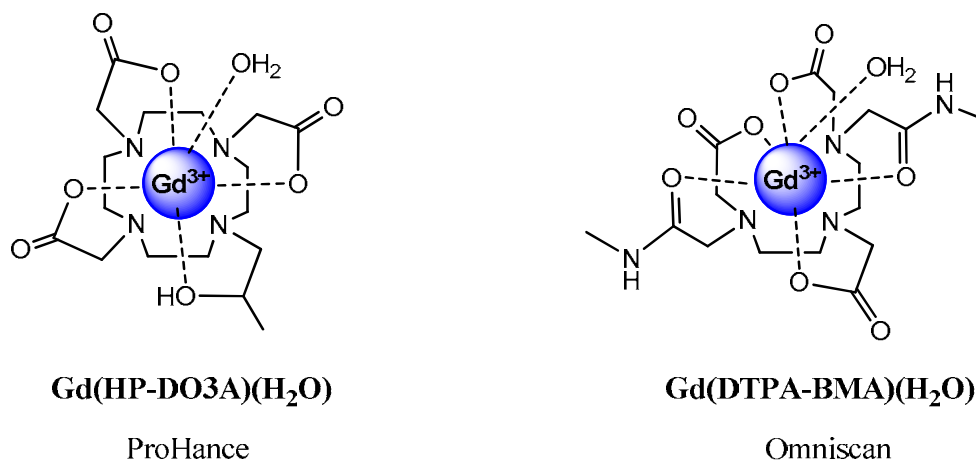
Omniscan

Figure 1.6 Structures of Gd-HP-DO3A (ProHance) and Gd-DTPA-BMA (Omniscan)

ProHance and Omniscan were developed to be charge neutral to alleviate patient discomfort

experienced when injecting solutions with high osmolality. Many other contrast agents have

been synthesized for which the reader is directed to an excellent review of this subject.[27]

The relaxivities of clinical contrast agents (4.2 $mM^{-1}s^{-1}$ for Gd-DOTA, 4.3 $mM^{-1}s^{-1}$ for

Gd-DTPA, measured at 20 MHz, 25 $^{\circ}$C, pH 7.4)[30] are far from the theoretical maximum of ~100

$mM^{-1}s^{-1}$. The difficulty of designing a high relaxivity contrast agent lies in the simultaneous

optimization of the relaxation parameters q, τ_m, and τ_R.

According to equation 1.8, an elementary assessment of contrast agent design would be

to increase q in order to increase relaxivity. In practice, however, one must take into

consideration the deleterious effects associated with an increase in q, namely the reduction in the

coordination number of the ligand and the concomitant effect of reduced complex stability.

Increasing q to 2, as in Gd-DO3A (Figure 1.7), resulted in a decrease in the thermodynamic

formation constant by 4 orders of magnitude (Gd-DO3A $logK_{GdL}= 21.1$ compared to Gd-DOTA

$logK_{GdL}= 25.3$) [28]. Further increasing q to 3, as in Gd-NOTA (Figure 1.7), resulted in a dramatic

decrease in the thermodynamic formation constant by almost 12 orders of magnitude ($logK_{GdL}=$

13.7) and rendered agents of this type unsuitable for human imaging due to the possibility of

Gd^{3+} dissociation from the ligand.[31]

Gd(DO3A)(H$_2$O)$_2$ **Gd(NOTA)(H$_2$O)$_3$**
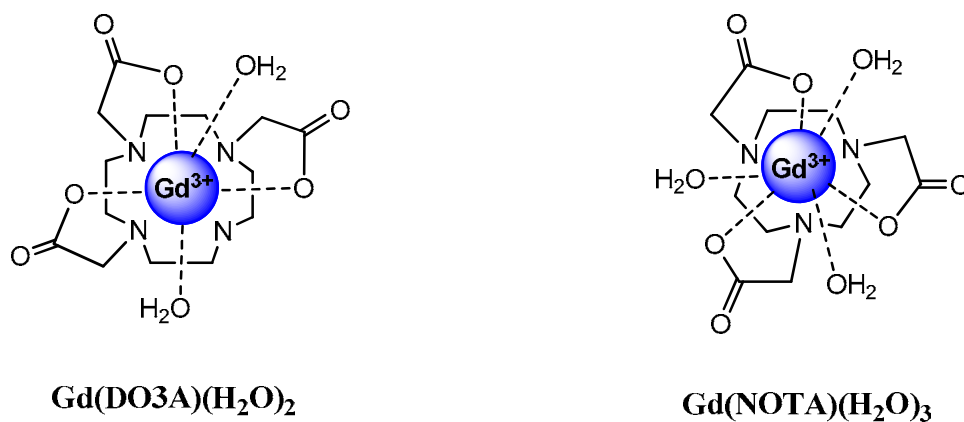
Figure 1.7 Structures of Gd-DO3A and Gd-NOTA

The $1/r^6$ dependence of the dipolar relaxation (Equation 1.11) suggests that a small

decrease in the distance between the protons of the inner sphere water and the paramagnetic Gd^{3+}

(r_{GdH}) would have a profound increase in the observed relaxivity. Unfortunately, r is difficult to

control and varies little (2.41-2.50 Å) among a wide range of chelates.[27]

In the case of very slow water exchange ($T_{1m} \ll \tau_m$), Equation 1.8 shows that the relaxivity is limited by τ_m. Substituting the ubiquitous acetate pendant coordinating groups (found in most clinically used contrast agents) with amide-based pendant coordinating groups causes τ_m to slow from 244 ns (for Gd-DOTA) to 19 μs (for Gd-DTMA, the tetra-substituted N-methyl amide version of DOTA).[32,33] Sherry and coworkers have extensively studied the factors influencing τ_m and discovered a dependence of τ_m on the overall complex geometry.[7]

In the case of fast water exchange ($T_{1m} \gg \tau_m$), Equation 1.8 can no longer be used to easily predict the factors influencing relaxivity, and a more thorough approach involving Equations 1.10-1.14 is warranted. Since most gadolinium-based contrast agents are small molecule chelates with fast water exchange, the limiting factor in τ_c (Equations 1.13-1.14) is τ_R, the rotational correlation time. Increasing τ_R results in increased relaxivities and has been the subject of investigation by many research groups.[34] An increased τ_R can be afforded by associating the contrast agent with a macromolecule such that the τ_R of the small molecule contrast agent approaches that of the macromolecule. Examples of efforts to optimize the τ_R of gadolinium-based contrast agents include association with proteins;[35] covalent attachment to polymers[36] and dendrimers;[37] and encapsulation within liposomes,[38] virus capsids,[39] and C_{60}.[40]

Enzyme-Activated T_1 Contrast Agents

While many research groups aim to increase the relaxivity of contrast agents through the optimization of q, τ_m, and/or τ_R, others have been concerned with the development of enzyme-activated contrast agents. Termed "smart" agents, these complexes are able to report on physiological processes due to a change in relaxivity.

A paradigm of this class of agents, EGad, was developed in the Meade laboratory.[1] The agent features a DO3A-based Gd^{3+} chelate with a galactopyranose sugar appended as a pendant arm of the macrocycle. The sugar acts to block water access to Gd^{3+}, resulting in a $q = 0.7$ complex. Upon enzymatic cleavage of the sugar by β-galactosidase, the blocking sugar is removed, resulting in a $q = 1.2$ complex and a concomitant 20% increase in relaxivity (Figure 1.8). Through this novel approach, the agent is able to be "turned on" by the enzyme. A modified version of this agent, EGadMe (Figure 1.8), was used to track β-galactosidase activity in vivo.[2]

R = H (EGad), CH_3 (EGadMe)
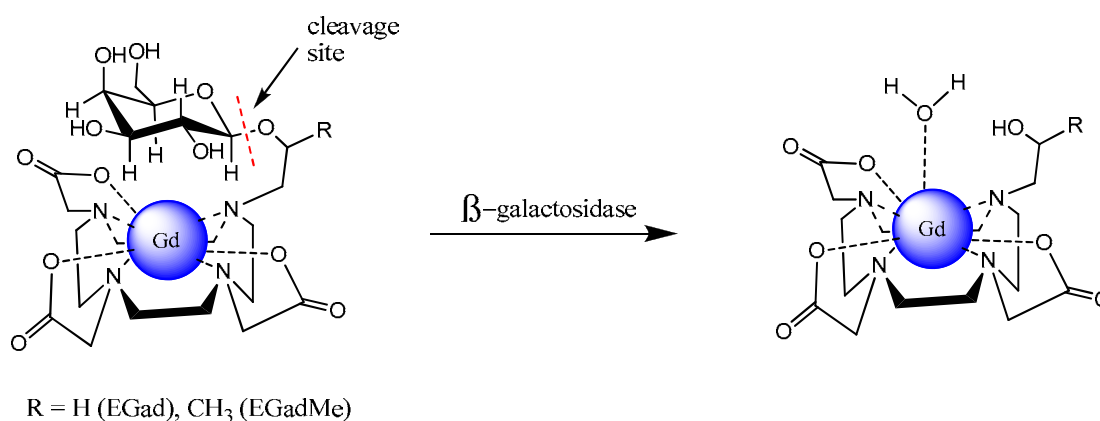
Figure 1.8 β-Galactosidase-activated contrast agents, EGad[1] and EGadMe[2]

Lauffer and coworkers developed a contrast agent activated by alkaline phosphatase.[3] Upon the cleavage of a phosphate group by the enzyme, the aryl group becomes more hydrophobic, binds to human serum albumin, and results in a 70% increase in relaxivity due to an increase in τ_R (Figure 1.9).
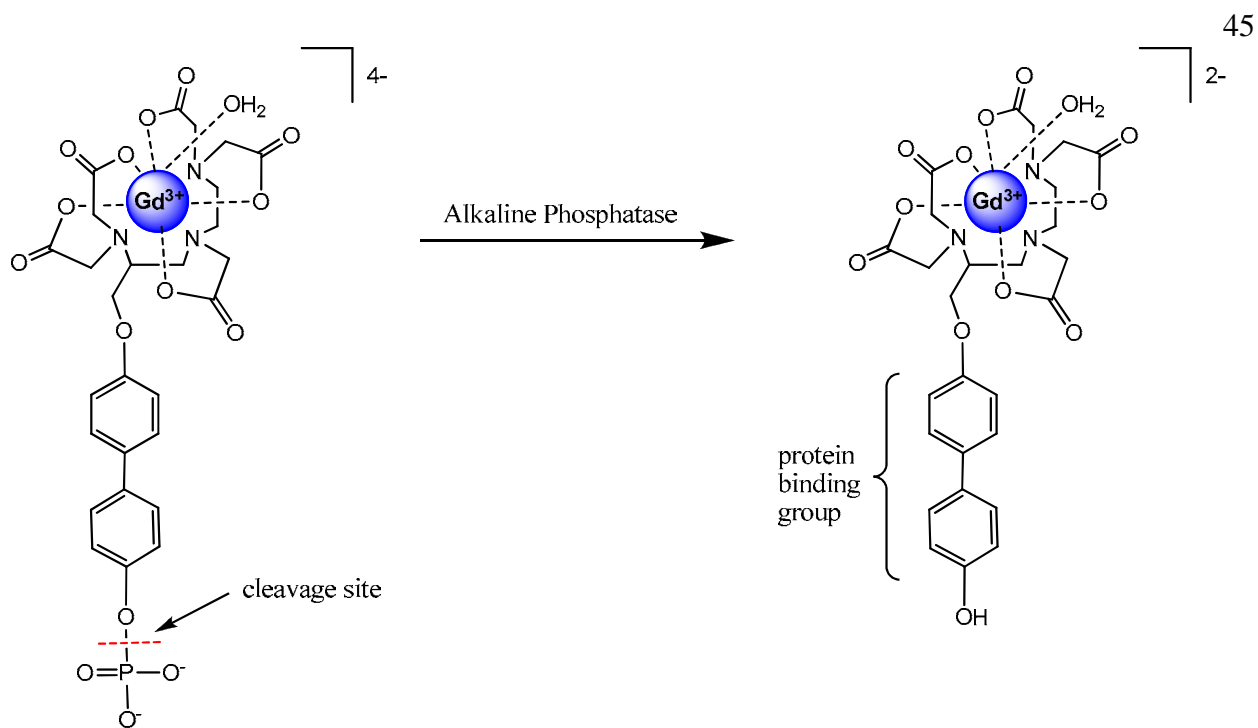
Figure 1.9 Phosphatase-activated contrast agent[3]

Duimstra and co-workers involved the use of a self-immolative linker to create an agent which is activated by β-glucuronidase.[4] Upon enzymatic cleavage of the β-glucuronic acid, the linker undergoes an electron cascade which changes the relaxivity of the contrast agent (Figure 1.10). The agent was hypothesized to increase in relaxivity upon cleavage due to the binding of carbonate, however in vitro enzyme studies displayed an increase in T_1 (decrease in relaxivity) upon enzymatic cleavage.
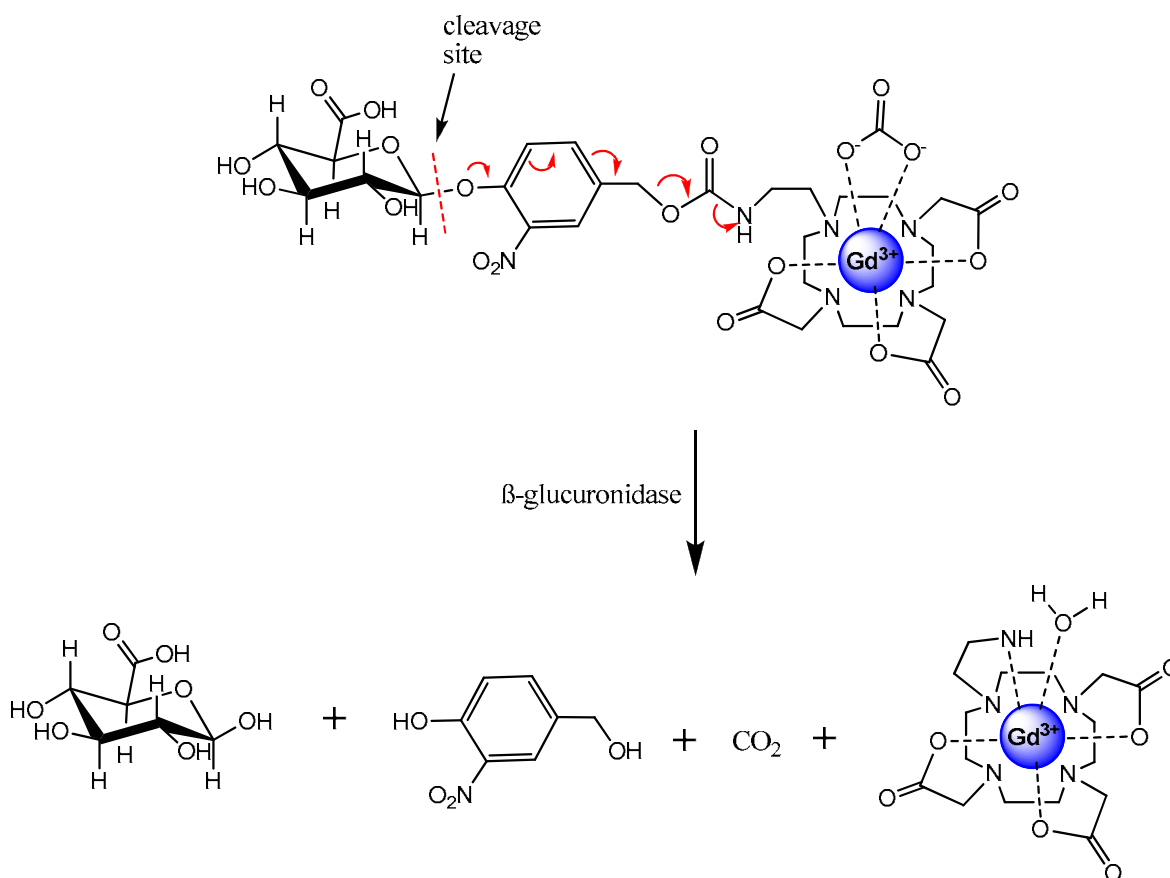
Figure 1.10 β-Glucuronidase-activated contrast agent showing self-immolative electron cascade[4]

<u>PARACEST MR Imaging</u>

Paramagnetic chemical exchange saturation transfer (PARACEST) MR imaging is an alternative method of introducing contrast based on modulation of the overall intensity of the water proton signal. PARACEST imaging utilizes a presaturation pulse to selectively saturate inner-sphere water protons.[41] As the inner-sphere water exchanges with bulk water, the saturated magnetization is effectively transferred to bulk water. As a result, PARACEST agents produce negative contrast (resulting in a darker image) by decreasing the intensity of the bulk water signal. For most DOTA or DTPA-based MRI contrast agents, fast inner-sphere water exchange

results in a reduction of water proton hyperfine shifts to near zero (making them unsuitable for

use as PARACEST imaging agents). Therefore, the mean residence lifetime of the inner-sphere

water must be sufficiently long ($\tau_m \geq \mu s$ time scale) to observe a PARACEST effect from inner-

sphere water. The long (μs) mean water residence lifetimes observed for amide-derivatives of

DOTA satisfy this requirement.[41] In addition to the PARACEST effect due to slowly

exchanging inner-sphere water, the presence of exchangeable NH or OH protons in close

proximity to the lanthanide(III) allows PARACEST imaging based on this second pool of

protons which are able to exchange with bulk water.

Commonly, europium(III), dysprosium(III), and terbium(III) are used in place of the

gadolinium(III) used in T_1 contrast agents due to the ability of the former metals to induce

considerable NMR hyperfine shifts in nearby nuclei.[41] For both pools of exchangeable protons

(inner-sphere water and/or NH/OH protons), the substitution of various lanthanide(III) ions into

the same ligand results in different chemical shifts for the exchangeable protons due to the

unique Lanthanide Induced Shift (LIS) of each metal (see Chapter II, Table 2.2 for a list of LIS).

The tuning of the saturation frequency to the chemical shift of the exchangeable protons within

each PARACEST agent allows the imaging of the individual components of a mixture of

PARACEST agents containing different lanthanide(III) ions. In this regard, Aime and coworkers

imaged a mixture of europium(III) and terbium(III) complexes of a DotamGly ligand, thus

exploiting the different PARACEST saturation frequencies of each metal.[42]

SCOPE OF THESIS

This thesis concerns the design, synthesis, and characterization of novel peptide-based, enzyme-activated MRI contrast agents. Agents of this type have the potential to monitor enzyme activity in vivo. Specifically, these agents have been designed to monitor two very important classes of enzymes, caspases and matrix metalloproteinases, which are instrumental in the biological processes of apoptosis and tumor metastasis, respectively. The in vivo imaging of these key biological processes has the potential to revolutionalize the detection of diseased tissue. The agents are proposed to undergo structural changes upon cleavage of a substrate peptide, ultimately resulting in a change in relaxivity. Five approaches to modulate the relaxivity of gadolinium(III) chelates through enzymatic activation are described. Chapter I provides an introduction to MRI and explains the theory required to understand the design and development of novel contrast agents. Chapter II starts with an early design of an agent in which a peptide is proposed to block inner-sphere water access to gadolinium(III). The cleavage site of the peptide was varied to determine the effect of distance of the cleavage site to the gadolinium(III) chelate (details in Appendix I). The results of this initial study lead to the development of the peptide-bridged macrobicyclic MRI contrast agents. The linker length of the peptide-bridged macrobicyclic agents was varied in a systematic manner in order to study the effects of proximity of the peptide to the macrocycle in blocking inner-sphere water access. Chapter III takes a different approach to modulate relaxivity by employing a self-immolative linker between a peptide and a gadolinium(III) chelate. In comparison to previous self-immolative MRI contrast agents, the substrate was changed in order to target caspase-3 and the chelate structure was altered to enhance the binding affinity of the carbonate anion. Chapter IV investigates a simplified version of the contrast agent presented in Chapter III and displays a novel mechanism

of coordination which has great potential for use in restricting inner-sphere water access to gadolinium(III). Chapter IV explores new methods of modulating T_1 and T_2 relaxation through the covalent attachment of a gadolinium(III) chelate (T_1 contrast agent) to a cobalt ferrite nanoparticle (T_2 contrast agent). The use of two different linker lengths sets the stage for determining the effect of distance between the T_1 and T_2 contrast agents on the overall observed relaxivity of the conjugate. The inclusion of an enzyme-cleavable linker between the T_1 and T_2 contrast agents gives this conjugate the potential to track enzyme activity. Each of the agents in Chapters II, III, IV, and V and Appendix I share a common thread of peptide-based enzyme substrates covalently attached to a gadolinium(III) chelate. The results contained in this work open doors to new classes of MRI contrast agents which have the potential to track enzymatic activity in vivo.

CHAPTER II

PEPTIDE-BRIDGED MACROBICYCLES FOR THE DETECTION OF

PROTEASES

INTRODUCTION

In 1997, the Meade group pioneered enzyme-activated MRI contrast agents.[1] Termed "smart" agents, they are able to report on physiological processes due to a change in relaxivity. The premier agent features a DO3A-based, Gd^{3+} chelate with a galactopyranose sugar appended as a pendant arm of the macrocycle. The sugar partially blocks inner-sphere water access to Gd^{3+}, resulting in a $q = 0.7$ complex. Upon enzymatic cleavage of the sugar by β-galactosidase, the blocking sugar is removed, resulting in a $q = 1.2$ complex and a concomitant 20% increase in relaxivity (Figure 2.1). A modified version of this agent, EGadMe (Figure 2.1), was reported in 2000 to track β-galactosidase activity in vivo.[2]

R = H (EGad), CH$_3$ (EGadMe)
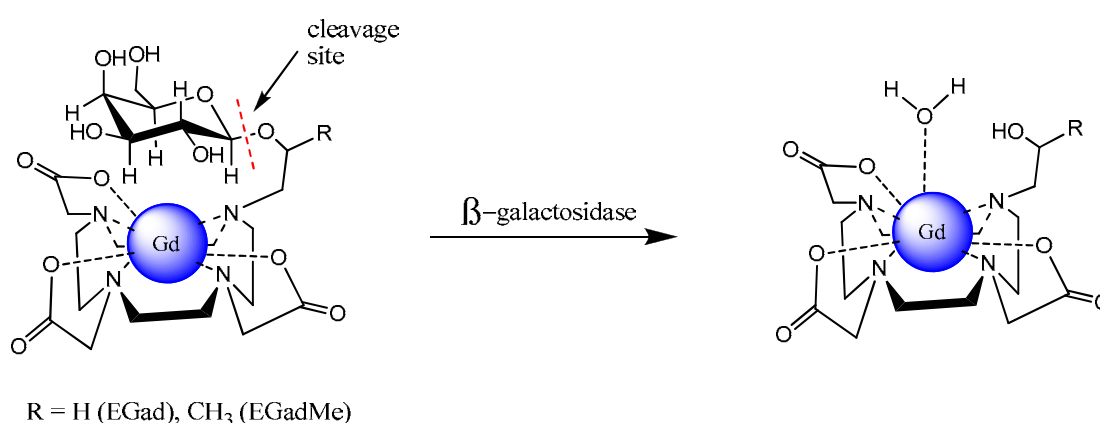
Figure 2.1 β-Galactosidase-activated contrast agents, EGad[1] and EGadMe[2]

The present work started with the goal of extending the limited collection of enzyme-activated agents to include agents sensitive to proteases. Proteases are ubiquitous in biological systems; currently there are 460 known human proteases.[3] The cleavage of specific peptide sequences by proteases is crucial for numerous processes including ovulation, fertilization, embryonic development, tissue remodeling, cell-cycle regulation, immune cell activation, and

apoptosis.[4] The misregulation of proteases in humans has been linked to cancer, arthritis,

osteoporosis, neurodegenerative disorders, and cardiovascular diseases.[3] Therefore, the ability to

non-invasively monitor protease activity in vivo is of paramount importance in advancing the

detection of numerous diseases. Towards this end, a protease-cleavable MRI contrast agent was

designed based on previous enzyme-activated agents. Replacing the sugar blocking moiety used

in the β-galactosidase agents with an enzyme-cleavable substrate peptide has the potential to

create agents that can track protease activity in vivo using MRI.[1,2,5] The substrate peptide was

used to modulate inner sphere water access to Gd^{3+} in a manner analogous to that achieved by

earlier reported β-galactosidase agents.[1,2,5] The substrate consisted of a consensus sequence for

Matrix Metalloproteinase-7 (Described in detail in Appendix I).

A series of agents was synthesized in which the distance of cleavage site to the Gd^{3+}

chelator was systematically varied. In order to simulate the effect of enzymatic cleavage and

serve as authentic standards for comparison, the corresponding "cleaved" agents were

synthesized (Figure 2.2).

Uncleaved Agents
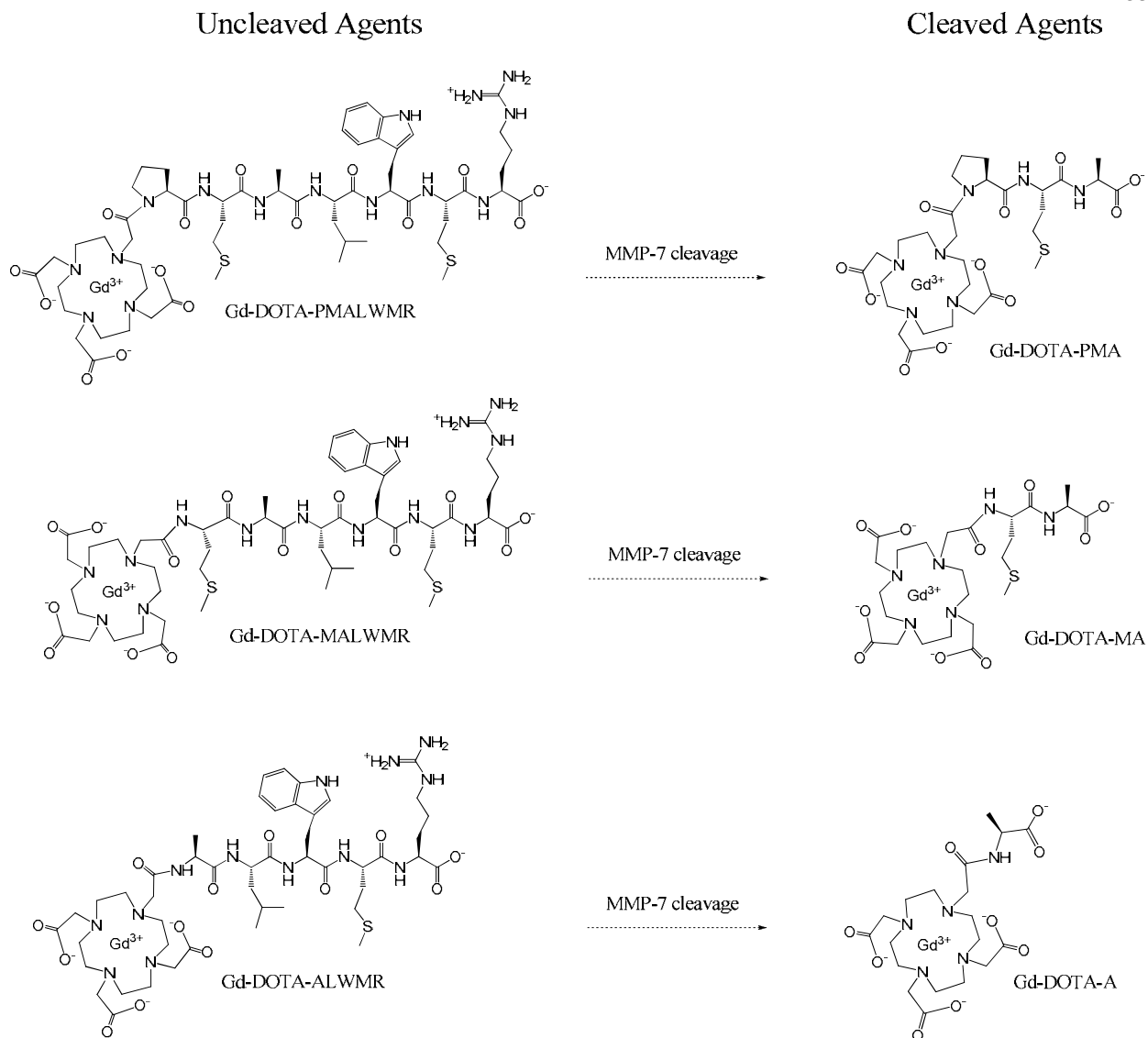
Cleaved Agents

Figure 2.2 Contrast agents for the detection of MMP-7 (details in Appendix I)

Analysis of the uncleaved and cleaved agents revealed that the number of inner-sphere water molecules was unchanged between the uncleaved and cleaved agents (Figure 2.3, details in Appendix I). These results lead to the development of the peptide-bridged agents discussed in detail in this chapter.

Uncleaved Agents

Cleaved Agents

Eu-DOTA-PMALWMR
$q = 1.0 \pm 0.1$

Eu-DOTA-PMA
$q = 1.1 \pm 0.1$

Eu-DOTA-MALWMR
$q = 1.1 \pm 0.1$

Eu-DOTA-MA
$q = 1.0 \pm 0.1$

Eu-DOTA-ALWMR
$q = 1.0 \pm 0.1$

Eu-DOTA-A
$q = 1.0 \pm 0.1$
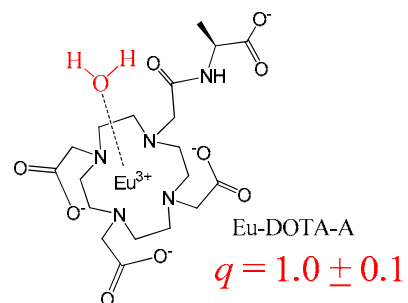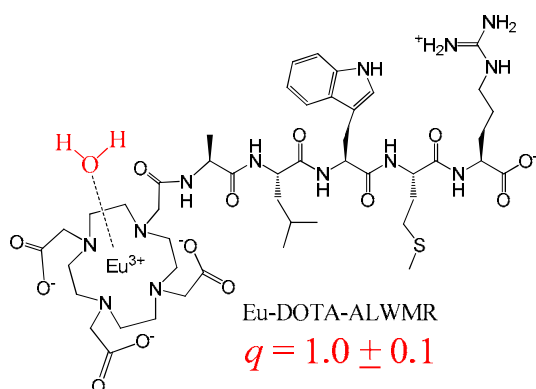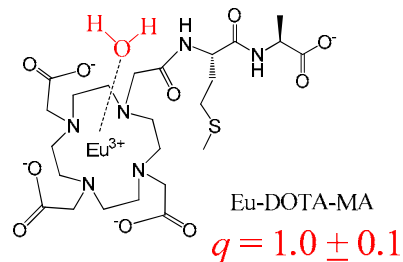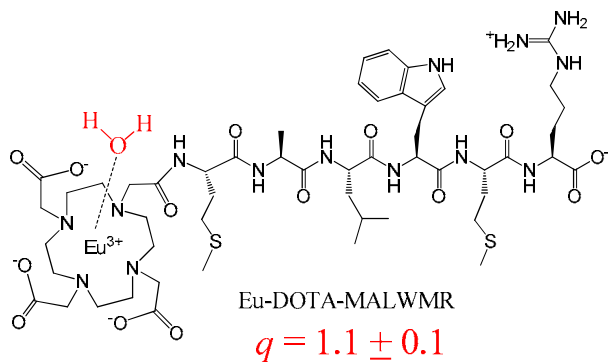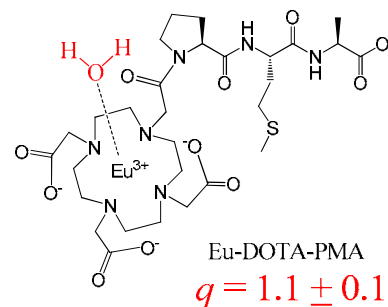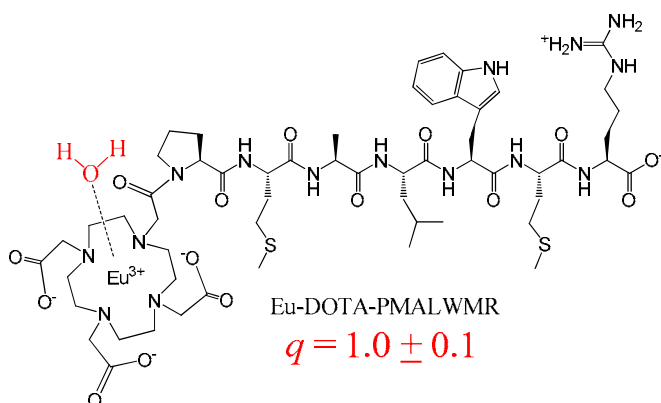
Figure 2.3 Structures and associated number of inner-sphere water molecules (q) determined for the Eu^{3+} analogs of the contrast agents depicted in Figure 2.2[6]

Design of Peptide-Bridged Macrobicycles

Due to the lack of water blocking by the initial peptide-based agent ($q = 1$, Figure 2.3), it was determined that the peptide exists in a conformation in which the N-terminal amide oxygen coordinates to the lanthanide, leaving the ninth coordination site open to water exchange. This is supported by literature precedence of macrocyclic pendant amide carbonyl oxygens coordinating to lanthanides.[6,7] Therefore, a new methodology was designed in which the peptide would to occupy the space covering the ninth coordination site for a DOTA-based macrocylic chelate. By bridging the peptide across the macrocyclic chelator, it was hypothesized that the peptide would act to sterically block inner-sphere water access to Gd^{3+} (Figure 2.4). Such an effect would decrease water relaxation by the agent. Placing the enzyme cleavage site of the substrate between the amino acid residues attached to the chelate allows the structure to open upon enzymatic cleavage of the substrate peptide. This opening of the bridge is hypothesized to allow inner-sphere water access to Gd^{3+} resulting in an increase in relaxivity of the agent.
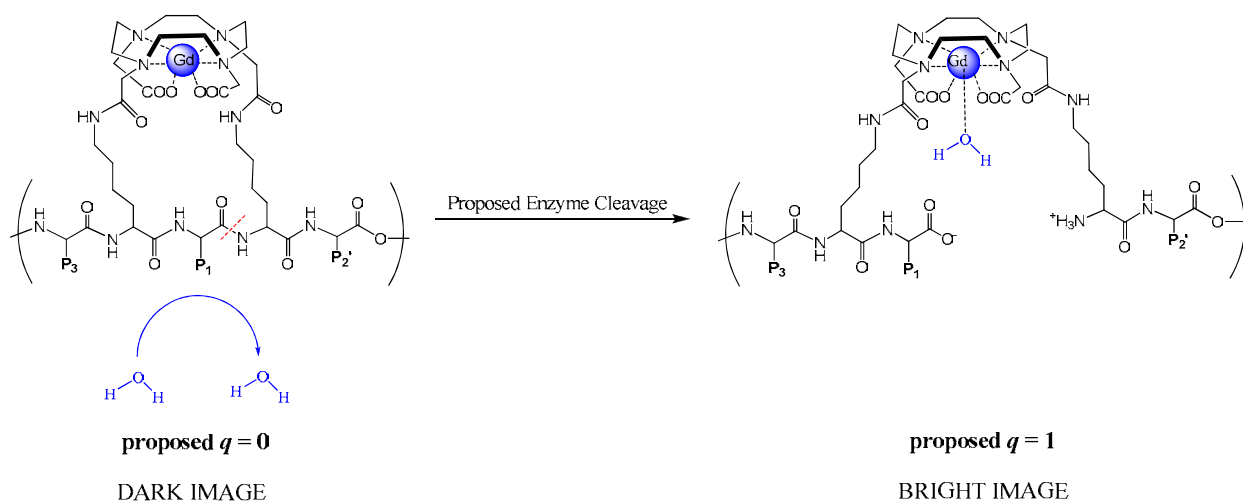
Figure 2.4 General structure of peptide-bridged macrobicycles and proposed mechanism of *q*-modulation (enzyme cleavage site is denoted with red dashed line)

Through CPK modeling, it was estimated that an "n + 2" approach should be used where the macrocycle is covalently attached to the side chains of a peptide with a single amino acid spanning the gap. This arrangement accommodates the stereochemistry of naturally occurring L-amino acids, thereby allowing the peptide to adopt a stable, unstrained conformation. An "n + 2" approach allows recognition of the amino acid side-chains adjacent to the cleavage site (P_1 or P_1' amino acid side-chains; see Figure 2.5 for protease substrate nomenclature[8]), which are often necessary for enzymatic cleavage of the substrate.
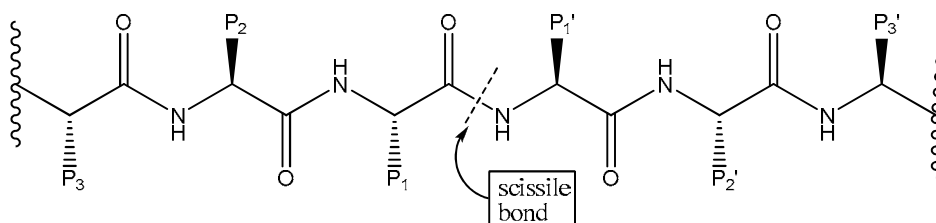
Figure 2.5 Protease Substrate Nonmenclature[8]

After several approaches to form a bridge between the peptide and a macrocyclic chelate were investigated (details in Appendix II), the design eventually evolved into the amide linkage shown in Figure 2.4. This general methodology was used as a blueprint in the synthetic schemes of Parts I and II.

PART I. Peptide-Bridged MRI Contrast Agents for the Detection of Caspase-3

Part I. Introduction: Caspases

Apoptosis is the process of programmed cell death and is paramount to a number of biological processes including normal cell turnover, embryonic development, and metamorphosis.[9] Increased apoptosis has been linked to autoimmune disorders and neurodegenerative diseases such as Alzheimer's and Huntington's diseases.[9] Inhibition of apoptosis has been attributed to several forms of cancer.[9] Due to the severity of the aforementioned afflictions, it is evident that apoptosis plays a crucial role in multiple human pathologies.

Caspases have long been heralded as the executioners of apoptosis.[9] The ten known caspases can be divided into three groups based on their respective substrate specificities.[10] Within this family of proteases, caspase-3 is responsible either wholly or in part for the proteolysis of a large number of substrates during the execution phase of apoptosis.[9]

The imaging of caspase-3 activity in vivo would provide valuable information regarding apoptotic processes and the role of caspases in life-threatening diseases. Current methods of assessing caspase-3 activity include colorimetric and fluorescent assays in which a chromophore is covalently attached to the C-terminus of a substrate peptide. Cleavage of a substrate peptide from a chromophore results in a change of the UV/visible or fluorescence spectrum of the chromophore, thereby monitoring caspase-3 activity in vitro. The practical applications of visible and fluorescence techniques are restricted to the observation of cells and small animals due to the limited penetration of light (<10 mm).[11] MRI provides an alternative to optical

microscopy, allowing the imaging of opaque organisms in three dimensions at cellular resolution.[2]

Design of a Peptide-Bridged Contrast Agent for Caspase-3

Caspase-3 cleaves substrates containing the DEXD^X motif, where X denotes a variety of amino acids and ^ denotes the cleavage site.[10] Placement of the bridge linking the lanthanide chelate to the peptide at the variable residues of the substrate peptide was hypothesized to not interfere with substrate recognition and cleavage by caspase-3. The incorporation of a tryptophan residue on the N-terminus of the peptide provides a chromophore for HPLC purification of synthetic intermediates. It was hypothesized that the substrate peptide could act to sterically block inner-sphere water access to Gd^{3+} (Figure 2.4), resulting in decreased water relaxation by the agent. Upon enzymatic cleavage of DEXD^X by caspase-3, the bridge was hypothesized to open, allowing inner-sphere water access to Gd^{3+} and resulting in an increase in relaxivity of the agent.

It should be noted that the near similar sequence specificity[10] of caspases 3 and 7 would most likely make the agents described in Part I of this chapter substrates for both enzymes. However, for simplicity, only caspase-3 cleavage will be addressed in the following discussion.

Part I. A. (Lysine Linker) Results and Discussion

Synthesis of a Peptide-Bridged Contrast Agent for Detection of Caspase-3

The overall method used to synthesize the target compound, **5,** can be broken down into two segments: the synthesis of the macrocyclic ligand used to chelate Gd^{3+} and the 7-mer peptide which acts as a substrate for caspase-3. Besides serving as a substrate, the peptide includes two lysine residues which serve as points of attachment for the lanthanide chelate. Through the use of convergent synthesis, appreciable quantities of **5** were synthesized, despite a lengthy, 24-step route.

The synthesis of **2** was accomplished in 5 steps with 41% overall yield (Schemes 2.1 and 2.2). The selective functionalization of cyclen, developed by Kovacs and coworkers, provided a convenient method of stereochemical control which was carried through the remainder of the steps to produce **2**.[12] Of particular interest are the NMR spectra of **1** and **2**. The bulky benzyl protecting groups of **1** cause it to be locked in two different conformations. At room temperature, the interconversion of the isomers is slow on the NMR timescale, resulting in twice the number of expected resonances in the ${}^{1}H$ and ${}^{13}C$ NMR spectra. Removal of the benzyl protecting groups from **1** by hydrogenation to produce **2** results in solvent-dependent fluxionality. In $CDCl_3$ and CD_3OD, the ${}^{1}H$ NMR resonances for **2** show the broadening characteristics of fluxional behavior. However, in D_2O, the ${}^{1}H$ NMR resonances of **2** are sharper, presumably due to hydrogen bonding of the pendant carboxylic acid functionalities. Due to the limited solubility of **2** in $CDCl_3$ and D_2O, ${}^{13}C$ NMR analysis was only performed in CD_3OD.

72%

90%

91%
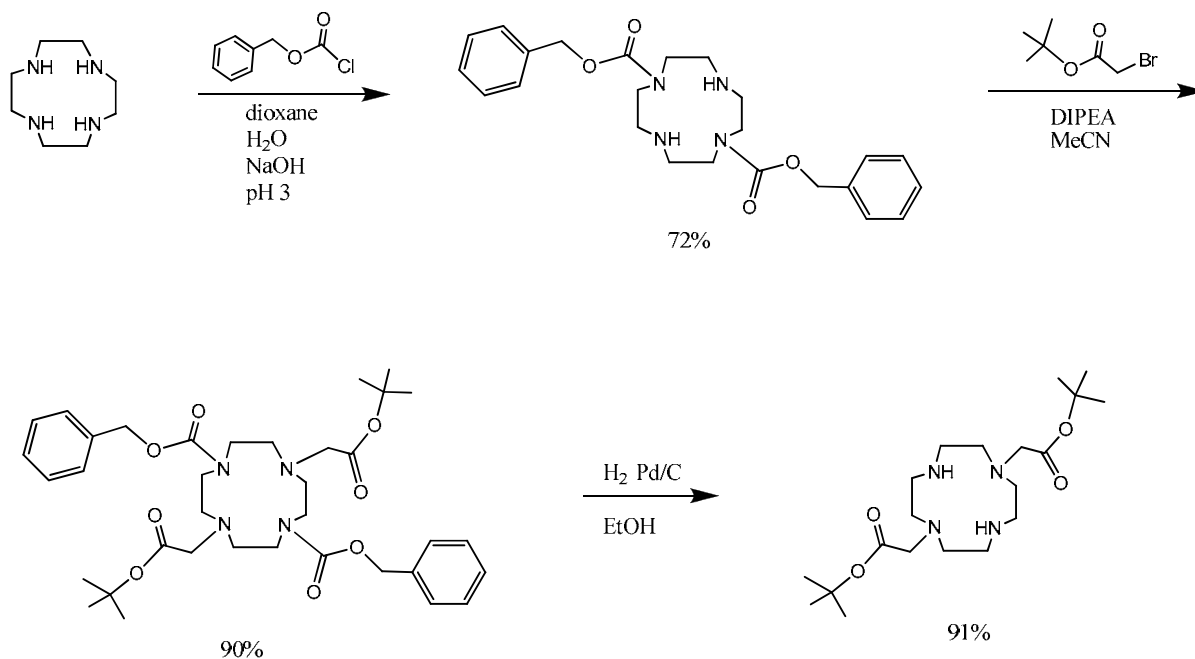
Scheme 2.1 Synthesis of 1,7-bis(*tert*-butoxycarbonylmethyl)-1,4,7,10-tetraazacyclododecane[12]

1

80%

2

87%
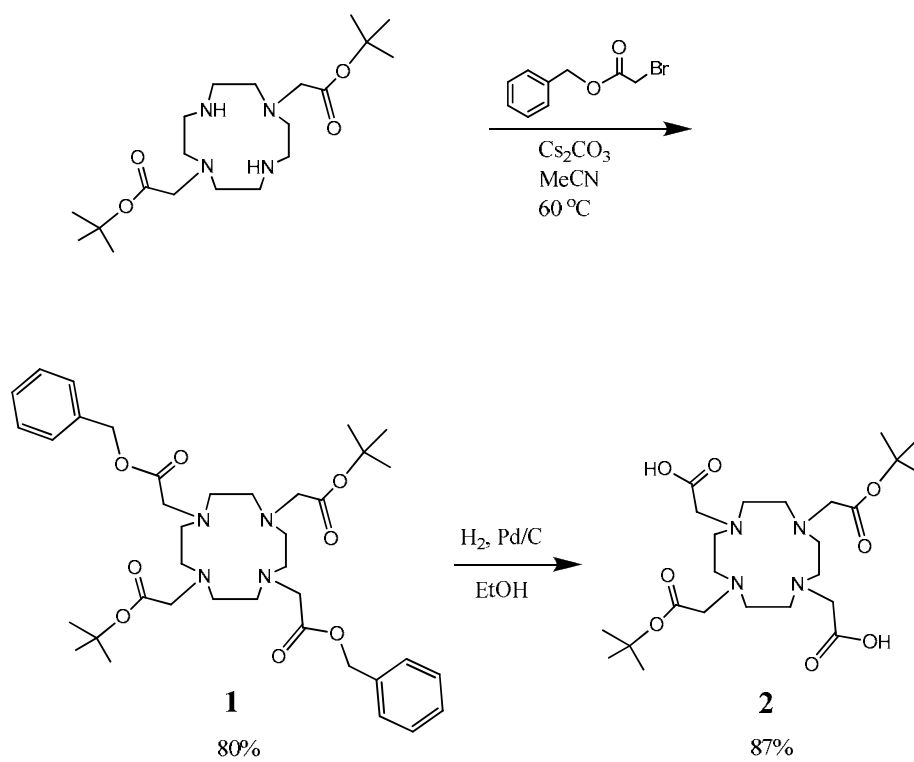
Scheme 2.2 Synthesis of 1 and 2

The peptide was synthesized using Solid-Phase Peptide Synthesis (SPPS) (Scheme 2.3). The use of a 4-way orthogonal protecting strategy allowed precise control over the reactivities of the multiple functional groups present on the peptide. Each deprotection and coupling reaction via SPPS occurred in near quantitative yield (> 99% as determined by the Kaiser test[13]). Reactions were driven towards completion by the use of excess reagents, which can be easily washed away from the resin after each step. The use of three distinct amine protecting groups, 9-fluorenylmethoxycarbonyl (fmoc), methyltrityl (Mtt), and *N*-[1-(4,4-dimethyl-2,6-dioxocyclohex-1-ylidene)ethyl] (Dde), allowed stepwise coupling of the pendant carboxylic acids of **2** with the lysine side-chain amines (Scheme 2.4). To confirm the stepwise addition of **2** to the peptide, a portion of resin was removed, and the intermediate product, [**3]**, was cleaved from the resin to produce **3**, which was characterized by ESI-MS (Scheme 2.5).

1. piperidine/DMF

2. fmoc-lys(Mtt)-OH
   HATU, DIPEA, DMF

3. piperidine/DMF

4. fmoc-asp(OtBu)-OH
   HATU, DIPEA, DMF

5. piperidine/DMF

6. Dde-lys(fmoc)-OH
   HATU, DIPEA, DMF

R = Wang Resin

fmoc removed with piperidine

Mtt removed with 1% TFA

Dde removed with hydrazine

tBu removed with 95% TFA

Cleavage from resin with 95% TFA
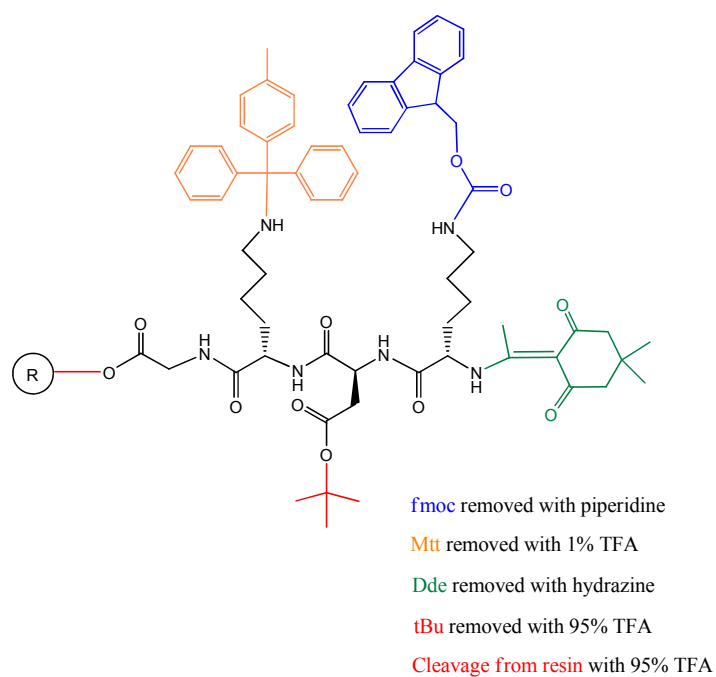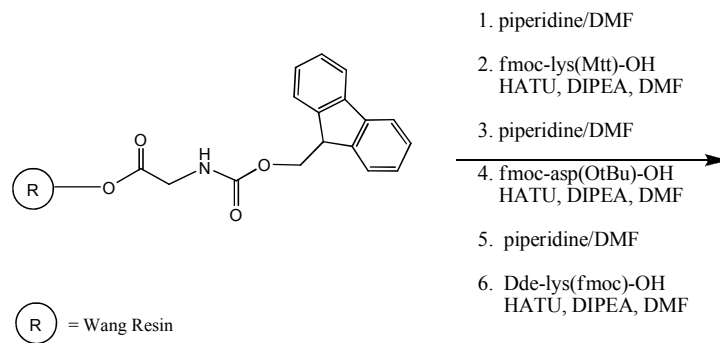
Scheme 2.3 Solid-Phase Peptide Synthesis with 4-way orthogonal protecting strategy
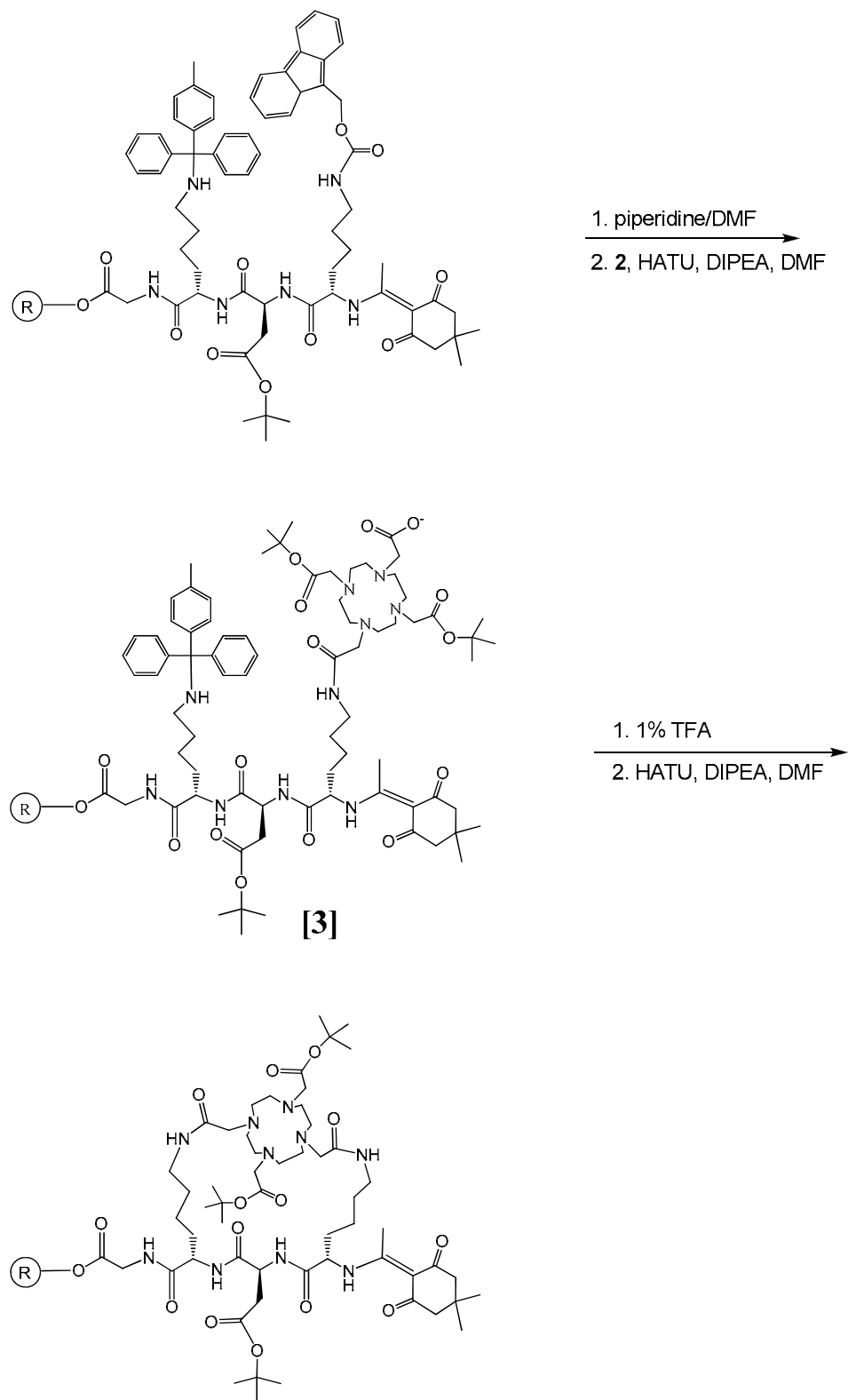
Scheme 2.4 Addition of 2 to the peptide followed by closing of the 28-membered macrobicycle
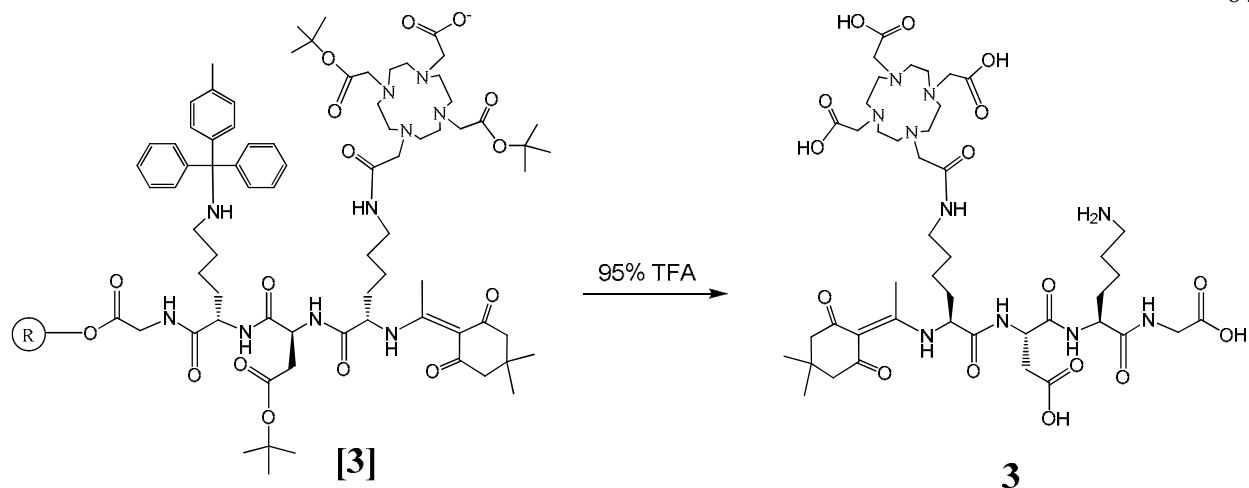
Scheme 2.5 Cleavage of resin-bound intermediate [3] to produce 3 for characterization by ESI-MS

The selectivity of the protecting group strategy and the high-yielding capabilities of SPPS

afforded the macrobicyclic structures in high yield. In contrast, solution-based syntheses of ring

closing steps are notoriously difficult and often result in low yields and mixed products.[14,15]

After successful closure of the macrobicycle, the remaining N-terminal amino acid residues were

added to the peptide (Scheme 2.6). Cleavage of the peptide from the resin with TFA

concomitantly removed the Boc protecting group on the tryptophan side-chain as well as the t-Bu

protecting groups located on the aspartic acid side-chains, the glutamic acid side-chain, and the

pendant carboxylic acids of the chelate (Scheme 2.7). This global Boc and tBu deprotection

allowed the removal of six protecting groups in a single step. The free ligand was purified by

HPLC and characterized by analytical HPLC, ESI-MS, and 2D-NMR. Metalation was

accomplished using the appropriate lanthanide hydroxide (lanthanide = Gd^{3+}, Eu^{3+}, Dy^{3+},

compounds **5**, **6**, **7**, respectively) followed by HPLC purification with overall yields of 3%, 1%,

and 1%, respectively, after 24 steps.

1. hydrazine/DMF

2. fmoc-glu(OtBu)-OH
   HATU, DIPEA, DMF

3. piperidine/DMF

4. fmoc-asp(OtBu)-OH
   HATU, DIPEA, DMF

5. piperidine/DMF

6. fmoc-trp(Boc)-OH
   HATU, DIPEA, DMF
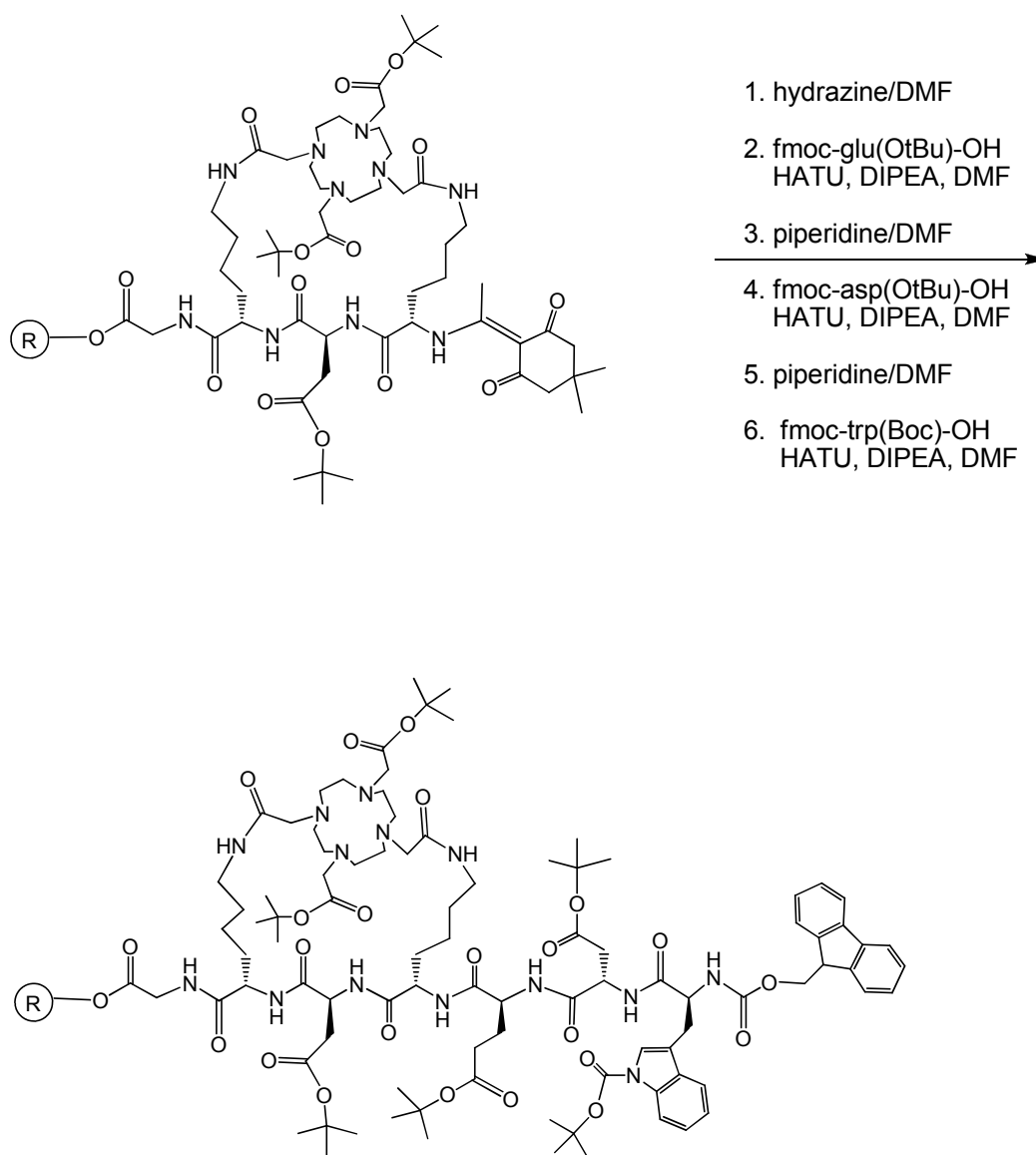
Scheme 2.6 Addition of N-terminal amino acids to the peptide

1. piperidine/DMF

2. 95%TFA
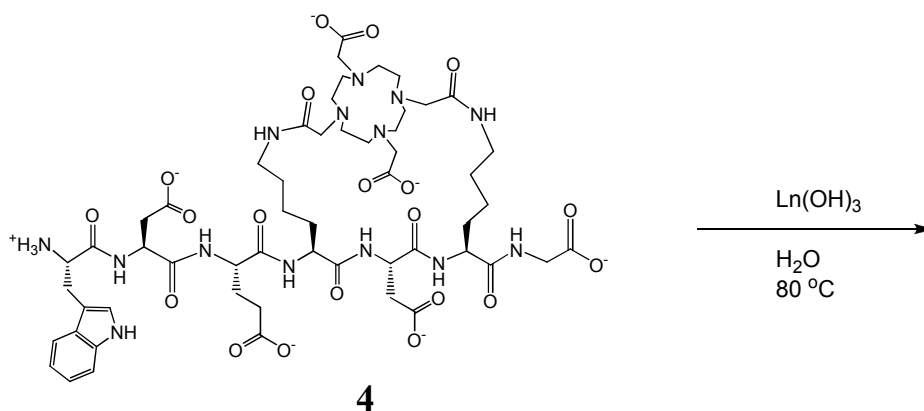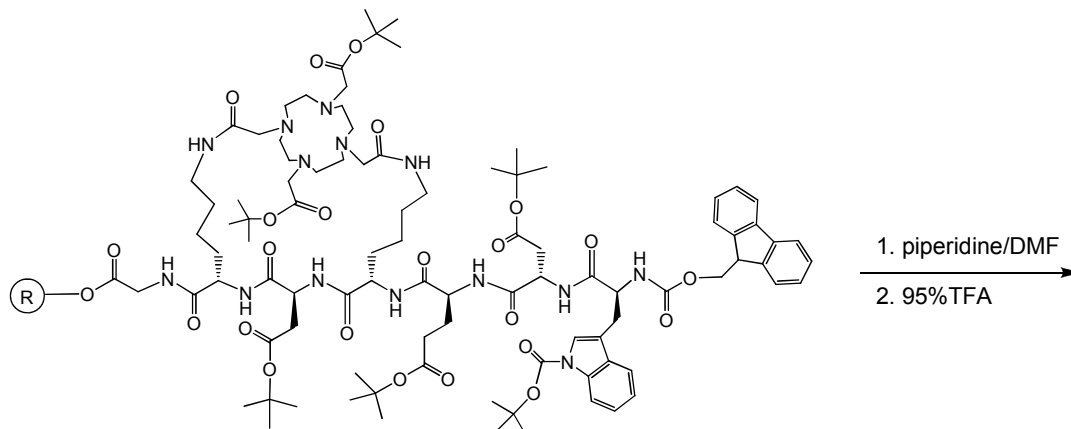
4

27% yield after 18 SPPS steps;
11% overall yield after 23 steps (includes synthesis of **2**)

Ln(OH)$_3$

H$_2$O
80 °C
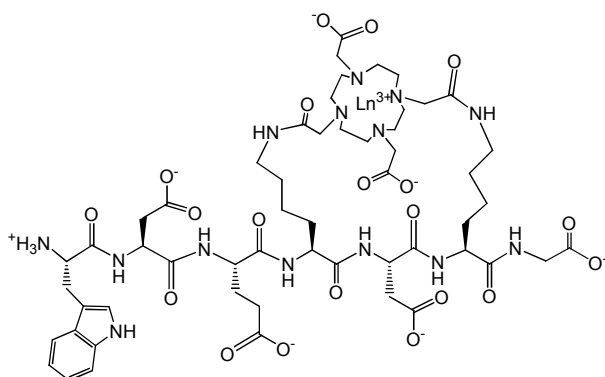
Ln^{3+} = Gd^{3+}, **5** (26% yield, 3% overall)
Eu^{3+}, **6** (12% yield, 1% overall)
Dy^{3+}, **7** (12% yield, 1% overall)

Scheme 2.7 Synthesis of 4 and metalation to produce 5, 6, 7

2D-NMR of **4**

To verify the structure of **4**, a series of 2-dimensional NMR (2D-NMR) experiments were performed at 600 MHz. Upon initial inspection of the 1-D ^{1}H-NMR of **4**, the spectrum was complex and displayed non-first order coupling. The overlapping of resonances was complicated by the fluxionality of the chelate (vida infra, compound **2**). An intensive investigation using several 2-D NMR techniques confirmed the expected structure of **4**.

Total correlation spectroscopy (TOCSY) was a good starting point for assigning the ^{1}H-NMR spectrum of **4**. TOCSY uses long mixing times such that all protons within a spin system show coupling. A spin system can be defined as a continuous chain of alkyl groups. With peptides, the use of TOCSY is particularly advantageous because the backbone nitrogen atom of each amino acid residue is a heteroatom which acts to disrupt coupling. This translates into each amino acid residue being a unique spin system. Therefore each residue can be expected to exhibit cross peaks among all its protons and none with protons of other residues.[16] TOCSY was useful in establishing connectivity between α protons (which are easily distinguished by their unique chemical shifts) and protons found on the side-chain of each amino acid. Lysine side-chain CH_2 resonances were easily identified due to their extensive number of coupled resonances in the TOCSY experiment. Further assignment of H_β, H_γ, H_δ, and H_ε of the lysine side chain were accomplished using proton-proton correlation spectroscopy (COSY) and nuclear Overhauser and exchange spectroscopy (NOESY) (Figure 2.6 and Table 2.1). Identification of the tryptophan protons proved facile due to the downfield shift of the aromatic protons, as well as strong COSY and NOESY interactions within the aromatic spin system. The lack of TOCSY,

COSY, or NOESY interactions with the protons at 3.96 ppm supports the assignment of this resonance as the α protons of glycine.

NOESY allowed several through-space interactions to be identified, which gives insight into the 3-dimensional conformation of **4** in aqueous solutions. Of particular interest is the observed coupling between E_α and K_γ. Nuclear Overhauser effects are observed only when the proton-proton distance is less than 5 Å.[16] Therefore the observed NOESY correlation between E_α and K_γ suggests that these two sets of protons are in close proximity. The use of high-field magnetic frequencies (600 MHz) allowed resolution of two sets of K_δ protons. These two resonances could be due to one of two scenarios: either the geminal protons are experiencing slightly different environments despite being chemically equivalent or the two lysine side-chains are in slightly different environments despite being related through symmetry. Because neither a COSY nor a NOESY interaction between $K_{\delta 1}$ and $K_{\delta 2}$, was observed, it can be concluded that these two sets of protons represent the latter of the two scenarios. The NOESY interaction between the K_ε protons and the acetate protons located on the pendant arms of the chelate corroborates the general capping structure shown in Figure 2.4 and dispels notions of the structure being inverted (in which the peptide would reside on the hydrophobic side of the chelate, opposite the water exchange site).

Due to the similar chemical shifts of the D_β protons and the cyclen backbone protons, unambiguous assignments could not be made for these resonances. The α protons of the aspartic acid residues and the tryptophan residue proved difficult to differentiate. This difficulty was exacerbated by the resonance at 4.8 ppm due to residual water. Efforts to reduce the residual water peak included repeated cycles of dissolving **4** in D_2O followed by lyophilization. Water

suppression through NMR pulse sequences was not pursued due to the potential loss of

information from α protons which may reside within the same region of the NMR spectrum. A

complete list of assigned 2-D coupling interactions can be found in Table 2.1.
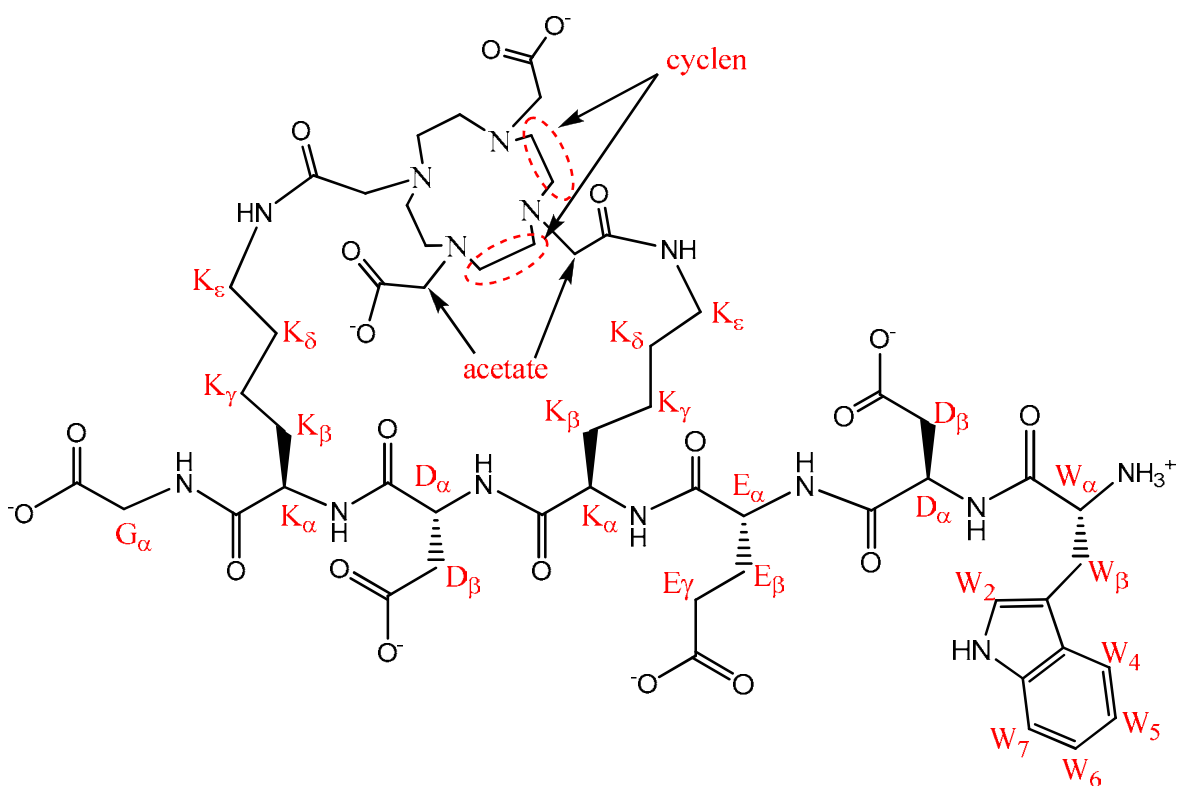
Figure 2.6. Proton nomenclature for 2-D NMR assignments of 4 (as used in Table 2.1)

Proton Identity[a]	Chemical Shift (ppm)	Observed Coupling Interactions (ppm)		
		TOCSY	COSY	NOESY
W_α	4.68[a]			
W_β	3.42	7.29		7.29, 7.60
W_2	7.29	3.42		3.42
W_4	7.60		7.15, 7.25, 7.50	3.42, 7.15, 7.25
W_5	7.15		7.25, 7.50, 7.60	7.25, 7.60
W_6	7.25		7.15, 7.50, 7.60	7.15, 7.50, 7.60
W_7	7.50		7.15, 7.25, 7.60	7.25
D_α	4.68[b]			
D_β	2.3-2.9[c]			
E_α	4.19	1.92, 2.10, 2.39	1.92, 2.10	1.92, 2.10
E_β	2.06[d] 1.92[e], 2.10[e]	1.92[f], 2.10[f], 2.39, 4.19	2.39, 4.19	1.92[f], 2.10[f], 2.39, 4.19
E_γ	2.39	1.92, 2.10, 4.19	1.92, 2.10	1.92, 2.10
K_α	4.33[g]	1.35, 1.38		
K_β	1.47, 1.50	2.97	1.35, 1.38	1.35, 1.38, 1.70
K_γ	1.35, 1.38	2.97, 4.33	1.47, 1.50, 1.70, 1.75	1.47, 1.50, 1.70, 4.19
$K_{\delta 1}$	1.70	2.97	1.35, 1.38, 2.97	1.35, 1.38, 1.47, 1.50
$K_{\delta 2}$	1.75	2.97	1.35, 1.38	4.19
K_ε	2.97	1.35, 1.38, 1.47, 1.50, 1.70, 1.75	1.70	3.75
G_α	3.96			
cyclen	2.3-2.9[c]			
acetate	3.30, 3.75			2.97, 3.30, 3.75

Table 2.1. 2-D ^{1}H-NMR coupling interactions observed for 4

[a]one-letter amino acid abbreviations used with subscripts denoting proton position, see Figure 2.6 for nomenclature; [b]overlapping resonances and overlap with water residual resonance at 4.80 ppm prevents unambiguous assignments; [c]overlapping resonances preclude unambiguous assignments; [d]geminal protons not resolved in 1-D spectrum (500 MHz); [e]geminal protons resolved in 2-D spectrum (600 MHz); [f]geminal coupling; [g]resonances not resolved in 1-D or 2-D spectra

Number of inner-sphere water molecules, q

The determination of q for **5** was performed through the measurement of the luminescence lifetime decay of the Europium analog, **6**, in water and deuterium oxide. Excitation of the Europium $^7F_0 \rightarrow {}^5D_0$ transition at 580 nm results in luminescence due to $^5D_0 \rightarrow {}^7F_2$ emission. The $^5D_0$ state is long-lived (millisecond timescale), however, vibrational energy transfer can occur with solvent molecules bound to the Europium, resulting in quenching of the luminescence. The quenching effect of OH oscillators is approximately 200 times faster than the quenching of OD oscillators. This difference in luminescence quenching by OH oscillators and OD oscillators has been exploited as a method to determine the number of inner-sphere water molecules of Europium chelates.[17] Measurement of the Europium luminescence lifetime decays in water (τ_{H2O}) and deuterium oxide (τ_{D2O}) can be used to calculate q through the use of Equation 2.1, where A has been empirically derived to be 1.05 water molecules*ms and k_{XH} is a correction factor to account for amine NH and alcoholic OH oscillators (from the ligand) in the first coordination sphere of Europium.

$$\textbf{Equation 2.1}^{[17]} \quad q = A[\tau_{H2O}^{-1} - \tau_{D2O}^{-1} - k_{XH}]$$

Because Europium and Gadolinium differ in ionic radii by only 0.9%, the substitution of the former for the latter has minimal perturbation on the overall structure of the chelate.[18]

The determination of q for **6** was attempted using a Hitachi F-4500 fluorescence spectrometer. The luminescence decay constant of **6** in D_2O (τ_{D2O}) was determined to be 1.90 ms after fitting ($R^2 = 0.996$) (Figure 2.7). The luminescence decay constant of **6** in H_2O (τ_{H2O}),

however, was too fast (< 0.5 ms) to be accurately determined using the Hitachi F-4500. Due to

the limited capabilities of the Hitachi F-4500, an alternate method of determining *q* was pursued.
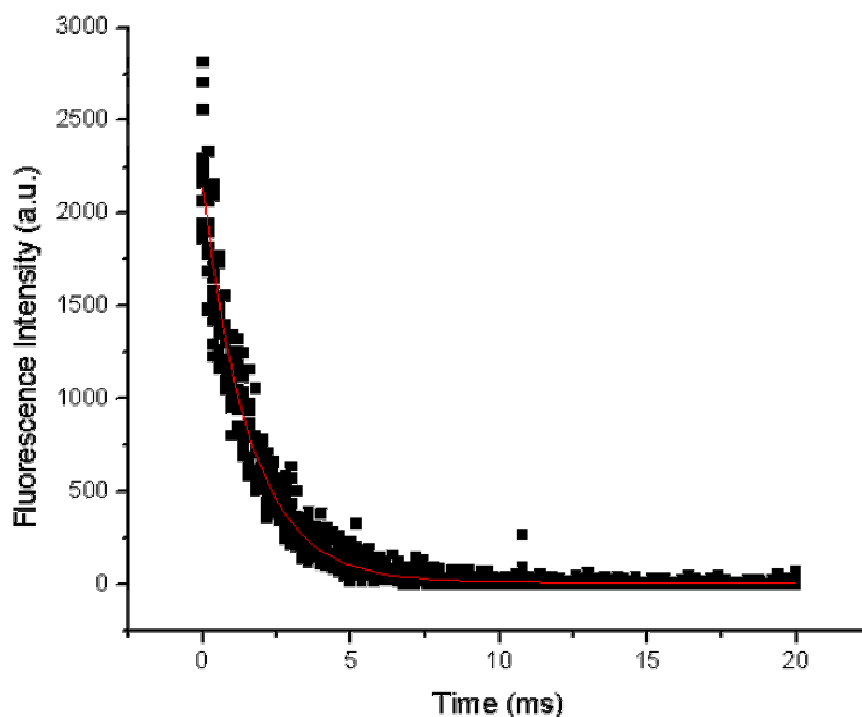
Figure 2.7. Luminescence decay of 6 in D₂O (50 replicates; black squares = experimental data; red line = fit to monoexponential decay with decay constant 1.90 ms, (R^2 = 0.996)

The next approach for determining *q* invoked the use of NMR and required the synthesis

of **7**, the Dysprosium (III) analog of **5**. Lanthanides produce characteristic paramagnetic shifts in

NMR spectra; this phenomenon is known as the Lanthanide Induced Shift (LIS).[19] Table 2.2

shows the relative shifts observed for various lanthanides. Dysprosium has been employed as a

shift reagent due to its large paramagnetic shift in ¹H-NMR.[19] The method of Alpoim and

coworkers was used to determine q by measuring the Dysprosium Induced Shift (DIS) of ^{17}O-

enriched water as a function of the concentration of **7**.[20] Assuming fast water exchange, the DIS

is linear with Dysprosium concentration. As q increases, the observed DIS of the bulk water ^{17}O-

NMR resonance will increase. The slope of the DIS vs. **7** concentration (Figure 2.8) was

compared to that of a solution of $DyCl_3$, with the ratio being equal to q.

Lanthanide	LIS of Ln^{3+}-bound water δ (ppm)
Pr^{3+}	-60
Nd^{3+}	-32
Sm^{3+}	-4
Eu^{3+}	50
Tb^{3+}	-600
Dy^{3+}	-720
Ho^{3+}	-360
Er^{3+}	200
Tm^{3+}	500
Yb^{3+}	200

Table 2.2 Lanthanide Induced Shifts of Ln^{3+}-bound water for DOTA-tetra(amide) chelates[19]

Concentration (M)

$y = -69.07x - 0.2535$
$R^2 = 0.9919$
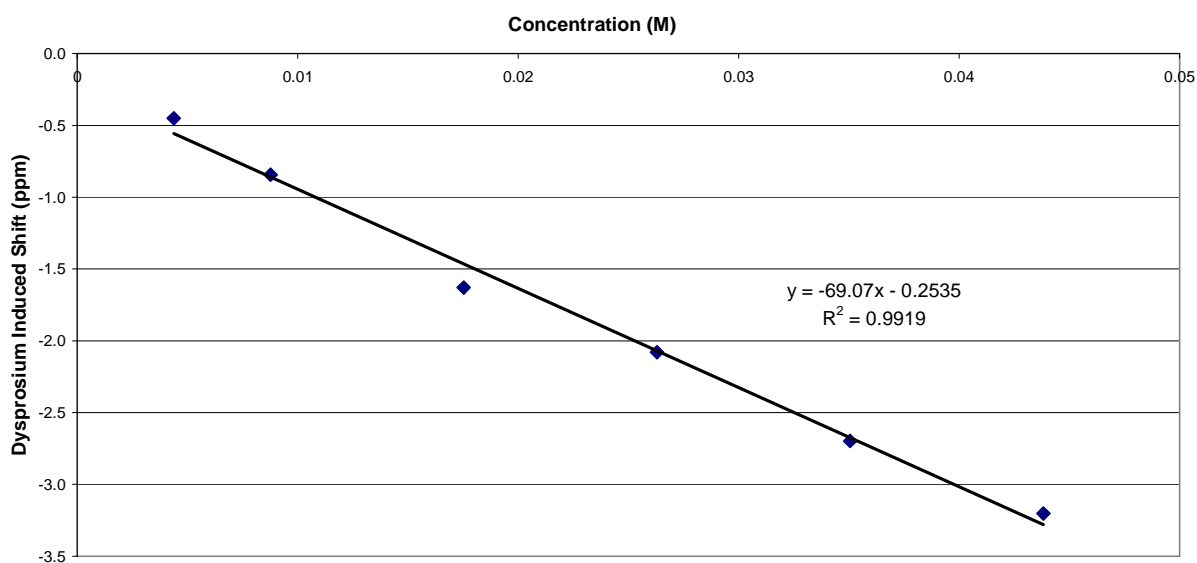
Figure 2.8. Dysprosium Induced Shift of water ^{17}O-NMR resonance by 7

The DIS experiment resulted in $q = 1.73$ (assuming the lanthanide ion is 9-coordinate) or

$q = 1.44$ (assuming the lanthanide ion is 8-coordinate).[20,21] Conflicting literature reports of the

exact coordination number for the Dysprosium aquo ion (the standard of comparison for this

experiment) prompted further investigation of the coordination geometry of **5**.

The DIS results suggest that **5** could potentially have two inner sphere water molecules.

To test this hypothesis, a relaxivity profile of **5** as a function of pH was obtained (Figure 2.9).

Lanthanide chelates with two inner sphere waters show a characteristic decrease in relaxivity at

high pH due to the binding of carbonate anion (which increases in concentration at higher pH) in

a bidentate fashion.[22] Figure 2.9 shows that **5** exhibits an increase in relaxivity at high pH, which

argues against a $q = 2$ complex. The increased relaxivities observed for **5** at extreme pH values

($2 > pH > 11$) can be explained by prototropic exchange. Prototropic exchange occurs when the

protons on the lanthanide-bound water molecule are exchanging with bulk water protons faster

than the inner-sphere water is exchanging with the bulk water.[23] Prototropic exchange is observed at extreme pH values due to acid or base assisted proton exchange with bulk water.[23,24] The result of prototropic exchange is an increase in relaxivity because more protons are effectively being relaxed by the paramagnetic Gd^{3+} in a given period of time.

An interesting feature of the pH dependent relaxivity of **5** is the increase in relaxivity at pH 3.5 and pH 10. These local maxima in relaxivity correspond to the expected pK_a values for the carboxylic acids and amides, respectively, of **5**. Similar phenomena are reported in the literature for compounds with exchangeable protons in the vicinity of the paramagnetic center.[23] At pH values near the pK_a of the exchangeable protons, an increase in relaxivity is observed due to increased proton exchange. Since the protons are close to the paramagnetic center, they are effectively relaxed in a manner akin to that of a second sphere water molecule.
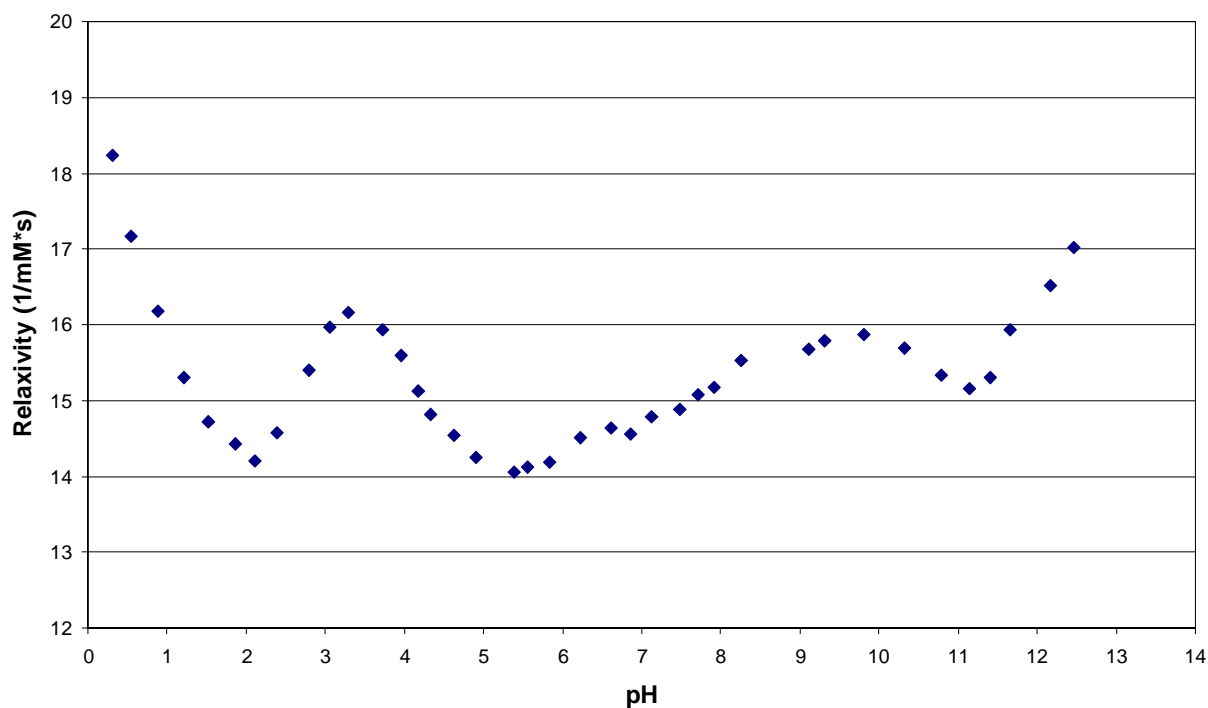
Figure 2.9. Relaxivity vs. pH of compound 5

The results of the pH dependent relaxivity study helped eliminate the possibility of **5** having two inner-sphere waters, but did not ease the ambiguity of q being either 1.44 or 1.73 (as determined by the DIS experiment). Therefore, the luminescence decay measurements were re-visited with improved instrumentation. Time resolved laser luminescence of **6** measurements were acquired using a Nd: YAG pump laser. The use of the laser resulted in precise measurements of the luminescence decay lifetimes of **6** in water and deuterium oxide (Figure 2.10). Fitting the laser luminescence data to a monoexponential decay resulted in decay constants of 0.5496 ± 0.0003 ms ($R^2 = 0.9994$) and 1.752 ± 0.002 ms ($R^2 = 0.998$) for water and deuteriuim oxide, respectively. Application of Equation 2.1 resulted in $q = 1.2 \pm 0.1$ for **6**.

Data: Data1_B
Model: ExpDec1
Equation: y = A1*exp(-x/t1) + y0
Weighting:
y   No weighting

Chi^2/DoF   = 7.3738E-10
R^2   = 0.99942

y0   -0.00122   ±4.5134E-7
A1   0.00488   ±1.4665E-6
t1   0.54957   ±0.00031

Data: Data1_B
Model: ExpDec1
Equation: y = A1*exp(-x/t1) + y0
Weighting:
y   No weighting

Chi^2/DoF   = 1.7839E-9
R^2   = 0.99871

y0   -0.00119   ±8.5146E-7
A1   0.00482   ±2.0385E-6
t1   1.75249   ±0.00157
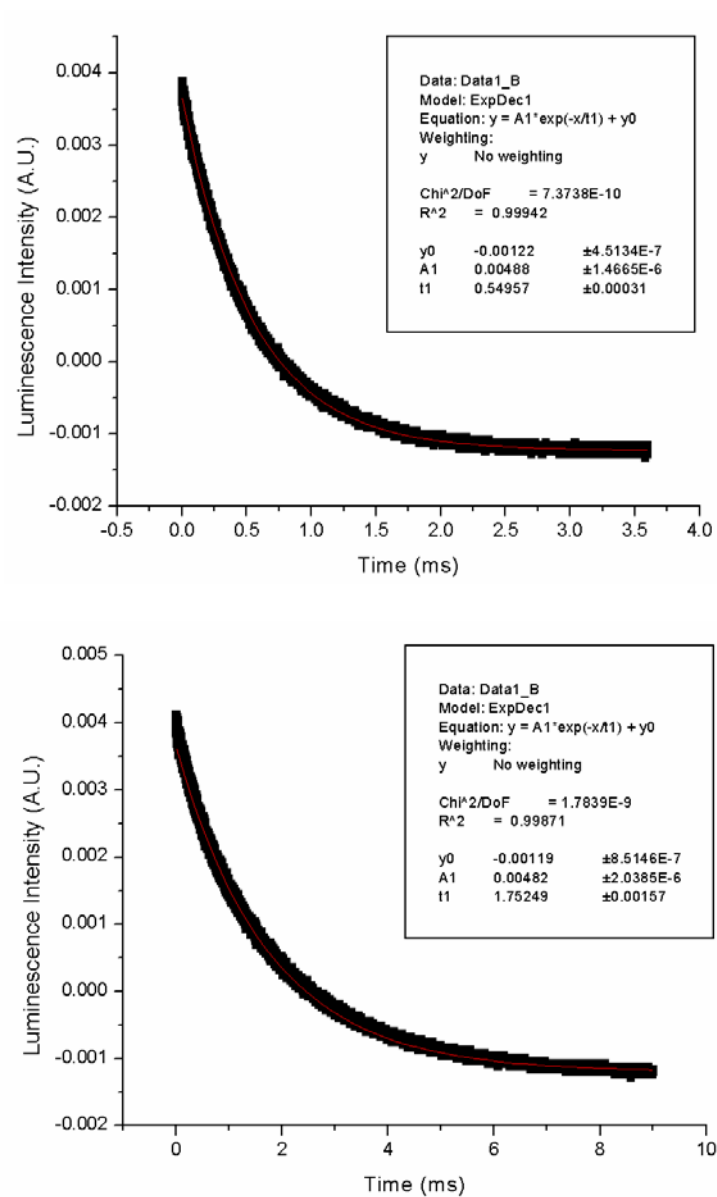
Figure 2.10 Luminescence lifetime decays of 6 in H$_2$O (top) and D$_2$O (bottom).
*Note: different units on x-axis

Mean Water Residence Lifetime, τ_m

The mean water residence lifetime, τ_m, of **5** was determined using literature methods.[25,26] These methods were originally developed by Swift and Connick for paramagnetic metal ions and later applied to the determination of τ_m of MRI contrast agents by Micskei and coworkers.[25,26]

The effect of the paramagnetic complex, **5**, on the transverse relaxation time of ^{17}O in water was studied. Due to the low natural abundance of ^{17}O in water, the samples were doped with ^{17}O-enriched water. The difference of the linewidth of the water ^{17}O resonance in the presence and absence of **5** was measured as a function of temperature. The experimental results were compared to the theoretical equations previously developed by Swift and Connick.[25] A fit to the established theory for a single species (only one isomer of **5** present in solution) could not be obtained. The unique features of the low temperature portion of the ^{17}O-NMR data led to the hypothesis that **5** could exist as two isomers. Reworking the Swift and Connick equations to incorporate terms for two distinct isomers (Equation 2.2 in Experimental Section), allowed the experimental data to be fit to the theoretical model, resulting in τ_m values of 1159 ns and 70 ns (Figure 2.11). Similar phenomena have been reported in the literature by Zhang and coworkers where a closely related bis-amide complex, Gd-DOTA-2DMA (Figure 2.12), was shown to exist as two isomers with drastically different τ_m values of 1350 ns and 14.2 ns.[27] Zhang and coworkers attributed the faster τ_m value to the minor twisted square anti-prismatic (TSAP) isomer, while the slower τ_m value belonged to the more prevalent square anti-prismatic (SAP) isomer (Figure 2.13 shows the TSAP and SAP isomers of Gd-DOTA). In order to disseminate the contribution of each of the TSAP and SAP isomers to the overall observed τ_m, Zhang and coworkers determined the ratio of the isomers as a function of temperature by variable

temperature (VT) ^{1}H-NMR of Eu-DOTA-2DMA. In a study akin to that of Zhang and

coworkers, VT ^{1}H-NMR of **6** (the Eu^{3+} analog of **5**) was acquired, however the separate

resonances due to the TSAP and SAP isomers could not be discerned. Therefore **6** was

determined to be in the intermediate fluxional regime throughout the entire temperature range

studied (1 ^{o}C to 85 ^{o}C), and the determination of the TSAP/SAP isomer ratio was proscribed by

this method. Due to the solution being aqueous, analysis of the compound outside of this

temperature range was not admissible.
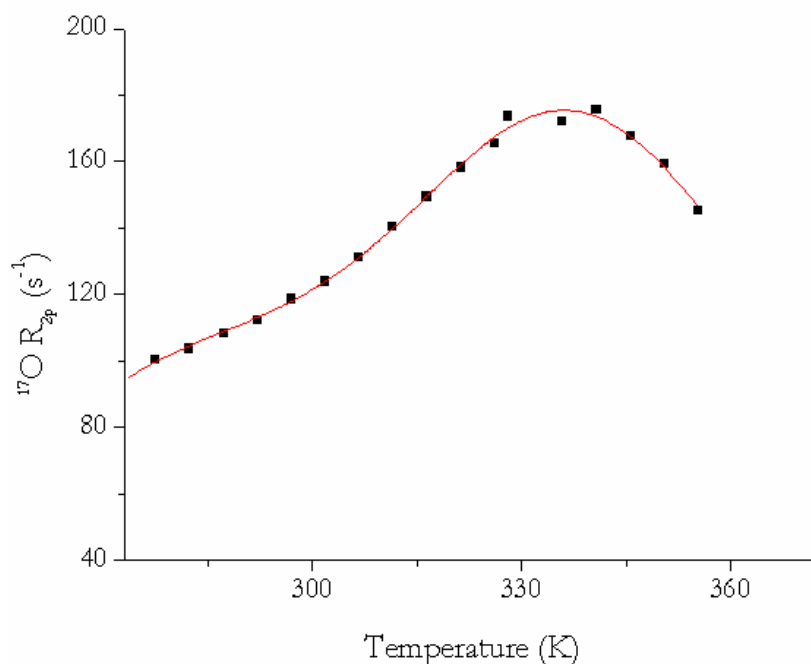
Figure 2.11 Fit (red line, R^2 = 0.997) of experimental data (black squares) to a two isomer theoretical model in the determination of τ_m for 5 by VT ^{17}O-NMR
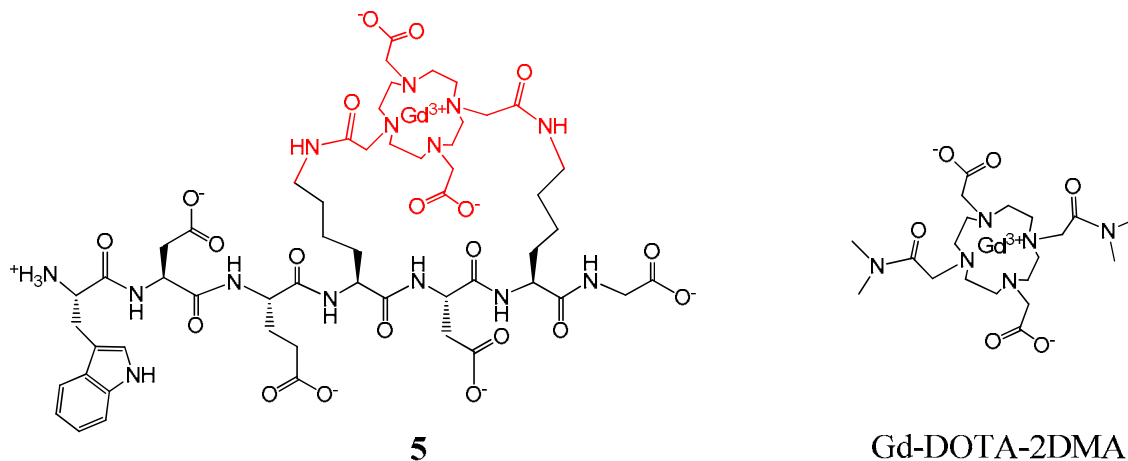
5   Gd-DOTA-2DMA

Figure 2.12. Comparison of compound 5 chelate structure (highlighted red) with related literature compound, Gd-DOTA-2DMA[27]

TSAP   SAP
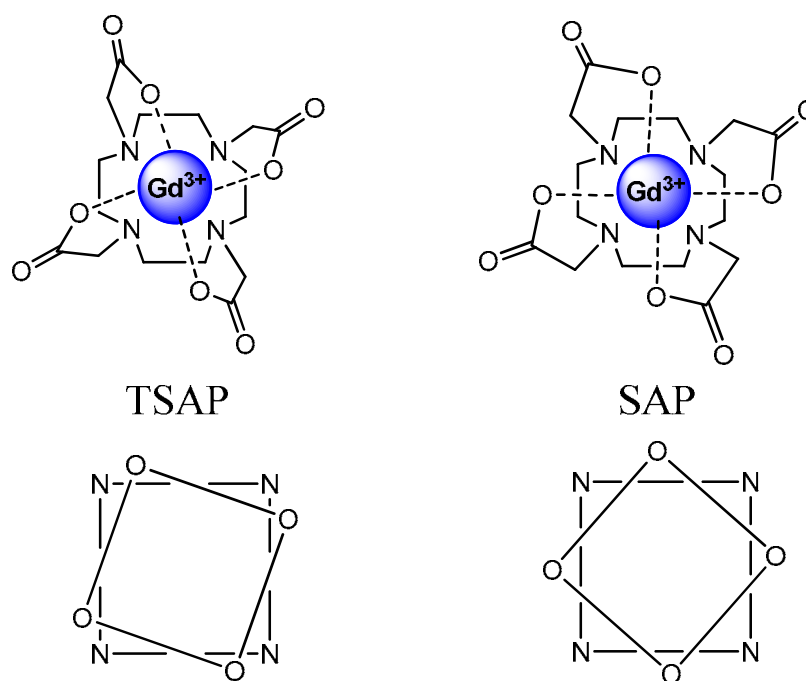
Figure 2.13 TOP: Structures of the twisted square anti-prismatic (TSAP) and square antiprismatic (SAP) isomers of Gd-DOTA

BOTTOM: Geometry of the TSAP and SAP isomers, showing the difference in twist angle between the plane of nitrogen atoms of the cyclen backbone and the plane of oxygen atoms of the pendant acetate groups

<u>Relaxivity</u>

The independent determination of the relaxometric parameters q and τ_m were critical in understanding the factors influencing the relaxivity of **5**. When measured in the caspase-3 enzyme buffer (50 mM HEPES, 100 mM NaCl, 10 mM DTT, 1 mM EDTA, 10% sucrose, 0.1% CHAPS, 1 mg/mL BSA, pH 7.4), **5** displayed a relaxivity of 10.8 mM^{-1}s^{-1}. This value is much higher than the relaxivities of ~4 mM^{-1}s^{-1} reported for clinical contrast agents.[28] Contrast agents have been reported which attribute high relaxivity to increased molecular reorientation time (τ_R) due to interaction with serum albumin proteins.[29-31] In order to exclude the possibility of the high relaxivity of **5** being attributed to an increase in τ_R due to interaction with bovine serum albumin (BSA), the relaxivity measurements were repeated using the same buffer system without BSA. The relaxivity of **5** in the presence and absence of BSA were within experimental error, therefore it was concluded that the high relaxivity of **5** is not due to interaction with BSA. The high relaxivity of **5** is purported to be due to two factors: high molecular mass and the presence of second-sphere water molecules which are H-bonded within the macrobicycle.

With a molecular mass of 1402 g/mole, **5** has almost triple the molecular mass of Gd-DOTA (561 g/mole). The molecular reorientation time, τ_R, of molecules increases linearly with overall size, and the relaxivity of small molecule Gd^{3+}-based contrast agents is limited by τ_R (explained in Chapter I, see Equations 1.13-1.14). Resultantly, the relaxivity of small molecule Gd^{3+}-based agents increases linearly with molecular mass.[32] The high molecular mass of **5**, however, is only partially responsible for the observed high relaxivity.

The other factor responsible for the high relaxivity of **5** is a putative second-sphere water molecule. Second-sphere water molecules are defined as solvent molecules that are not directly

bound in the first coordination sphere, yet remain in proximity of the paramagnetic metal for a relatively long time.[33] Second-sphere water molecules can be due to hydrogen bridges to the ligand and/or to the bound water.[33] The contribution of second-sphere water can be described using the same theory as used for the inner-sphere water.[33] Second-sphere relaxation was reported to be responsible for the unexpectedly high relaxivity observed for a contrast agent which lacked an inner-sphere water molecule.[23] The absence of an inner-sphere water molecule would lead to an expected relaxivity of ~2 $mM^{-1}s^{-1}$, because approximately half of the relaxivity observed for small molecule Gd^{3+}-based agents is due to inner-sphere relaxation (the other half being due to outer-sphere effects of closely diffusing water molecules).[32,33] The $q = 0$ agent displayed a relaxivity of 4.2 $mM^{-1}s^{-1}$ due to the presence of a second-sphere water molecule tightly interacting with a negatively charged functional group on the contrast agent.[23] Another example of a contrast agent with high relaxivity attributed to second-sphere water was reported by Anelli and coworkers for a contrast agent which was designed for imaging of the hepatobiliary system.[34] The agent displayed a relaxivity of 8.5 $mM^{-1}s^{-1}$, despite having a molecular mass of only 1100 g/mole. The high relaxivity was attributed to the presence of an H-bonded second-sphere water in addition to an inner-sphere water. Aime and coworkers, reporting on H-bonded second-sphere water, stated, "This additional contribution to the relaxivity when a negative charge is located in close proximity of the coordination cage appears to be a rather general phenomenon".[23] As such, it seems plausible that the multiple negative charges located in close proximity of the coordination cage of **5** could result in an H-bonded second-sphere water molecule. This second-sphere water molecule, coupled with the high molecular mass of **5**, explains the observed high relaxivities.

Part I. A. (Lysine Linker) Conclusions

The synthesis of target compound **5** was accomplished in 24 steps with an overall yield of 3%. A thorough 2-D NMR structural analysis of the free ligand, **4**, confirmed the overall structure of the macrobicycle. The number of inner-sphere water molecules, q, of the lanthanide complexes was studied using the NMR lanthanide induced shift and laser luminescence methods and determined to be 1.2 ± 0.1. A relaxivity vs. pH profile of **5** confirmed a $q = 1$ complex and revealed interesting features. The mean water residence lifetime, τ_m, of **5** was determined by VT ^{17}O-NMR. The τ_m study revealed that **5** exists as a mixture of the TSAP and SAP isomers with τ_m values of 70 ns and 1159 ns, respectively. These values of τ_m for **5** agree with literature τ_m values of closely related compounds. The high relaxivity of 10.8 mM^{-1}s^{-1} for **5** is due to its high molecular mass and a purported H-bonded second-sphere water molecule. The presence of an inner-sphere water for **5** prompted a redesign of the linker between the chelate and the peptide (Part I. B) in an effort to limit inner-sphere water access to the paramagnetic lanthanide.

Part I. B. (Diaminopropionic Acid Linker) Results and Discussion

Due to the presence of inner-sphere water for **5**, the linker length between the chelate and the peptide was shortened. During the time of this study, a macrobicyclic lanthanide chelate which lacked an inner-sphere water was published by Vipond and coworkers.[35] The literature complex, 8O$_2$-bridged DOTAM, featured a 21-membered macrobicycle with a chelate structure very similar to the peptide-bridged macrocycles in the present work (Figure 2.14). The lack of an inner-sphere water for 8O$_2$-bridged DOTAM provided the impetus to redesign the peptide-bridged macrocycle to consist of a 22-membered macrobicycle (Figure 2.15).

5

(28-membered macrobicycle)

8O₂-bridged DOTAM

(21-membered macrobicycle)
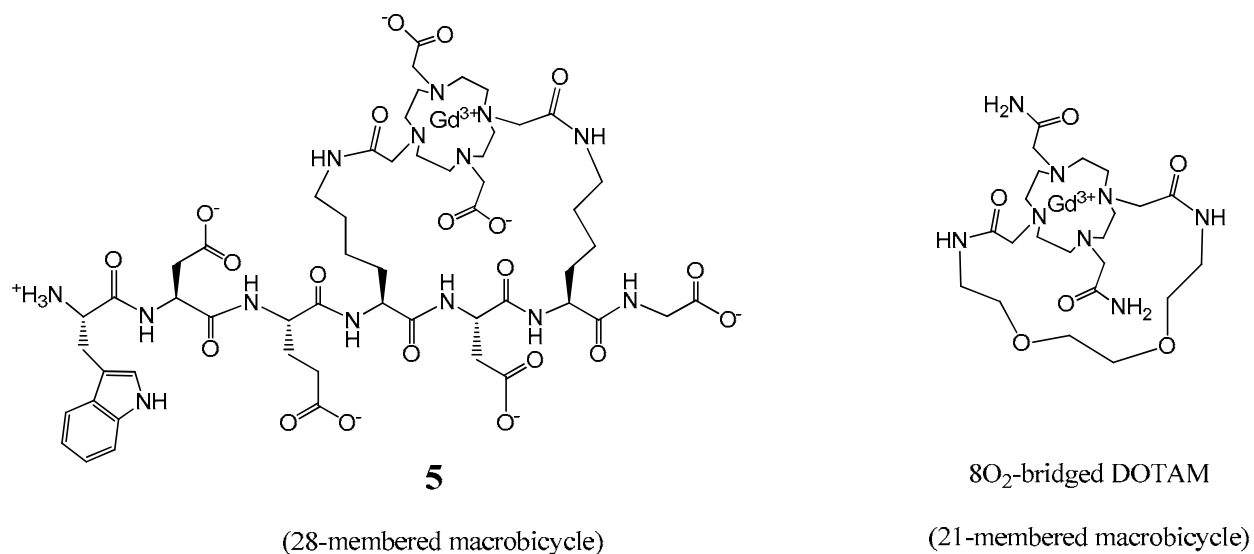
Figure 2.14 Comparison of the 28-membered macrobicyclic structure of 5 with the 21-membered macrobicyclic literature compound, 8O₂-bridged DOTAM[35]

5

(28-membered macrobicycle)

12

(22-membered macrobicycle)
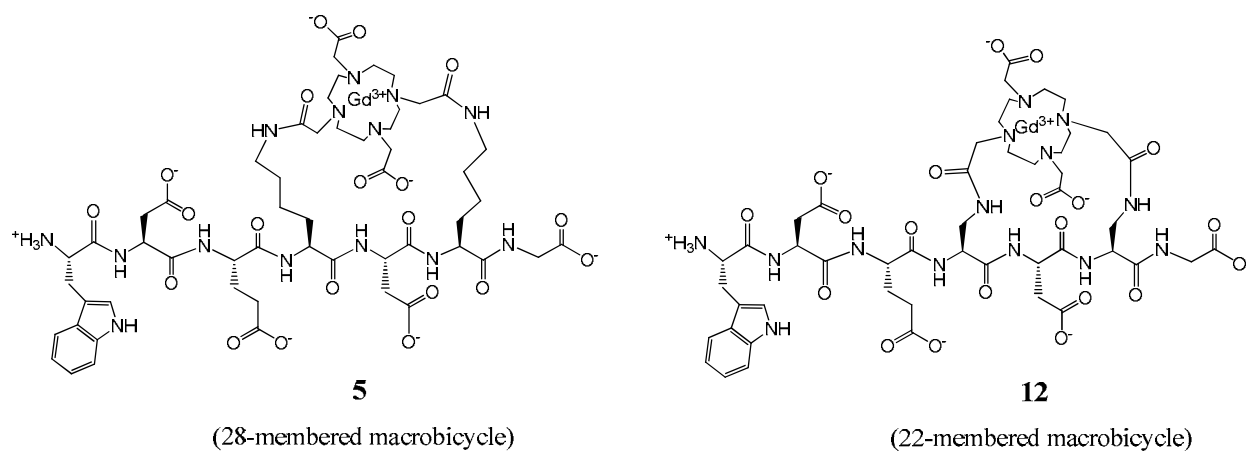
Figure 2.15 Comparison of the structures of the 28-membered macrobicyclic structure of 5 (Part I. A) and the 22-membered macrobicyclic structure of 12 (Part I. B)

Synthesis

By substituting commercially available diaminopropionic acid for lysine, target

compounds **12** and **13** were synthesized in 24 steps (with overall yields of 6% and 9%,

respectively) using the methods and protecting strategy developed in Part I. A (Schemes 2.8,

2.10, 2.13, 2.14). To confirm the stepwise formation of the bridge between **2** and the protected

peptide during SPPS, key intermediates were cleaved from the resin and characterized by ESI-

MS (Schemes 2.9, 2.11, 2.12).

1. piperidine/DMF

2. fmoc-Dap(Mtt)-OH
   HATU, DIPEA, DMF

3. piperidine/DMF

4. fmoc-asp(OtBu)-OH
   HATU, DIPEA, DMF

5. piperidine/DMF

6. Dde-Dap(fmoc)-OH
   HATU, DIPEA, DMF

R = Wang Resin

[8]
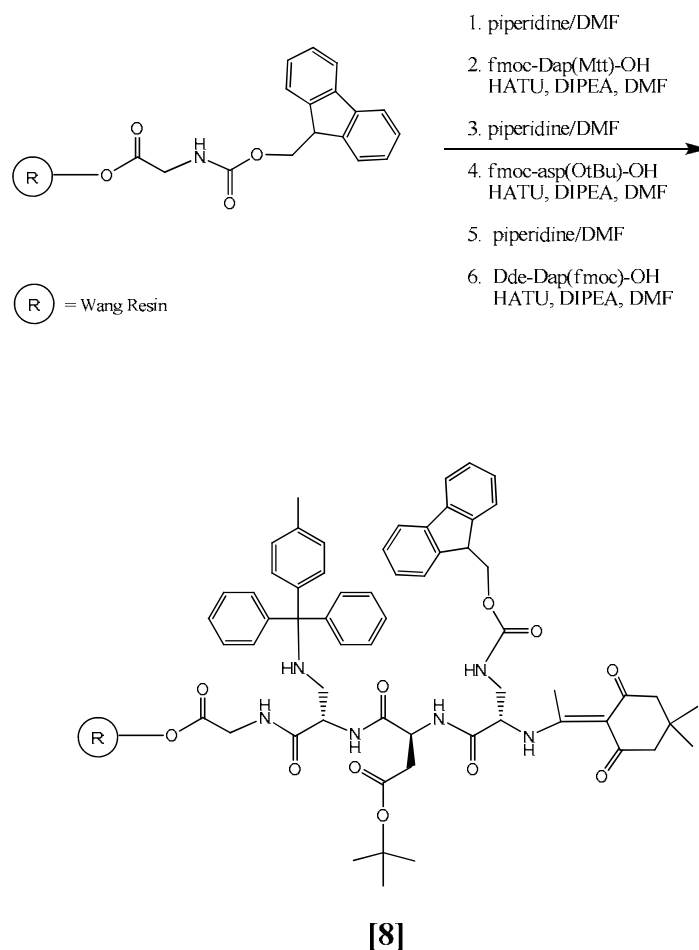
Scheme 2.8 Synthesis of resin-bound peptide intermediate [8]

1. piperidine/DMF

2. 95% TFA

[8]

8
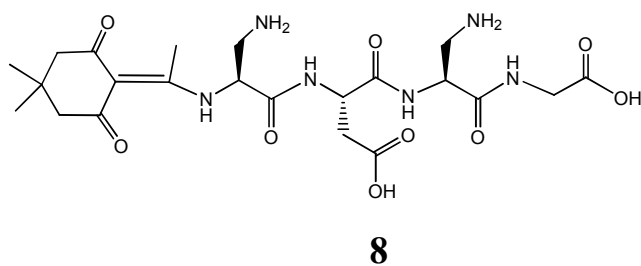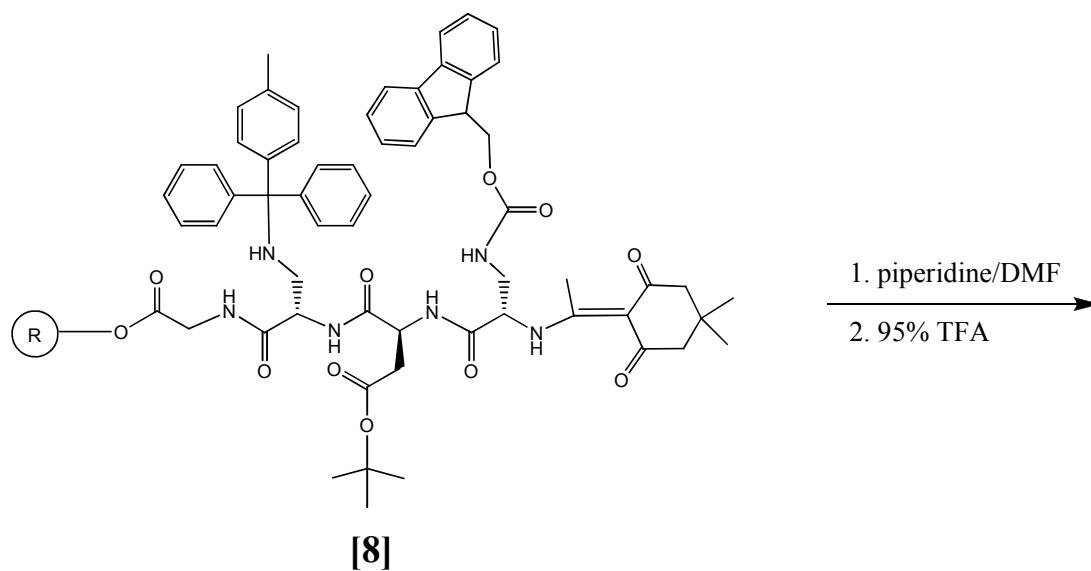
Scheme 2.9 Cleavage of resin-bound intermediate [8] to yield 8 for characterization by ESI-MS
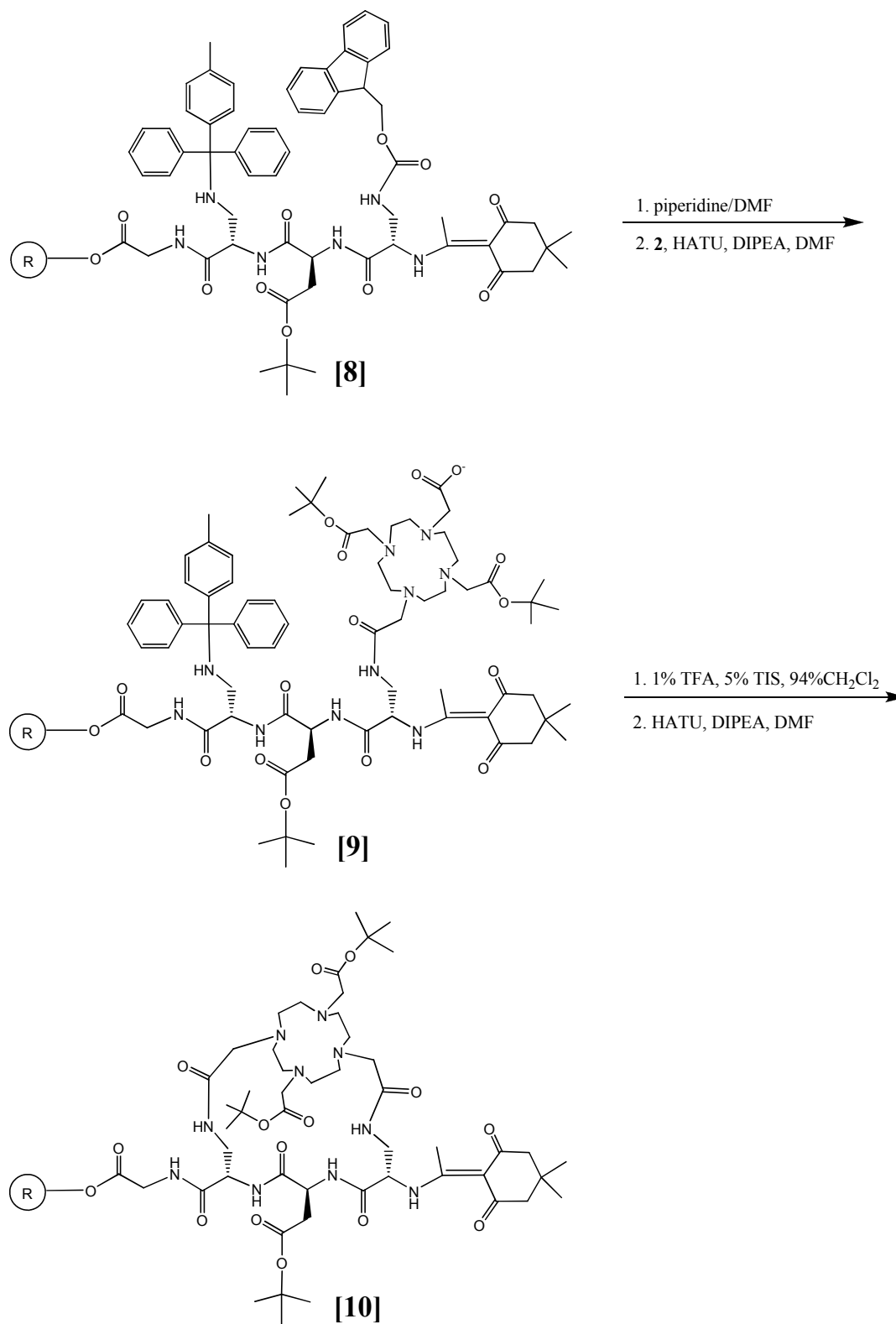
Scheme 2.10 Addition of 2 to the peptide followed by closing of the 22-membered macrobicycle

95% TFA

[9]

9
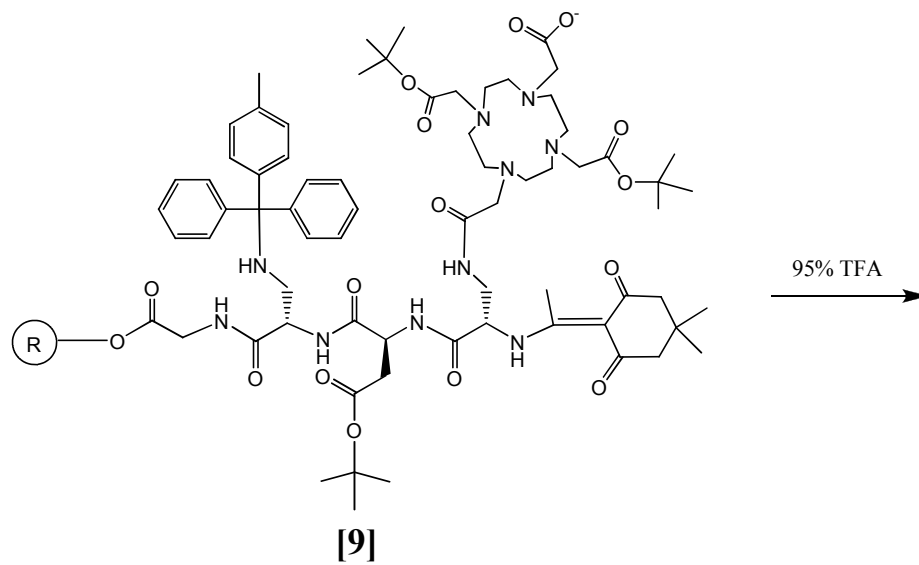
Scheme 2.11 Cleavage of resin-bound intermediate [9] to yield 9 for characterization by ESI-MS
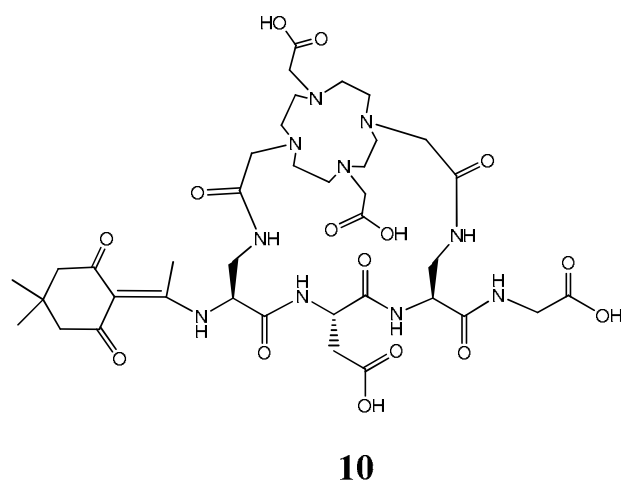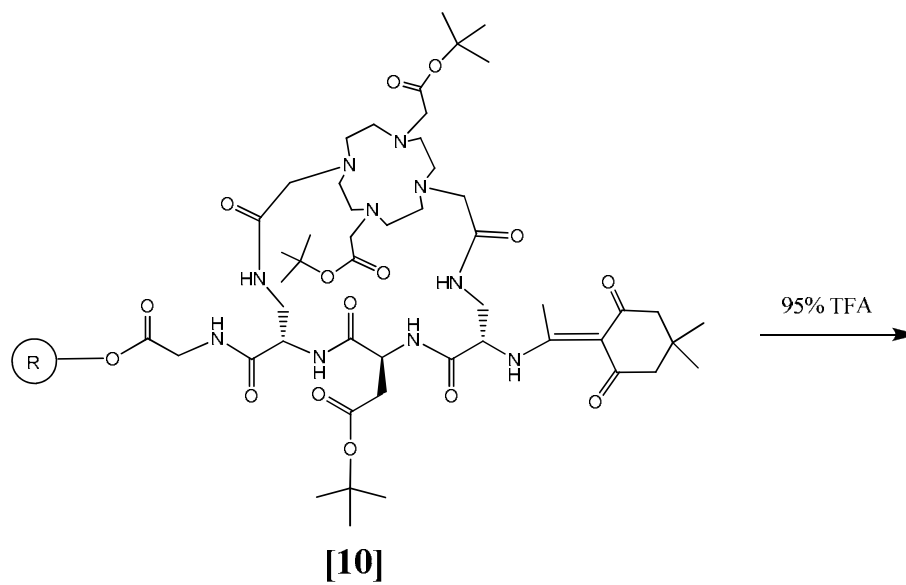
Scheme 2.12 Cleavage of resin-bound intermediate [10] to yield 10 for characterization by ESI-MS

1. hydrazine/DMF

2. fmoc-glu(OtBu)-OH
   HATU, DIPEA, DMF

3. piperidine/DMF

4. fmoc-asp(OtBu)-OH
   HATU, DIPEA, DMF

5. piperidine/DMF

6. fmoc-trp(Boc)-OH
   HATU, DIPEA, DMF

[10]

[11]
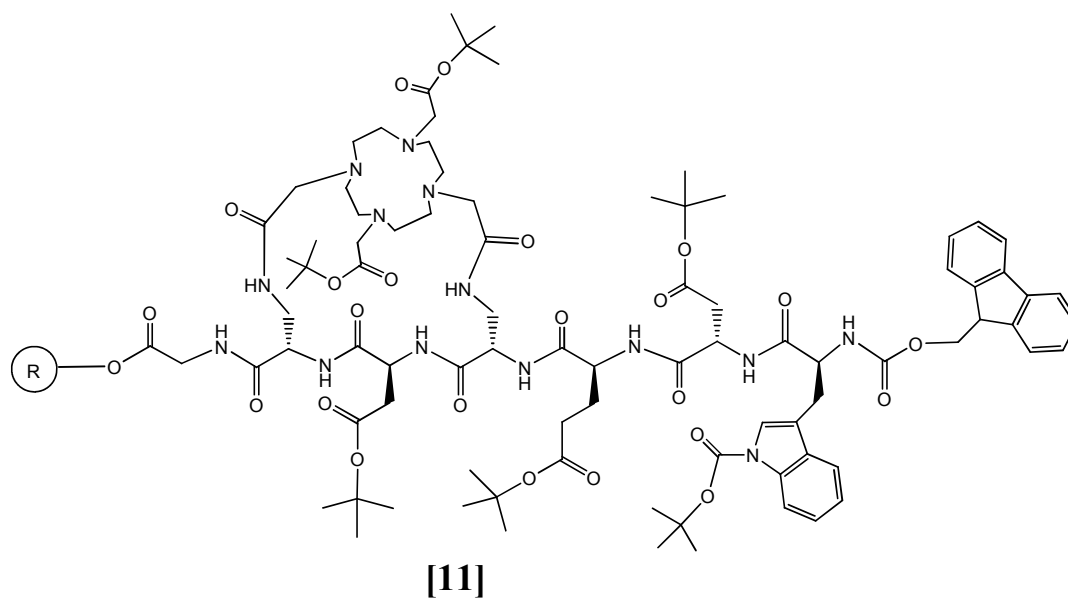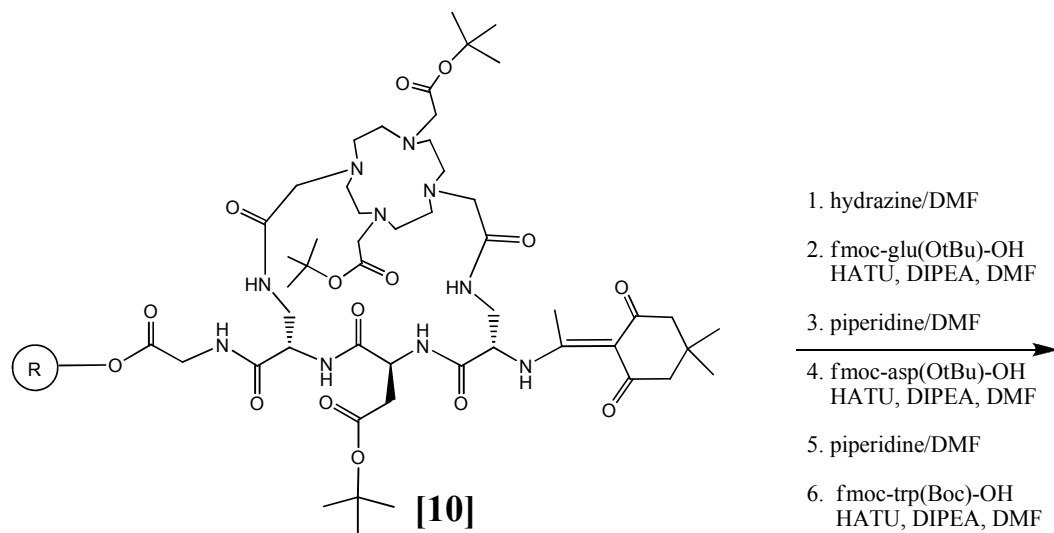
Scheme 2.13 Addition of N-terminal amino acids to resin-bound intermediate [10] to produce resin-bound intermediate [11]

[11]

1. piperidine/DMF

2. 95%TFA, 2.5% TIS, 2.5% H₂O
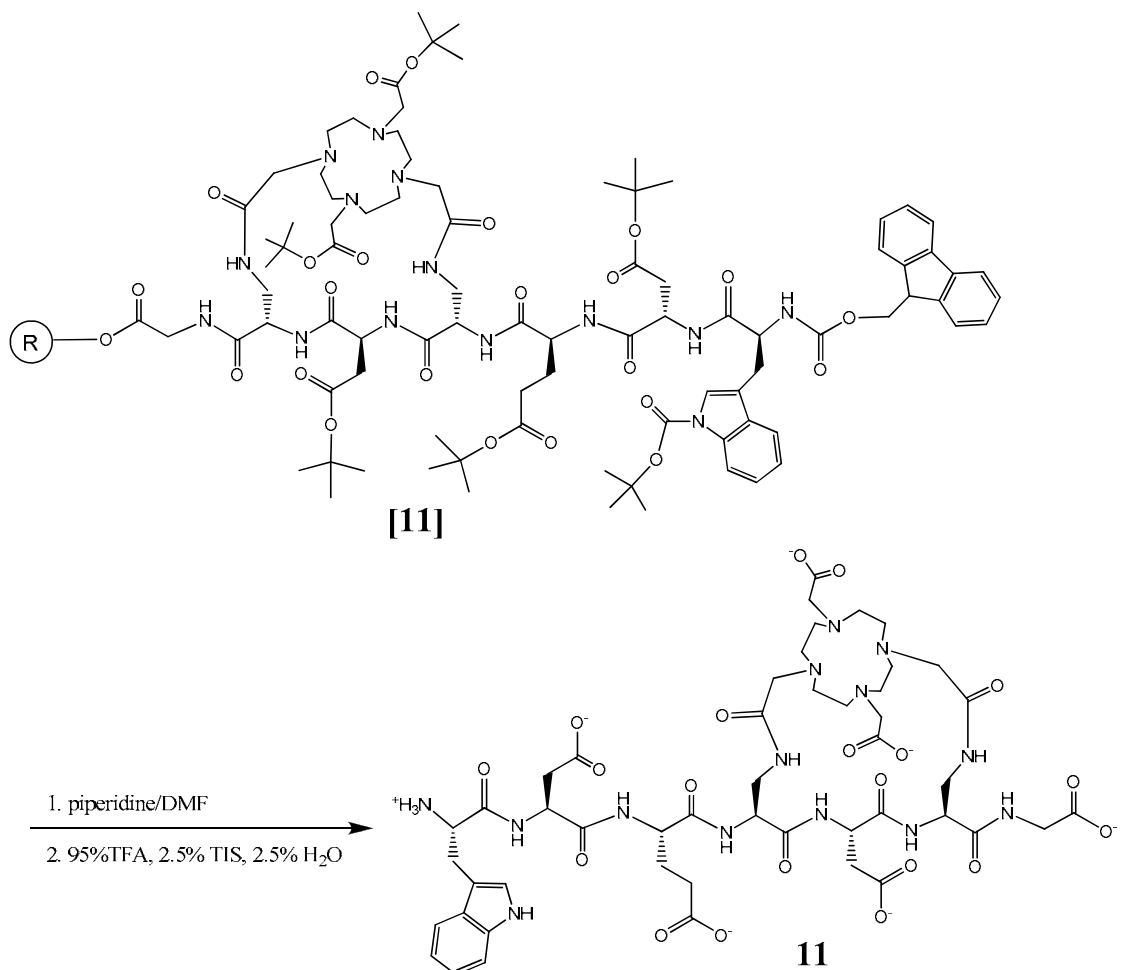
11
54% yield after 18 SPPS steps;
22% overall yield after 23 steps (includes synthesis of **2**)

Ln(OH)₃

H₂O
80 °C

Ln³⁺ = Gd³⁺, **12** (27% yield, 6% overall)
Eu³⁺, **13** (41% yield, 9% overall)
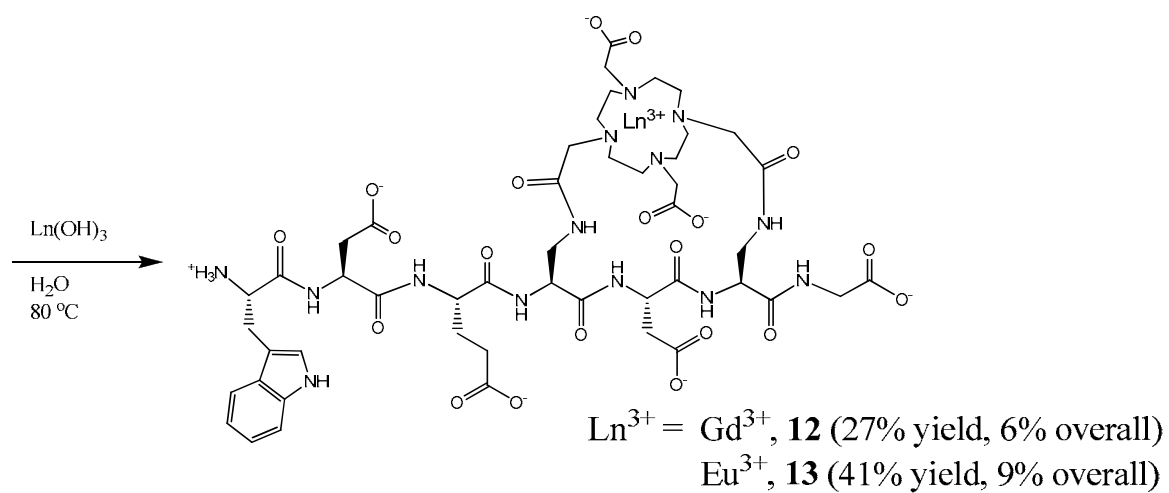
Scheme 2.14 Synthesis of 11 and metalation to produce 12 and 13

Relaxometric Properties (q, τ_m, relaxivity)

The determination of q for **13** and of relaxivity and τ_m for **12** were accomplished using methods described in Part I. A. The luminescence decay constants for **13** in water and deuterium oxide were 0.4744 ± 0.0003 ms ($R^2 = 0.9994$) and 1.6412 ± 0.0006 ms ($R^2 = 0.9998$), respectively, resulting in a calculated $q = 1.4 \pm 0.1$. Due to the error of ± 0.1 inner sphere water molecules, the q value for **13** is within experimental error of the q value of 1.2 determined for the related lysine-bridged agent, **6** (Part I. A). These results obviate the possibility of water blockage by the peptide for **12**. The relaxivity of 9.6 mM^{-1}s^{-1} for **12** is similar to the value of 10.8 mM^{-1}s^{-1} determined for **6** (Part I. A). The ^{17}O-NMR data displayed an overall shape similar to that of **6** and was thus fit to a two isomer model, resulting in τ_m values of 839 ns and 32 ns (Figure 2.16).
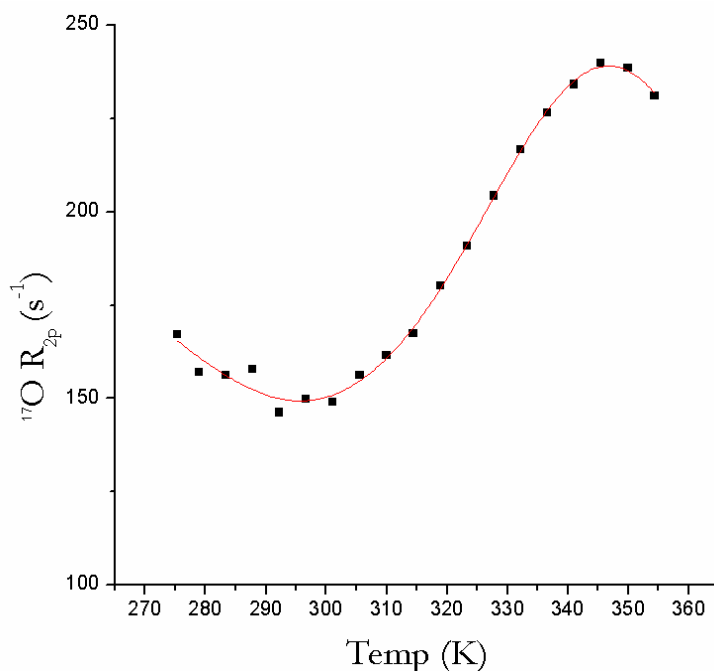
Figure 2.16 Fit (red line, $R^2 = 0.996$) of experimental data (black squares) to a two isomer theoretical model in the determination of τ_m for 12 by VT ^{17}O-NMR

Part I. B (Diaminopropionic Acid Linker) Conclusions

The synthesis of **12** was accomplished in 24 steps with an overall yield of 6%. The synthesis and the determination of the relaxometric properties of **12** paralleled that of the previously discussed **5**. The shortening of the lysine linker found in **5** to the diaminopropionic acid linker found in **12** had a minimal effect on the relaxometric properties. Proximity of the peptide to the chelate was not sufficient to block inner-sphere water access.

It was hypothesized that the shortening of the 28-membered macrobicyclic structure of **5** to the 22-membered macrobicyclic structure of **12** would lead to a decrease in q. This hypothesis was supported by the literature complex, $8O_2$-bridged DOTAM (Figure 2.14), which consists of a 21-membered macrobicyclic structure and lacks inner-sphere water.[35] The authors attributed the lack of an inner-sphere water to distortions of the coordination sphere induced by steric constraints imposed by the bridging unit. Crystallographic analysis of the ytterbium(III) complex of $8O_2$-bridged DOTAM confirmed a constrained system which existed only as the TSAP isomer. In the present work, the peptide did not induce sufficient strain on the macrocyclic chelate to exclude water access to the lanthanide. The VT ^{17}O-NMR studies of **5** and **12** revealed that both of these complexes display fluxionality between the TSAP and SAP isomers. The overall implications of the peptide-bridged contrast agents and future directions are discussed at the end of this chapter.

PART II. Peptide-Bridged MRI Contrast Agents for the Detection of Matrix Metalloproteinase-7

(*Note: Part II is a derivative of the efforts and ideas presented in Part I and many of the experiments in Part II were run in parallel with the analogous experiments of Part I. For brevity, the majority of the information in Part II will be presented in Schemes and Figures. For details, the reader is directed to the analogous section in Part I.)

Part II. Introduction: Matrix Metalloproteinases

Matrix metalloproteinases (MMPs) are a family of zinc containing enzymes that mediate the breakdown of connective tissues.[36] MMPs are important in many physiological processes including wound healing, bone resorption, and uterine and breast involution.[37] The enzymes are generally expressed at low levels, but these levels rise rapidly during inflammation, wound healing, and cancer.[38] Overexpression of MMPs has been linked to several degenerative diseases such as multiple sclerosis,[39-42] corneal ulceration,[43] periodontal disease,[44] gastrointestinal ulceration,[45] abdominal aortic aneurysm,[46] rheumatoid arthritis,[47] osteoarthritis,[47,48] cancer invasion,[49-52] and tumor metastasis.[51,53-57]

As early as 1949, MMPs were recognized as depolymerizing enzymes that were believed to facilitate tumor growth by degrading connective tissues.[58] Recently, the mechanistic role of MMPs in tumor metastasis and invasion has been shown to be much more complex. However, the positive correlation between MMP expression levels and the invasive potential of a tumor

remains.[57] Of the twenty-four known MMPs, MMP-7 has been closely linked to events

occurring during tumor metastasis and invasion.[38,49-52,56,57]

Cancer is one of the leading causes of death in the United States, accounting for

approximately 25% of all deaths.[59] Patients with metastatic cancer have significantly lower odds

of survival; approximately 50% of cancer patients die when the primary tumor becomes

metastatic.[11,59] As a result, there is a growing need for a reliable MMP activity marker.[60]

The detection of MMP activity is critical for identifying metastatic cancer and could be

used to monitor the efficacy of MMP inhibitors, leading to the optimization of anti-cancer

therapeutic protocols.[11,60,61] The current method of monitoring MMP activity consists of ex vivo

assays on excised tissues or fluid samples. In order to detect MMP activity in vitro, fluorescent

probes have been developed.[62,63] The practical applications of fluorescence techniques are

restricted to the observation of cells, small animals, and tumors near the surface of the skin due

to the limited penetration of light (<10 mm).[11] MRI provides an alternative to optical

microscopy, allowing the imaging of opaque organisms in three dimensions at cellular

resolution.[2]

Design of a Peptide-Bridged Contrast Agent for MMP-7

MMP-7 cleaves substrates containing the PLX^LXAX motif, where X denotes a variety

of amino acids and ^ denotes the cleavage site.[64] Placement of the bridge linking the lanthanide

chelate to the peptide at the variable (X) residues of the substrate peptide was hypothesized to not

interfere with substrate recognition and cleavage by MMP-7. The incorporation of a tryptophan

residue on the C-terminus of the peptide provides a chromophore for HPLC purification of

intermediates. It was hypothesized that the substrate peptide could act to sterically block inner-sphere water access to Gd^{3+} (Figure 2.4), resulting in ineffective water relaxation by the agent. Upon enzymatic cleavage of PLKLKAW by MMP-7, the bridge was hypothesized to open, allowing inner-sphere water access to Gd^{3+} and resulting in an increase in relaxivity of the agent.

Part II. A. (Lysine Linker) Results and Discussion

<u>Synthesis</u>

Target compounds **18** and **19** were synthesized in 24 steps (with overall yields of 1%) using the methods and protecting strategy developed in Part I. A (Schemes 2.15, 2.17, 2.20, 2.21). To confirm the stepwise formation of the bridge between **2** and the peptide to form the macrobicyclic structure, key intermediates were cleaved from the resin and characterized by ESI-MS (Schemes 2.16, 2.18, 2.19).

1. piperidine/DMF

2. fmoc-ala-OH
   HATU, DIPEA, DMF

3. piperidine/DMF

4. fmoc-lys(Mtt)-OH
   HATU, DIPEA, DMF

5. piperidine/DMF

6. fmoc-leu-OH
   HATU, DIPEA, DMF

7. piperidine/DMF
   HATU, DIPEA, DMF

8. Dde-lys(fmoc)-OH
   HATU, DIPEA, DMF

R ⃝ = Wang Resin
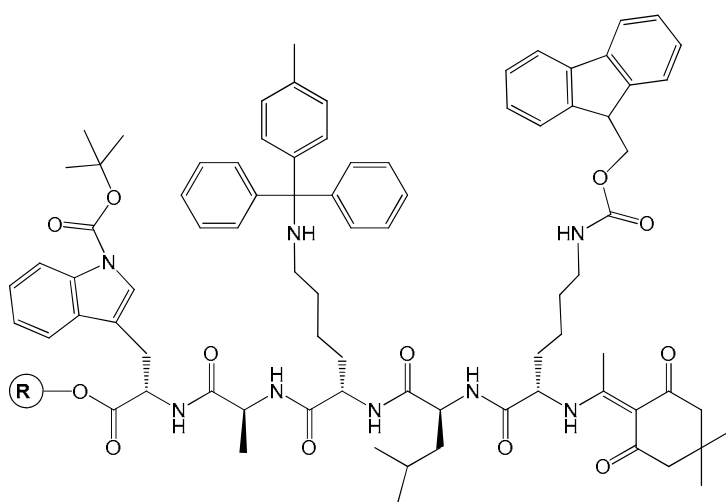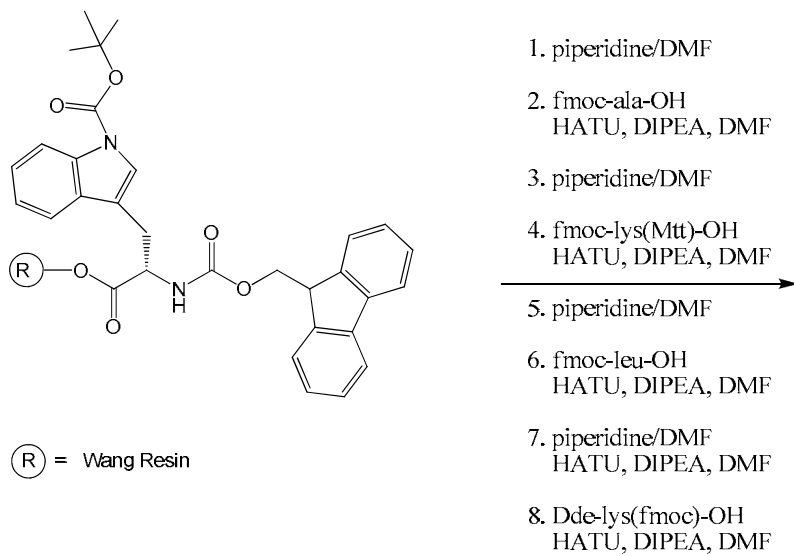
[14]

Scheme 2.15 Synthesis of resin-bound peptide intermediate [14]

1. piperidine/DMF

2. 95% TFA

[14]

14
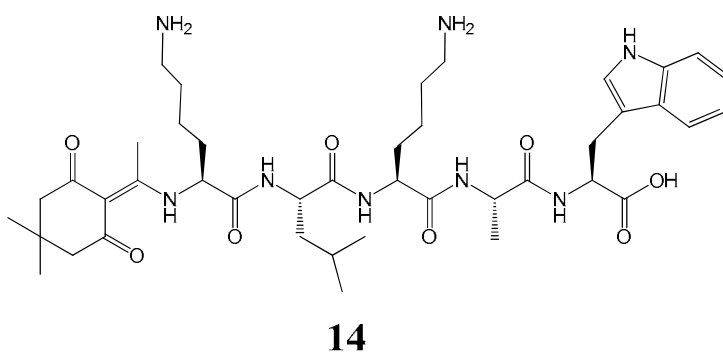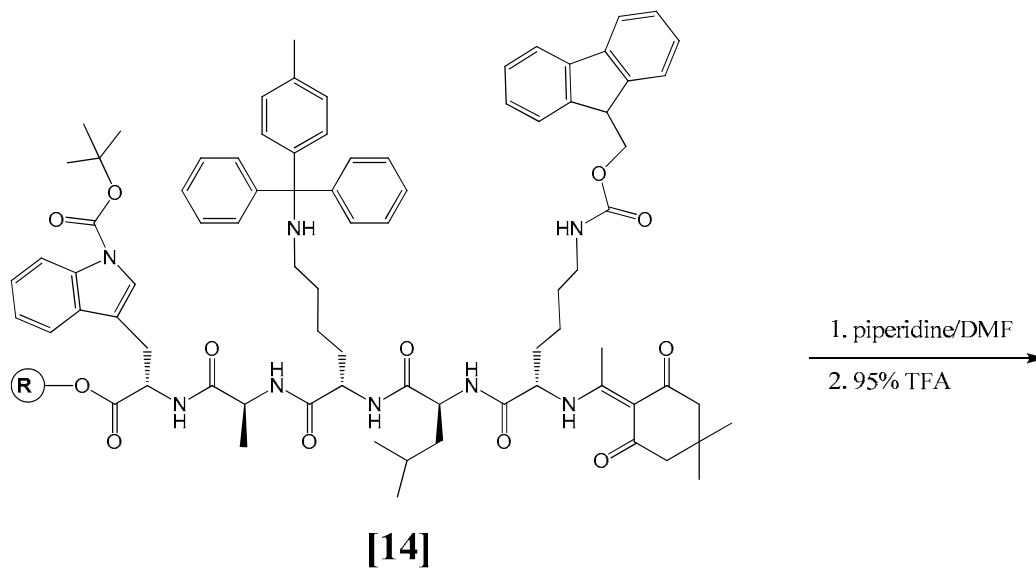
Scheme 2.16 Cleavage of resin-bound intermediate [14] to yield 14 for characterization by ESI-MS

1. piperidiine/DMF

2. **2**, HATU, DIPEA, DMF

[14]

1. 1% TFA

2. HATU/ DIPEA

[15]

[16]
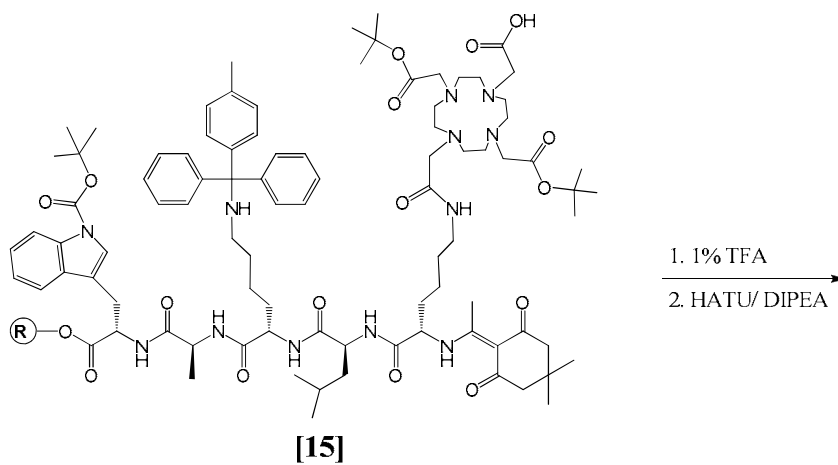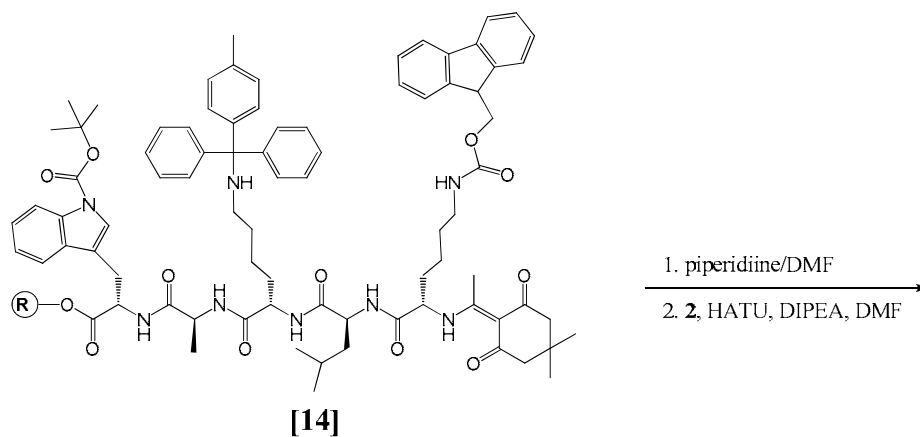
Scheme 2.17 Addition of 2 to the peptide followed by closing of the 28-membered macrobicycle

[15]

95% TFA

15
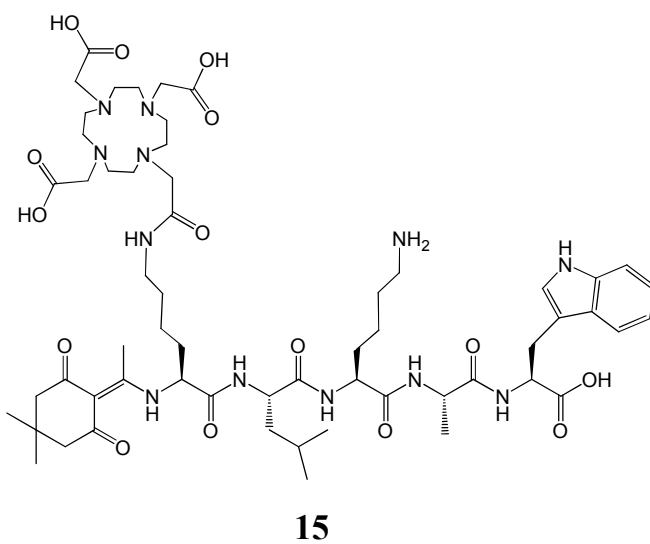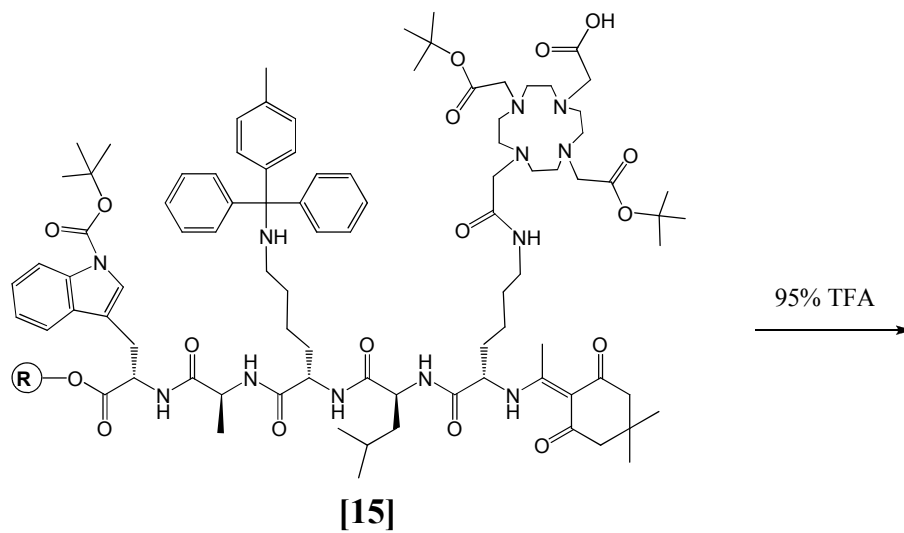
Scheme 2.18 Cleavage of resin-bound intermediate [15] to yield 15 for characterization by ESI-MS

95% TFA

[16]

16
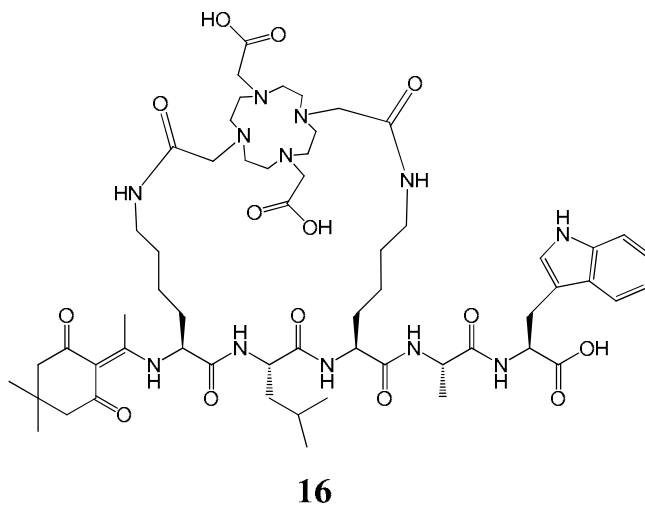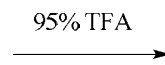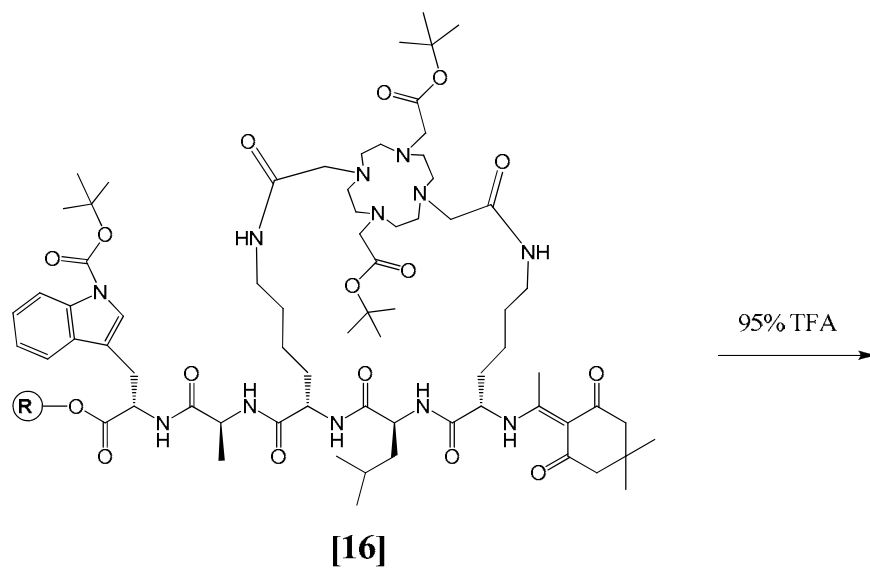
Scheme 2.19 Cleavage of resin-bound intermediate [16] to yield 16 for characterization by ESI-MS

1. hydrazine/DMF

2. fmoc-leu-OH
   HATU, DIPEA, DMF

3. piperidine/DMF

4. fmoc-pro-OH
   HATU, DIPEA, DMF

[16]

[17]
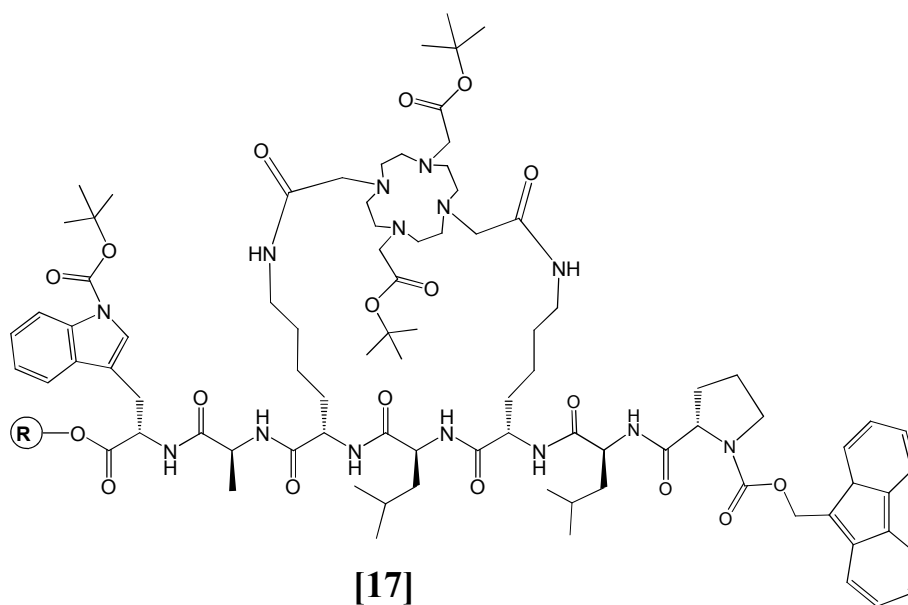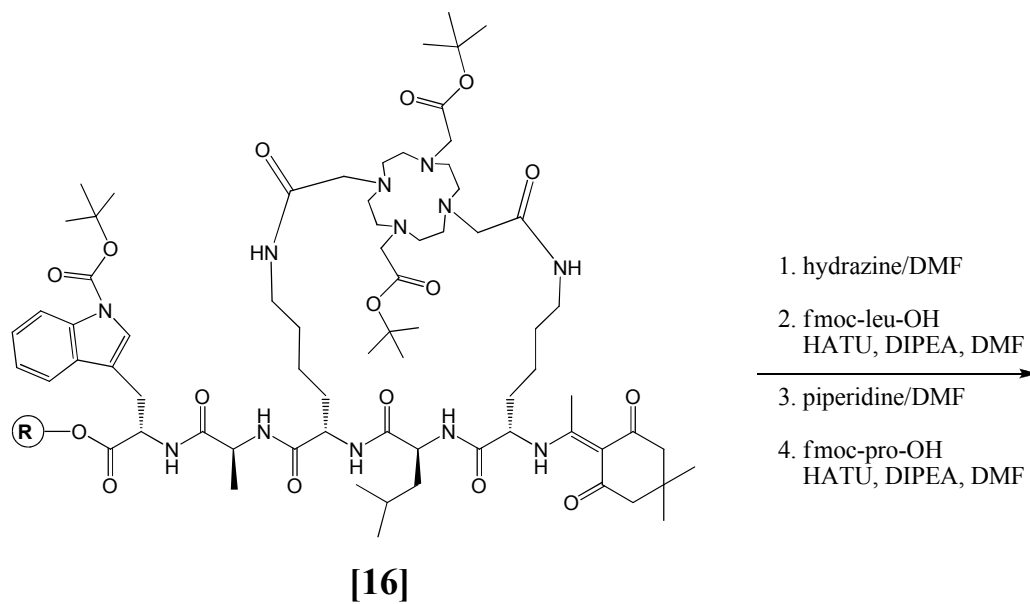
Scheme 2.20 Addition of N-terminal amino acids to resin-bound intermediate [16] to produce resin-bound intermediate [17]

[17]

1. piperidine/DMF
2. 95%TFA

17
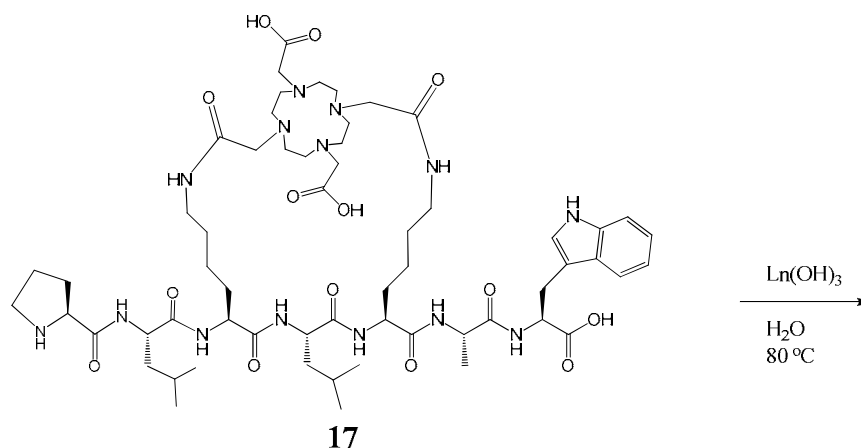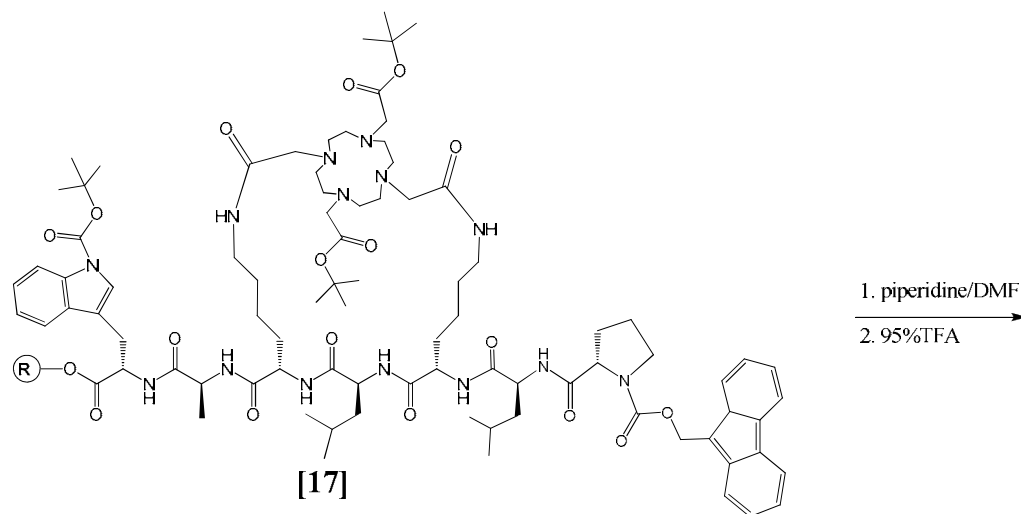
10% yield after 18 SPPS steps;
4% overall yield after 23 steps (includes synthesis of **2**)

Ln(OH)$_3$

H$_2$O
80 °C

Ln^{3+} = Gd^{3+}, **18** (24% yield, 1% overall)
Eu^{3+}, **19** (23% yield, 1% overall)
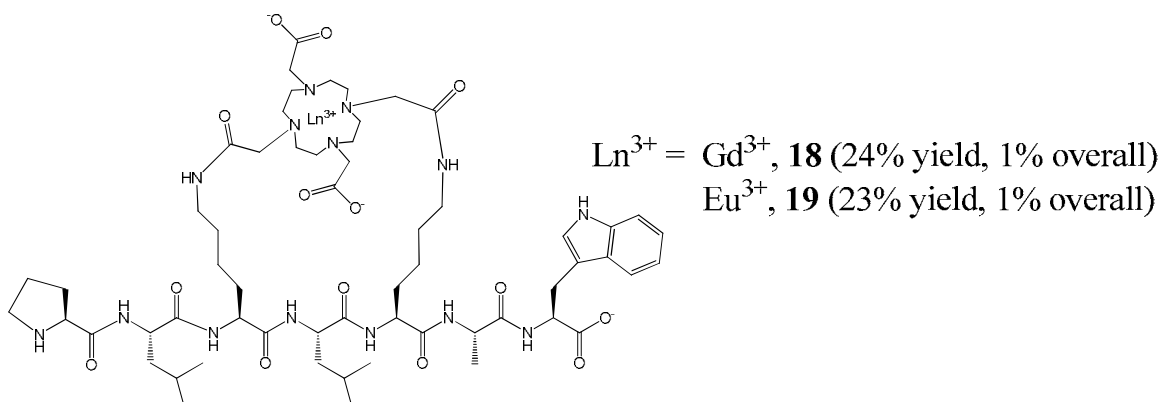
Scheme 2.21 Synthesis of 17 and metalation to produce 18 and 19

Relaxometric Properties (q, τ_m, relaxivity)

The determination of q for **19** and relaxivity and τ_m for **18** were accomplished using methods described in Part I. A. The luminescence decay constants for **19** in water and deuterium oxide were 0.4963 ± 0.0003 ms ($R^2 = 0.9992$) and 1.422 ± 0.002 ms ($R^2 = 0.997$), respectively, resulting in a calculated $q = 1.2 \pm 0.1$. This value of q is the same as that determined for the structurally similar lysine-based caspase-3 agent, **5**. The relaxivity of 12.5 mM^{-1}s^{-1} for **18** is slightly higher than the value of 10.8 mM^{-1}s^{-1} determined for **5** (Part I. A). The minor differences in relaxivity between the two lysine-based contrast agents could be due to slight structural variations resulting from the different amino acid sequences and/or the different buffer constituents used (**18** and **5** were measured in MMP-7 and caspase-3 assay buffer solutions, respectively; details of buffer constituents listed in Experimental). The ^{17}O-NMR linewidth analysis of **18** was fit to a two isomer model, resulting in τ_m values of 1073 ns and 68 ns (Figure 2.17).
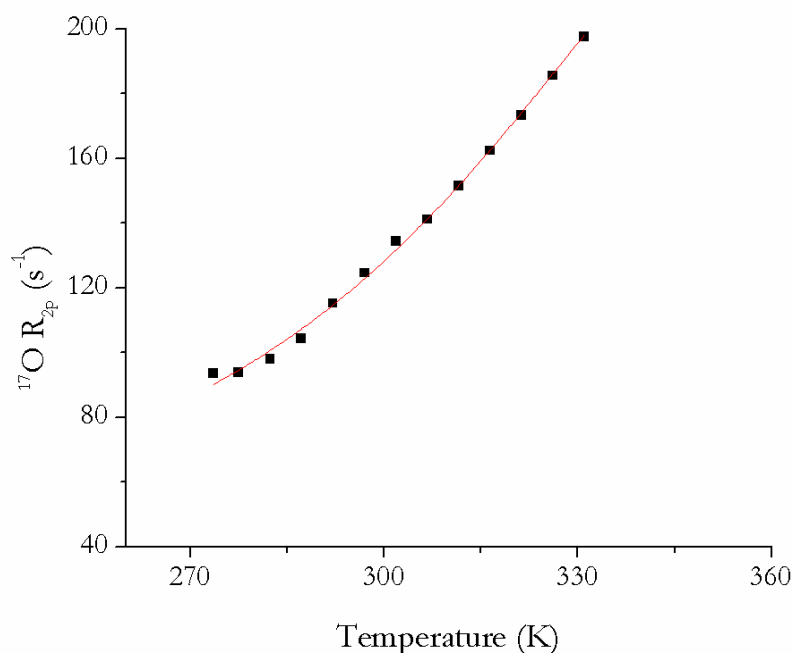
Figure 2.17 Fit (red line, R^2 = 0.9991) of experimental data (black squares) to a two isomer theoretical model in the determination of τ_m for 18 by VT ^{17}O-NMR

Part II. A. (Lysine Linker) Conclusions

The synthesis of compound **18** was accomplished in 24 steps with an overall yield of 1%. The relaxometric properties of the lysine-based MMP-7 agent, **18**, are consistent with the structurally similar lysine-based caspase-3 agent, **5** (Part I. A). The slight differences between **18** and **5** are likely due to the differing amino acid sequences used to construct each agent.

The presence of an inner-sphere water for **18** prompted a redesign of the linker between the chelate and the peptide (Part II. B) in an effort to prohibit inner-sphere water access to the paramagnetic lanthanide.

Part II. B. (Diaminopriopionic Acid Linker) Results and Discussion

Due to the presence of an inner-sphere water for **18**, the linker length between the chelate

and the peptide was shortened using the methodology described in Part I. B.

<u>Synthesis</u>

By substituting commercially available diaminopropionic acid for lysine, target

compounds **24** and **25** were synthesized in 24 steps (with overall yields of 1% and 0.3%,

respectively) using schemes similar to those in Part II.A (Schemes 2.22, 2.24, 2.27, 2.28). In

order to confirm the stepwise formation of the bridge between **2** and the peptide to form the

macrobicyclic structure, key intermediates were cleaved from the resin and characterized by ESI-

MS (Schemes 2.23, 2.25, 2.26).
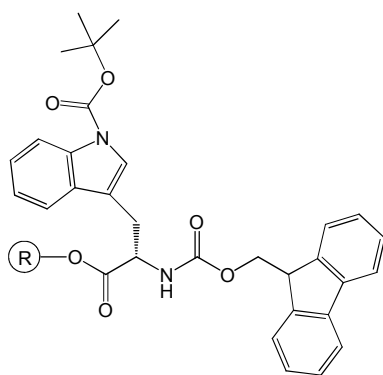
1. piperidine/DMF

2. fmoc-ala-OH
   HATU, DIPEA, DMF

3. piperidine/DMF

4. fmoc-Dap(Mtt)-OH
   HATU, DIPEA, DMF

5. piperidine/DMF

6. fmoc-leu-OH
   HATU, DIPEA, DMF

7. piperidine/DMF
   HATU, DIPEA, DMF

8. Dde-Dap(fmoc)-OH
   HATU, DIPEA, DMF

R = Wang Resin
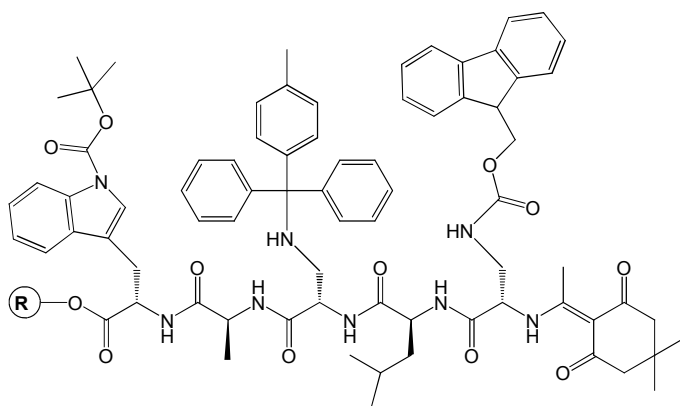
[20]

Scheme 2.22 Synthesis of resin-bound peptide intermediate [20]

1. piperidiine/DMF

2. 95% TFA

[20]

20
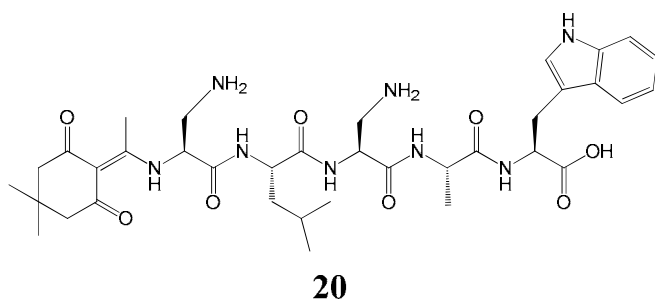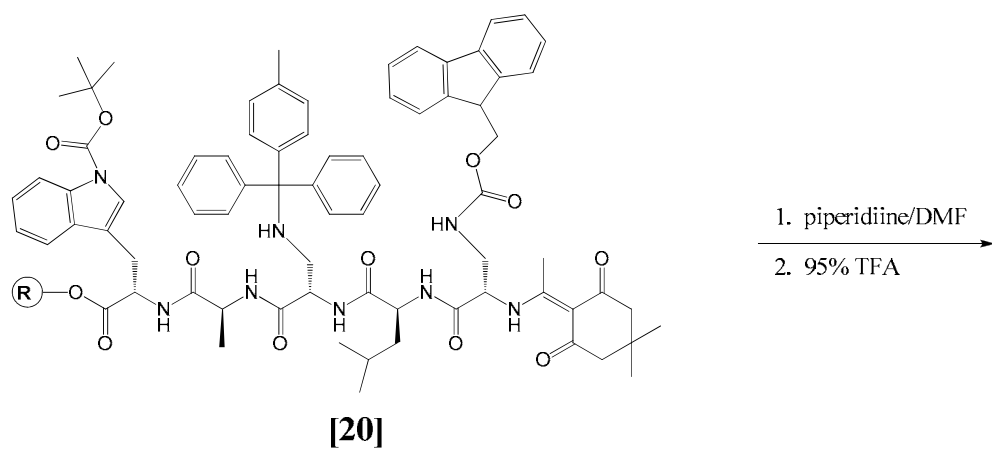
Scheme 2.23 Cleavage of resin-bound intermediate [20] to yield 20 for characterization by ESI-MS

1. piperidiine/DMF

2. **2**, HATU, DIPEA, DMF

[20]

1. 1% TFA

2. HATU, DIPEA, DMF

[21]

[22]
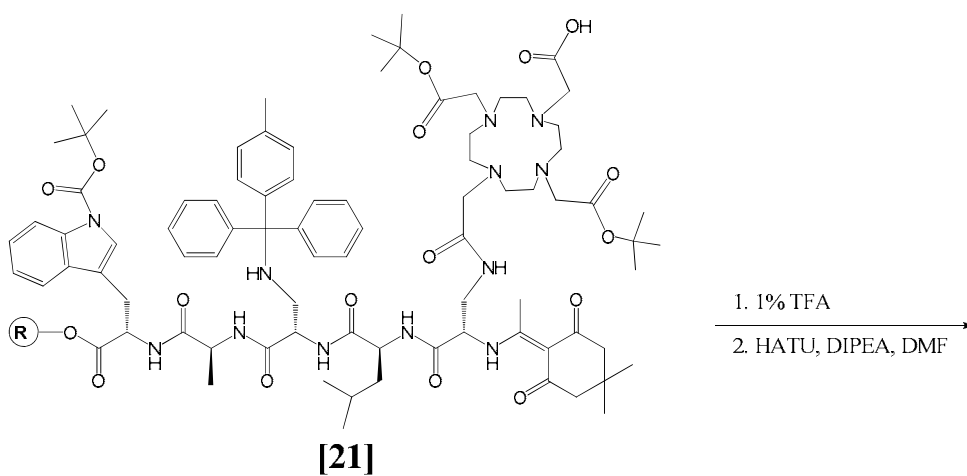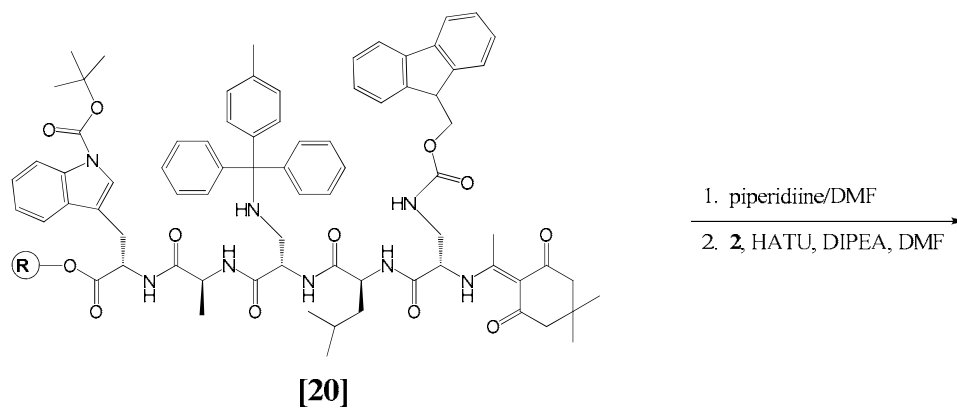
Scheme 2.24 Addition of 2 to the peptide followed by closing of the 22-membered macrobicycle

95% TFA

[21]

21
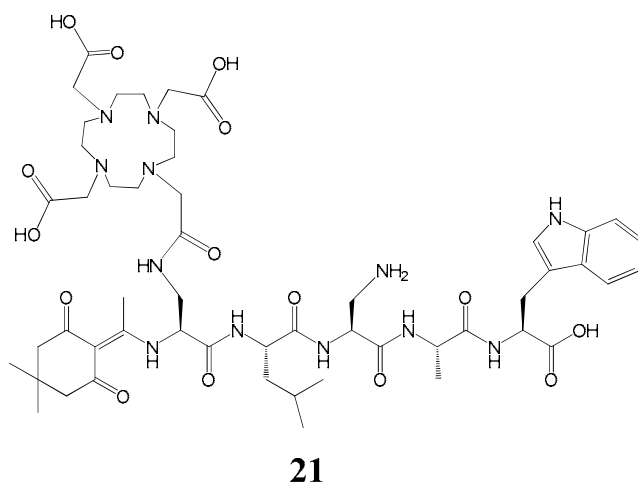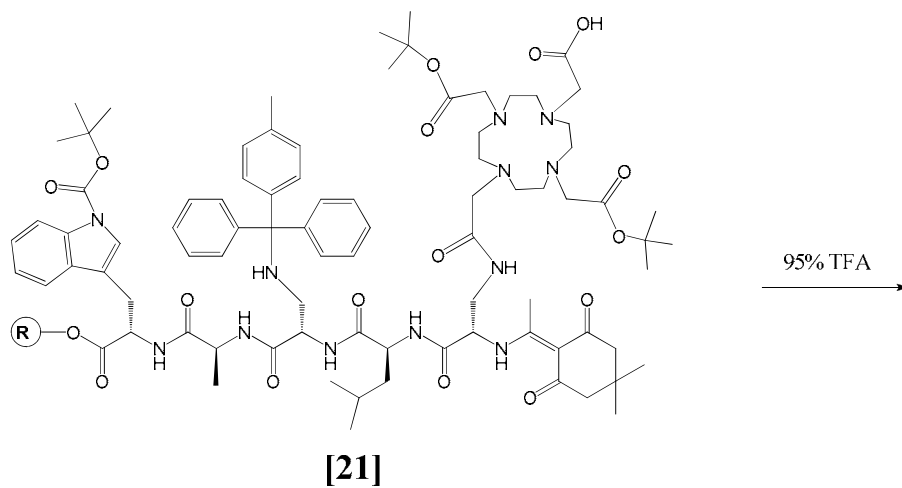
Scheme 2.25 Cleavage of resin-bound intermediate [21] to yield 21 for characterization by ESI-MS

95% TFA

[22]

22
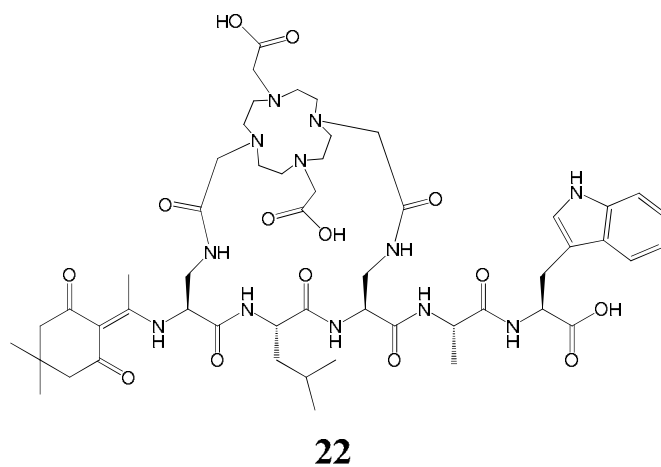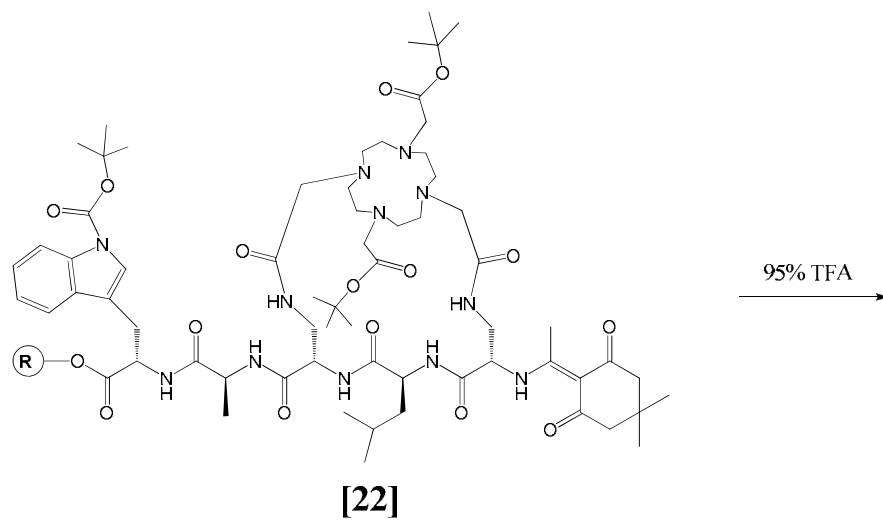
Scheme 2.26 Cleavage of resin-bound intermediate [22] to yield 22 for characterization by ESI-MS

1. hydrazine/DMF

2. fmoc-leu-OH
   HATU, DIPEA, DMF

3. piperidine/DMF

4. fmoc-pro-OH
   HATU, DIPEA, DMF

[22]

[23]
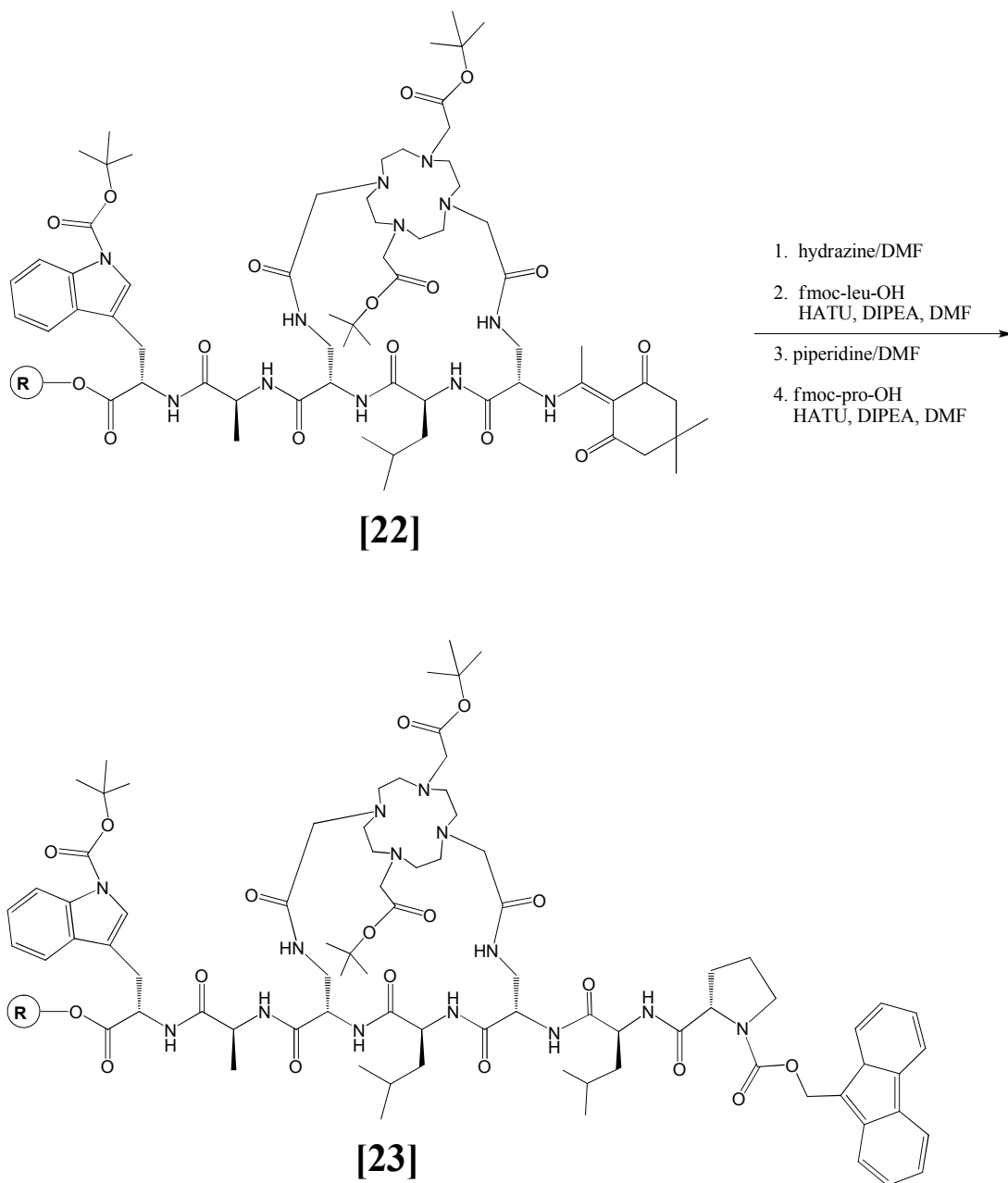
Scheme 2.27 Addition of N-terminal amino acids to resin-bound intermediate [22] to produce resin-bound intermediate [23]

[23]

1. piperidine/DMF

2. 95%TFA

23
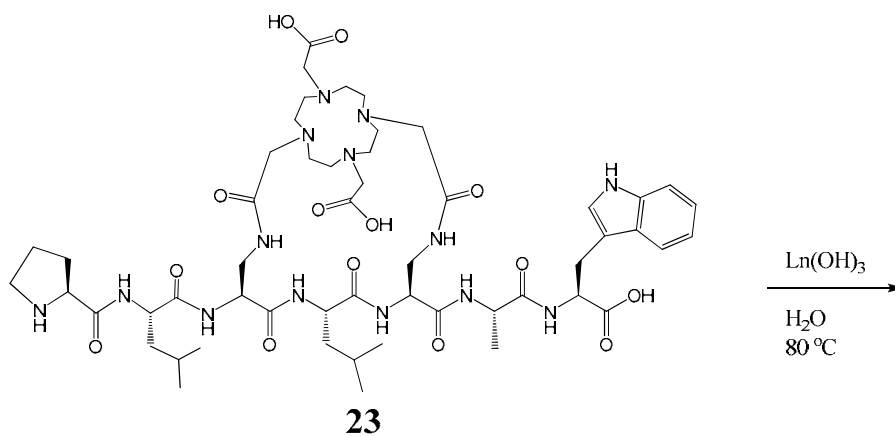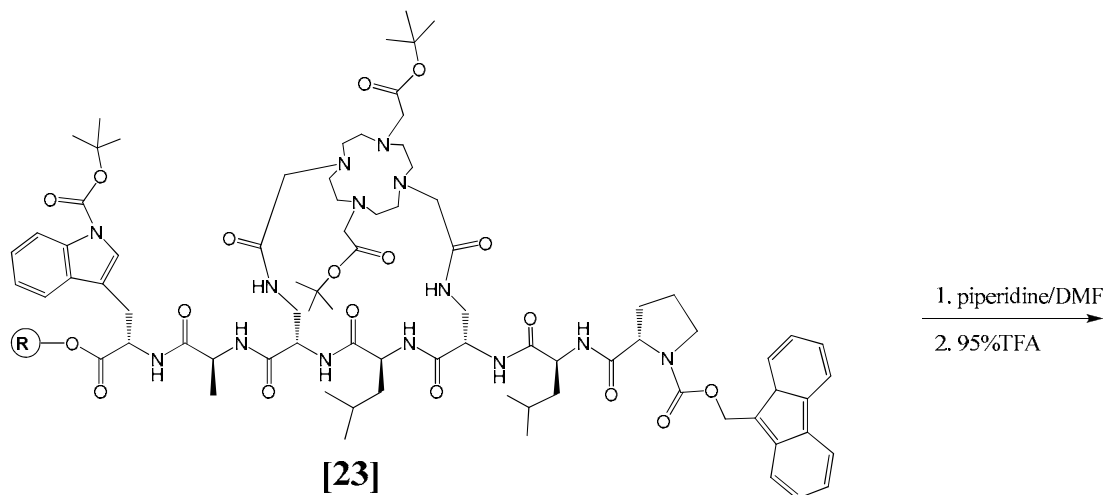
8% yield after 18 SPPS steps;
3% overall yield after 23 steps (includes synthesis of **2**)

Ln(OH)$_3$

H$_2$O
80 °C

Ln^{3+} = Gd^{3+}, **24** (33% yield, 1% overall)

Eu^{3+}, **25** (9% yield, 0.3% overall)
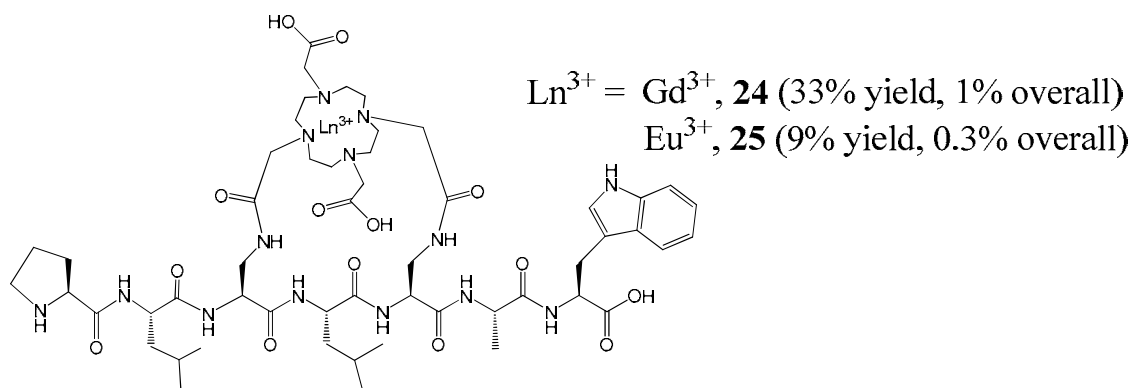
Scheme 2.28 Synthesis of 23 and metalation to produce 24 and 25

<u>Relaxometric Properties (q, τ_m, relaxivity)</u>

The determination of q for **25** and of τ_m and relaxivity for **24** were accomplished using methods described in Part I. A.

The luminescence decay constants for **25** in water and deuterium oxide were 0.6112 ± 0.0004 ms ($R^2 = 0.9991$) and 1.564 ± 0.002 ms ($R^2 = 0.998$), respectively, resulting in a calculated $q = 0.9 \pm 0.1$. This value of q is slightly lower than the value of 1.2 obtained for the lysine-based agent, **18** (Part II. A). The ^{17}O-NMR linewidth analysis of **24** was fit to a two isomer model which includes contributions from both the SAP and TSAP isomers, resulting in τ_m values of 1323 ns and 635 ns, respectively (Figure 2.18). The τ_m value for the TSAP isomer of **24** is an order of magnitude longer than the TSAP τ_m value of 68 ns reported for **18,** and the τ_m value for the SAP isomer of **24** is considerably greater than the SAP τ_m value of 1073 ns reported for **18** (Part II. A). These drastic differences in τ_m help explain the differences in relaxivity between **24** and **18**. The relaxivity of **24** was 5.9 mM^{-1}s^{-1}, which is considerably lower than the value of 12.5 mM^{-1}s^{-1} determined for **18** (Part II. A). The differences in relaxivity between **24** and **18** is best explained by a combination of the slightly lower q values and the significantly longer τ_m values of **24**.
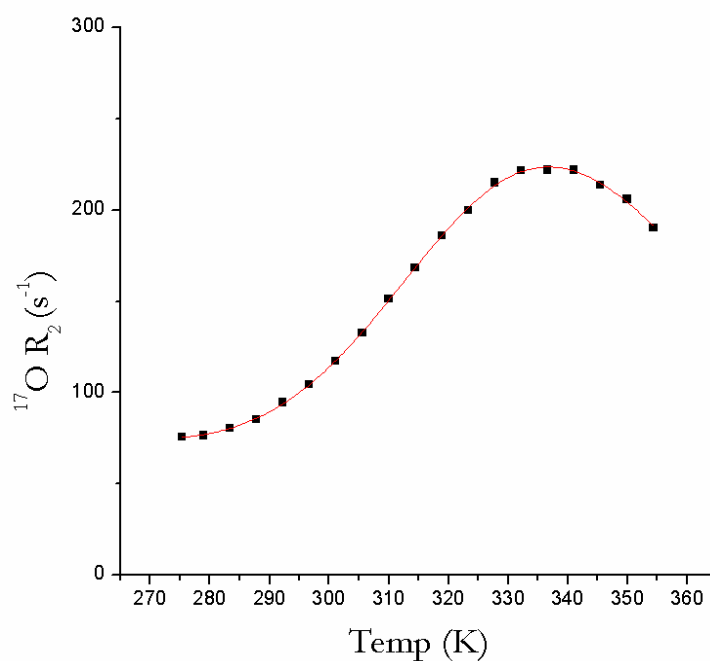
Figure 2.18 Fit (red line, R^2 = 0.9997) of experimental data (black squares) to a two isomer theoretical model in the determination of τ_m for 24 by VT ^{17}O-NMR

Enzyme Studies

The relatively low relaxivity of **24** prompted an investigation of the relaxivity of the agent in the presence of MMP-7. The T_1 of a solution of **24** in the presence of active MMP-7 was measured as a function of time. A control solution consisting of **24** without added MMP-7 was subjected to the same conditions and the T_1 of the solution was monitored over time. After repeating the experiments several times, it was determined that there was not a significant difference between the experimental and control solutions. These results suggest that either the enzyme is unable to cleave the substrate peptide of **24** or there is a lack of change in relaxivity of **24** before and after enzymatic cleavage. Further investigation of these two possible scenarios was examined using mass spectrometry. The enzymatic hydrolysis of **24** by MMP-7 should

result in an increase in mass by 18 a.m.u. due to the addition of water into the scissile amide bond. This increase in mass should be detectable by mass spectrometry. Despite repeated efforts, neither **24** nor the enzymatic cleavage product of **24** could be detected by ESI-MS or MALDI-TOF MS.

Part II. B (Diaminopropionic Acid Linker) Conclusions

The synthesis of **24** was accomplished in 24 steps with an overall yield of 1%. The relaxometric properties of **24** differ significantly from those of the related lysine-based **18** from Part II.A. The slightly lower q value of 0.9 and significantly longer τ_m values of 1323 ns for the SAP isomer and 635 ns for the TSAP isomer (as compared to $q = 1.2$ and $\tau_m = 1073$ ns for the SAP isomer and 68 for the TSAP isomer of **18**) help explain why the relaxivity of **24** (5.9 mM^{-1}s^{-1}) is approximately half that of **18 (**12.5 mM^{-1}s^{-1}). The steric constraint due to proximity of the peptide to the gadolinium(III) chelate is a likely culprit for the longer τ_m values of **24** as compared to the larger 28-membered macrobicyclic structure of **18**.

The relatively low relaxivity of **24** prompted enzyme studies with MMP-7. It was hypothesized that the relaxivity of **24** would increase upon cleavage by MMP-7 due to increased water access to the paramagnetic gadolinium(III) (proposed mechanism, Figure 2.4). An investigation of the relaxivity of **24** after incubation with MMP-7 was not significantly different from the control solutions which lacked enzyme. Mass spectrometry failed to detect either **24** or the enzymatically cleaved product in the complex milieu of the MMP-7 assay buffer. Due to the prohibitively high cost of synthesis and low overall yield (1% after 24 steps), further studies of **24** where not attempted.

OVERALL SUMMARY AND FUTURE DIRECTIONS

The macrobicyclic chelates presented in this chapter are a systematic approach towards controlling the coordination environment of lanthanide chelates. The first generation (compounds **5** and **18**) featured chelates attached via amide bonds to the side chain amine of lysine. These agents incorporated a 28-membered macrobicyclic structure. The relaxometric properties of the agents were thoroughly evaluated, and it was determined that the peptide did not effectively block inner-sphere water access to the lanthanide chelate. The results of these studies led to the second generation of agents where diaminopropionic acid was used in place of lysine in the bridging amino acid residues. Using the synthetic methodology developed for the first generation, the second generation of agents (compounds **12** and **24**) consisted of a 22-membered macrobicyclic structure. For both **12** and **24**, the peptide did not completely block inner-sphere water access, however, for **24**, the water exchange rate ($k_{ex} = 1/\tau_m$) was slowed by an order of magnitude. The slower water exchange rate for **24** resulted in the overall relaxivity being half that of the analogous first generation agent, **18**. Interestingly, **12** did not show a decrease in water exchange rate as compared to **5**. It is hypothesized that the functionality and conformation of the individual amino acids of the peptide have a great influence on the water exchange rate of the chelate. Further investigation of this hypothesis involves synthesizing a variety macrobicyclic complexes with systematic changes of the amino acids. The influence of charged vs. hydrophobic amino acid side-chains leaves an interesting topic for future studies of peptide-based macrobicyclic lanthanide chelates.

The novel chelates developed both in this chapter and in Appendix II will serve as valuable synthons for future projects. The controlled functionalization of cyclen resulting in **2**

has potential applications in the development of novel MRI contrast agent conjugates. For instance, the pseudo-*trans* carboxylic acids of **2** could be used to synthesize molecules which feature MRI contrast agents incorporated into a linear chain of amino acids, polymers, or other relevant structures. Incorporation of the lanthanide chelate within the backbone of a linear macromolecule (as opposed to current designs which feature MRI contrast agents appended to the periphery of the macromolecule) would help fully take advantage of the increased molecular tumbling of the macromolecule, resulting in a great increase in relaxivity of the contrast agent.

The methodology developed during the synthesis of the macrobicyclic structures involved multi-step synthesis with 4-way orthogonal protecting strategy. This protecting strategy will be useful for future projects involving the covalent attachment of multiple unique moieties to a peptide. For instance, a peptide could be functionalized with a fluorophore and an MRI contrast agent to allow multimodal imaging of biological systems.

The use of solid-phase peptide synthesis was instrumental in maintaining high yields throughout the lengthy, 24-step syntheses. With the general synthetic strategy developed in the present work, multiple permutations of the structure are possible with minimal changes to the overall synthetic steps. This chapter represents only two examples of the potential target enzymes (Part I., Caspase-3 and Part II., MMP-7) out of the plethora of known enzymes. By simply changing the amino acid sequence of the substrate peptide, this methodology can be used to synthesize countless potential imaging agents. Since subtle changes in the amino acid structure can have a drastic influence on the relaxometric properties of the resultant contrast agent, the investigation of peptide-based macrobicyclic MRI contrast agents leaves much to be explored.

EXPERIMENTAL (Parts I. and II.)

General

<u>Abbreviations</u>

DMF = N,N-dimethylformamide, TFA = trifluoroacetic acid, MeCN = acetonitrile, TIS = triisopropylsilane, fmoc = 9-fluorenylmethoxycarbonyl, Boc = *tert*-butoxycarbonyl, Mtt = methyltrityl, HATU = *o*-(7-azabenzotriazol-1-yl)-N,N,N',N'-tetramethyluronium hexafluorophosphate, DIPEA = N,N-diisopropylethylamine, DOTA = 1,4,7,10-tetraazacyclododecane N,N',N'',N'''-tetraacetic acid, NMR = nuclear magnetic resonance, HPLC = high performance liquid chromatography, RP-HPLC = reverse phase high performance liquid chromatography, PDA = photodiode array, ESI-MS = electrospray ionization mass spectrometry, MALDI-TOF MS = matrix assisted laser desorption ionization time of flight mass spectrometry, CHCA = α-cyano-4-hydroxycinnamic acid, Dde = (4,4-dimethyl-2,6-dioxocyclohex-1-ylidene)ethyl, tris = 2-amino-2-hydroxymethylpropane-1,3-diol, BSA = bovine serum albumin, APMA = 4-aminophenylmercuric acetate, HEPES = 4-(2-hydroxyethyl)-1-piperazineethanesulfonic acid, DTT = dithiothreitol, EDTA = ethylenediaminetetraacetic acid, CHAPS = 3-[(3-chloramidopropyl) dimethylammonio]-1-propane sulfonate, Dap = diaminopropionic acid

<u>Chemicals</u>

Fmoc-L-amino acids and fmoc-L-amino acids with side chain protecting groups were purchased (NovaBiochem, San Diego, California) and used as received. Diaminopropionic acid

derivatives and Diaminobutanoic acid derivatives were purchased (IRIS Biotech GmbH, Germany) and used as received. All other chemicals and solvents were purchased (Sigma Aldrich, St. Louis, Missouri) and used as received.

Instrumentation

UV/visible spectra for the Kaiser test were performed on an Agilent 8453 UV/vis spectrophotometer. ESI-MS was performed on a Varian Quadrupole 1200L or a Thermo Finnigan LCQ Advantage. Samples were dissolved in MeOH and 0.22 µm filtered prior to injection. MALDI-TOF MS was performed on a PerkinElmer Voyager DE Pro operating in reflector mode using CHCA as matrix. Aqueous samples (1 µL) were spotted on a stainless steel plate along with matrix solution (1 µL of saturated CHCA solution in 1:1 MeCN : 0.1% TFA). Samples were dried under ambient conditions before acquiring spectra. Analytical HPLC-MS was performed on a reverse-phase C_{18} Atlantis T3 column (Waters, T3 5µm, 4.6 X 250mm) with a Varian Prostar 363 fluorescence detector, a Varian Prostar PDA 330 UV/vis detector, and a Varian Quadrupole 1200L MS to determine the appropriate gradients to be used for preparative HPLC. Preparative HPLC was performed on a reverse-phase C_{18} Atlantis T3 column (Waters, T3 10µm, 19 X 250mm with 19 X 10mm guard) with a Hewlett-Packard 1046A fluorescence detector and a Varian Prostar UV/vis dual wavelength detector.

1-D NMR spectra were acquired on either a Varian Mercury 400 MHz or Varian Inova 500 MHz instrument. 2-D NMR were acquired on a Varian 600 MHz instrument. Fluorescence measurements were recorded on a Hitachi F-4500 using quartz cuvettes. T_1 measurements were determined using a Bruker mq60 Minispec operating at 60 MHz and 37 ^{o}C. Lanthanide

concentrations were determined using Inductively Coupled Plasma Mass Spectrometry (ICP-MS) on a Thermo Electron Corporation XSeries[II] ICP-MS with Thermo PlasmaLab software. ICP-MS samples were performed in triplicate using a standard calibration for each Lanthanide with an internal standard consisting of 50 ppb In^{3+}.

Other

Pt stain for TLC consists of 150 mg K_2PtCl_6 in 90 mL H_2O, 10 mL 1 N HCl, 3 g KI. CAM stain for TLC consists of 900 mL water, 100 mL concentrated H_2SO_4, 100 g ammonium molybdate, and 4 g ceric (IV) sulfate. The Kaiser test for free amines was used to determine reaction progress during solid-phase peptide synthesis.[13] All water used was purified using a Milli-Q (Millipore Billerica, Massachusetts) purification system. Millipore Millex-GN 0.22 μm Nylon filters were used for aqueous solutions and Millipore Millex-FG 0.22 μm hydrophobic PTFE filters were used for non-aqueous solutions.

Part I.A.

1,7-bis(*tert*-butoxycarbonylmethyl)-4,10-bis(benzyloxycarbonylmethyl)-1,4,7,10-tetraazacyclododecane (1)

1,7-bis(*tert*-butoxycarbonylmethyl)-1,4,7,10-tetraazacyclododecane (synthesized according to literature methods[12]) (5.00537 g, 12.4959 mmol) was dissolved in 12 mL MeCN and placed in a 100 mL roundbottom flask with magnetic stirbar. Cs_2CO_3 (3.4 eq., 14.03217 g, 43.0672 mmol)

and benzyl 2-bromoacetate (2.1 eq., 4.120 mL, 26.26 mmol) were added and the flask was

attached to a water-cooled reflux condenser equipped with a Drierite drying tube. The flask was

placed in a 60 $^{\circ}$C oilbath and stirred overnight. The reaction was determined complete by TLC

(silica gel, 1:9:90 saturated KNO_3:H_2O:MeCN, Pt stain, product R_f = 0.53). The solution was

cooled to room temperature and paper filtered to remove Cs_2CO_3. MeCN was removed by rotary

evaporation under reduced pressure to afford the crude product as a yellow oil. The crude

product was dissolved in CH_2Cl_2 and loaded onto a silica gel column (8 cm diameter X 10 cm

height). Excess benzyl 2-bromoacetate was eluted with CH_2Cl_2, followed by a gradient up to

10% MeOH in CH_2Cl_2 to elute the desired product. Solvents were removed by rotary

evaporation under reduced pressure followed by pumping vacuum overnight to afford **1** as a

yellow oil (6.9290 g, 80% yield).

ESI-MS: Calc. 696.41; Found positive mode 719.4 (M + Na^+)

^{1}H NMR ($CDCl_3$): δ = 1.4 (s, 18H, *t*-Bu), 2.3-2.9 (br, 16H, cyclen), 3.1-3.7 (8H, C*H$_2$*COO-tBu

and C*H$_2$*COO-Bz), 5.1 (s, 4H, Bz C*H$_2$*), 7.3 (br, Bz aromatic, Note: integration of aromatics not

available due to solvent residual peak at 7.26 ppm)

^{13}C NMR ($CDCl_3$): δ = 28.1, 28.3, 48.5, 52.0, 55.7, 55.9, 56.6, 56.8, 66.2, 66.6, 67.1, 81.9, 82.2,

128.4, 128.5, 128.6, 128.7, 135.2, 135.9, 170.1, 171.4, 173.3, 173.7

1,7-bis(*tert*-butoxycarbonylmethyl)-4,10-bis(carboxymethyl)-1,4,7,10-

tetraazacyclododecane (2)

1 (6.9290 g, 9.9430 mmol) was dissolved in 125 mL absolute ethanol and transferred to a glass

hydrogenation vessel with Pd/C catalyst (10% catalyst loading, 5.8000 g). The vessel was

purged four times with H_2/vacuum then charged with H_2 (40 psi) and reacted for 48 hours with

mechanical shaking. The mixture was paper filtered and 0.22μm filtered to remove the catalyst.

Solvent was removed by rotary evaporation under reduced pressure, forming an off-white solid.

The product was placed under vacuum to dry, resulting in **2** as a white powder (4.4444 g, 87%

yield).

ESI-MS: Calc. 516.32; Found positive mode 517.3 $(M + H^+)$, 539.3 $(M + Na^+)$, negative mode

515.4 (M^-), 537.4 $[(M + Na^+)^-]$

^{1}H NMR (CDCl$_3$): δ = 1.4 (s, 18H, *t*-Bu), 2.2-3.8 (br, 24H, cyclen, C*H*$_2$COO-tBu, and

C*H*$_2$COOH)

^{1}H NMR (D$_2$O): δ = 1.4 (s, 18H, *t*-Bu); 3.0 (br, 4H), 3.1 (br, 4H), 3.4-3.6 (br, 12H), 4.0 (s, 4H)

[cyclen, C*H*$_2$COO-tBu, and C*H*$_2$COOH]

^{1}H NMR (CD$_3$OD): δ = 1.4 (s, 18H, *t*-Bu), 2.0-3.9 (br, 24H, cyclen, C*H*$_2$COO-tBu, and

C*H*$_2$COOH)

^{13}C NMR (CD$_3$OD): δ = 28.4, 28.5, 28.6, 52.5, 52.9(br), 55.1(br), 55.6, 56.2, 57.6(br), 58.2, 58.4,

61.6, 83.3(br), 83.9, 86.5, 165.7, 169.7(br), 170.1, 170.4, 170.6, 171.2, 171.8, 171.9, 172.2(br),

172.8, 173.6, 174.1

Dde-Lys(2*)-Asp-Lys-Gly (3)

[Note: 2* denotes site of attachment for 2 to the peptide side-chain; please see appropriate

scheme for structure]

The protected peptide was synthesized according standard solid-phase peptide synthesis methods using manual batch-type synthesis and fmoc protected amino acids.[65]

A Wang resin consisting of 100-200 mesh 1% cross-linked polystyrene beads functionalized with p-benzyloxybenzyl alcohol handle was used as a solid support for the stepwise addition of amino acids. The Wang resin was purchased (NovaBiochem, San Diego, California) with the N-terminal amino acid, fmoc-glycine, preloaded onto the resin. The resin (2.50498 g, 0.78 mmol/g resin loading, 1.95 mmol glycine) was added to a fritted glass reactor vessel fitted with a 3-way valve for switching between N_2 (used to mix during all reactions and rinses) and vacuum (used to drain rinses and excess reactants). The dry Wang resin was pre-swelled with CH_2Cl_2 (1 X 10 minute rinse) followed by DMF (4 X 10 minute rinses). The N-terminal fmoc protecting group was removed using 20% piperidine in DMF (until determined >99% complete by the Kaiser test; typically 4 X 10 minutes). The resin was rinsed with DMF (4 X 10 minutes). The next amino acid (2.5 equivalents relative to the N-terminal glycine on the Wang resin) to be added to the peptide was dissolved in a minimal amount of DMF. To this solution, HATU (2.0 equivalents) and DIPEA (5.0 equivalents) were added to form a yellow solution of the preactivated fmoc-amino acid. This solution was added to the resin and reacted while gently bubbling N_2 to mix the reactants until determined >99% complete (typically 2-12 hours) by the Kaiser test. Upon completion, the resin was rinsed with DMF (4 X 10 minutes). This process of fmoc removal and addition of the next amino acid was repeated for each amino acid until the desired sequence, Dde-Lys(fmoc)-Asp(OtBu)-Lys(Mtt)-Gly-Wang resin, was obtained. The lysine side-chain fmoc protecting group was removed using 20% piperidine in DMF. **2** was coupled to the lysine side-

chain amine using the same conditions as used for the amino acid couplings and monitored by

the Kaiser test. Upon reaction completion, the resin was rinsed with DMF (4 X 10 minutes).

At this point, a small amount (typically ~10 mg) of resin-bound intermediate Dde-Lys(**2**)-

Asp(OtBu)-Lys(Mtt)-Gly-Wang resin, **[3]**, was removed for cleavage to produce **3** (see

"Cleavage of the peptide from the resin") while the remainder was carried through to the next

step of the synthesis. Intermediate compound **3** was characterized by mass spectrometry.

ESI-MS: Calc. 996.51; Found positive mode 997.5 (M + H$^+$), 1019.5 (M + Na$^+$), negative mode

995.5 (M$^-$), 1017.5 [(M + Na$^+$)$^-$]

Trp-Asp-Glu-Lys(2*)-Asp-Lys(2*)-Gly (4)

[Note: 2* denotes sites of attachment for 2 to the peptide side-chains; please see

appropriate scheme for structure]

Starting with **[3]**, the resin was swelled in CH$_2$Cl$_2$ (4 X 10 minutes) and the Mtt protecting group

was removed from the side chain of the lysine using 94% CH$_2$Cl$_2$, 5% TIS, 1% TFA until

determined >99% complete (typically 6 X 2 minutes) by the Kaiser[13] test. The resin was rinsed

with DMF (4 X 10 minutes). The remaining unprotected pendant carboxylate arm of **2** was

reacted with the lysine side chain amine under coupling conditions [HATU (2.0 equivalents) and

DIPEA (5.0 equivalents) were dissolved in a minimum amount of DMF to form a yellow

solution which was added to the resin and reacted overnight while gently bubbling N$_2$ to mix]

and was monitored using the Kaiser[13] test. This intramolecular coupling resulted in the closing

of the bridge to form a 28-membered macrocycle. Upon reaction completion, the resin was

rinsed with DMF (4 X 10 minutes). The Dde protecting group was removed from the N-terminus

using 2% hydrazine in DMF until determined >99% complete (typically 3 X 3 minutes) by the

Kaiser[13] test. The resin was rinsed with DMF (4 X 10 minutes) and the remaining amino acids

(glu, asp, trp) were added as fmoc-glu(OtBu), fmoc-asp(OtBu), fmoc-trp(Boc) sequentially in a

manner as described above. After the desired sequence was obtained, the peptide was cleaved

from the resin (see "Cleavage of peptide from resin") to yield (1.78250 g) of crude product. The

crude product was purified using preparative RP-HPLC (Solvent A = 0.05% TFA in H_2O,

Solvent B = MeCN; flow rate = 15 mL/min; gradient starting at 0% B and ramping to 10% B

over 5 minutes, hold isocratic 10% B for 30 minutes, ramp to 100% B over 5 minutes, hold

isocratic 100% B for 5 minutes, ramp to 0% B over 5 minutes, hold isocratic 0% B for 5 minutes;

fluorescence detection of tryptophan λ_{ex} = 250 nm, λ_{em} = 350 nm; UV/vis detection at 205 nm

and 270 nm) by injecting sample (typically ~150 mg per injection) dissolved in water (3 mL, 0.22

μm filtered) with the desired product eluting at ~40 minutes. MeCN was removed by rotary

evaporation under reduced pressure. The remaining aqueous solution was frozen in liquid N_2

and lyophilized (typically ~90 mg isolated product per injection) to yield 644.63 mg (27% overall

yield for SPPS reactions, 11% overall yield including the 5 steps required to synthesize **2**) of **4** as

a white powder.

ESI-MS: Calc. 1244.56; Found positive mode 1245.5 (M + H$^+$), 1267.5 (M + Na$^+$), negative

mode 1243.4 (M$^-$), 1265.4 [(M + Na$^+$)$^-$]

^{1}H NMR (D_2O): Non-first order spectra; assignments made using 2-D TOCSY, COSY, NOESY

(Table 2.1, Part I., Results and Discussion) δ = 1.35, 1.38 (K_γ); 1.47, 1.50 (K_β); 1.70, 1.75 (K_δ);

2.06 (E_β); 2.3-2.9 (cyclen, D_β); 2.39 (E_γ); 2.97 (K_ϵ); 3.30 (C*H₂*COOH); 3.42 (W_β); 3.75

(C*H₂*COOH); 3.96 (G_α); 4.19 (E_α); 4.33 (K_α); 4.68 (W_α, D_α); 7.15, 7.25, 7.29, 7.50, 7.60 (W

aromatic)

Cleavage of peptide from resin:

Resin was placed in a fritted reactor column and (where appropriate) remaining fmoc groups were removed with piperidine as described above. The resin was rinsed with DMF (4 X 10 minutes), CH_2Cl_2 (4 X 10 minutes), methanol (4 X 10 minutes); and dried under vacuum overnight. To the dried resin was added a cleavage cocktail (35 mL) consisting of 95% TFA, 2.5% TIS, 2.5% H_2O. The resin was reacted in the cleavage cocktail for one hour, after which the solution was drained into a vial. Fresh cleavage cocktail (10 mL) was added to the resin and reacted for 10 minutes, followed by draining into a vial. Fresh cleavage cocktail (5 mL) was added to the resin and immediately drained into a vial. The TFA filtrates were combined and stored in capped vials overnight to fully remove all tBu and Boc protecting groups. TFA was evaporated by passing N_2 over the vial. The volume was reduced to ~7.5 mL followed by addition of cold (-20 ^{o}C) diethyl ether to precipitate the crude product as an off-white solid. The suspension was centrifuged and decanted. The diethyl ether extraction was repeated 4 times followed by evaporation of residual diethyl ether by passing N_2 over the vial. The solid cake was dissolved in water (20 mL), frozen in liquid N_2 and lyophilized.

Gadolinium(III)-Trp-Asp-Glu-Lys(2*)-Asp-Lys(2*)-Gly (5)

4 (97.0 mg, 0.0782 mmol) was placed in a 100 mL round bottom flask with magnetic stirbar and dissolved in 40 mL H_2O. The pH was adjusted to 5.5 using 5% NaOH followed by addition of $Gd(OH)_3 \cdot 6H2O$ (18.85 mg, 0.05960 mmol, 0.8 equivalents). The flask was capped with a rubber septum and sonicated briefly to reduce the size of the $Gd(OH)_3$ particulates before placing in a 80

^{o}C oilbath with stirring. Over the course of the reaction, the pH gradually increased due to the release of OH$^-$ and there was a visible decrease in the amount of Gd(OH)$_3$ solids. The pH was periodically monitored and adjusted to 5.5 using HCl vapor. The reaction was determined to be complete when the pH ceased to change (typically 48-72 hours). The pH was raised to 10 using 20% NaOH [typically 2 µL, to precipitate any excess Gd^{3+} as Gd(OH)$_3$] and 0.22 µm filtered. The filtrate was then frozen in liquid nitrogen and lyophilized. The crude product was purified using preparative RP-HPLC (Solvent A = H$_2$O, Solvent B = MeCN; flow rate = 15 mL/min; gradient starting at 0% B and ramping to 1% B over 15 seconds, hold isocratic 1% B for 29 minutes 45 seconds, ramp to 100% B over 5 minutes, hold isocratic 100% B for 5 minutes, ramp to 0% B over 5 minutes, hold isocratic 0% B for 15 minutes; fluorescence detection of tryptophan λ_{ex} = 250 nm, λ_{em} = 350 nm; UV/vis detection at 205 nm and 270 nm) by injecting sample (typically ~90 mg per injection) dissolved in water (3 mL, 0.22 µm filtered) with the desired product eluting at ~35 minutes 45 seconds. MeCN was removed by rotary evaporation under reduced pressure. The remaining aqueous solution was frozen in liquid nitrogen and lyophilized (typically ~12 mg isolated product per injection) to yield 28.50 mg (26% yield) of **5** as a white powder. Metalation was confirmed by ICP-MS.

Europium(III)-Trp-Asp-Glu-Lys(2*)-Asp-Lys(2*)-Gly (6)

EuCl$_3$·6H$_2$O (1.07676 g, 2.93868 mmol) was dissolved in 5mL water and precipitated by addition of 2 mL 2M NaOH. The white precipitate was vacuum filtered, washed with water, and lyophilized to give Eu(OH)$_3$ as a white powder (577.55 mg, 96.8% yield).

4 (87.89 mg, 0.07086 mmol) was metalated with Eu(OH)$_3$ (17.06 mg, 0.08404 mmol, 1.2

equivalents) and purified using the same method as described for **5** to produce 12.07 mg (12%

yield) of **6** as a white powder. Metalation was confirmed by ICP-MS.

Dysprosium(III)-Trp-Asp-Glu-Lys(2*)-Asp-Lys(2*)-Gly (7)

Dy(OH)$_3$ was prepared from DyCl$_3$·6H$_2$O using the same method as described for Eu(OH)$_3$.

4 (99.63 mg, 0.08033 mmol) was metalated with Dy(OH)$_3$ (19.53 mg, 0.09147 mmol, 1.1

equivalents) and purified using the same method as described for **5** to produce 13.90 mg (12%

yield) of **7** as a white powder. Metalation was confirmed by ICP-MS.

Part I.B.

The diaminopropionic acid (Dap) -based contrast agent was synthesized using the same methods

as the lysine-based agent (above), starting with tryptophan(Boc)-Wang resin (706.90 mg, 0.78

mmol/g resin loading, 0.55 mmol glycine) and substituting fmoc-Dap(Mtt)-OH and Dde-

Dap(fmoc)-OH residues for fmoc-Lys(Mtt)-OH and Dde-Lys(fmoc)-OH residues, respectively.

Key intermediates were characterized using ESI-MS.

Dde-Dap-Asp-Dap-Gly (8)

ESI-MS: Calc. 526.23; Found positive mode 527.20 (M + H$^+$), 549.17 (M + Na$^+$), negative mode

525.23 (M$^-$), 547.24 [(M + Na$^+$)$^-$]

Dde-Dap(2*)-Asp-Dap-Gly (9)

ESI-MS: Calc. 912.41; Found positive mode 913.39 (M + H$^+$), 935.36 (M + Na$^+$), negative mode 911.42 (M$^-$), 933.32 [(M + Na$^+$)$^-$]

Dde-Dap(2*)-Asp-Dap(2*)-Gly (10)

ESI-MS: Calc. 894.40; Found positive mode 895.34 (M + H$^+$), 917.34 (M + Na$^+$), negative mode 893.32 (M$^-$), 915.36 [(M + Na$^+$)$^-$]

Trp-Asp-Glu-Dap(2*)-Asp-Dap(2*)-Gly (11)

Crude **11** (488.88 mg) was purified using preparative RP-HPLC (Solvent A = 0.05% TFA in H$_2$O, Solvent B = MeCN; flow rate = 15 mL/min; gradient starting at 0% B and ramping to 10% B over 5 minutes, hold isocratic 10% B for 30 minutes, ramp to 100% B over 5 minutes, hold isocratic 100% B for 5 minutes, ramp to 0% B over 5 minutes, hold isocratic 0% B for 5 minutes; fluorescence detection of tryptophan λ_{ex} = 250 nm, λ_{em} = 350 nm; UV/vis detection at 205 nm and 270 nm) by injecting sample (typically ~100 mg per injection) dissolved in water (3 mL, 0.22 µm filtered) with the desired product eluting at ~40 minutes. MeCN was removed by rotary evaporation under reduced pressure. The remaining aqueous solution was frozen in liquid N$_2$ and lyophilized (typically ~75 mg isolated product per injection) to yield 345.66 mg (54% overall yield SPPS reactions, 22% overall yield including the 5 steps required to synthesize **2**) **11** as a white powder.

ESI-MS: Calc. 1160.48; Found positive mode 1161.49 (M + H$^+$), 1183.37 (M + Na$^+$), negative mode 1159.28 (M$^-$), 1181.76 [(M + Na$^+$)$^-$]

Gadolinium(III)-Trp-Asp-Glu-Dap(2*)-Asp-Dap(2*)-Gly (12)

11 (65.05 mg, 0.05627 mmol) was metalated with Gd(OH)$_3$·6H$_2$O (19.54 mg, 0.06184 mmol, 1.1 equivalents) using the same method as described for **5**. The crude product (72.74 mg) was purified using preparative RP-HPLC (Solvent A = H$_2$O, Solvent B = MeCN; flow rate = 15 mL/min; gradient starting at 0% B and ramping to 1% B over 15 seconds, hold isocratic 1% B for 29 minutes 45 seconds, ramp to 100% B over 5 minutes, hold isocratic 100% B for 5 minutes, ramp to 0% B over 5 minutes, hold isocratic 0% B for 15 minutes; fluorescence detection of tryptophan λ_{ex} = 250 nm, λ_{em} = 350 nm; UV/vis detection at 205 nm and 270 nm) by injecting crude product dissolved in water (3 mL, 0.22 μm filtered) with the desired product eluting at ~35 minutes 45 seconds. MeCN was removed by rotary evaporation under reduced pressure. The remaining aqueous solution was frozen in liquid N$_2$ and lyophilized to yield 20.06 mg (27% yield) of **12** as an off-white powder. Metalation was confirmed by ICP-MS.

Europium(III)-Trp-Asp-Glu-Dap(2*)-Asp-Dap(2*)-Gly (13)

11 (80.37 mg, 0.06952 mmol) was metallated with Eu(OH)$_3$ (16.02 mg, 0.07892 mmol, 1.1 equivalents) using the same method as described for **5** to yield 116.97 mg crude **13**. The crude product was purified using RP-HPLC using the same method as described for **12** to yield 37.69 mg (41% yield) of **13** as an off-white solid. Metalation was confirmed by ICP-MS.

Part II.A.

Dde-Lys-Leu-Lys-Ala-Trp (14)

The protected peptide was synthesized according standard solid-phase peptide synthesis methods using manual batch-type synthesis and fmoc protected amino acids.[65]

A Wang resin consisting of 100-200 mesh 1% cross-linked polystyrene beads functionalized with *p*-benzyloxybenzyl alcohol handle was used as a solid support for the stepwise addition of amino acids. The Wang resin was purchased (NovaBiochem, San Diego, California) with the N-terminal amino acid, fmoc-tryptophan(Boc), preloaded onto the resin. The resin (2.51022 g, 0.59 mmol/g resin loading, 1.5 mmol tryptophan) was added to a fritted glass reactor vessel fitted with a 3-way valve for switching between N_2 (used to mix during all reactions and rinses) and vacuum (used to drain rinses and excess reactants). The dry Wang resin was pre-swelled with CH_2Cl_2 (1 X 10 minute rinse) followed by DMF (4 X 10 minute rinses). The N-terminal fmoc protecting group was removed using 20% piperidine in DMF (until determined >99% complete by the Kaiser[13] test; typically 4 X 10 minutes). The resin was rinsed with DMF (4 X 10 minutes). The next amino acid (2.5 equivalents relative to the N-terminal tryptophan on the Wang resin) to be added to the peptide was dissolved in a minimal amount of DMF. To this solution, HATU (2.0 equivalents) and DIPEA (5.0 equivalents) were added to form a yellow solution of the pre-activated fmoc-amino acid. This solution was added to the resin and reacted while gently bubbling N_2 to mix the reactants until determined >99% complete (typically 2-12 hours) by the Kaiser test. Upon reaction completion, the resin was rinsed with DMF (4 X 10 minutes). This process of fmoc removal and addition of the next amino acid was repeated for each amino acid until the desired intermediate sequence, Dde-Lys(fmoc)-Leu-Lys(Mtt)-Ala-Trp(Boc)-Wang resin,

[14], was obtained. At this point, a small amount (typically ~10 mg) of resin was removed for

cleavage (see "Cleavage of the peptide from the resin") while the remainder was carried through

to the next step of the synthesis.

ESI-MS: Calc. 808.48; Found positive mode 809.50 (M^+), 831.50 ($M + Na^+$), negative mode

807.59 (M^-)

Dde-Lys(2*)-Leu-Lys-Ala-Trp (15)

The fmoc protecting group was removed from the lysine side chain of **[14]** using 20% piperidine

(as described above), followed by overnight coupling to **2** (using same conditions as amino acid

couplings described above) and monitored by the Kaiser[13] test. Upon reaction completion, the

resin was rinsed with DMF (4 X 10 minutes).

At this point, a small amount (typically ~10 mg) of resin-bound intermediate **[15]** was removed

for cleavage to produce **15** (see "Cleavage of the peptide from the resin") while the remainder of

[15] was carried through to the next step of the synthesis.

ESI-MS: Calc. 1194.66; Found positive mode 1195.55 ($M + H^+$), 1217.55 ($M + Na^+$), negative

mode 1193.48 (M^-)

Dde-Lys(2*)-Leu-Lys(2*)-Ala-Trp (16)

[15] was swelled in CH_2Cl_2 (4 X 10 minutes) and the Mtt protecting group was removed from

the side chain of the lysine using 94% CH_2Cl_2, 5% TIS, 1% TFA until determined >99%

complete (typically 6 X 2 minutes) by the Kaiser[13] test. The resin was rinsed with DMF (4 X 10

minutes). The remaining unprotected pendant carboxylate arm of **2** was reacted with the lysine

side chain amine under coupling conditions [HATU (2.0 equivalents) and DIPEA (5.0

equivalents) were dissolved in a minimum amount of DMF to form a yellow solution which was

added to the resin and reacted overnight while gently bubbling N_2 to mix] and was monitored

using the Kaiser test. This intramolecular coupling resulted in the closing of the bridge to form a

28-membered macrocycle. Upon reaction completion, the resin was rinsed with DMF (4 X 10

minutes).

At this point, a small amount (typically ~10 mg) of resin-bound intermediate **[16]** was removed

for cleavage to produce **16** (see "Cleavage of the peptide from the resin") while the remainder of

[16] was carried through to the next step of the synthesis.

ESI-MS: Calc. 1176.65, Found negative mode 1175.44 (M⁻)

Pro-Leu-Lys(2*)-Leu-Lys(2*)-Ala-Trp (17)

The Dde protecting group was removed from the N-terminus of **[16]** using 2% hydrazine in DMF

until determined >99% complete (typically 3 X 3 minutes) by the Kaiser[13] test. The resin was

rinsed with DMF (4 X 10 minutes) and the remaining amino acids (leu, pro) were added as their

respective fmoc protected amino acid derivatives sequentially in a manner as described above.

After the desired sequence was obtained, the peptide was cleaved from the resin (see "Cleavage

of peptide from resin" below) to yield (985.89 mg) of crude product. The crude product was

purified using preparative RP-HPLC: (Solvent A = 0.05% TFA in H_2O, Solvent B = MeCN; flow

rate = 15 mL/min; gradient starting at 0% B and ramping to 30% B over 5 minutes, hold isocratic

30% B for 15 minutes, ramp to 100% B over 3 minutes, hold isocratic 100% B for 5 minutes,

ramp to 0% B over 5 minutes, hold isocratic 0% B for 7 minutes; fluorescence detection of

tryptophan λ_{ex} = 250 nm, λ_{em} = 350 nm; UV/vis detection at 205 nm and 270 nm) by injecting

crude product (typically ~100 mg per injection) dissolved in water (3 mL, 0.22 μm filtered) with

the desired product eluting at ~24-25 minutes. MeCN was removed by rotary evaporation under

reduced pressure. The remaining aqueous solution was frozen in liquid N_2 and lyophilized

(typically ~22 mg isolated product per injection) to yield 177.15 mg (10% yield overall yield

SPPS reactions, 4% overall yield including the 5 steps required to synthesize **2**) of **17** as a white

solid.

ESI-MS: Calc. 1222.71; Found positive mode 1245.71 (M + Na^+)

Gadolinium(III)-Pro-Leu-Lys(2*)-Leu-Lys(2*)-Ala-Trp (18)

17 (15.91 mg, 0.01301 mmol) was metallated using $Gd(OH)_3 \cdot 6H_2O$ (3.20 mg, 0.01536 mmol, 1.2

equivalents) using the same method as described for **5**. The crude product was purified using

preparative RP-HPLC (Solvent A = H_2O, Solvent B = MeCN; flow rate = 15 mL/min; gradient

starting at 0% B and ramping to 1% B over 15 seconds, hold isocratic 1% B for 29 minutes 45

seconds, ramp to 100% B over 5 minutes, hold isocratic 100% B for 5 minutes, ramp to 0% B

over 5 minutes, hold isocratic 0% B for 15 minutes; fluorescence detection of Gd^{3+} λ_{ex} = 275 nm,

λ_{em} = 314 nm; UV/vis detection at 205 nm and 270 nm) by injecting sample (11.44 mg)

dissolved in water (3 mL, 0.22 μm filtered) with the desired product eluting at ~35 minutes 45

seconds. MeCN was removed by rotary evaporation under reduced pressure. The remaining

aqueous solution was frozen in liquid N_2 and lyophilized to yield 4.39 mg (24% yield) of **18** as a

white powder. Metalation was confirmed by ICP-MS.

Europium(III)-Pro-Leu-Lys(2*)-Leu-Lys(2*)-Ala-Trp (19)

17 (10.41 mg, 0.008512 mmol) was metallated with Eu(OH)$_3$ (2.98 mg, 0.01468, 1.7 equivalents) using the same method as described for **5** to yield 5.4 mg crude **19** which was purified using the same method as described for **18** to yield 2.70 mg (23% yield) of **19** as a white powder. Metalation was confirmed by ICP-MS.

Part II.B.

The diaminopropionic acid (Dap) -based contrast agent was synthesized using the same methods as the lysine-based agent (above), starting with tryptophan(Boc)-Wang resin (758.09 g, 0.59 mmol/g resin loading, 0.45 mmol tryptophan) and substituting fmoc-Dap(Mtt)-OH and Dde-Dap(fmoc)-OH residues for fmoc-Lys(Mtt)-OH and Dde-Lys(fmoc)-OH residues, respectively. As above, key intermediates were characterized using ESI-MS.

Dde-Dap-Leu-Dap-Ala-Trp (20)

ESI-MS: Calc. 724.39; Found negative mode 725.45 (M$^-$)

Dde-Dap(2*)-Leu-Dap-Ala-Trp (21)

ESI-MS: Calc. 1110.57; Found positive mode 1113.36 (M + H$^+$), 1135.82 (M + Na$^+$)

Dde-Dap(2*)-Leu-Dap(2*)-Ala-Trp (22)

ESI-MS: Calc. 1092.56; Found negative mode 362.86 (M/3)

Pro-Leu-Dap(2*)-Leu-Dap(2*)-Ala-Trp (23)

The crude product (275.42 mg) was purified using preparative RP-HPLC: Solvent A = H_2O,

Solvent B = MeCN; flow rate = 15 mL/min; gradient starting at 0 % B and ramping to 10% B

over 5 minutes, hold isocratic 10% B for 10 minutes, ramp to 20% B over 5 minutes, hold

isocratic 20% B for 5 minutes, ramp to 30% B over 5 minutes, hold isocratic 30% B for 5

minutes, ramp to 100% B over 5 minutes, hold isocratic 100% B for 5 minutes, ramp to 0%B

over 5 minutes, hold isocratic 0% B for 5 minutes; fluorescence detection of tryptophan λ_{ex} =

250 nm, λ_{em} = 350 nm; UV/vis detection at 205 nm and 270 nm) by injecting sample (typically

~131 mg per injection) dissolved in water (3 mL, 0.22 µm filtered) with the desired product

eluting at ~24-26 minutes. MeCN was removed by rotary evaporation under reduced pressure.

The remaining aqueous solution was frozen in liquid N_2 and lyophilized (typically ~21.40 mg

isolated product per injection) to yield 38.60 mg (8% overall yield SPPS reactions, 3% overall

yield including the 5 steps required to synthesize **2**) of **23** as a white solid.

ESI-MS: Calc. 1138.61, Found negative mode 1137.63 (M⁻), positive mode 1159.54 (M + Na⁺)

Gadolinium(III)-Pro-Leu-Dap(2*)-Leu-Dap(2*)-Ala-Trp (24)

23 (11.54 mg, 0.01016 mmol) was metallated with $Gd(OH)_3 \cdot 6H_2O$ (3.54 mg, 0.0112 mmol, 1.1

equivalents) using the same method as described for **5**. The crude product (12.24 mg) was

purified using preparative RP-HPLC (Solvent A = H_2O, Solvent B = MeCN; flow rate = 15

mL/min; gradient starting at 0% B and ramping to 1% B over 15 seconds, hold isocratic 1% B for

29 minutes 45 seconds, ramp to 100% B over 5 minutes, hold isocratic 100% B for 5 minutes,

ramp to 0% B over 5 minutes, hold isocratic 0% B for 15 minutes; fluorescence detection of Gd^{3+}

$\lambda_{ex} = 275$ nm, $\lambda_{em} = 314$ nm; UV/vis detection at 205 nm and 270 nm) by injecting sample (11.44

mg dissolved in 3 mL water; 0.22 μm filtered) with the desired product eluting at ~35 minutes

45 seconds.) MeCN was removed by rotary evaporation under reduced pressure. The remaining

aqueous solution was frozen in liquid N_2 and lyophilized to yield 4.39 mg (33% yield) of **24** as a

white powder. Metalation was confirmed by ICP-MS.

ESI-MS: Calc. 1294.52, Found positive mode 1409.86 (M + TFA$^+$)

Europium(III)-Pro-Leu-Dap(2*)-Leu-Dap(2*)-Ala-Trp (25)

23 (7.30 mg, 0.00641 mmol) was metallated with Eu(OH)$_3$ (2.36 mg, 0.007589 mmol, 1.2

equivalents) using the same method as described for **5** to yield 9.36 mg crude **25** of which 8.73

mg was purified using the same method as described for **24** to yield 0.78 mg (9%) of **25** as a

white powder. Metalation was confirmed by ICP-MS.

Determination of *q*:

Luminescence Decay method:

1 mg of **6** or **18** was dissolved in 500μL of H_2O. Time-resolved luminescence spectra were

acquired with the following parameters: 395 nm excitation wavelength, 614 nm emission

wavelength, 10nm excitation slit width, 10nm emission slit width, 950V PMT, 50 replicates.

Data were fit to a single exponential decay using Origin version 7.0. The equation from

Supkowski and coworkers (Equation 2.1, Results and Discussion), with corrections applied for 2

amide functionalities, was used to determine *q*.[17]

Dysprosium Induced Shift method:

The number of inner-sphere water molecules of **7** was determined using the method of Alpoim and coworkers.[20] 40 µL of ^{17}O enriched water (10% ^{17}O enrichment; Medical Isotopes, Inc., Pelham, New Hampshire) was added to 760 µL of 80% H_2O/ 20% D_2O solution and split into two 400 µL aliquots. One aliquot was used to dissolve 56.0 mg of **7** to form a 100 mM stock solution. The other aliquot was used to dilute the stock solution to final solutions consisting of 0, 10, 20, 40, 60, 80, 100 mM **7**. 50 µL of each solution was placed in an NMR tube insert while 25 µL of the remaining sample was used for determining Dy^{3+} concentration in each sample by ICP-MS. The ^{17}O NMR chemical shift of bulk water was measured for each concentration at 25.0 ^{o}C on a Varian Inova 400 (tuned to 54.310 MHz ^{17}O frequency) and compared to similarly prepared solutions of $DyCl_3$.

Laser Luminescence Decay method:

Laser luminescence was performed in collaboration with the research group of Professor Janet Morrow at the University at Buffalo, SUNY. Samples in water were prepared consisting of 0.5 mM **6**, **13**, **19**, or **25**; 100 mM $NaNO_3$ (to control ionic strength); and 20 mM HEPES buffer. D_2O samples were prepared by three successive lyophilizations/reconstitutions of **6**, **13**, **19**, or **25** with D_2O (to fully substitute deuterium for exchangeable protons) followed by preparation in D_2O as described for the H_2O samples. Spectra were acquired on a Spectra-Physics Quanta Ray PRO-270-10 Q-switched Nd: YAG pump laser (10 Hz, 60-70 mJ pulse^{-1}) with a MOPO SL. Excitation spectra of the Eu^{3+} $^{7}F_o \rightarrow {}^{5}D_o$ transition were recorded at 0.01 nm increments between 578-581 nm for each complex to determine the excitation frequency to be used for lifetime

decays. The $^5D_0 \rightarrow {}^7F_2$ emission was passed through a 628 nm band-pass filter (Semrock, model

FF01-628/27-25) and focused onto a time-grated photomultiplier tube module (Hamamatsu,

model H 7680-01 MOD). Time resolved luminescence measurements were collected using a

digital Tektronix TDS 3034B oscilloscope. An average of three trials was used for **6** and **19**. An

average of five trials was used for **13** and **25**. Data were fit to a single exponential decay (with

$R^2 > 0.99$ for each fit) using Origin version 7.0. The equation from Supkowski and coworkers

(Equation 2.1, Results and Discussion), with corrections applied for 2 amide functionalities, was

used to determine q.[17]

Relaxivity

Stock solutions consisting of 0.200 mM of **5** or **12** in Caspase-3 assay buffer (50 mM HEPES,

100 mM NaCl, 10 mM DTT, 1 mM EDTA, 10% sucrose, 0.1% CHAPS, 1 mg/mL BSA, pH 7.4)

or **18** or **24** in MMP-7 assay buffer (50 mM tris HCl, 150 mM NaCl, 10 mM $CaCl_2$, 1 mg/mL

BSA, pH 7.5) were prepared. Serial dilutions of the stock solutions produced concentrations of

0.100 mM, 0.050 mM, 0.025 mM. Twenty five microliters of each sample were used for

determining Gd^{3+} concentration using ICP-MS. Samples were equilibrated to 37 ^{o}C in a water

bath for 10 minutes prior to T_1 measurement. The T_1 of each solution was determined using an

inversion recovery pulse sequence with appropriate recycle delays (>5*T_1). The resulting curves

were fit to a monoexponential function to obtain T_1. A plot of 1/T_1 vs. concentration was fit to a

straight line yielding the relaxivity as the slope.

Relaxivity vs. pH

A 1 mM solution of **5** was prepared in 2 mL water. The solution was split into two 800 μL

aliquots: one was used for the acidic range and the other for the basic range. The pH was

adjusted into either the acidic range using HCl vapor (as to not change the concentration of the

solution) or the basic range using NaOH (using 0.5 μL additions of 5 mM, 50 mM, or 500 mM

NaOH; more concentrated NaOH solutions were used as the solution became increasingly basic).

For the basic range, the volume of NaOH added was recorded and used to correct the final

concentrations (the correction proved negligible as a total of 47.5 μL of NaOH was added to 800

μL initial solution; a 5.9% increase in volume). Gd^{3+} concentration was determined using ICP-

MS. The samples were allowed to equilibrate at 37 ^{o}C for 5 minutes before each T_1

measurement. The T_1 of each solution was determined using an inversion recovery pulse

sequence with appropriate recycle delays ($>5*T_1$). The resulting curves were fit to a

monoexponential function to obtain T_1. The difference in T_1 values vs. water were used to

determine the relative relaxivity at each pH.

Mean Water Residence Lifetime

The method of Micskei and coworkers was used to determine the mean water residence

lifetime.[26] Samples were prepared as 225 microliters of 20 mM **5**, **12**, **18**, or **24** in water with 25

microliters of ^{17}O enriched water (10% ^{17}O enrichment; Medical Isotopes, Inc., Pelham, New

Hampshire) added, resulting in 1% ^{17}O enrichment in the final sample. This solution was placed

in an NMR tube with an insert containing D_2O (for lock reference). A water standard was

prepared consisting of 1% ^{17}O enriched water with D_2O insert. VT-NMR was acquired on a

Varian Inova 400 (tuned to 54.310 MHz ^{17}O frequency) at 5 $^{\circ}$C intervals between 1 $^{\circ}$C and 90 $^{\circ}$C.

Temperatures were corrected using a calibration plot. The samples were equilibrated for 10

minutes at each temperature, followed by lock and shim. The ^{17}O linewidth of the bulk water

was measured at each temperature. The pH of the samples was recorded and Gd^{3+} concentrations

were determined by ICP-MS. Data were fit using equation 2.2 in Origin version 7.0.

Equation 2.2 (adapted from literature[25,26] to incorporate 2-isomer model):

F=400;s=3.5;univ=8.31;wi=6.28e6*F*0.13557;ws=6.28e6*F*658.21; tmB=((tm0B^(-1)*x/298.15)*exp((HmB/univ)*(0.003354-(1/x))))^-1; tmA=((tm0A^(-1)*x/298.15)*exp((HmA/univ)*(0.003354-(1/x))))^-1; trB=((tr0B^(-1)*x/298.15)*exp((HrB/univ)*(0.003354-(1/x))))^-1; trA=((tr0A^(-1)*x/298.15)*exp((HrA/univ)*(0.003354-(1/x))))^-1; tvB=((tv0B^(-1)*x/298.15)*exp((HvB/univ)*(0.003354-(1/x))))^-1; tvA=((tv0A^(-1)*x/298.15)*exp((HvA/univ)*(0.003354-(1/x))))^-1; T1eB=((1/25)*deltaB*tvB*(4*s^2+4*s-3)*((1/(1+ws^2*tvB^2))+(4/(1+4*ws^2*tvB^2))))^-1; T1eA=((1/25)*deltaA*tvA*(4*s^2+4*s-3)*((1/(1+ws^2*tvA^2))+(4/(1+4*ws^2*tvA^2))))^-1; T2eB=((0.02*(4*s^2+4*s-3)*tvB*deltaB*(3+(5/(1+(ws^2*tvB^2)))+(2/(1+(4*ws^2*tvB^2))))))^(-1);
T2eA=((0.02*(4*s^2+4*s-3)*tvA*deltaA*(3+(5/(1+(ws^2*tvA^2)))+(2/(1+(4*ws^2*tvA^2))))))^(-1); tc1B=(T1eB^(-1)+trB^(-1)+tmB^(-1))^(-1); tc1A=(T1eA^(-1)+trA^(-1)+tmA^(-1))^(-1); tc2B=(T2eB^(-1)+trB^(-1)+tmB^(-1))^(-1); tc2A=(T2eA^(-1)+trA^(-1)+tmA^(-1))^(-1); te1B=(T1eB^-1+tmB^-1)^(-1); te1A=(T1eA^-1+tmA^-1)^(-1); te2B=(T2eB^(-1)+tmB^(-1))^(-1); te2A=(T2eA^(-1)+tmA^(-1))^(-1);
contB=(1/3)*s*(s+1)*accB^2*(te1B+(te2B/(1+ws^2*te2B^2))); contA=(1/3)*s*(s+1)*accA^2*(te1A+(te2A/(1+ws^2*te2A^2))); dip1B=((1/15)*4.535671e-33*s*(s+1))/(rB^6); dip1A=((1/15)*4.535671e-33*s*(s+1))/(rA^6); dip2B=4*tc1B; dip2A=4*tc1A; dip3B=(13*tc2B)/(1+ws^2*tc2B^2); dip3A=(13*tc2A)/(1+ws^2*tc2A^2); dip4B=(3*tc1B)/(1+wi^2*tc1B^2); dip4A=(3*tc1A)/(1+wi^2*tc1A^2); dip9=1.6995e14*0.32; dip5B=(0.2*trB)/(1+wi^2*trB^2); dip5A=(0.2*trA)/(1+wi^2*trA^2); dip6B=(0.8*trB)/(1+4*wi^2*trB^2); dip6A=(0.8*trA)/(1+4*wi^2*trA^2); dip7B=(2/5)*(wi^2*1.1890597e-79*s^2*(s+1)^2)/(9*1.9063324e-32*x^2*rB^6); dip7A=(2/5)*(wi^2*1.1890597e-79*s^2*(s+1)^2)/(9*1.9063324e-32*x^2*rA^6); dip8B=(3*tc1B)/(1+wi^2*tc1B^2); dip8A=(3*tc1A)/(1+wi^2*tc1A^2); dipB=dip1B*(dip2B+dip3B+dip4B); dipA=dip1A*(dip2A+dip3A+dip4A); quadB=dip9*(dip5B+dip6B); quadA=dip9*(dip5A+dip6A); curB=dip7B*dip8B; curA=dip7A*dip8A; diptotB=dipB+curB+quadB; diptotA=dipA+curA+quadA; T2mB=(contB+diptotB)^-1; T2mA=(contA+diptotA)^-1; gauss=F*1e6/4255.319; dwmB=(1.856953e-20*s*(s+1)*accB*gauss)/(3*1.3807e-16*x); dwmA=(1.856953e-20*s*(s+1)*accA*gauss)/(3*1.3807e-16*x); numB=(T2mB^-2)+(T2mB*tmB)^-1+dwmB^2;

numA=(T2mA^-2)+(T2mA*tmA)^-1+dwmA^2; denomB=(tmB^-1+T2mB^-1)^2+dwmB^2; denomA=(tmA^-1+T2mA^-1)^2+dwmA^2; ScamB=numB/denomB; ScamA=numA/denomA ; pmB=n*(1-XA)*conc/55.56; pmA=n*XA*conc/55.56; y=(pmA*scamA/tmA)+(pmB*scamB/tmB)

Note: A and B refer to each of the two isomers; because the relative ratios of isomers A and B as a function of temperature could not be determined experimentally (see Results and Discussion, Part I. A.), the mole fraction of A and B was allowed to vary during the fitting.

Definitions of fitting parameters:

deltaA, deltaB = the trace of the zero-field-splitting tensor for isomers A and B; tm0A, tm0B = the mean water residence lifetime of isomers A and B; HmA, HmB = enthalpy of water exchange for isomers A and B; tr0A, tr0B = the rotational correlation time of isomers A and B (set 50 ps to agree with literature values[66] of small molecule Gd^{3+} contrast agents); HrA, HrB = enthalpy of rotation for isomers A and B; tv0A, tv0B = the correlation time for the modulation of the zero-field-splitting tensor for isomers A and B; HvA, HvB is the enthalpy of the tv0 correlation time for isomers A and B; accA, accB = $A/\hbar$ = the scalar coupling constant between the electrons of Gd^{3+} and the protons of the inner sphere water for isomers A and B (set to -3800000 rad/s); rA, rB = the distance between the paramagnetic ion and the oxygen of the inner-sphere water for isomers A and B (set to literature value[26] for DOTA, 2.5 Å); n = the number of inner sphere waters (set to 1; determined experimentally – see Results and Discussion, Part I. A.); conc = concentration of the paramagnetic ion (determined experimentally by ICP-MS); XA = the fraction of isomer A present in solution

MMP-7 Enzyme Study

Enzyme activity

Human recombinant MMP-7 was purchased from Anaspec (San Jose, CA). MMP-7 was divided

into either 2 μL aliquots (used for fluorescence) or 20 μL aliquots (used for T_1 measurements).

Each aliquot contained 10 μg/mL units each [> 600 units/μg; one unit hydrolyzes 1 pmol of

Mca-Pro-Leu-Gly-Leu-Dap(Dnp)-Ala-Arg-NH$_2$ per minute at pH 7.5 at 25 ^{o}C] and was stored at

-80 ^{o}C. The MMP-7 assay buffer consisted of 50 mM tris HCl, 150 mM NaCl, 10 mM CaCl$_2$, 1

mg/mL BSA, pH 7.5. MMP-7 was activated by incubation in 1mM APMA in assay buffer for 1

hour at 37 ^{o}C prior to use. Enzyme activity was confirmed using a SensoLyte 490 MMP-7

fluorescence assay kit (purchased from Anaspec; used according to manufacturer instructions).

The enzyme was active for up to 50 hours (indicated by periodic addition of fresh substrate and

monitoring the fluorescence intensity), however the activity decreased slowly with time.

T_1 Enzyme Study

0.49 mg of **24** was added to 17.5μL H$_2$O to form a 20 mM solution (exact concentration later

determined using ICP-MS) and used in place of the fluorescent substrate in the MMP-7 assay kit.

T_1 measurements of MMP-7 assay buffer with and without 1 mM APMA and **24** in buffer with

and without 1 mM APMA were recorded. 3.5μL of the 20 mM solution of **24** was added to the

activated enzyme and T_1 measurements were immediately taken at periodic time intervals for 48

hours. 3.5μL of the fluorescent peptide substrate from the MMP-7 assay kit was placed in a

separate 350 μL vial of activated MMP-7 and fluorescence measurements were taken in parallel

to T_1 measurements to confirm enzyme activity throughout the experiment. As a control, T_1

measurements were taken of **24** in buffer solution (with 1 mM APMA) lacking active MMP-7.

Gd^{3+} concentrations of all solutions were determined by ICP-MS.

CHAPTER III

A SELF-IMMOLATIVE MAGNETIC RESONANCE IMAGING CONTRAST AGENT FOR THE DETECTION OF CASPASE-3

The text in this chapter is taken in part from:

INTRODUCTION

Caspase-3

An introduction to caspase-3 can be found in Chapter II, Part I.

Design of a Self-Immolative Agent Activated by Caspase-3

Caspase-3 cleaves substrates containing the DEVD^X motif, where X denotes a variety

of amino acids and ^ denotes the cleavage site.[1] The variability in the P_1' residue (the amino

acid on the C-terminal side of the cleavage site; see Figure 2.5, Chapter II for nomenclature) that

is tolerated by caspase-3 allows non-natural substrates to be cleaved by the enzyme. This has

allowed the development of colorimetric assays. The commercially available caspase-3

colorimetric assay used in the present work consists of a *para*-nitroaniline (pNA) moiety on the

C-terminus of Ac-DEVD (Figure 3.1). Upon cleavage by caspase-3, the liberated pNA gives a

distinct yellow color, which can be quantified by measuring the absorbance of the assay solution

at 405 nm. By exchanging the pNA chromophore with a structurally similar linkage to a MRI

contrast agent, an MR version of this reporter system has been developed.
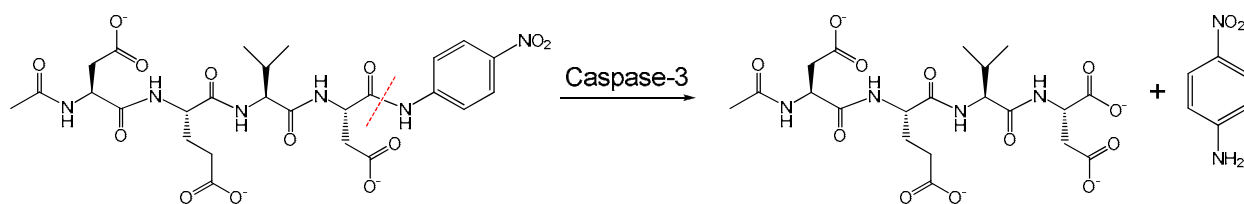
Figure 3.1 Commercially available colorimetric assay for caspase-3 consisting of Ac-DEVD-pNA, which releases the chromophore pNA upon enzymatic cleavage (enzymatic cleavage site denoted with red dashed line)

The linkage chosen for the MRI contrast agent is based on previous reports of self-immolative linkers. Originally developed as an integral part of a prodrug, the self-immolative linker features a substituted benzyl alcohol which rearranges to a reactive quinone intermediate. Nucleophilic attack by water (which is ubiquitous in biological systems) causes a rearrangement which releases the active drug.[2] Since this seminal report, several variations of self-immolative linkers have surfaced in the literature. With publication dates differing by only one week, de Groot and coworkers and Amir and coworkers independently developed an interesting series of dendrimers with self-immolative linkages.[3,4] A single cleavage event initiates a propagation of self-immolation throughout the dendrimer core, ultimately releasing an active drug. Jones and coworkers developed a fluorescence assay based on a self-immolative linkage between a peptide sequence cleaved by prostate specific antigen and Rhodamine 110.[5] De Graaf and coworkers used a self-immolative linkage to create a prodrug in order to improve the therapeutic index of the potent cytotoxic anti-cancer drug doxorubicin.[6] Alaoui and coworkers shortly thereafter developed a similar prodrug system for paclitaxel.[7,8] Abraham and coworkers recently enhanced the capabilities of prodrug therapy by adding a targeting antibody to a self-immolative doxorubicin prodrug.[9]

Recent efforts in the Meade laboratory involve the use of a self-immolative linker between β-glucuronic acid and an MRI contrast agent.[10] Upon cleavage of the substrate by β-glucuronidase, the linker rearranges and releases a contrast agent, resulting in up to a 15% change in T_1. This relaxivity of this prototype agent was dependent on the buffer system employed. The addition of carbonate and/or phosphate had an influence on the relaxivity of the agent, due to the ability of these anions to coordinate to the paramagnetic metal. The binding of carbonate to the gadolinium(III) complex was determined to be weak due to the lack of

saturation upon titration of up to 36 mM carbonate. The weak carbonate binding was attributed to the overall neutral charge of the complex.

Work described in the present chapter aimed to build upon the information obtained by Duimstra and coworkers to develop a self-immolative MRI contrast agent for the detection of caspase-3. Exchanging the β-glucuronic acid used by Duimstra and coworkers with the caspase-3 substrate, DEVD, allowed the detection of a different class of enzymes. Due to the restriction that caspase-3 only cleaves amide bonds, the self-immolative linker used by Duimstra and coworkers[10] (which featured a glycosidic linkage) had to be substituted with a version similar to that used by Alaoui and coworkers[7] (which featured an aniline-based linkage). The resulting cleavage by-product, 4-aminobenzyl alcohol, has been shown to be non-toxic.[6] Exchanging the lanthanide chelate pendant arms from negatively charged acetate groups to neutral amides resulted in a greater affinity for carbonate anion.

The anion-binding of lanthanide complexes containing amides was extensively studied by Bruce and coworkers.[11] In particular, lanthanide complexes of the tris-amide ligand (RRR)-1,4,7-tris[1-(1-phenyl)ethylcarbomoylmethyl]-(1,4,7,10-tetraazacyclododecane) displayed a high affinity for carbonate and other biologically relevant anions such as citrate, lactate, and acetate.[11] Using europium(III) luminescence, Bruce and coworkers showed that carbonate can bind to tris-amide complexes and displace inner-sphere water molecules, resulting in $q = 0$ complexes.[11] It was hypothesized that a variation of this ligand could be used with the present system in an effort to effectively block inner-sphere water access through the binding of endogenous carbonate to the lanthanide. Cleavage of the DEVD substrate by caspase-3 and subsequent degradation of the self-immolative linker would result in the formation of a primary amine pendant arm (Figure 3.2). It was hypothesized that this newly formed primary amine would coordinate to the

lanthanide, displacing the carbonate, resulting in a complex with one inner-sphere water

molecule ($q = 1$). The hypothesized change in q from 0 (carbonate bound) to 1 would result in a

dramatic increase in the relaxivity of the contrast agent. This change in relaxivity could be used

as a method to monitor caspase-3 activity in vivo.

It should be noted that the near similar sequence specificity[1] of caspase-3 and caspase-7

would most likely make **5** a substrate for both enzymes. However, for simplicity, only caspase-3

cleavage will be addressed in the following discussion.
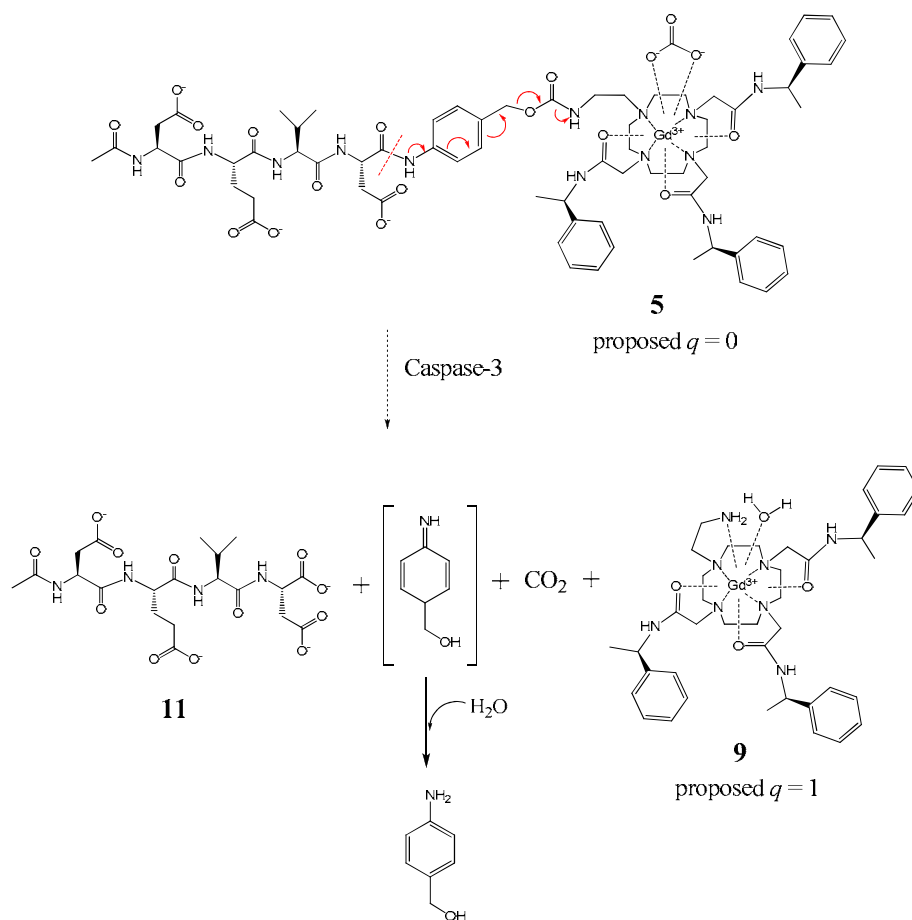
Figure 3.2. Proposed mechanism of relaxivity change upon cleavage by caspase-3. Carbonate is proposed to bind to 5 resulting in a $q = 0$ complex. Enzymatic cleavage (at red dashed line) initiates an electron cascade (red arrows), producing 9 in which the amine is proposed to bind to gadolinium(III), displacing carbonate, and allowing inner-sphere water access.

RESULTS AND DISCUSSION

<u>Synthesis</u>

The synthesis of **5** was accomplished in 15 steps with an overall yield of 2% (Schemes 3.1-3.4). The convergent synthesis of **5** involved two facets: synthesis of the substrate peptide with a self-immolative linker and synthesis of the lanthanide chelate.

The protected peptide, **1**, was synthesized by Solid-Phase Peptide Synthesis (SPPS) using standard fmoc protecting strategy, with *tert*-butyl protection of the aspartic and glutamic acid side-chains (Scheme 3.1). The extremely acid-labile NovaSyn TGT resin allowed **1** to be cleaved from the resin without removal of the side-chain *tert*-butyl protecting groups. The use of excess reagents and repeated SPPS reactions allowed the synthesis of **1** in gram quantities in exceptionally high yield (87% after 9 steps).

Coupling of 4-aminobenzyl alcohol to the C-terminus of **1** followed by reaction with bromoethylisocyanate resulted in the formation of the self-immolative linker. The alkyl bromide of **3** proved to be an efficient leaving group for nucleophilic substitution by the secondary amine of the chelate.

The chelate was synthesized from commercially available cyclen in one step according to published procedures[12] (Scheme 3.3). The separation of the mono-, di-, tri-, and tetra-substituted products proved to be non-trivial. After several attempts of the published procedures[11,12] to separate the byproducts using alumina chromatography, the use of RP-HPLC was warranted to obtain the chelate in acceptable purity. Within the present work, the yield of the desired tris-alkylated product was reproducibly 27-29%; the reported literature[12] yield of 78% is disproportionately high for reactions of this type and warrants suspicion.

The S_{N2} reaction between the chelate and **3** combined the self-immolative linker with the chelate, producing **4** (Scheme 3.3). Initial attempts at removal of the *tert*-butyl groups from **4** using strong acid (TFA or formic acid) resulted in unwanted hydrolysis of the carbamate of the self-immolative linkage. Seeking to avoid harsh acidic treatment, an inspection of the literature revealed reports of the use of $ZnBr_2$ in the removal of *tert*-butyl groups from carboxylic acids in the presence of acid-labile groups.[13,14] The use of $ZnBr_2$ was effective in removing the *tert*-butyl groups from **4**, however, the resulting product had appreciable amounts of Zn^{2+} (as evidenced by ICP-MS and the distinctive Zn^{2+} isotope pattern in ESI-MS), which was presumably bound in the macrocyclic chelate. The affinity of tetraazacyclododecanes for Zn^{2+} is well documented.[15] Subsequent metalation with $Gd(OH)_3$ resulted in low yields due to the considerable amount of undesired Zn^{2+}-adduct (64% zinc, 33 % gadolinium by ICP-MS; ESI-MS showed Zn^{2+}-adduct as major peak and Gd^{3+}-adduct as minor peak). The problem of undesired zinc metalation was circumvented by simple reversal of the final two synthetic steps (Scheme 3.4). The insolubility of **4** in the aqueous solutions normally employed for metalation with gadolinium(III) warranted the use of the triflate salt such that the metalation could be carried out in organic solvents. After **4** was metallated with $Gd(CF_3SO_3)_3$, the *tert*-butyl groups were removed using $ZnBr_2$ followed by a phase transfer into aqueous conditions. After purification by preparative RP-HPLC, **5** showed no signs of Zn^{2+} metalation (as evidenced by ICP-MS and ESI-MS). Using an analogous method, **6** was synthesized for luminescence studies.
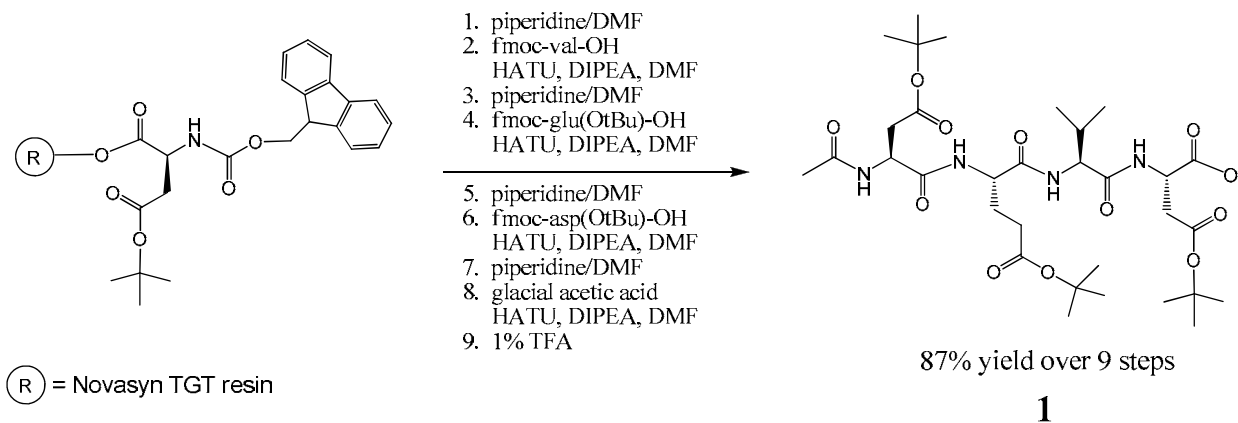
Scheme 3.1 Synthesis of 1 using solid-phase peptide synthesis
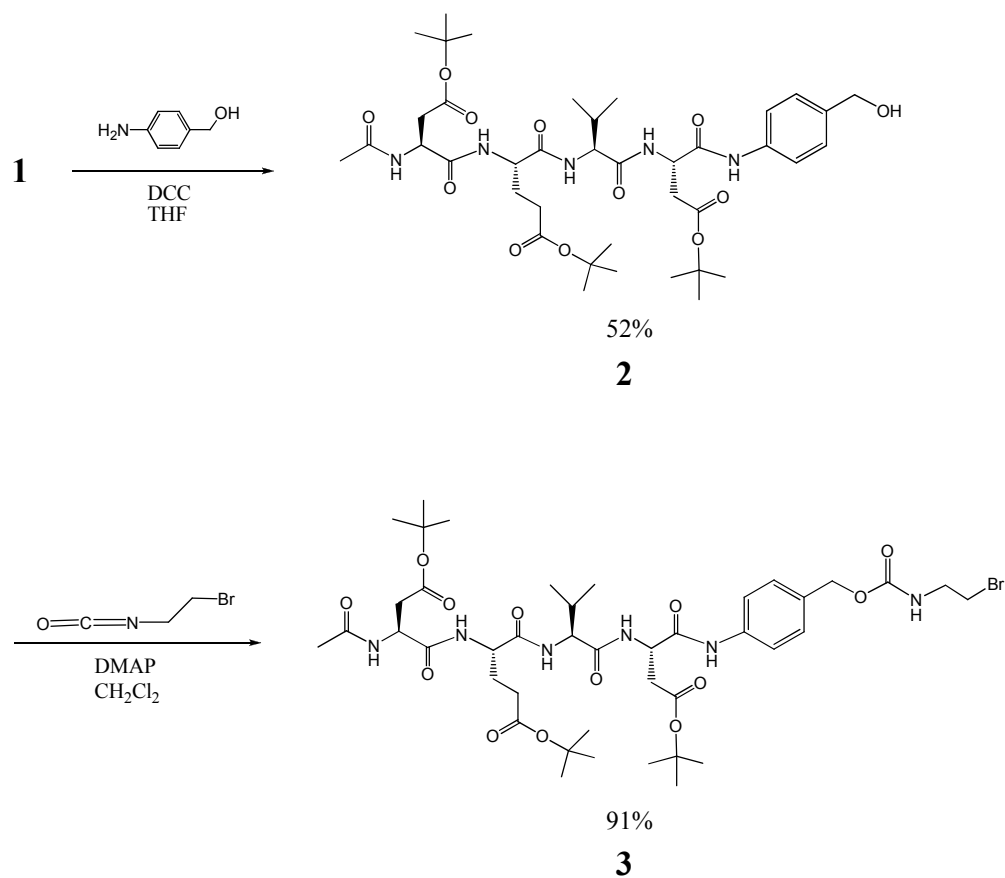
Scheme 3.2 Synthesis of intermediates 2 and 3

28%

55%

4
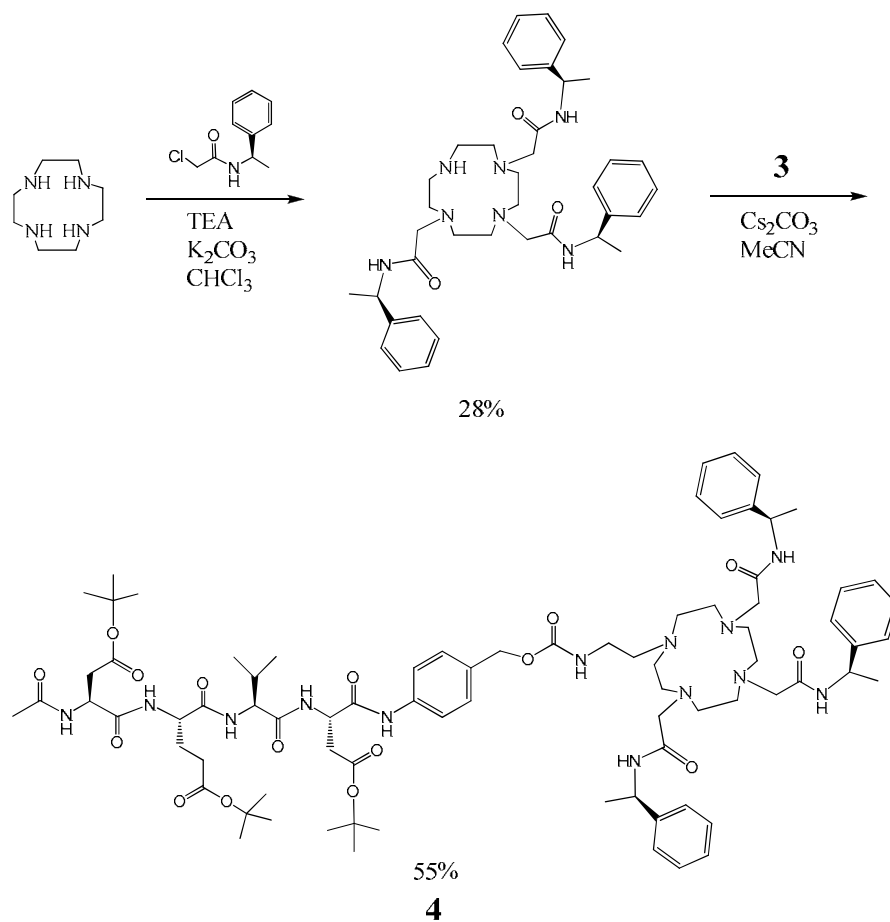
Scheme 3.3 Synthesis of chelate and coupling to 3 to yield 4 (step 1 based on literature[12])

$Ln^{3+} = Gd^{3+}$, **5**, 37%
Eu^{3+}, **6**, 41%
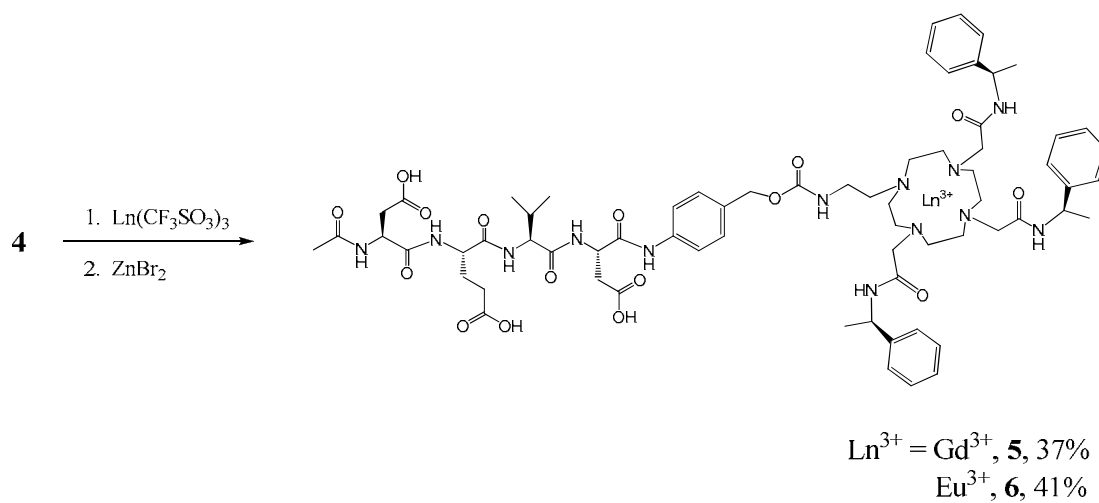
Scheme 3.4 Metalation of 4 with gadolinium(III) or europium(III) followed by *tert*-butyl deprotection using ZnBr$_2$ results in target compounds 5 and 6, respectively.

In order to simulate the effects of enzymatic cleavage and to provide authentic standards for comparison, the "cleaved" components, **9-11**, were synthesized (Schemes 3.5 and 3.6). Since **9-11** do not contain the acid-sensitive self-immolative linker, the synthesis was markedly straightforward and the use of TFA to remove *tert*-butyl groups proved effective.
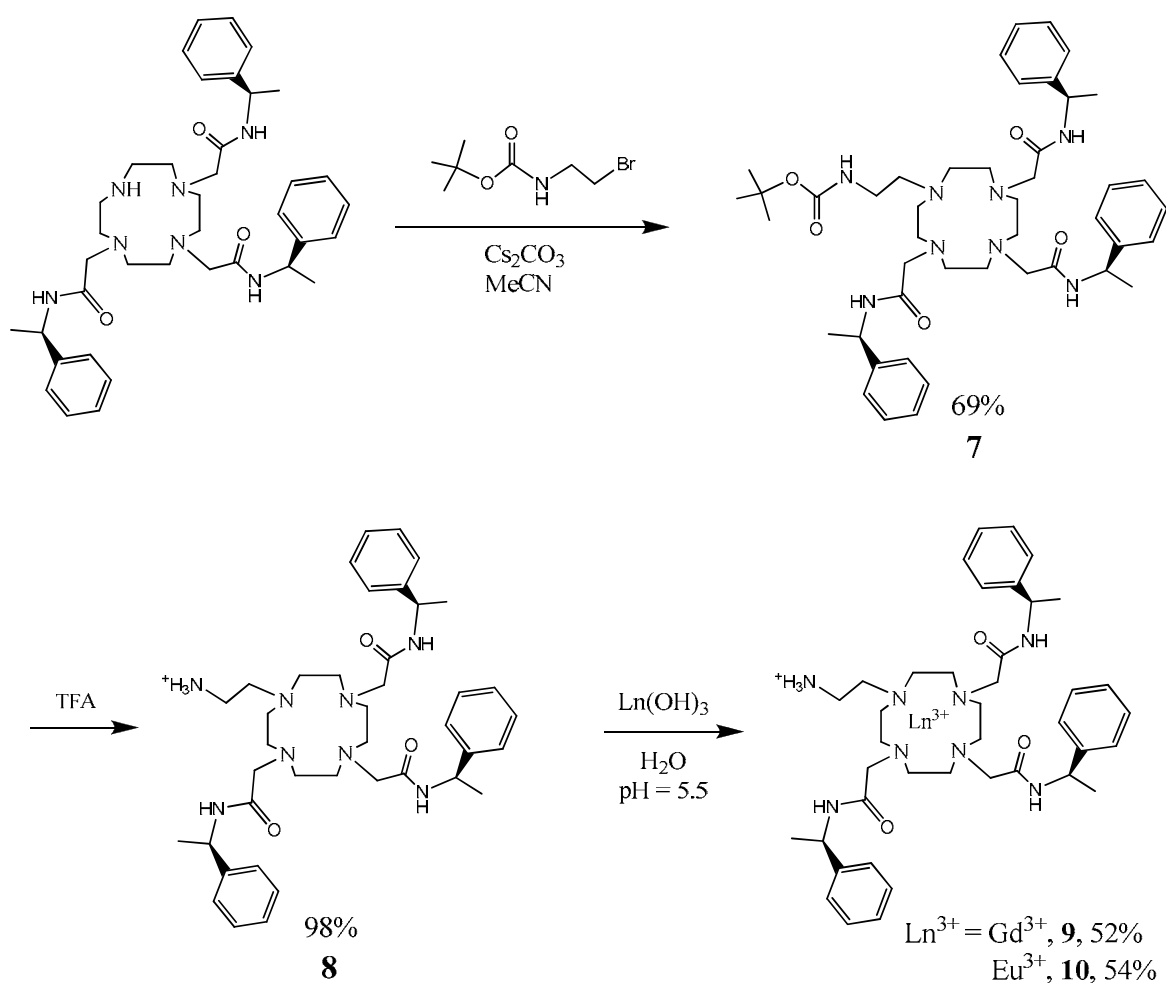
Scheme 3.5 Synthesis of 9 and 10, the chelate portion of the expected enzymatic cleavage products of 5 and 6, respectively.

TFA

99%

1 → **11**
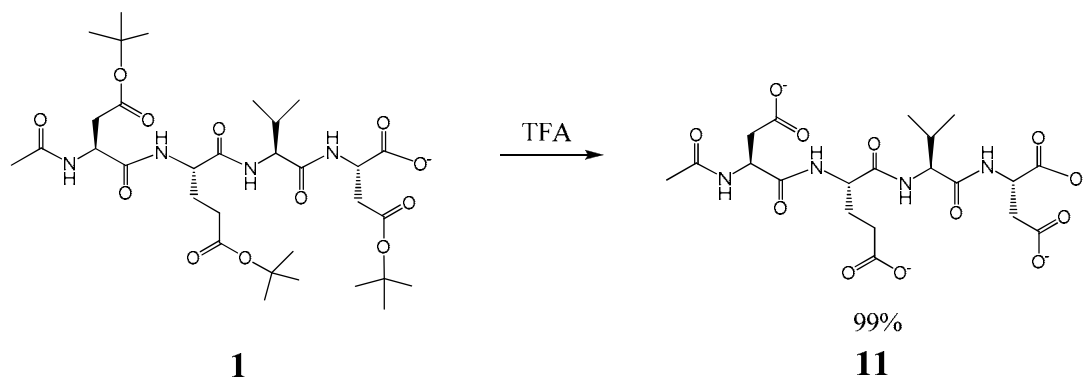
Scheme 3.6 Synthesis of peptide 11, the peptide portion of the expected enzymatic cleavage product of 5 and 6.

Relaxometric Properties (relaxivity, q, τ_m)

The determination of relaxivity and τ_m for **5** and **9** and the determination of q for **6** and **10** were performed using methods described in Chapter II, Part I.A.

The relaxivity of **5** in caspase-3 assay buffer (20 mM HEPES, 2 mM EDTA, 5 mM DTT, 0.1% CHAPS, 1 mg/mL BSA, pH 7.4) is 5.31 mM^{-1}s^{-1} while the relaxivity of the expected enzymatic cleavage product, **9**, is 4.13 mM^{-1}s^{-1}. Since MRI contrast agents have been reported to associate with serum albumin proteins,[16-18] these values were measured in the same buffer without the addition of bovine serum albumin (BSA) and resulted in relaxivities of 4.65 mM^{-1}s^{-1} for **5** and 3.76 mM^{-1}s^{-1} for **9**. The slight increases in relaxivity for **5** and **9** in the presence of BSA can be attributed to the increased viscosity of the solution and are far from the ~10 fold increase in relaxivity experienced by contrast agents which are known to associate with serum albumin proteins.[16-18]

To determine whether carbonate binds to **5** and **9**, the relaxivity of each agent was determined as a function of pH. Lanthanide chelates which bind carbonate show a characteristic

decrease in relaxivity at high pH due to displacement of inner-sphere water by carbonate

(carbonate concentrations increase at high pH).[19] Consequently, the relaxivity vs. pH profile of **5**

shows a significant decrease in relaxivity at pH > 8 which can be attributed to carbonate binding

and displacing the inner-sphere water (Figure 3.3). In contrast, **9** does not display a dramatic

decrease in relaxivity at pH > 8, and it can therefore be concluded that **9** does not bind carbonate

to a significant degree (Figure 3.3). The lack of carbonate binding by **9** is attributed to the

primary amine pendant functionality which is able to coordinate to gadolinium(III), thus

preventing carbonate from binding in a bidentate fashion.

Further analysis of the relaxivity vs. pH profile reveals interesting insight into the

relaxometric behavior of **9**. At low pH values, the increase in relaxivity for **9** is likely due to

increased prototropic exchange. Related amide complexes display an increase in relaxivity at

low pH due to increased prototropic exchange.[19] Dissociation of gadolinium(III) from the

chelate is not expected given that closely related DOTA-tetraamides are reported to be

kinetically inert toward acid-catalyzed dissociation (half-life in 2.5 M HNO_3 at 298 K = 0.2 –

639 hours).[19] The 25-30 fold higher stability of DOTA-tetraamides (as compared to DOTA)

towards acid-catalyzed dissociation is attributed to the difficulty of protonating an amide pendant

arm (as compared to the relative ease of protonating the carboxylic acid pendant arms of

DOTA).[20]

A close inspection of the relaxivity vs. pH profile of **5** and **9** reveals that at physiological

pH (7.4), the relaxivity of **5** in water is higher than that of **9** (Figure 3.3). This trend is in

agreement with the observed differences in relaxivity between **5** and **9** in caspase-3 assay buffer.

At pH 7.4, the majority of carbonate species in solution exists as hydrogencarbonate (carbonate

accounts for <0.2% of carbonated species at pH 7.4 while hydrogencarbonate accounts for

45%).[11] Carbonate binds to 7-coordinate lanthanide chelates in a bidentate fashion while hydrogencarbonate binds in a monodentate fashion.[11] Since the amount of carbonate is extremely low at physiological conditions, the relaxivity change between **5** and **9** does not operate under the proposed carbonate mechanism depicted in Figure 3.2. The relaxivity vs. pH profile shows that carbonate binds to **5** and not to **9**, however, this mechanism of relaxivity modulation can only function when carbonate is present in substantial concentrations (pH > 8) (Figure 3.3). Therefore, at the physiologically relevant pH 7.4, the conversion of **5** to **9** by caspase-3 will result in a change in resultant MR image intensity from bright to dark.
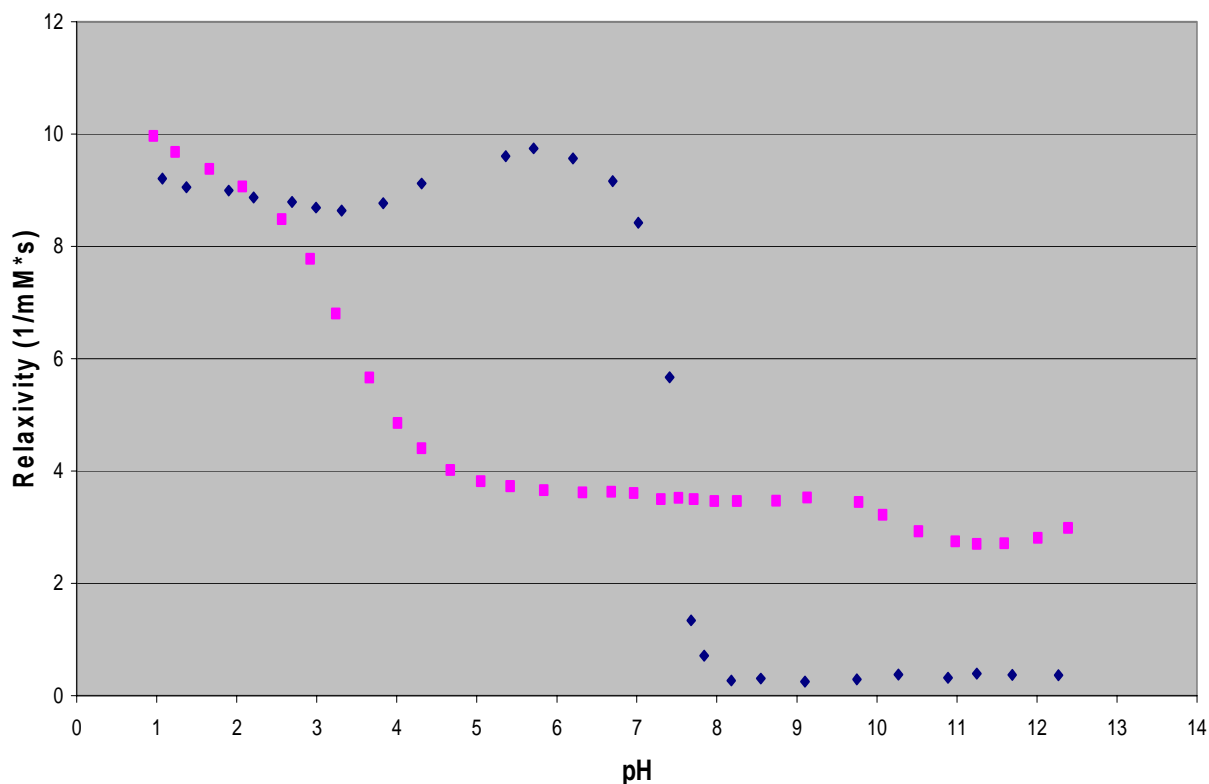
Figure 3.3 Relaxivity vs. pH profiles for 5 (blue diamonds) and 9 (pink squares). The binding of carbonate to 5 displaces inner-sphere water, resulting in a marked decrease in relaxivity at pH > 8 (carbonate concentrations increase dramatically at pH = 8).[11] In contrast, 9 does not exhibit behavior indicative of carbonate binding.

To discern the mechanism by which **5** and **9** differ in relaxivity, the number of inner-sphere waters (q) and the mean water residence lifetime (τ_m) were measured for each complex. The q values obtained using the method of Supkowski and coworkers[21] resulted in $q = 1.8 \pm 0.1$ and $q = 1.7 \pm 0.1$ for **6** and **10**, respectively [the europium(III) analogs of **5** and **9**, respectively]. Since the q values measured for **5** and **9** are within experimental error, this parameter cannot account for the relaxivity difference observed between these two complexes. The τ_m values for **5** and **9** were determined by measuring the transverse relaxation rate of ^{17}O as a function of temperature (Figure 3.4) using the method developed by Micskei and coworkers.[22] The τ_m values of 1.3 ± 0.3 µs and 5.3 ± 0.5 µs for **5** and **9**, respectively, are responsible for the relaxivity difference observed between **5** and **9**. These τ_m values are in accord with published values for related DOTA-trisamide complexes (1.5 µs).[11] It should be noted that τ_m values are strongly influenced by the functionality present on the pendant arms of the chelate: the τ_m values of trisamide-based chelates and tetraamide-based chelates differ by one and two orders of magnitude, respectively, from the τ_m values of acetate-based chelates ($\tau_m = 1.5$ µs for Gd-DOTA-trisamide, $\tau_m = 19$ µs for Gd-DOTA-tetraamide, and $\tau_m = 244$ ns for the acetate-based Gd-DOTA).[11,22,23] Consequently, while acetate-based derivatives of Gd-DOTA have short τ_m values (fast water exchange; $\tau_m = 1/k_{ex}$) and are thus limited in relaxivity by their rotational correlation time (τ_R), the amide-based derivatives of Gd-DOTA are limited in relaxivity by their long τ_m.[24] According to Equation 1.8 (Chapter I), when τ_m is > 0.5 µs, the relaxivity of the complex is limited by τ_m. Therefore, the relaxivity of Gd-DOTA-trisamide complexes is limited by their slow τ_m.[19] In the present work, the tris-amides **5** and **9** are limited in relaxivity by their slow τ_m and the difference in relaxivity observed between **5** and **9** can be attributed to their differences in τ_m.

Further support for the relaxivity of **9** being dominated by a slow τ_m can be found in a simple experiment involving the addition of phosphate anion to a buffered solution of **9**. An interesting phenomenon reported by Bruce and coworkers is the dramatic decrease in τ_m from 1.5 μs to 175 ns upon addition of excess Na_2HPO_4 to a Gd-DOTA-trisamide at pH 7.45.[11] Since the relaxivity of Gd-DOTA-trisamide complexes is limited by τ_m, the addition of Na_2HPO_4 to a Gd-DOTA-trisamide chelate should result in a dramatic increase in relaxivity. Accordingly, in the present work, the addition of 10-fold excess Na_2HPO_4 to **9** resulted in a relaxivity increase from 4.13 $mM^{-1}s^{-1}$ to 6.28 $mM^{-1}s^{-1}$.

In conclusion, the mechanism of relaxivity change between **5** and **9** at physiological pH does not follow the originally proposed q-modulated carbonate mechanism depicted in Figure 3.2. Instead, the relaxivity difference between **5** and **9** is attributed to differing τ_m values and thus **5** can be considered a τ_m-modulated MRI contrast agent. Despite the actual mechanism of action differing from the originally proposed mechanism, **5** still holds much promise to be used as a caspase-3 responsive MRI contrast agent.
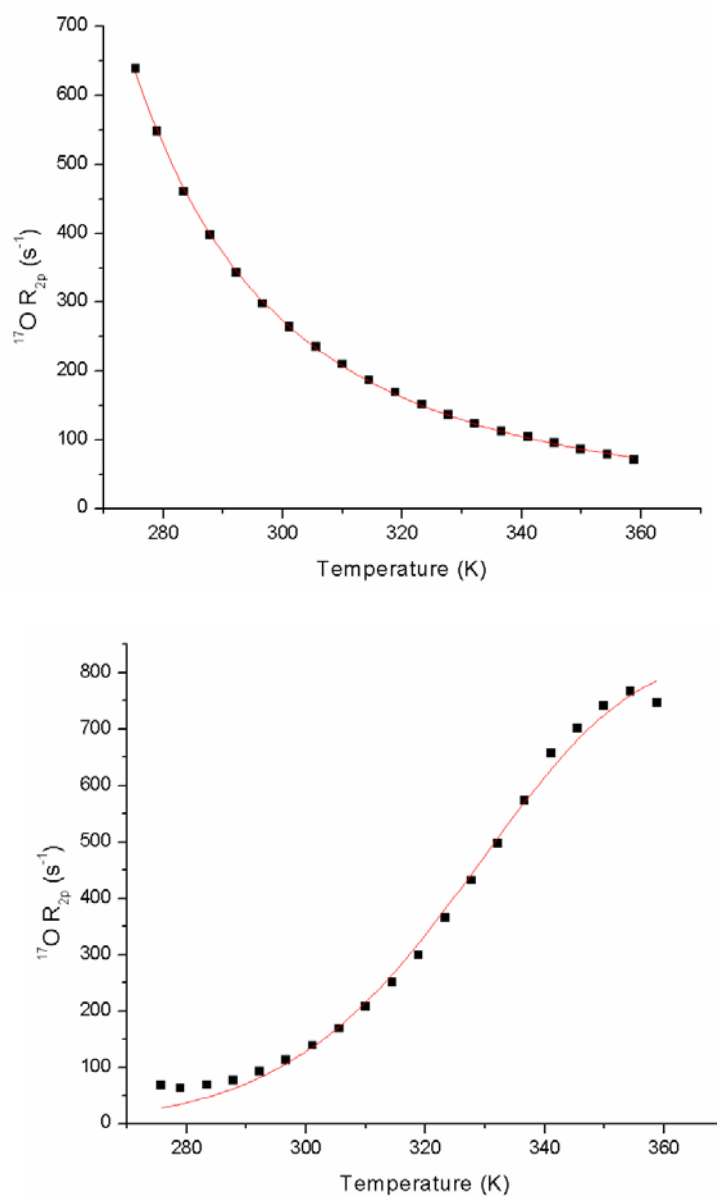
Figure 3.4 ^{17}**O transverse relaxation rate as a function of temperature for 5 (top) and 9 (bottom). Black squares are experimental data, red lines are fit (R^2 = 0.9997 and 0.994 for 5 and 9, respectively) to the Swift and Connick equation[25] in the determination of τ_m. The values of τ_m for 5 and 9 are 1.3 $\pm$ 0.3 μs and 5.3 $\pm$ 0.5 μs , respectively, and account for the observed relaxivity differences between 5 and 9.**

<u>Enzymatic Cleavage of **5** by Caspase-3</u>

The difference in relaxivity between **5** and **9** was sufficient to warrant an investigation of the change in relaxivity of **5** upon cleavage by caspase-3. Upon exposure to active human caspase-3, a solution of **5** exhibited up to a 50 % increase in T_1. The change in T_1 was monitored as a function of time with varying amounts of **5** (Figure 3.5). The T_1 of a solution containing **5** in enzyme buffer without caspase-3 (negative control) did not change. The addition of a competitive inhibitor (Ac-DEVD-CHO) slowed the rate of enzymatic cleavage of **5**.

A closer inspection of the T_1 changes observed upon enzymatic cleavage of **5** revealed features which are unique to the measurement of enzymatic processes by changes in T_1. Since the T_1 observed (T_{1obs}) is a bulk property of a solution which contains diamagnetic and paramagnetic contributions (Equation 1.6, Chapter I), the data must be interpreted with caution. The presence of multiple paramagnetic species in solution (**5** and, after enzymatic cleavage, **9**), each with differing effects on T_1 (equimolar solutions of **5** and **9** will produce different T_1 values), adds complexity to the factors influencing T_{1obs}. Since T_{1obs} is dependent on the concentration of **5** (even before enzymatic cleavage), the data in Figure 3.5 is presented as percent change in T_1. The percent change in T_{1obs} upon enzymatic cleavage of **5** increased with increasing initial concentrations of **5** due to the lower initial value of T_{1obs} for higher concentrations of **5** [% change = (final – initial)/initial] (Figure 3.5). Therefore, the greater the amount of **5**, the greater the amount of change in T_{1obs} upon enzymatic cleavage. Another unique feature which deserves clarification is the trial involving the addition of the competitive inhibitor. The change in T_{1obs} for this trial is confounded by the increase in viscosity of the enzyme cleavage solution upon addition of the inhibitor solution (the inhibitor was dissolved in DMSO and added to the enzyme assay buffer). The increased viscosity of DMSO causes a

significant decrease in T_{1obs} due to slower molecular rotation. Therefore the change in T_{1obs}

for this trial is amplified due to the lower initial value of T_{1obs} and the percentage change in T_{1obs}

appears greater than expected. It is important to note that the rate of change in T_{1obs} vs. time

(represented by the slope) is less than the rate of change for a solution containing the same

concentration of **5** without inhibitor (Figure 3.5). Since Ac-DEVD-CHO is a competitive

inhibitor of caspase-3, it is expected to decrease the effective cleavage rate of the enzyme.
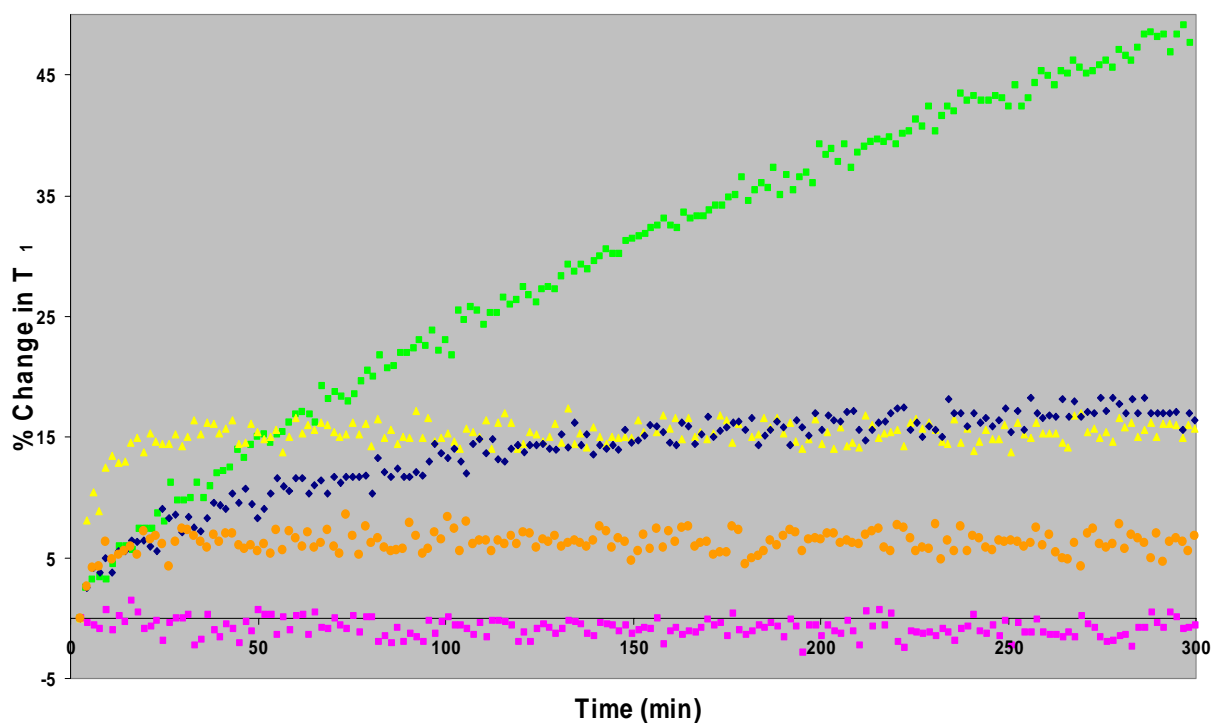
Figure 3.5   Change in T_1 vs. time for the cleavage of **5** by caspase-3 using various concentrations of **5**: 400 μM (orange circles), 600 μM (yellow triangles), and 800 μM (green squares); see explanation of concentration dependence in text.   Addition of a competitive inhibitor slowed the rate of enzymatic cleavage (dark blue diamonds). A solution of 800 μM **5** lacking enzyme did not change significantly over time (negative control, pink squares).

Enzyme Kinetics

In order to experimentally determine the kinetic parameters for the cleavage of **5** by caspase-3, several criteria must be met. The Briggs-Haldane steady-state approximation of the Michaelis-Menten model for enzyme kinetics assumes a steady-state concentration of the enzyme-substrate complex [ES].[26,27] In order to meet the [ES] steady state requirement, the substrate must be present in excess such that the enzyme is saturated with substrate.[27] Within the present system, an excess of **5** would lead to the T_{1obs} being dominated by the effects of **5**, and therefore the small amounts of **9** present during the initial cleavage by caspase-3 would not significantly change T_{1obs} (because T_{1obs} is composed of the intrinsic diamagnetic component and the paramagnetic components due to **5** and **9**, vida supra). This caveat makes the detection of **9** in the presence of excess **5** very difficult because the T_{1obs} is dominated by the contributions from **5**. This situation is in stark contrast to fluorescent or UV/visible substrates (often used to determine enzymatic rate constants), which have little or no fluorescence or absorbance attributed to the uncleaved substrate. In conclusion, the determination of the Michaelis-Menten kinetics for the cleavage of **5** by caspase-3 cannot be performed using T_1 measurements because of the intrinsic background of the uncleaved substrate (**5** has a pronounced effect on T_1). In contrast, UV/visible and fluorescence spectroscopy have the potential to be convenient methods for the determination of enzyme kinetic parameters.

The cleavage of **5** by caspase-3 results in the liberation of 4-aminobenzyl alcohol (Figure 3.2). It was hypothesized that the UV absorbance of 4-aminobenzyl alcohol could be used to measure the kinetics of the cleavage of **5** by caspase-3. The UV absorbance spectrum of 4-aminobenzyl alcohol in water contains maxima at 198 nm, 238 nm, and 285 nm. In order to determine the limit of detection (LOD) of 4-aminobenzyl alcohol by UV spectroscopy, the

absorbance of increasingly dilute solutions was measured. It was empirically determined that the LOD of an aqueous solution of 4-aminobenzyl alcohol on our instrument is approximately 5 µM. The LOD of 4-aminobenzyl alcohol was attempted in caspase-3 assay buffer, however the strong absorbance of the buffer constituents prohibited detection of the analyte. Caspase-3 assay buffer contains very strong (3 AU) UV absorbances at 205 nm and 280 nm. Fluorescence detection of 4-aminobenzyl alcohol in caspase-3 assay buffer produced similar results. Therefore, the cleavage of **5** by caspase-3 cannot be monitored using UV/visible or fluorescence spectroscopy.

In a further attempt to determine the enzyme kinetics of caspase-3 cleavage of **5**, high performance liquid chromatography-mass spectrometry (LC-MS) was performed on the enzyme solution. It was reasoned that the separation of the buffer components from 4-aminobenzyl alcohol using chromatography would allow the detection of each analyte without interference from the overlapping UV absorbances. Using an Atlantis T3 reverse-phase column with water (solvent A) and acetonitrile (solvent B) as the mobile phases, a concentrated solution (500 µM) of 4-aminobenzyl alcohol in caspase-3 assay buffer was analyzed by LC-MS. Using a gradient of solvents (starting at 0% B then ramp to 5% B over 30 min, ramp to 100% B over 15 min, hold 100% B 5 min, ramp 0% B over 5 min, hold 0% B 5 min), the UV detection of 4-aminobenzyl alcohol in caspase-3 assay buffer was accomplished (retention time = 26 minutes). Even though the mass spectrometer failed to detect 4-aminobenzyl alcohol (probably due to ionization suppression from buffer salts), the UV absorbance spectrum matched previous results with maxima at 198 nm, 238 nm, and 285 nm. In addition, using the current gradient conditions, two of the buffer components were identified by MS (HEPES, retention time = 5 minutes; CHAPS, retention time = 40 minutes).

At the low concentrations of 4-aminobenzyl alcohol expected during caspase-3 cleavage of **5**, however, the peak at 26 minutes (due to 4-aminobenzyl alcohol) could not be detected in the LC chromatogram. Assuming 100% cleavage of **5**, there would be 400 μM of 4-aminobenzyl alcohol in the caspase-3 assay buffer. Since the caspase-3 cleavage reactions were performed at small volumes (50 μL) due to the high cost of enzyme, the sample must be diluted (to an injection volume of 200 μL) prior to LC-MS (resulting in an injection concentration of 100 μM). Therefore a solution of 4-aminobenzyl alcohol mimicking these concentrations was prepared and analyzed by LC-MS. The LC-MS chromatogram of the concentration mimic solution failed to detect 4-aminobenzyl alcohol and only revealed peaks due to the buffer components, HEPES and CHAPS. Furthermore, solutions containing **5** and **9** at the concentrations used in the caspase-3 cleavage reaction were prepared. The LC-MS chromatogram of these solutions failed to detect either **5** or **9** and, once again, only exhibited peaks due to the HEPES and CHAPS buffer components. Larger scale studies of the enzymatic cleavage reaction were prohibited due to the excessive cost of human recombinant caspase-3.

MR Imaging and Analysis of T_1 and T_2 (Acquired by Keith MacRenaris, Meade Research Group)

MR images confirm the specific cleavage of **5** by caspase-3 (Figure 3.6). The MRI samples were prepared to have equal amounts of gadolinium(III) (confirmed by ICP-MS) such that the differences observed are not due to variations in concentration. The cleavage of **5** by caspase-3 produces a significant change in the T_1-weighted MR image intensity (Figure 3.6, compare sample 1 to 5). The image intensity of the enzymatically cleaved solution is similar to that of the independently synthesized cleaved agent **9** (Figure 3.6, compare sample 5 to 3). As a

negative control, **5** was incubated with heat denatured, inactive caspase-3, which produced an image intensity similar to that of **5** without enzyme (Figure 3.6, compare sample 2 to 1).

The T_1 and T_2 values associated with the MR image in Figure 3.6 are given in Table 3.1 and help quantify the results of the image. An inspection of the T_1 and T_2 values for each sample confirms the conclusions made from the MR images and reveals subtle features which are less prevalent in the MR images. A comparison of the intensity of the enzymatically cleaved solution (sample 5) and the buffer blank (sample 4) look similar in the MR image, however the associated T_1 values of 1840 ± 70 ms and 3500 ± 100 ms, respectively, are significantly different. The slight difference in the MR image intensity between the enzymatically cleaved product (sample 5) and the independently synthesized cleaved agent, **9** (sample 3) can be attributed to the decrease in T_2 which occurs upon addition of enzyme. This phenomenon is evident when comparing samples 1, 2, and 5 which contain 0 units/µL, 0.1 units/µL, and 0.2 units/µL of caspase-3, respectively, and have T_2 values of 110 ± 20 ms, 69 ± 8 ms, and 28 ± 3 ms, respectively.
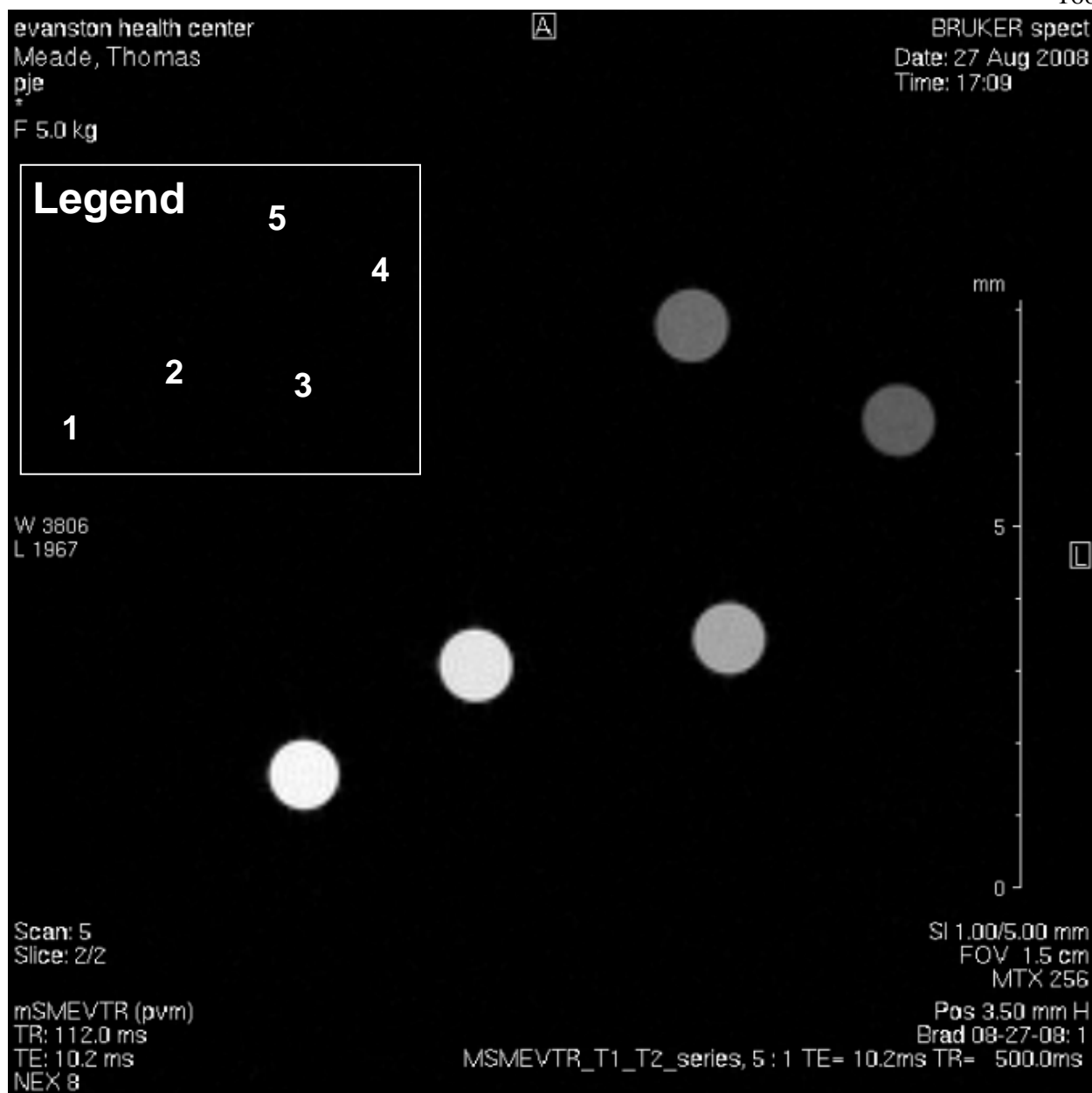
Figure 3.6 T_1-weighted MR image of in vitro caspase-3 cleavage of 5.
(14.1 Tesla, 25 $^{\circ}$C, slice thickness = 1.0 mm, FOV = 1.5 cm, scalebar on right = 8 mm).
(Legend located in upper left corner of image): sample 1 = **5** in buffer; sample 2 = **5** in buffer
after incubation with 0.1units/μL inactive caspase-3 (negative control); sample 3 = **9** in buffer;
sample 4 = buffer blank; sample 5 = **5** in buffer after incubation with 0.2units/μL active caspase-
3. Buffer consists of caspase-3 assay buffer (20 mM HEPES, 2 mM EDTA, 5 mM DTT, 0.1%
CHAPS, 1 mg/mL BSA, pH 7.4). Samples 1-3,5 contain 105 μM gadolinium(III) (by ICP-MS).
T_1 and T_2 values for each sample are listed in Table 3.1

T$_1$ Values

	sample 1	sample 2	sample 3	sample 4	sample 5
Slice 1	1310 ± 50 ms	1290 ± 50 ms	1950 ± 70 ms	3500 ± 100 ms	1840 ± 70 ms
Slice 2	1320 ± 50 ms	1300 ± 50 ms	1980 ± 70 ms	3500 ± 100 ms	1840 ± 70 ms

T$_2$ Values

	sample 1	sample 2	sample 3	sample 4	sample 5
Slice 1	110 ± 20 ms	70 ± 10 ms	110 ± 20 ms	80 ± 10 ms	28 ± 3 ms
Slice 2	110 ± 20 ms	69 ± 8 ms	110 ± 10 ms	73 ± 5 ms	28 ± 3 ms

Table 3.1 T$_1$ values (top) and T$_2$ values (bottom) for MR images in Figure 3.6 Data is given for two distinct regions (slices) within the sample. Sample 1 = **5** in buffer; sample 2 = **5** in buffer after incubation with 0.1units/µL inactive caspase-3 (negative control); sample 3 = **9** in buffer; sample 4 = buffer blank; sample 5 = **5** in buffer after incubation with 0.2units/µL active caspase-3. Buffer consists of caspase-3 assay buffer (20 mM HEPES, 2 mM EDTA, 5 mM DTT, 0.1% CHAPS, 1 mg/mL BSA, pH 7.4). Samples 1-3,5 contain 105 µM gadolinium(III) (by ICP-MS).

<u>Cell Uptake and Viability</u> (performed by Allison Harney, Meade Research Group)

Cellular uptake of **5** and **9** in MDA-MB-231 cells was performed in triplicate at both high and low incubation concentrations. The high incubation concentrations consisted of 190 µM and 546 µM of **5** and **9**, respectively. The low incubation concentrations were performed at 10-fold lower concentrations: 19 µm and 55 µM of **5** and **9**, respectively. At both high and low incubation concentrations, the amount of **9** associated with the cells was not significant compared to untreated cells based on a one-way ANOVA t-test ($P < 0.05$) (Figure 3.7). In contrast, the amount of **5** associated with the cells increases significantly with time at both the high and low incubation concentrations (Figure 3.7). The amount of gadolinium(III) associated

with cells incubated with **5** did not reach a plateau after 48 hours. Cells exposed to the high

incubation concentrations accumulated 1000-fold more **5** than **9** after 48 h. After 48 hours at the

low incubation concentrations, cells treated with **5** retain significantly more gadolinium(III) per

cell than cells treated with **9**. The mechanism of cellular uptake of **5** is currently under

investigation.
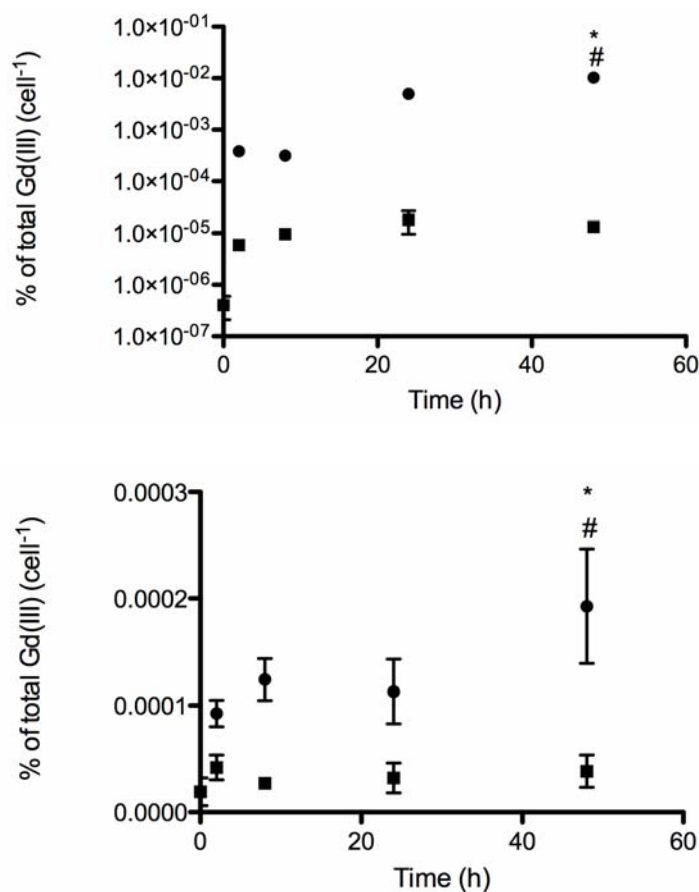
Figure 3.7 Uptake of **5** (circles) and **9** (squares) in MDA-MB-231 cells.
TOP: high incubation concentrations (190 µM and 546 µM of **5** and **9**, respectively)
BOTTOM: low incubation concentrations (19 µM and 55 µM of **5** and **9**, respectively)

*Denotes statistically significant difference within series. #Denotes statistically significant difference between series. The amount of **5** associated with the cells increases significantly with time at both high and low incubation concentrations. For cells incubated with both high and low incubation concentrations of **9**, the amount of gadolinium(III) associated with the cells is not significantly different from untreated cells. (Note: the ordinate of the top graph is a logarithmic scale while the ordinate of the bottom graph is a linear scale.)

The viability of cells exposed to **5** or **9** was performed at high and low incubation concentrations (same concentrations as used in uptake studies) to determine an appropriate concentration range for cell labeling and physiological applications. At the high incubation concentrations, **5** was highly toxic to the cells after 2 hours of incubation, with only 23% of cells surviving treatment (Figure 3.8). The low incubation concentrations of **5** proved less toxic, with viabilities which were comparable to the untreated control cells. To test whether the toxicity of the high incubation concentrations of **5** was due to the substrate peptide or the chelate, **11** and **9** were administered to cells at a high (50 μM and 550 μM, respectively) and low (5 μM and 55 μM) concentrations. Neither **11** nor **9** proved to be toxic at either high or low incubation concentrations. It is hypothesized that the toxicity of the high incubation concentrations of **5** is due to intracellular concentrations that are sufficiently high to produce cytotoxicity. Further cell viability studies are currently underway.
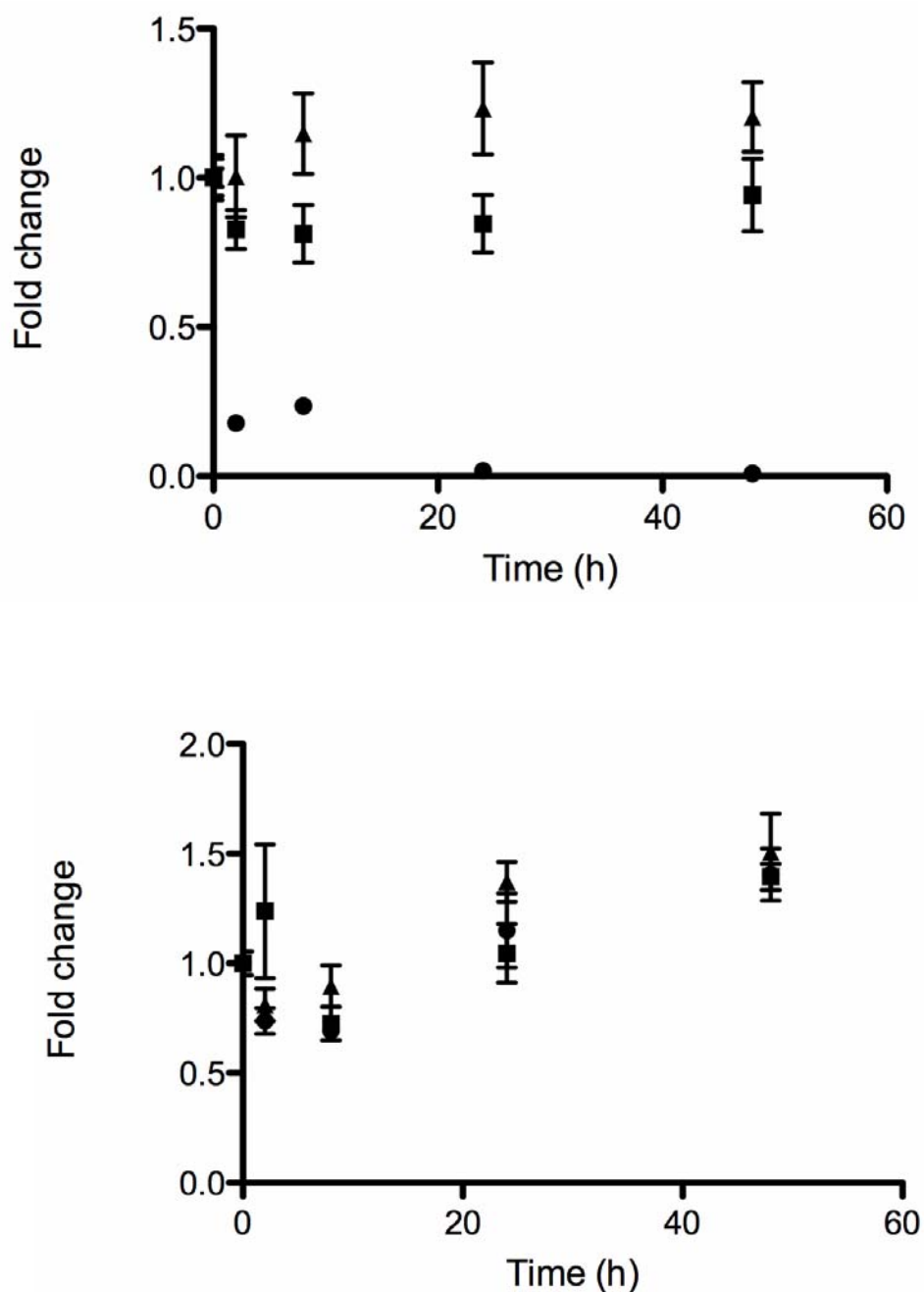
Figure 3.8 Viability of cells incubated with **5** (circles), **9** (triangles), and **11** (squares).
TOP: high incubation concentrations (190 μM, 546 μM, and 50 μM of **5**, **9**, and **11,**
respectively)
BOTTOM: low incubation concentrations (19 μM, 55 μM, and 5 μM of **5**, **9**, and **11**,
respectively) At the high incubation concentration, **5** is toxic to cells. At the low incubation
concentrations, both **5** and **9** did not hinder cellular viability.
Note: viability is presented as the fold change in the number of cells as compared to untreated
control cells (where 1.0 = 100% viability)

SUMMARY AND FUTURE DIRECTIONS

A self-immolative MRI contrast agent, **5**, has been synthesized for the detection of caspase-3. The agent was synthesized in 15 steps with an overall yield of 2%. The products (chelate **9** and peptide **11**) corresponding to enzymatic cleavage of **5** were synthesized for use as authentic standards for comparison.

Through study of the pH dependence of relaxivity, **5** displays a decrease in relaxivity at pH > 8 due to the displacement of inner-sphere water by carbonate. In contrast, the primary amine functionality of **9** coordinates to gadolinium(III) and prohibits carbonate binding. At physiological pH, the amount of carbonate is low, and therefore the observed relaxivity difference between **5** and **9** is not governed by the initially proposed carbonate mechanism. The difference in relaxivity observed between **5** and **9** (5.31 mM^{-1}s^{-1} and 4.13 mM^{-1}s^{-1}, respectively) at physiological pH is attributed to their differing τ_m values (1.3 μs and 5.3 μs, respectively). The 22% difference in relaxivity between **5** and **9** was sufficient to warrant in vitro testing of **5**.

The cleavage of **5** by human caspase-3 was demonstrated using a time-dependent study of the spin-lattice relaxation time (T_1). Cleavage of **5** by caspase-3 resulted in the expected increase in T_1. Control samples lacking active enzyme failed to show a change in T_1 over time, and the presence of a caspase-3 competitive inhibitor slowed the rate of cleavage of **5**. MR images verified a significant change in the T_1 of a solution containing **5** upon cleavage by caspase-3.

The uptake of **5** by MDA-MB-231 cells was measured using gadolinium(III) ICP-MS. Incubation with **5** shows cellular uptake which is both time-dependent and concentration dependent. In contrast, the amount of gadolinium(III) in cells incubated with **9** is not

significantly different from untreated control cells. At 190 μM incubation concentration, **5** is

toxic to cells, however at 19 μM, the cells remained viable. The toxicity of **5** at 190 μM is

speculated to be due to the high amount of cell uptake. Cells treated with 546 μM or 55 μM **9**

were viable. Cells treated with 50 μM or 5 μM **11** were viable.

The mechanism of the uptake of **5** is currently unknown. Comparison of the cellular

uptake of **5** with the coordinatively saturated agent from Chapter IV (which is similar in

structure, but lacks the self-immolative linker) is currently being investigated. Future work

includes tritium labeling the N-terminal acetate group located on **11** such that the cellular uptake

of the peptide can be quantified. These studies will help deduce whether the self-immolative

linker or the peptide (or an additive effect of each) is responsible for the cellular uptake of **5**.

The mechanism of cell uptake will be thoroughly investigated to determine whether **5** operates

under a passive or active mechanism. Results from these studies will be beneficial in designing

future cell-permeable MRI contrast agents.

Induction of Apoptosis and MR Imaging

Caspase-3 is responsible for the proteolysis of a large number of substrates during the

execution phase of apoptosis.[28] The induction of apoptosis in cells leads to increased caspase-3

activity. The induction of apoptosis in MDA-MB-231 cells using tamoxifen is currently

underway. Upon treatment with tamoxifen, the MDA-MB-231 cells will be lysed and caspase-3

activity will be confirmed using a colorimetric caspase-3 assay kit. Upon confirmation of

caspase-3 activity, **5** will be added to the lysate and the T_1 of the solution will be monitored over

time. A control cell line, consisting of MCF-7 cells (which are currently cultured in our

laboratory) will be used, as this ovarian cancer cell line does not express caspase-3. These

experiments will serve as validation of the ability of the self-immolative contrast agent to detect caspase-3 activity in a complex mixture (cell lysate). Further studies include incubation of cells with **5** prior to apoptosis induction and MR imaging of apoptosis in a cellular environment.

Variations of structure

The self-immolative agent presented in the current work is amenable to many variations in structure. Currently underway is the synthesis of a tris(acetate)-based chelate which is hypothesized to change relaxivity in a mechanism similar to that reported by Duimstra and coworkers.[10] A comparison of the relative mechanisms of relaxivity modulation for these agents will be valuable in the design of future self-immolative agents. Other variations of structure include changing the peptide, such that other proteases can be imaged using this self-immolative approach.

Two-Photon Microscopy

Two-photon confocal microscopy of the europium(III) analog, **6**, has the potential to provide useful information about the subcellular localization of the self-immolative agent in MDA-MB-231 cells. Two photon confocal microscopy of europium(III) analogs of MRI contrast agents has been previously used in our laboratory to image intracellular localization.[29] The imaging of the intracellular localization of **6** has the potential to reveal much information concerning the mechanism of cellular uptake as well as the fate of the agent once it is inside the cell.

PARACEST MR Imaging

In addition to T_1 MR imaging, the long τ_m of **5** and **9** (1.3 μs and 5.3 μs, respectively) make lanthanide(III) chelates of these agents [such as the europium(III) analog, **6**] candidates for use as paramagnetic chemical exchange saturation transfer (PARACEST) agents (see Chapter I for a description of PARACEST). Furthermore, the exchangeable amide protons located on the pendant arms of the chelate make **6** amenable to PARACEST imaging.

The cleavage of **6** by caspase-3 could be potentially detected through PARACEST effects from both the inner-sphere water protons and the exchangeable amide protons. The inner-sphere water protons could be probed using PARACEST by exploiting the change in τ_m observed upon enzymatic cleavage of the self-immolative agent by caspase-3. Recently, Ratnakar and coworkers reported tetraamide PARACEST agents which are responsive to the modulation of the water exchange rate ($k_{ex} = 1/\tau_m$) of the complex.[30] Second, the cleavage of the self-immolative agent by caspase-3 is associated with the change of a chelate pendant arm from an amide to a primary amine. This change in functionality results in a change in chemical shift of the presaturation pulse required to produce a PARACEST effect as well as the intensity of the PARACEST effect (which is proportional to the number of exchangeable protons).[31] Yoo and coworkers exploited these principles with a PARACEST agent consisting of a DEVD peptide attached to DOTA.[32] Caspase-3 cleavage of the amide bond between the C-terminus of the peptide and the pendant arm of DOTA liberates a primary amine, resulting in a change in the PARACEST spectrum.[32] The potential for the self-immolative agent described in the present work to be used as a PARACEST agent provides another mechanism by which caspase-3 activity may be monitored.

Multimodal Imaging

An interesting potential application of the self-immolative agent presented in this work involves the mixing of **5** and **6** [as well as other lanthanide(III) chelates thereof for PARACEST imaging] into a single solution. While counter-intuitive from a chemists' perspective (as we strive to make pure compounds), the mixing of **5** and **6** would effectively produce a multimodal agent. The ligand of **5** and **6** is exactly the same, which translates into similar in vivo pharmacokinetics such that the mixture of agents should behave in a similar manner as either of its pure constituents, as has been reported by Aime and coworkers for solutions of mixed PARACEST agents.[33] A similar approach could be used with the self-immolative agent presented in this chapter. A mixture of **5** and **6** has the potential to monitor caspase-3 activity in vivo using T_1 and/or PARACEST [using different saturation frequencies for each lanthanide(III)] MRI followed by co-validation of the intracellular localization of the agent using two-photon microscopy of excited tissues. The deep-tissue capabilities of in vivo MR imaging coupled with the resolution of confocal microscopy has the potential to revolutionize the imaging of enzymatic processes in a research setting.

EXPERIMENTAL

General experimental details can be found in Chapter II.

Abbreviations

THF = tetrahydrofuran, DMF = dimethylformamide, TFA = trifluoroacetic acid, MeCN = acetonitrile, TIS = triisopropylsilane, fmoc = 9-fluorenylmethoxycarbonyl, Boc = *tert*-butoxycarbonyl, HATU = *o*-(7-azabenzotriazol-1-yl)-N,N,N',N'-tetramethyluronium hexafluorophosphate, DIPEA = N,N-diisopropylethylamine, DCC = dicyclohexylcarbodiimide, DMAP = dimethylamino pyridine, DOTA = 1,4,7,10-tetraazacyclododecane N,N',N'',N'''-tetraacetic acid, HPLC = high performance liquid chromatography, RP-HPLC = reverse phase high performance liquid chromatography, PDA = photodiode array, ESI-MS = electrospray ionization mass spectrometry, cyclen = 1,4,7,10-tetraazacyclododecane, Ac = acetyl, pNA = *para*-nitroaniline, BSA = bovine serum albumin, EDTA = ethylenediamine pentaacetic acid, HEPES = 4-(2-hydroxyethyl)-1-piperazine ethanesulfonic acid, DTT = dithiothreitol, CHAPS = 3-[(3-cholamidopropyl)dimethylammonio]-1-propanesulfonate, MEM = modified Eagle's media, DPBS = Dulbecco's phosphate buffered saline

Chemicals

Fmoc-L-amino acids and fmoc-L-amino acids with side chain protecting groups were purchased (NovaBiochem, San Diego, California) and used as received. (R)-*N*-(2-chloroethanoyl)-2-phenylethylamine was purchased (ASDI, Newark, Delaware) and used as received. All other chemicals and solvents were purchased (Sigma Aldrich, St. Louis, Missouri) and used as

received. Anhydrous THF, MeCN, and CH_2Cl_2 were obtained from a Glass Contour (San Diego, CA) solvent system.

Instrumentation

UV/visible spectra for the Kaiser test were performed on an Agilent 8453 UV/vis spectrophotometer. ESI-MS was performed on a Varian Quadrupole 1200L or a Thermo Finnigan LCQ Advantage. ESI-MS samples were dissolved in MeOH and 0.22 μm filtered. Analytical HPLC-MS was performed on a reverse-phase C18 Atlantis T3 column (Waters, T3 5μm, 4.6 X 250mm) with a Varian Prostar 363 fluorescence detector, a Varian Prostar PDA 330 UV/vis detector, and a Varian Quadrupole 1200L MS. Preparative HPLC was performed on a reverse-phase C18 Atlantis T3 column (Waters, T3 10μm, 19 X 250mm with 19 X 10mm guard) with a Hewlett-Packard 1046A fluorescence detector and a Varian Prostar UV/vis dual wavelength detector. NMR spectra were recorded on either a Varian Mercury 400 MHz or Varian Inova 500 MHz instrument. Fluorescence measurements were recorded on a Hitachi F-4500 using quartz cuvettes. T_1 measurements were determined using a Bruker mq60 Minispec operating at 60 MHz and 37 ^{o}C. Lanthanide concentrations were determined using Inductively Coupled Plasma Mass Spectrometry (ICP-MS) on a Thermo Electron Corporation XSeries[II] ICP-MS with Thermo PlasmaLab software. ICP-MS samples were performed in triplicate using a standard calibration with an internal standard consisting of 50 ppb In^{3+}.

Solid-Phase Extraction

Solid-phase extraction was performed using Oasis HLB 6 cc, 500 mg solid-phase extraction cartridges (Waters Corp, Milford, MA). The cartridges were conditioned using MeCN (3 mL)

and 0.1% TFA in water (3 mL). Samples (typically 50 mg crude product was loaded per

cartridge) were dissolved in 5 mL of 0.1% TFA in water and loaded onto the cartridge. The

cartridge was washed with 0.1% TFA in water (4 X 4 mL) and water (4 mL). Product was eluted

using 70% MeCN in water, frozen in liquid N_2, and lyophilized.

Ac-Asp(OBu-*t*)-Glu(OBu-*t*)-Val-Asp(OBu-*t*) (1)

The protected peptide was synthesized according standard solid-phase peptide synthesis

methods[34] using manual batch-type synthesis and fmoc protected amino acids.

NovaSyn TGT resin consisting of 90μm 1% cross-linked polystyrene beads functionalized with

extremely acid-sensitive 4-carboxytrityl linker was used as a solid support for the stepwise

addition of amino acids. NovaSyn TGT resin was purchased (NovaBiochem, San Diego,

California) with the N-terminal amino acid, fmoc-asp(OtBu), preloaded onto the resin. The resin

(10.4924 g, 0.23 mmol/g resin loading, 2.4 mmol) was added to a fritted glass reactor vessel

fitted with a 3-way valve for switching between N_2 (used to mix during all reactions and rinses)

and vacuum (used to drain rinses and excess reactants). The dry NovaSyn TGT resin was pre-

swelled with CH_2Cl_2 (1 X 10 minute rinse) followed by DMF (4 X 10 minute rinses). The N-

terminal fmoc protecting group was removed using 20% piperidine in DMF (until determined

>99% complete by the Kaiser test; typically 4 X 10 minutes). The resin was rinsed with DMF (4

X 10 minutes). The next amino acid (2.5 equivalents relative to the N-terminal amino acid on

the resin) to be added to the peptide was dissolved in a minimal amount of DMF. To this

solution, HATU (2.0 equivalents) and DIPEA (5.0 equivalents) were added to form a yellow

solution of the preactivated fmoc-amino acid. This solution was added to the resin and allowed

to react while gently bubbling N_2 to mix the reactants until determined >99% complete (typically

2-12 hours) by the Kaiser test[35]. Upon completion, the resin was rinsed with DMF (4 X 10

minutes). This process of fmoc removal and addition of the next amino acid was repeated for

each amino acid until the desired sequence, Ac-Asp(OBu-*t*)-Glu(OBu-*t*)-Val-Asp(OBu-*t*)-

Novasyn TGT resin, was obtained. The N-terminal amino functionality was capped using glacial

acetic acid in a manner similar to the addition of amino acids described above. The resin was

then rinsed with DMF (4 X 10 minutes), CH_2Cl_2 (4 X 10 minutes), methanol (4 X 10 minutes);

and dried under vacuum overnight. The dried resin was swelled with anhydrous CH_2Cl_2 for 10

minutes. Excess CH_2Cl_2 was drained from the resin, followed by reaction with 1% TFA in

anhydrous CH_2Cl_2 (10 X 2 minutes, 10 mL each). The solution was drained and collected. The

resin was rinsed with CH_2Cl_2 (3 X 30 seconds, 30 mL each), methanol (3 X 30 seconds, 30 mL

each), CH_2Cl_2 (3 X 30 seconds, 30 mL each), and methanol (3 X 30 seconds, 30 mL each). The

rinses were collected in separate vials and tested for presence of product using TLC (CAM

stain). Rinses containing product were combined with the original cleavage solutions, then the

volume was reduced to 5 mL using rotary evaporation under reduced pressure. Cold water (40

mL) was added to the solution, resulting in a colorless precipitate. The flask was placed in an

icebath to increase precipitation. The precipitate was vacuum filtered using a glass frit, washed

with cold water, transferred to a vial. The vial was placed under vacuum for one hour, then

placed in a KOH desiccator under vacuum for 3 days resulting in a white powder. Yield (1.4289

g, 87%) R_f = 0.58 (silica gel, 12:4:1 $CHCl_3$: methanol : conc NH_4OH, CAM stain)

ESI-MS: Calc. 686.37; Found negative mode 685.40 (M⁻)

^{1}H NMR ($CDCl_3$): Note: non-first order coupling δ = 0.9 (br, 6H, V$_\gamma$); 1.4 (s, 27H, *t*-Bu C*H₃*);

2.0-2.2 (m, 6H, acetyl C*H₃*, E$_\beta$, V$_\beta$); 2.4 (br, 2H, Eγ); 2.7-2.8 (br, 4H, D$_\beta$); 4.3, 4.4, 4.7, 4.8 (br,

4H, D$_\alpha$, E$_\alpha$, V$_\alpha$); 5.7 (br, C-terminal O*H*); 7.5 (br, 1H, N*H*), 7.6 (br, 1H, N*H*), 7.9 (br, 1H, N*H*)

^{1}H NMR (CD$_3$OD): Note: non-first order coupling δ = 0.9 (br, 6H, Vγ); 1.4 (s, 27H, *t*-Bu

C*H$_3$*); 1.8-3.0 (br, 12H, acetyl C*H$_3$*, E$_\beta$, V$_\beta$, E$_\gamma$, D$_\beta$); 4.2 (br, 1H, V$_\alpha$), 4.4 (br, 1H, E$_\alpha$); 4.7 (br, 2H,

D$_\alpha$); 8.0, 8.1, 8.3 (br, N*H*)

^{13}C NMR (CD$_3$OD): δ = 18.8, 19.9 (V$_\gamma$, acetyl *CH$_3$*); 22.7 (V$_\beta$); 28.5 (*t*-Bu *CH$_3$*); 32.2, 32.7 (E$_\beta$,

E$_\gamma$); 38.3, 38.5 (D$_\beta$); 50.4, 51.5, 54.1, 60.1 (D$_\alpha$, E$_\alpha$, V$_\alpha$); 81.9, 82.5, 82.6 (*t*-Bu); 171.3, 171.4,

173.2, 173.3, 173.4, 173.5, 173.7, 174.2 (carbonyl)

N-[Ac-Asp(OBu-*t*)-Glu(OBu-*t*)-Val-Asp(OBu-*t*)]-4-aminobenzylalcohol (2)

1 (1.4289 g, 2.0849 mmol) was dissolved in 100 mL anhydrous THF followed by addition of 4-aminobenzyl alcohol (256.91 mg, 2.0860 mmol) and DCC (862.42 mg, 4.1798 mmol). The reaction was stirred at room temperature under N$_2$ atmosphere for two days and monitored using TLC (100% ethyl acetate eluent, UV detection, Ac-Asp(OBu-*t*)-Glu(OBu-*t*)-Val-Asp(OBu-*t*) R$_f$ = 0.00, 4-aminobenzyl alcohol R$_f$ = 0.55, product R$_f$ = 0.27). The reaction mixture was diluted with 150 mL ethyl acetate and filtered to remove the urea byproduct. The solvent was removed by rotary evaporation under reduced pressure then the solid was dried under vacuum. The crude product was dissolved in 1:1 CH$_2$Cl$_2$: methanol and absorbed onto 18 g silica gel and dried using rotary evaporation under reduced pressure. The silica gel was loaded onto a column (silica gel column slurry packed using 100% ethyl acetate; 7.5 cm diameter, 8.5 cm height) and eluted using 100% ethyl acetate followed by 10% methanol in ethyl acetate. Solvent was removed by rotary evaporation under reduced pressure followed by drying under vacuum to afford a yellow solid. Yield: 862.9 mg, 52%

ESI-MS: Calc. 791.43; Found positive mode 814.46 (M + Na$^+$), negative mode 826.43 (M + Cl$^-$)

^{1}H NMR (CD$_3$OD): Note: non-first order coupling δ = 0.9 (d, 6H, V$_\gamma$); 1.4 (s, 27H, *t*-Bu

C*H$_3$*); 2.0 (s, 3H, acetyl C*H$_3$*); 2.1, 2.3, 2.6, 2.8, 2.9 (m, 9H, E$_\beta$, V$_\beta$, Eγ, D$_\beta$); 4.4, 4.7, 4.8, 4.9

(4H, D$_\alpha$, E$_\alpha$, V$_\alpha$); 4.6 (s, 2H, PhC*H$_2$*OH); 7.3 (m, 2H, aromatic); 7.6 (d, 1H, aromatic, *J* = 8.5

Hz); 7.7 (d, 1H, aromatic, *J* = 8.5 Hz)

^{13}C NMR (CD$_3$OD): δ = 19.2, 19.8 (V$_\gamma$, acetyl C*H$_3$*); 22.7 (V$_\beta$); 28.5 (*t*-Bu C*H$_3$*); 31.8, 32.0,

32.2, 32.6, 34.9, 38.3 (E$_\beta$, E$_\gamma$, D$_\beta$); 50.4, 50.5, 51.5, 51.6, 52.1, 52.3, 53.0, 53.1, 54.0, 54.1, 54.5,

60.1, 61.0, 61.6 (D$_\alpha$, E$_\alpha$, V$_\alpha$); 64.9 (PhC*H$_2$*OH); 81.8, 82.5, 82.6 (*t*-Bu); 121.4, 128.7 (aromatic);

138.7, 138.9 (aromatic ipso *C*); 170.8, 171.3, 171.5, 173.2, 173.4, 173.5, 174.0, 174.1 (carbonyl)

N-[Ac-Asp(OBu-*t*)-Glu(OBu-*t*)-Val-Asp(OBu-*t*)]-4-(2-bromo-ethylcarbamoyloxymethyl)-aniline (3)

2 (162.34 mg, 0.20499 mmol) was dissolved in 10 mL anhydrous CH$_2$Cl$_2$ followed by addition

of DMAP (24.89 mg, 0.2037 mmol) and 2-bromoethylisocyanate (0.0278 mL, 0.308 mmol).

The solution was capped and stirred at room temperature overnight. The reaction was monitored

using ESI-MS. After 17 hours, an additional 0.308 mmol of 2-bromoethylisocyanate was added

and the reaction was stirred for 4 hours. The reaction was determined complete after

disappearance of *N*-[Ac-Asp(OBu-*t*)-Glu(OBu-*t*)-Val-Asp(OBu-*t*)]-4-aminobenzylalcohol as

observed by ESI-MS. Solvent was removed using rotary evaporation under reduced pressure

followed by drying under vacuum. The yellow oil was dissolved in 1:1 CH$_2$Cl$_2$: ethyl acetate

and placed on a silica gel column (4.25 cm diameter, 14 cm height, eluent = 100% ethyl acetate).

TLC R$_f$ = 0.37 (silica gel, 100 % ethyl acetate, UV detection). Solvent was removed by rotary

evaporation under reduced pressure followed by drying under vacuum to afford a white solid.

Yield: 176.0 mg, 91%

ESI-MS: Calc. 940.38; Found positive mode 963.34 (M + Na$^+$), negative mode 977.41 (M + Cl$^-$)

^{1}H NMR (CDCl$_3$): Note: non-first order coupling δ = 1.0-1.4 (33H, V$_\gamma$, t-Bu CH_3); 2.0-2.9 (12H, acetyl CH_3, E$_\beta$, V$_\beta$, Eγ, D$_\beta$); 3.4-3.8 (4H, NHCH_2CH$_2$Br); 4.2-4.9 (4H, D$_\alpha$, E$_\alpha$, V$_\alpha$); 5.4 (s, 2H, PhCH_2OCO); 7.3 (aromatic, integration unavailable due to solvent residual); 7.6 (d, 1H, aromatic, J = 8.4 Hz); 7.8 (d, 1H, aromatic, J = 8.4 Hz)

^{13}C NMR (CDCl$_3$): δ = 18.7, 19.4 (V$_\gamma$, acetyl CH_3); 23.2 (V$_\beta$); 28.5 (t-Bu CH_3); 32.4 (br), 32.5, 33.9, 34.1 (E$_\beta$, E$_\gamma$, D$_\beta$, NHCH$_2$CH_2Br); 42.9, 43.4, 46.3, 47.6, 48.0, 49.2, 50.2 (br), 51.5 (br) (D$_\alpha$, E$_\alpha$, V$_\alpha$, NHCH_2CH$_2$Br); 64.5 (PhCH_2OCO); 81.4, 81.7, 81.9, 82.0 (t-Bu); 120.2, 120.5, 129.0, 131.9 (aromatic); 138.3, 138.5 (aromatic ipso C); 156.4, 157.1 (PhCH$_2$OCO); 169.0, 170.5, 170.7, 171.0. 171.2, 171.4, 171.8, 172.6 (carbonyl)

(RRR)-1,4,7-tris[1-(1-phenyl)ethylcarbomoylmethyl]-(1,4,7,10-tetraazacyclododecane)

(RRR)-1,4,7-tris[1-(1-phenyl)ethylcarbomoylmethyl]-1,4,7,10-tetraazacyclododecane

was prepared from cyclen according to literature[12] and purified using preparative RP-HPLC: (Solvent A = H$_2$O, Solvent B = MeCN; flow rate = 15 mL/min; gradient starting at 20% B and ramping to 100% B over 30 minutes, hold isocratic 100 % B for 5 minutes, ramp to 20% B over 5 minutes, hold isocratic 20% B for 5 minutes, UV/vis detection at 220 nm and 280 nm) by injecting sample (typically 262 mg per injection) dissolved in 40% MeCN/ 60% H$_2$O (4.5 mL, 0.22 μm filtered) with the desired product eluting at 8:30-9:45 (minutes:seconds). MeCN was removed by rotary evaporation under reduced pressure. The remaining aqueous solution was frozen in liquid N$_2$ and lyophilized (typically ~50 mg isolated product per injection). 28% yield after HPLC. ESI-MS, ^{1}H NMR, and ^{13}C NMR agreed with literature values.

N-[Ac-Asp(OBu-*t*)-Glu(OBu-*t*)-Val-Asp(OBu-*t*)]-4-(2-(1-((RRR)-4,7,10-tris[1-(1-phenyl)ethylcarbomoylmethyl])-(1,4,7,10-tetraazacyclododecyl)))ethylcarbamoyloxymethyl)-aniline (4)

3 (348.21 mg, 0.36969 mmol) and (RRR)-1,4,7-tris[1-(1-phenyl)ethylcarbomoylmethyl]-(1,4,7,10-tetraazacyclododecane) (192.05 mg, 0.29282 mmol, 0.8 equivalents) were dissolved in 8 mL anhydrous MeCN. Cs_2CO_3 (362.53 mg, 1.1127 mmol, 3.0 equivalents) was added and the flask was placed in a 60 ^{o}C oilbath with stirring overnight. The reaction was monitored with ESI-MS for the disappearance of (RRR)-1,4,7-tris[1-(1-phenyl)ethylcarbomoylmethyl]-(1,4,7,10-tetraazacyclododecane). Cs_2CO_3 was removed by vacuum filtration through paper; solvent was removed using rotary evaporation under reduced pressure followed by drying under vacuum. The crude product was purified using silica gel chromatography (3.75 cm diameter, 4 cm height, eluent 10% methanol in CH_2Cl_2). Solvent was removed by rotary evaporation under reduced pressure followed by drying under vacuum to afford a beige solid. Yield: 242.9 mg, 55%

ESI-MS: Calc. 1516.86; Found positive mode 1517.99 (M + H$^+$), 1539.91 (M + Na$^+$)

^{1}H NMR (CDCl$_3$): Note: non-first order coupling δ = 0.5-1.6 (42H, V$_\gamma$, *t*-Bu C*H$_3$*, CH$_2$CONHCHPhC*H$_3$*); 2.0-4.4 (38H, acetyl C*H$_3$*, E$_\beta$, V$_\beta$, Eγ, D$_\beta$, NHC*H$_2$*CH$_2$, C*H$_2$*CONHCHPhCH$_3$, cyclen); 4.4-5.4 (9H, D$_\alpha$, E$_\alpha$, V$_\alpha$, CH$_2$CONHC*H*PhCH$_3$, PhC*H$_2$*OCO); 7.0-7.4 (br, aromatic, integration unavailable due to solvent residual)

^{13}C NMR (CDCl$_3$): δ = 18.2, 19.4 (V$_\gamma$, acetyl C*H$_3$*); 22.1, 22.8, 23.1 (V$_\beta$, CH$_2$CONHCHPhC*H$_3$*); 28.2 (*t*-Bu C*H$_3$*); 32.0, 32.8, 37.4 (E$_\beta$, E$_\gamma$, D$_\beta$); 49.3-57.2 (br, D$_\alpha$, E$_\alpha$, V$_\alpha$, cyclen, NHC*H$_2$*C*H$_2$*, C*H$_2$*CONHC*H*PhCH$_3$); 70.6 (PhC*H$_2$*OCO); 81.3 (br, *t*-Bu C(CH$_3$)$_4$); 120.4, 126.0, 126.3, 126.4,

127.2, 127.8, 128.2, 128.6 (aromatic); 144.2 (br, aromatic ipso); 156.4, 156.9 (PhCH$_2$OCO); 169.9-173.3 (br, carbonyl)

Gadolinium(III)- *N*-(Ac-Asp-Glu-Val-Asp)-4-(2-(1-((RRR)-4,7,10-tris[1-(1-phenyl)ethylcarbomoylmethyl])-(1,4,7,10-tetraazacyclododecyl)))ethylcarbamoyloxymethyl)-aniline (H$_2$O) (5)

4 (100.59 mg, 0.066315 mmol) and Gd(CF$_3$SO$_3$)$_3$ (44.95 mg, 0.07436 mmol, 1.1 equivalents) were placed in a 100 mL flask with magnetic stirbar and purged with N$_2$. The reagents were dissolved in 10 mL anhydrous MeCN and placed in a 80 $^{\circ}$C oilbath overnight. Solvent was removed by rotary evaporation under reduced pressure followed by drying under high vacuum. ESI-MS of the intermediate confirmed metalation: calc for Gadolinium(III)-*N*-[Ac-Asp(OBu-*t*)-Glu(OBu-*t*)-Val-Asp(OBu-*t*)]-4-(2-(1-((RRR)-4,7,10-tris[1-(1-phenyl)ethylcarbomoylmethyl])-(1,4,7,10-tetraazacyclododecyl)))ethylcarbamoyloxymethyl)-aniline (H$_2$O) 1691.81; found positive mode Gd^{3+} isotope pattern centered at 1691.78 (M$^+$)

ZnBr$_2$ (233.87 mg, 1.0385, 15 equivalents) was added and the flask was purged with N$_2$ followed by addition of 10 mL anhydrous CH$_2$Cl$_2$. (Note: ZnBr$_2$ forms a suspension in CH$_2$Cl$_2$.) The reaction was stirred at room temperature for 24 hours during which an insoluble white ppt formed. After 24 hours, 60 mL water was added and the reaction was stirred for 2 hours. The crude product was lyophilized and purified by preparative RP-HPLC by dissolving in 40% MeCN in water followed by 0.2 μm filtering [typically ~150 mg crude product dissolved in 4.5 mL 40% MeCN per injection (contains considerable amount of ZnBr$_2$)]; (Solvent A = H$_2$O, Solvent B = MeCN; flow rate = 15 mL/min; starting at 20% B for 5 minutes, ramp to 100% B over 15 minutes, hold isocratic 100% B for 5 minutes, ramp to 0% B over 5 minutes, hold

isocratic 0% B for 5 minutes; UV/vis detection at 220 nm and 280 nm) with the desired

product eluting at 4.3 minutes. MeCN was removed by rotary evaporation under reduced

pressure. The remaining aqueous solution was frozen in liquid N_2 and lyophilized to yield a

white solid. Yield: 37.36 mg, 37 %. 38% metalated by mass as determined by Gd^{3+} ICP-MS.

ESI-MS: Calc (m/2) 761.31; Found positive mode Gd^{3+} isotope pattern centered at 762.10 (m/2)

Europium(III)- *N*-(Ac-Asp-Glu-Val-Asp)-4-(2-(1-((RRR)-4,7,10-tris[1-(1-

phenyl)ethylcarbomoylmethyl])-(1,4,7,10-

tetraazacyclododecyl)))ethylcarbamoyloxymethyl)-aniline (H_2O) (6)

4 (21.27 mg, 0.01402 mmol) was metallated with $Eu(CF_3SO_3)_3$ (10.65 mg, 0.01777 mmol, 1.3

equivalents) then deproteced with $ZnBr_2$ (52.74 mg, 0.2342 mmol, 16.7 equivalents) and purified

using RP-HPLC (product elutes at 4.4 minutes) using the same method as used for **5**.

ESI-MS of the intermediate confirmed metalation: calc for Europium(III)-*N*-[Ac-Asp(OBu-*t*)-

Glu(OBu-*t*)-Val-Asp(OBu-*t*)]-4-(2-(1-((RRR)-4,7,10-tris[1-(1-phenyl)ethylcarbomoylmethyl])-

(1,4,7,10-

tetraazacyclododecyl)))ethylcarbamoyloxymethyl)-aniline (H_2O) 1686.80; found positive mode

Eu^{3+} isotope pattern centered at 1686.79 (M^+)

6 was isolated as a white solid. Yield: 8.55 mg, 41 %.

ESI-MS: Calc (m/2) 758.81; Found positive mode Eu^{3+} isotope pattern centered at 759.99 (m/2)

1-(2-*t*Boc-aminoethyl)-(RRR)-4,7,10-tris[1-(1-phenyl)ethylcarbomoylmethyl]-(1,4,7,10-tetraazacyclododecane) (7)

(RRR)-1,4,7-tris[1-(1-phenyl)ethylcarbomoylmethyl]-(1,4,7,10-tetraazacyclododecane) (388.87 mg, 0.59291 mmol) and 2-(Boc-amino)ethyl bromide (201.40 mg, 0.89871 mmol, 1.5 equivalents) were dissolved in 5 mL anhydrous MeCN. Cs_2CO_3 (580.25 mg, 1.7809 mmol, 3.0 equivalents) was added and the reaction was stirred at 60 ^{o}C for 8 days. Additional 2-(Boc-amino)ethyl bromide (1.5 equivalents each 24 hour period) was added and the reaction was stirred at 60 ^{o}C until disappearance of (RRR)-1,4,7-tris[1-(1-phenyl)ethylcarbomoylmethyl]-(1,4,7,10-tetraazacyclododecane) as evidenced by TLC (1:9:90 sat KNO_3:H_2O:MeCN, Pt stain; R_f = 0.29, product R_f = 0.39) and ESI-MS. Cs_2CO_3 was removed by vacuum filtration through paper. Solvent was removed using rotary evaporation under reduced pressure followed by drying under vacuum. The crude product was dissolved in 10% MeOH/CH_2Cl_2 and placed on a silica gel column (4.5 cm diameter, 5.5 cm height, eluent = 10% MeOH/CH_2Cl_2). Solvent was removed by rotary evaporation under reduced pressure followed by drying under vacuum to afford 326.0 mg (69% yield) white solid.

ESI-MS: Calc. 798.52; Found positive mode 799.61 (M + H$^+$), 821.56 (M + Na$^+$)

^{1}H NMR (CDCl$_3$): Note: fluxional on NMR timescale resulting in broad resonances and making some integrations unavailable due to non-first order coupling δ = 0.8-1.2 (CH$_2$CONHCHPhC*H$_3$*), 1.4 (s, *t*-Bu C*H$_3$*), 1.5-3.4 (br, cyclen, C*H$_2$*C*H$_2$*NH-Boc, and C*H$_2$*CONHCHPhCH$_3$), 4.9 (br, 3H, CH$_2$CONHC*H*PhCH$_3$), 7.1-7.6 (br, 15H, aromatics)

^{13}C NMR (CDCl$_3$): δ = 22.3, 23.0 (CH$_2$CONHCHPhC*H$_3$*); 28.6 (*t*-Bu C*H$_3$*); 49.6-53.1 (br cyclen, C*H$_2$*C*H$_2$*NH-Boc, and C*H$_2$*CONHCHPhCH$_3$); 79.1 (*t*-Bu C(CH$_3$)$_4$); 126.2, 126.5, 126.7, 127.2,

128.7 (aromatic); 144.3, 144.8, 145.4 (aromatic ipso C); 156.5 (NHCOO-tBu); 170.2, 171.2 (CH$_2$$C$ONHCHPhCH$_3$)

1-(2-aminoethyl)-(RRR)-4,7,10-tris[1-(1-phenyl)ethylcarbomoylmethyl]-(1,4,7,10-tetraazacyclododecane) (8)

7 (326.0 mg, 0.4080 mmol) was dissolved in 10 mL of 95% TFA, 2.5% TIS, 2.5% H$_2$O and reacted overnight. TFA was evaporated by passing N$_2$ over the reaction solution, resulting in a yellow oil. Cold diethyl ether (30 mL) was used to precipitate the crude product as a white solid. The suspension was centrifuged and decanted. The diethyl ether extraction was repeated 4 times followed by evaporation of residual diethyl ether by passing N$_2$ over the solid cake. The crude product was dissolved in water (25 mL), frozen in liquid N$_2$, lyophilized, then purified using Solid-Phase Extraction to yield 281.06 mg white powder (98% yield).

ESI-MS: Calc. 698.46; Found positive mode 699.53 (M + H$^+$), 721.54 (M + Na$^+$)

^{1}H NMR (D$_2$O): Note: fluxional on NMR timescale resulting in broad resonances and non-first order coupling δ = 1.2-1.6 (br, 9H, CH$_2$CONHCHPhCH_3), 2.4-3.7 (br, 26H, cyclen, CH_2CH_2NH$_2$, and CH_2CONHCHPhCH$_3$), 4.4-5.2 (br, CH$_2$CONHCHPhCH$_3$, integration not available due to solvent residual peak), 7.0-7.4 (br, 15H, aromatics)

^{13}C NMR (D$_2$O with acetone reference): δ = 22.0 (br, CH$_2$CONHCHPhCH_3); 49.0-53.0 (br cyclen, CH$_2$$CH_2NH_2$, and CH$_2$CONHCHPhCH$_3$); 126.3, 126.4, 128.1, 128.3, 129.3, 129.6 (br, aromatic); 144.5, 144.0, 144.2 (aromatic ipso C); 171.0 (br, CH$_2$$C$ONHCHPhCH$_3$)

Gadolinium(III)-1-(2-aminoethyl)-(RRR)-4,7,10-tris[1-(1-phenyl)ethylcarbomoylmethyl]-(1,4,7,10-tetraazacyclododecane) (9)

8 (30.93 mg, 0.04419 mmol) was dissolved in 10 mL water and the pH was adjusted to 5.5 using 5% NaOH followed by addition of $Gd(OH)_3 \cdot 6H_2O$ (15.75 mg, 0.04979 mmol, 1.1 equivalents). The flask was capped with a rubber septum and placed in a 80 ^{o}C oilbath with stirring. The pH was periodically monitored and adjusted to 5.5 using HCl vapor. The reaction was determined to be complete when the pH stabilized (typically 48-72 hours). The crude reaction mixture was 0.22 μm filtered, frozen in liquid nitrogen, and lyophilized. The crude product was purified using preparative RP-HPLC (Solvent A = H_2O, Solvent B = MeCN; flow rate = 15 mL/min; gradient starting at 0% B and ramping to 100% B over 30 minutes, hold isocratic 100% B for 5 minutes, ramp to 0% B over 5 minutes, hold isocratic 0% B for 5 minutes; fluorescence detection of Gd^{3+} λ_{ex} = 274 nm, λ_{em} = 314 nm; UV/vis detection at 205 nm and 270 nm) by injecting crude product dissolved in water (3 mL, 0.22 μm filtered) with the desired product eluting at 12 minutes. MeCN was removed by rotary evaporation under reduced pressure. The remaining aqueous solution was frozen in liquid nitrogen and lyophilized to yield 19.56 mg white powder (52 % yield). 56% metalated by mass as determined by Gd^{3+} ICP-MS.

ESI-MS: Calc. 853.39; Found positive mode Gd^{3+} isotope pattern centered at 854.38 (M + H$^+$)

Europium(III)-1-(2-aminoethyl)-(RRR)-4,7,10-tris[1-(1-phenyl)ethylcarbomoylmethyl]-(1,4,7,10-tetraazacyclododecane) (10)

8 (13.16 mg, 0.01880 mmol) was metallated using $Eu(OH)_3$ (6.89 mg, 0.02215 mmol, 1.2 equivalents) and purified by RP-HPLC (product elutes at 12 minutes) using the same method as used for **9** to yield 8.67 mg white powder (54 % yield).

ESI-MS: Calc. 848.38; Found positive mode Eu^{3+} isotope pattern centered at 848.83 (M$^+$)

Ac-Asp-Glu-Val-Asp (11)

1 (42.92 mg, 0.06262 mmol) was dissolved in 5 mL of 95% TFA, 2.5% TIS, 2.5% H$_2$O and reacted overnight. TFA was evaporated by passing N$_2$ over the reaction solution, resulting in a yellow oil. Cold diethyl ether (30 mL) was used to precipitate the crude product as a white solid. The suspension was centrifuged and decanted. The diethyl ether extraction was repeated 4 times followed by evaporation of residual diethyl ether by passing N$_2$ over the solid cake. The crude product was dissolved in water (5 mL), frozen in liquid N$_2$, lyophilized, then purified using Solid-Phase Extraction to yield 31.76 mg white solid (99% yield).

ESI-MS: Calc. 518.19; Found negative mode 517.22 (M$^-$), positive mode 541.22 (M + Na$^+$)

^{1}H NMR (D$_2$O): Note: non-first order coupling $\delta = 0.9$ (d, 6H, V$_\gamma$), 1.9-2.1 (m, 6H, acetyl CH_3, E$_\beta$, V$_\beta$), 2.4 (t, 2H, Eγ), 2.7-2.9 (m, 4H, D$_\beta$), 4.0 (d, 1H, V$_\alpha$, $J = 7.6$ Hz), 4.4 (t, 1H, E$_\alpha$, $J = 7.4$ Hz), 4.6 (t, 1H, D$_\alpha$, $J = 6.4$ Hz), 4.7 (t, 1H, D$_\alpha$, $J = 6.0$ Hz)

^{13}C NMR (D$_2$O with acetone reference): $\delta = 18.3$, 18.9 (V$_\gamma$, acetyl CH$_3$); 22.4 (V$_\beta$); 26.5 (E$_\beta$); 30.4 (E$_\gamma$); 35.9, 36.0 (D$_\beta$); 49.7, 50.7, 53.5, 60.1 (D$_\alpha$, E$_\alpha$, V$_\alpha$); 173.2, 173.5, 174.3, 174.5, 174.8, 177.7 (carbonyl)

Luminescence Decay

3 mM solutions of **6** or **10** were prepared in 500μL of H$_2$O or D$_2$O. Time-resolved luminescence spectra were acquired with the following parameters: 395 nm excitation wavelength, 614 nm emission wavelength, 10 nm excitation slit width, 10 nm emission slit width, 950V PMT, 20 replicates. Data were fit to a single exponential decay using Origin version 7.0. Due to the fast

luminescence decay of **6** and **10** in pure water, solutions consisting of **6** or **10** in 0, 40, 60,

and 80% H_2O in D_2O were prepared. Plotting the decay constants obtained from each solution

resulted in a linear fit. The y-intercept of the linear fit allowed extrapolation to determine the

decay constant of **6** and **10** in pure water. The equation from Supkowski and coworkers[21] was

used to determine q with corrections for 4 amide/amines.

Relaxivity

Stock solutions consisting of 0.200 mM of **5** or **9** in Caspase-3 assay buffer (20 mM HEPES, 2

mM EDTA, 5 mM DTT, 0.1% CHAPS, 1 mg/mL BSA, pH 7.4) were prepared. Serial dilutions

of the stock solutions produced concentrations of 0.100 mM, 0.050 mM, 0.025 mM. Twenty

five microliters of each sample were used for determining Gd^{3+} concentration using ICP-MS.

Samples were equilibrated to 37 ^oC in a water bath for 10 minutes prior to T_1 measurement. The

T_1 of each solution was determined using an inversion recovery pulse sequence with appropriate

recycle delays (>5*T_1). The resulting curves were fit to a monoexponential function to obtain

T_1. A plot of $1/T_1$ vs. concentration was fit to a straight line yielding the relaxivity as the slope.

Relaxivity vs. pH

A 1 mM solution of **5** or **9** was prepared in 2 mL water. The solution was split into two 950 μL

aliquots: one was used for the acidic range and the other for the basic range. The pH was

adjusted into either the acidic range using HCl vapor (as to not change the concentration of the

solution) or the basic range using NaOH (using 0.5 μL additions of 5 mM, 50 mM, or 500 mM

NaOH; more concentrated NaOH solutions were used as the solution became increasingly basic).

For the basic range, the volume of NaOH added was recorded and used to correct the final

concentrations (the correction proved minimal as a total of only 22.5 μL of NaOH for **5** and 21.5 μL of NaOH for **9** was added to a 950 μL initial solution; corresponding to a 2.4% and 2.3% increase in volume, respectively). Gd^{3+} concentration was determined using ICP-MS. The samples were allowed to equilibrate at 37 ^{o}C for 5 minutes before each T_1 measurement. The T_1 of each solution was determined using an inversion recovery pulse sequence with appropriate recycle delays ($>5*T_1$). The difference in T_1 values vs. water were used to determine the relaxivity at each pH.

Mean Water Residence Lifetime

The method of Micskei and coworkers[22] was used to determine the mean water residence lifetime. Samples were prepared as 225 microliters of 20 mM **5** or **9** in water with 25 microliters of ^{17}O enriched water (10% ^{17}O enrichment; Medical Isotopes, Inc., Pelham, New Hampshire) added, resulting in 1% ^{17}O enrichment in the final sample. This solution was placed in an NMR tube with an insert containing D_2O (for lock reference). A water standard was prepared consisting of 1% ^{17}O enriched water with D_2O insert. VT-NMR was acquired on a Varian Inova 400 (tuned to 54.310 MHz ^{17}O frequency) at 5 ^{o}C intervals between 1 ^{o}C and 90 ^{o}C. Temperatures were corrected using a calibration plot. The samples were equilibrated for 10 minutes at each temperature, followed by lock and shim. The ^{17}O linewidth of the bulk water was measured at each temperature. The pH of the samples was recorded and Gd^{3+} concentrations were determined by ICP-MS. Data were fit to theory developed by Swift and Connick (Equation 3.1)[25] in Origin version 7.0.

Equation 3.1[25]

F=400;s=3.5;univ=8.31;wi=6.28e6*F*0.13557;ws=6.28e6*F*658.21;tm=((tm0^(-1)*x/298.15)*exp((Hm/univ)*(0.003354-(1/x))))^-1;tr=((tr0^(-1)*x/298.15)*exp((Hr/univ)*(0.003354-(1/x))))^-1;tv=((tv0^(-1)*x/298.15)*exp((Hv/univ)*(0.003354-(1/x))))^-1;T1e=((1/25)*delta*tv*(4*s^2+4*s-3)*((1/(1+ws^2*tv^2))+(4/(1+4*ws^2*tv^2))))^-1;T2e=((0.02*(4*s^2+4*s-3)*tv*delta*(3+(5/(1+(ws^2*tv^2)))+(2/(1+(4*ws^2*tv^2)))))))^(-1);tc1=(T1e^(-1)+tr^(-1)+tm^(-1))^(-1);tc2=(T2e^(-1)+tr^(-1)+tm^(-1))^(-1);te1=(T1e^-1+tm^-1)^(-1);te2=(T2e^(-1)+tm^(-1))^(-1);cont=(1/3)*s*(s+1)*acc^2*(te1+(te2/(1+ws^2*te2^2)));dip1=((1/15)*4.535671e-33*s*(s+1))/(r^6);dip2=4*tc1;dip3=(13*tc2)/(1+ws^2*tc2^2);dip4=(3*tc1)/(1+wi^2*tc1^2);dip9=1.6995e14*0.32;dip5=(0.2*tr)/(1+wi^2*tr^2);dip6=(0.8*tr)/(1+4*wi^2*tr^2);dip7=(2/5)*(wi^2*1.1890597e-79*s^2*(s+1)^2)/(9*1.9063324e-32*x^2*r^6);dip8=(3*tc1)/(1+wi^2*tc1^2);dip=dip1*(dip2+dip3+dip4);quad=dip9*(dip5+dip6);cur=dip7*dip8;diptot=dip+cur+quad;T2m=(cont+diptot)^-1;gauss=F*1e6/4255.319;dwm=(1.856953e-20*s*(s+1)*acc*gauss)/(3*1.3807e-16*x);num=(T2m^-2)+(T2m*tm)^-1+dwm^2;denom=(tm^-1+T2m^-1)^2+dwm^2;scam=num/denom;pm=n*conc/55.56;y=pm*scam/tm;

Definitions of parameters in Equation 3.1:

delta = the trace of the zero-field-splitting tensor; tm0 = the mean water residence lifetime; Hm = enthalpy of water exchange; tr0 = the rotational correlation time (set 50 ps to agree with literature values[36] of small molecule Gd^{3+} contrast agents); Hr = enthalpy of rotation; tv0 = the correlation time for the modulation of the zero-field-splitting tensor; Hv = the enthalpy of the tv0 correlation time; acc = $A/\hbar$ = the scalar coupling constant between the electrons of Gd^{3+} and the protons of the inner sphere water (set to -3800000 rad/s); r = the distance between the paramagnetic ion and the oxygen of the inner-sphere water (set to literature value[22] for DOTA, 2.5 Å); n = the number of inner sphere waters (set to 1.8 for **5** and 1.7 for **9**; determined experimentally – vida supra); conc = concentration of the paramagnetic ion (determined experimentally by ICP-MS)

Caspase-3 Activity

Active recombinant human caspase-3 was purchased from Biovision (Mountain View, CA) as a lyophilized powder, reconstituted in PBS with 15% glycerol, divided into 10 μL aliquots (each containing 1 unit per μL), and stored at -80 ^{o}C.

Unit definition: one unit cleaves 1 nmol DEVD-pNA per hour at 37 ^{o}C in 50 mM HEPES, 50 mM NaCl, 10 mM EDTA, 10 mM DTT, 5% glycerol, 0.1% CHAPS, pH 7.2.

Caspase-3 assay buffer (20 mM HEPES, 2 mM EDTA, 5 mM DTT, 0.1% CHAPS, 1 mg/mL BSA, pH 7.4) was prepared fresh daily.

Enzyme activity was confirmed using a caspase-3 colorimetric assay kit purchased from Aldrich (St. Louis, MO). The kit is based upon caspase-3 cleavage of Ac-DEVD-pNA, which produces a characteristic absorbance at 405 nm due to liberated pNA.

Caspase-3 T_1 Study

A 10 μL aliquot (containing 1 unit per μL) of frozen caspase-3 solution was thawed on ice and transferred to a vial using 39 μL assay buffer followed by addition of 1 μL 20 mM **5** in assay buffer, resulting in 50 μL solution containing 400 μM **5** (other concentrations of **5** were prepared in a similar manner, with adjustment of the amount of assay buffer such that the final solution was 50 μL). The solution was immediately placed in a glass tube (which was preheated to 37 ^{o}C), sealed with parafilm, and placed in the bore of a Bruker mq60 Minispec operating at 60 MHz and 37 ^{o}C. The T_1 was measured over a 15 hour time period using a saturation recovery pulse sequence with 4 s recycle delay, 10 ms initial pulse separation, 4000 ms final pulse separation, 0.05 ms delay sampling window, 0.02 ms sampling window, 2 scans per data point, 8 data points per T_1 measurement, 20 dB pulse attenuation, 65 dB gain. Repetitive measurements

were taken with a 4 second delay between measurements such that each T_1 measurement took a total of 101.3 s.

MR Imaging and Analysis of T_1 and T_2

Samples containing **5** and caspase-3 were prepared as described above for the T_1 time study and incubated at 37 ^{o}C for 15 hours prior to imaging. The T_1 of the solution containing **5** and active caspase-3 was monitored using the Bruker mq60 (60 MHz) minispec during the 15 hour incubation to ensure that the T_1 changed in the sample prior to imaging at 14.1 T. A solution of active caspase-3 enzyme was heat-denatured to produce inactive caspase-3 (for use as a negative control); lack of enzyme activity was confirmed using the colorimetric enzyme assay kit described above. The solution containing **5** and inactive caspase-3 was prepared in an identical manner as the active enzyme solution described above and incubated at 37 ^{o}C. The T_1 of the solution containing inactive caspase-3 and **5** was measured at the start and end of the 15 hour incubation, with no significant change in T_1. Samples containing **5** or **9** were prepared in assay buffer. ICP-MS was used to determine the exact gadolinium(III) content of each sample. The concentrations of the samples were adjusted by addition of assay buffer such that each solution contained equivalent amounts of gadolinium(III) (as confirmed by ICP-MS after concentration adjustment). Samples (40 μL of each solution) were prepared for imaging in glass capillary tubes and sealed with parafilm. MR measurements were performed on a General Electric/Bruker Omega 600WB 14.1 T imaging spectrometer fitted with Accustar shielded gradient coils at ambient temperature (~25 ^{o}C). Images were acquired using a T_1-weighted, spin-echo pulse sequence (T_E = 10.2 ms, T_R = 500.0 ms). Spin-lattice relaxation times (T_1) were acquired using a saturation recovery pulse sequence with static echo times (T_E = 10.18 ms) and variable repetition

times (T_R = 111.970, 200, 300, 400, 500, 750, 1000, 2000, 5000, 10000 ms). Spin-spin

relaxation times (T_2) were acquired using a saturation recovery pulse sequence with static T_R

(111.970 ms) and variable T_E (10.18, 20.36, 30.54, 40.72, 50.90 ms). Two independent trials

were performed per 1 mm slice and 2 slices of each sample were measured. Intensities of

selected regions of interest were fit to a monoexponential curve using Paravision version 3.02 to

obtain T_1 and T_2.

Cell Studies

MDA-MB-231 breast cancer cells were seeded in triplicate in 48-well plates at a density

of 2 x 10^5 cells/mL to reach 100% confluence after 48 hours. MDA-MB-231 cells were

maintained in Alpha-MEM supplemented with 10% fetal bovine serum, 2 mM glutamine, non-

essential amino acids, sodium pyruvate, 50 mM HEPES, and gentamicin. Cells were cultured at

37 °C in 5% CO_2. **5**, **9**, and **11** were dissolved in cell culture medium and sterilized with a 0.2

μM filter. Stock solutions of **5** and **9** were prepared at concentrations of 948 μM and 2.75 mM

respectively (concentrations determined by Gd^{3+} ICP-MS). The final concentration of **11**, based

on mass, was 500 μM. For high dose experiments, culture media was removed and fresh media

was added to 40 μL of **5**, 40 μL of **9**, or 20 μL of **11** to a final volume of 200 μl per well. For

low dose experiments, the same stock solutions were used, and 4 μL of **5**, 4 μL of **9**, or 2 μL of

11 were added to fresh media to a final volume of 200 μL per well. After incubation for 0, 2, 8,

24 or 48 h, cells were washed twice with cold 1 X DPBS and trypsinized. The trypsin reaction

was stopped with the addition of media to adjust the volume of the cell suspension to 100 μL.

The total viable cell population for each sample was counted using a Guava Easycite mini

personal cell analyzer. Viability was assessed using ViaCount reagent per manufacturers

instructions. Of the remaining cell suspension, 65 µL was digested in 90 µL of HNO_3 at 60

°C for a minimum of 3 hours. Gd^{3+} content was determined by ICP-MS and Gd^{3+} content of

cells was calculated.

CHAPTER IV

A COORDINATIVELY SATURATED GADOLINIUM(III) CHELATE FOR

THE DETECTION OF CASPASE-3

The text in this chapter is taken in part from:

Ulrich, B. D.; Harney, A. S.; MacRenaris, K. W.; Meade, T. J. "A Bioactivated Magnetic Resonance Agent for the Detection of Caspase-3", *Bioconjugate Chemistry, submitted*

INTRODUCTION

Caspase-3

An introduction to caspase-3 can be found in Chapter II, Part I.

Design of a Simplified MRI Contrast Agent for the Detection of Caspase-3

This chapter details the investigation of a contrast agent for the detection of caspase-3

activity. The agent is a derivative of the synthetic efforts found in Chapter III. The contrast

agent consists of a tris-amide derivative of DOTA, while the peptide consists of a caspase-3

substrate, DEVD (details of both in Chapter III). The difference between the contrast agent in

the present work and that of Chapter III lies in the linkage between the chelate and the peptide.

In the present work, the chelate was attached directly to the C-terminus of the peptide. The

direct attachment of the chelate to the peptide simplified the overall structure and synthesis of the

target molecule, as compared to the self-immolative agent of Chapter III.

It was hypothesized that **6** would change relaxivity upon enzymatic cleavage via a

carbonate mechanism similar to that initially proposed for the self-immolative agent in Chapter

III (Figure 4.1).
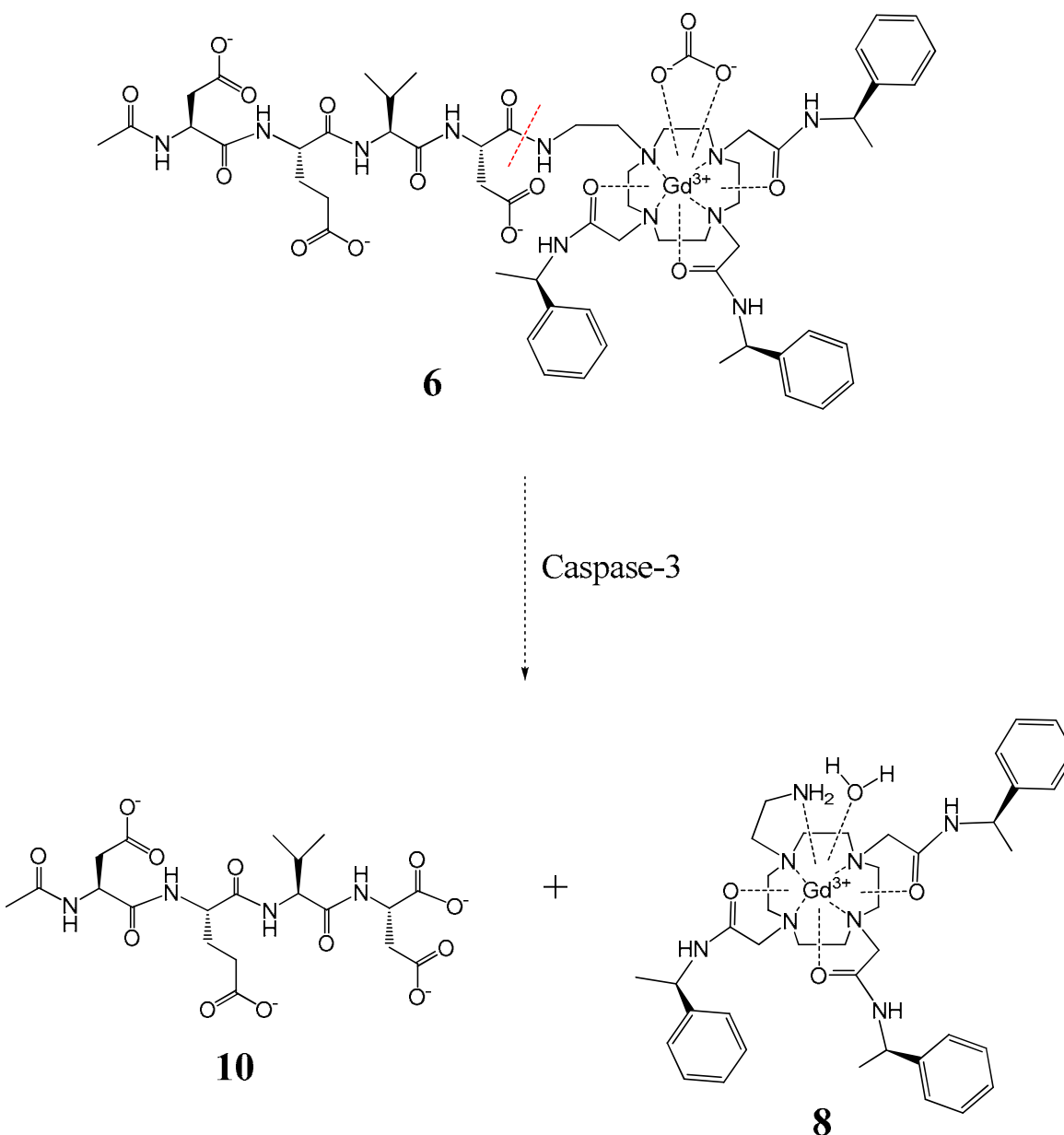
**Figure 4.1 Proposed mechanism to describe relaxivity change upon enzymatic cleavage.
Carbonate is expected to displace inner-sphere water of 6, resulting in a $q = 0$ complex.
Enzymatic cleavage of 6 produces 10 and 8. The pendant amine of 8 is proposed to
displace carbonate, leading to a $q = 1$ complex.**

RESULTS AND DISCUSSION

Synthesis

The synthesis of the target compound, **6**, was accomplished in 15 steps with an overall

yield of 3% (Schemes 4.1-4.3). The convergent synthesis of **6** involved two parts: synthesis of

the substrate peptide, **1**, and synthesis of the lanthanide chelate, **3**. Both syntheses are described

in detail in Chapter 3 (Schemes 4.1 and 4.2, respectively). Coupling of **1** and **3** to produce **4**

followed by deprotection with TFA yielded **5**. Metalation of **5** with either gadolinium(III) or

europium(III) yielded **6** and **7**, respectively (Scheme 4.3). The synthesis of **6** was more

straightforward than the synthesis of the self-immolative agent described in Chapter III, despite

having the same number of overall synthetic steps and only a slight increase in overall yield (3%

vs. 2%). The lack of an acid-sensitive self-immolative linker allowed the t-butyl deprotection of

4 to be conducted in TFA, resulting in easier workup and purification as compared to the $ZnBr_2$

mediated t-butyl deprotection of the self-immolative agent which required HPLC purification

(details in Chapter III).

The enzymatic cleavage products, **8**-**10**, were independently synthesized for use as

authentic standards during relaxometric measurements and enzyme studies (Schemes 4.4 and

4.5; discussed in Chapter 3).
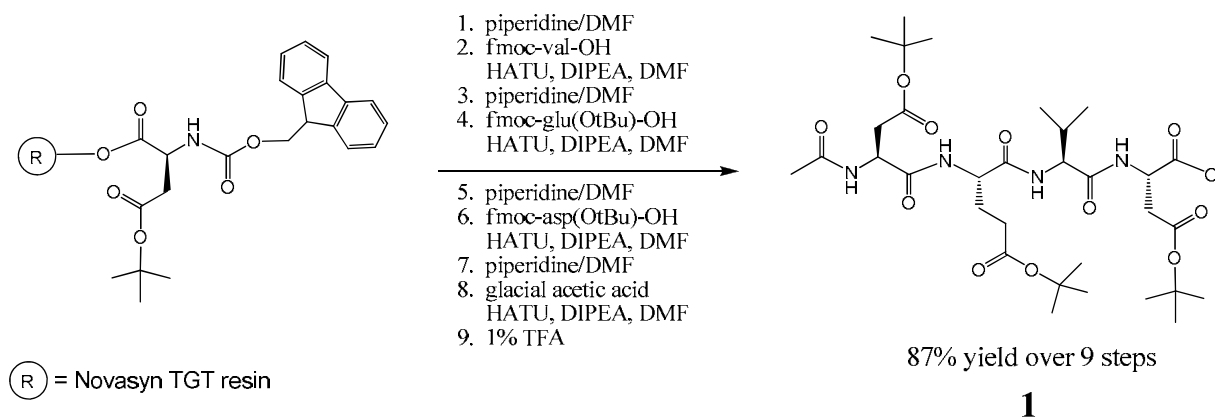
Scheme 4.1 Synthesis of 1 using solid-phase peptide synthesis
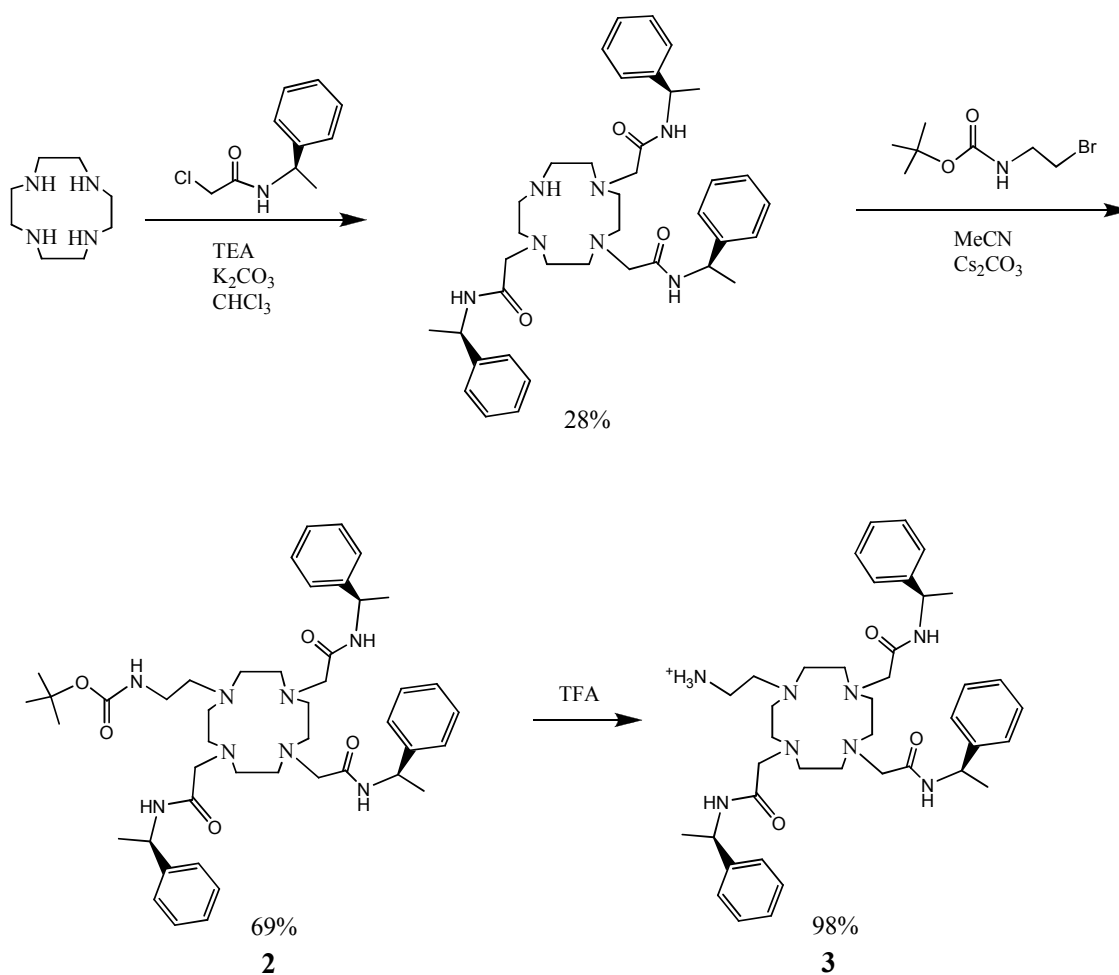
Scheme 4.2 Synthesis of 3 from cyclen (step 1 based on literature procedures[1])
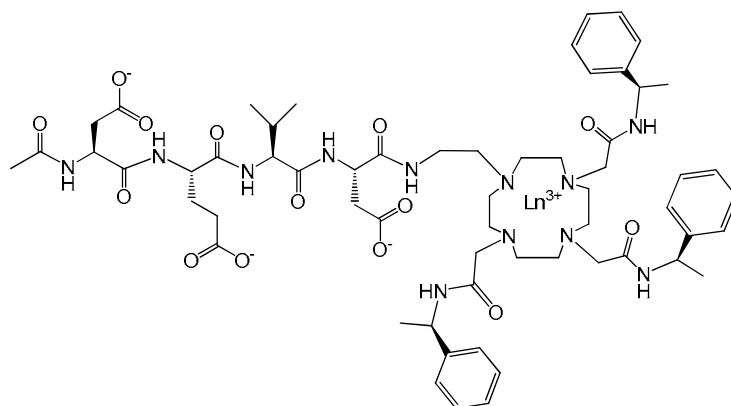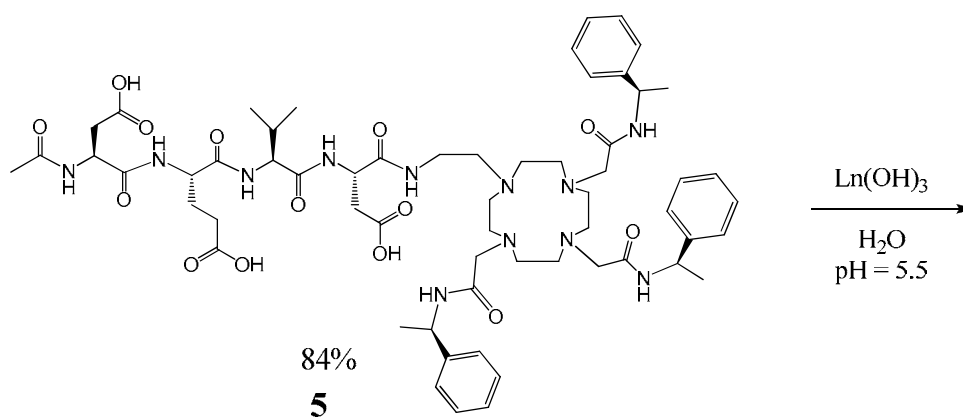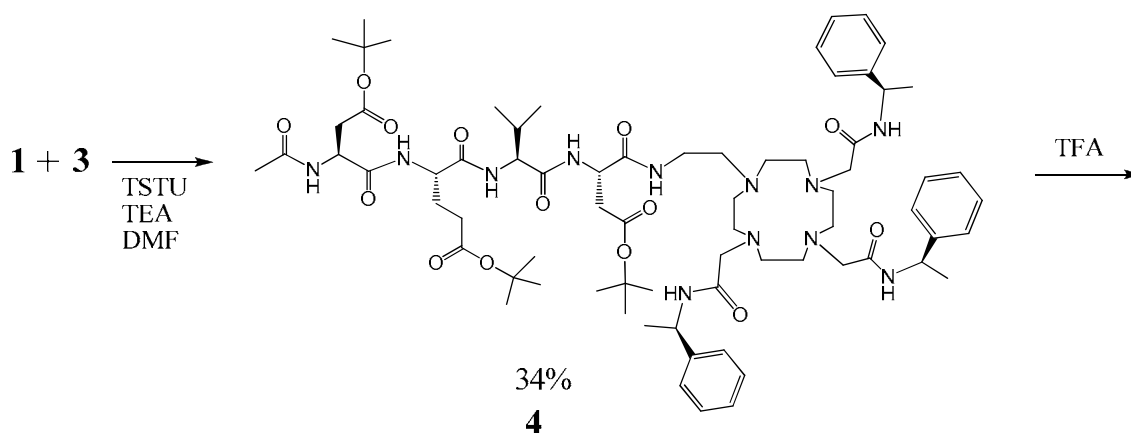
Scheme 4.3 Coupling of 1 to 3 to produce 4. Deprotection of 4 with TFA yields 5. Metalation of 5 with gadolinium(III) or europium(III) yields 6 and 7, respectively.
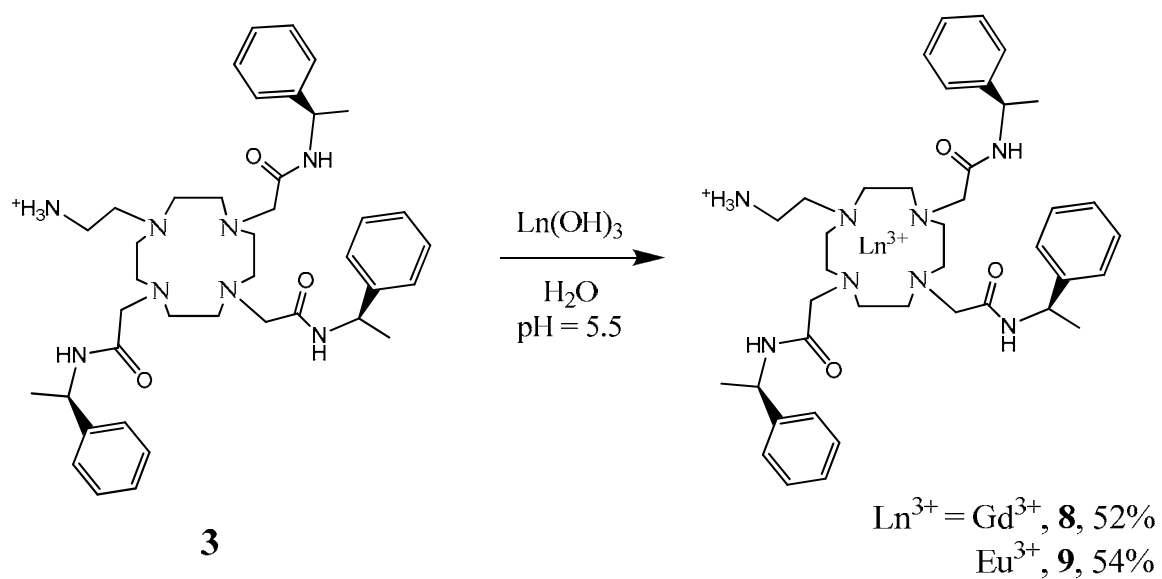
Scheme 4.4 Synthesis of 8 and 9, the chelate portion of the expected enzymatic cleavage products of 6 and 7, respectively.
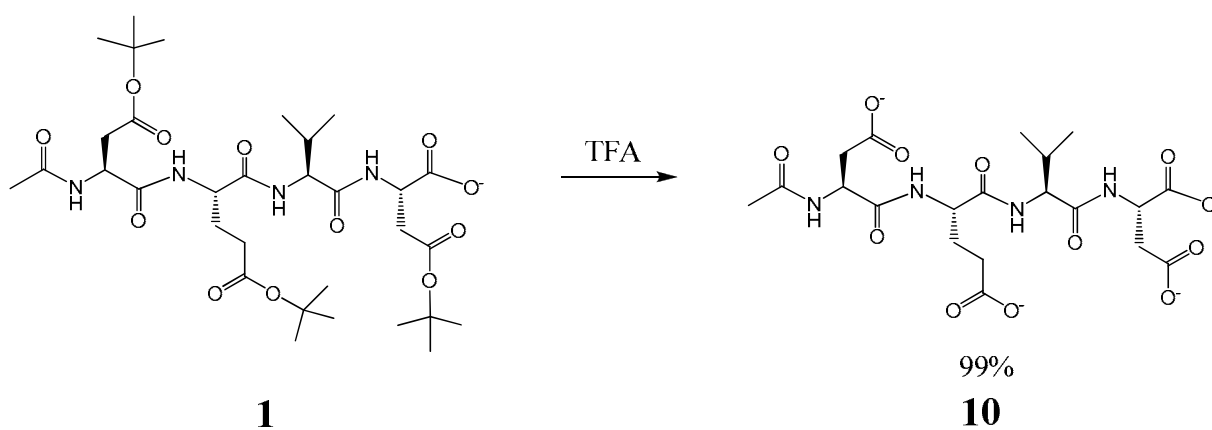
Scheme 4.5 Synthesis of peptide 10, the peptide portion of the expected enzymatic cleavage product of 6 and 7.

Relaxometric Properties (q, τ_m, relaxivity)

The determination of q for **7** and of τ_m and relaxivity for **6** were accomplished using methods described in Chapter II, Part I.A. The determination of q for **9** and of τ_m and relaxivity for **8** are described in Chapter III.

The number of inner-sphere water molecules for **7** was determined to be 0.2 ± 0.1. This value of q corresponds to essentially no inner-sphere water (with a small contribution due to outer-sphere water effects[2]). Using the same luminescence decay method as the present work, Vipond and coworkers recently reported a tetra-amide complex with $q = 0.15 \pm 0.1$ despite a lack of inner-sphere water as evidenced by single crystal X-ray analysis and variable temperature transverse relaxation rate measurements.[3] The transverse relaxation rate of **6** was independent of temperature over the range 275-359 K (Figure 4.2). The lack of a temperature dependence of the transverse relaxation rate is indicative of a $q = 0$ complex.[4] Therefore the q data and the variable temperature transverse relaxation data both suggest that **6** exists with virtually no inner-sphere water molecules.

The relaxivity of **6** in caspase assay buffer at pH 7.4 is 3.16 $mM^{-1}s^{-1}$. This value is significantly lower than that of the structurally similar self-immolative agent (5.31 $mM^{-1}s^{-1}$) described in Chapter III. Due to the lack of inner-sphere water, the relaxivity of **6** is almost entirely due to outer-sphere relaxivity (relaxation of closely diffusing water). For small molecule gadolinium(III)-based contrast agents, outer-sphere relaxivity accounts for approximately half of the overall observed relaxivity.[5-7] Therefore the observed relaxivity of 3.16 $mM^{-1}s^{-1}$ is appropriate given that it is approximately half of the relaxivity of the structurally similar self-immolative agent from Chapter III.
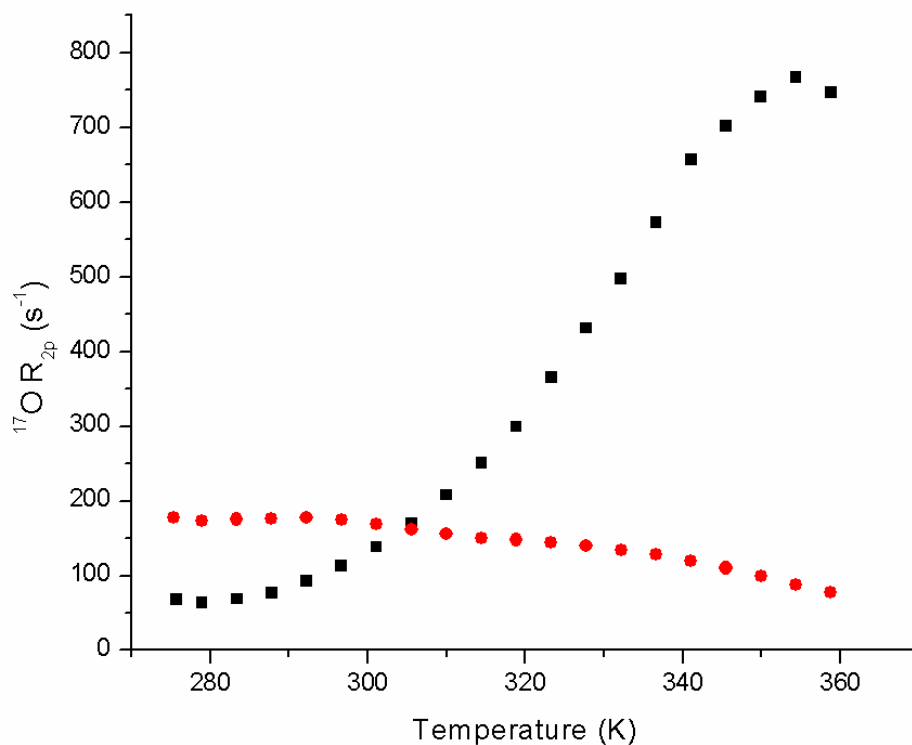
Figure 4.2 Transverse relaxation rate (^{17}O R$_{2p}$) as a function of temperature for 6 (red circles) and 8 (black squares). The lack of a ^{17}O R$_{2p}$ temperature dependence for 6 indicates a q = 0 complex. In contrast, 8 displays marked ^{17}O R$_{2p}$ temperature dependence due to inner-sphere water (q = 1.7, described in Chapter III)

It was originally hypothesized that **6** would bind carbonate, leading to a displacement of inner-sphere water in a manner similar to that observed by Bruce and coworkers for related tris-amide complexes.[4] Therefore, an initial inspection of the data suggested that the lack of inner-sphere water and resultant low relaxivity of **6** was due to the binding of carbonate to the complex. However, a search of the literature reveals that the amount of carbonate present in the relaxivity samples at pH 7.4 is extrememly low (carbonate accounts for less than 0.2% of carbonated species at pH 7.4 while hydrogencarbonate accounts for 45%).[4] This discrepancy

prompted additional studies of the coordination environment of **6**, as this raised doubts about carbonate being the species responsible for the lack of inner-sphere water.

In order to further investigate the lanthanide coordination environment of **6**, the relaxivity was measured as a function of pH (Figure 4.3). The variation of relaxivity with pH can reveal much information about a contrast agent, including both the binding of carbonate as well as the pK_a of exchangeable protons in close proximity to the paramagnetic gadolinium(III).[8,9] Lanthanide chelates which bind carbonate show a characteristic decrease in relaxivity at high pH. This is due to displacement of inner-sphere water by carbonate, as carbonate concentrations increase at high pH.[8] The relaxivity of **6** does not decrease at high pH, further ruling out the possibility of carbonate binding to **6**. At pH values less than 4, the relaxivity of **6** increases dramatically. This phenomenon was pivotal in understanding the lanthanide coordination environment of **6**. The change in relaxivity starting at pH 4 corresponds to protonation of the carboxylic acid of the C-terminal aspartic acid (the pK_a of the side-chain of aspartic acid is approximately 3.90).[10] This observation led to the conclusion that the side-chain of the C-terminal aspartic acid is coordinating to the lanthanide(III) center (Figure 4.4). At pH > 4, it is hypothesized that both the amide carbonyl and the aspartic acid side-chain coordinate to the metal, resulting in all 9 of the available lanthanide(III) coordination sites being occupied by the ligand (the metal is "coordinatively saturated"). As the pH is lowered below 4, the aspartic acid side-chain becomes protonated and no longer coordinates to the metal. The loss of coordination by the aspartic acid side-chain at low pH allows water to coordinate to gadolinium(III), thus explaining the observed increase in relaxivity. At low pH values, a further increase in relaxivity for **6** is likely due to increased prototropic exchange, as has been reported for structurally similar tetraamide complexes.[8] Dissociation of gadolinium(III) from the chelate is not expected because

closely related tetraamide derivatives of DOTA are kinetically inert toward acid-catalyzed

dissociation (half-life in 2.5 M HNO$_3$ at 298 K = 0.2 – 639 hours).[8] This stability at low pH is

attributed to the difficulty of protonating an amide pendant arm.[11]
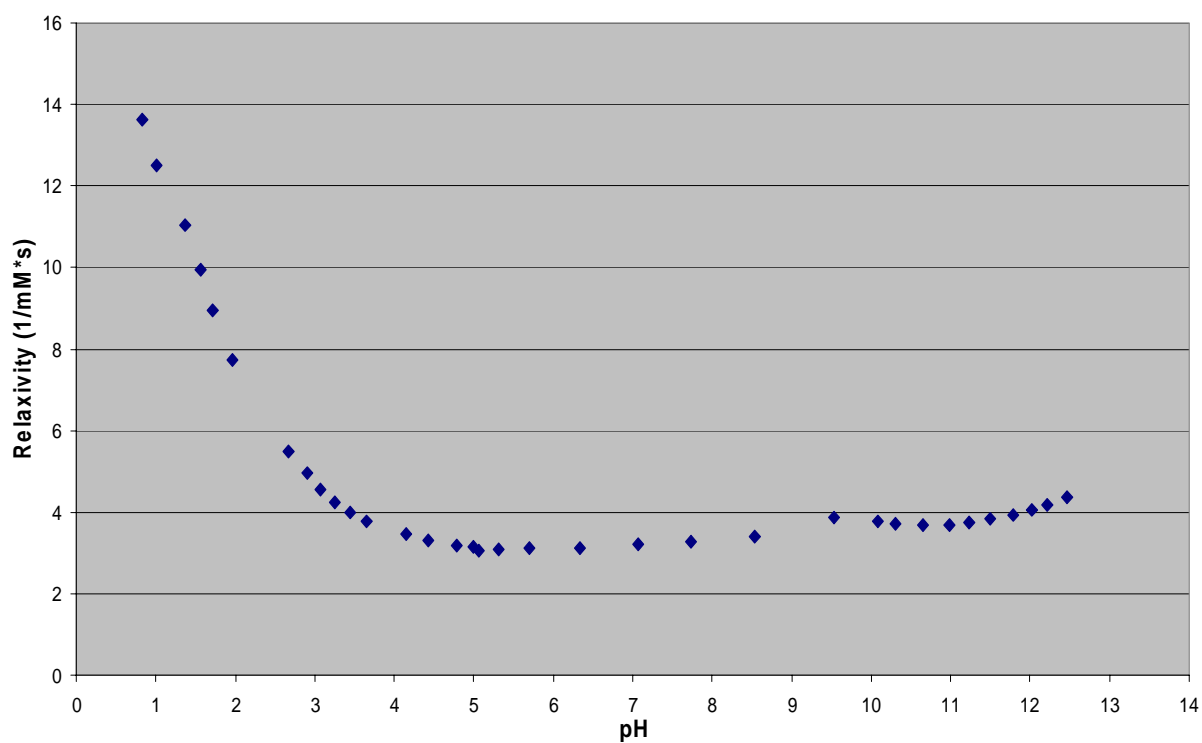
Figure 4.3 Relaxivity as a function of pH for 6
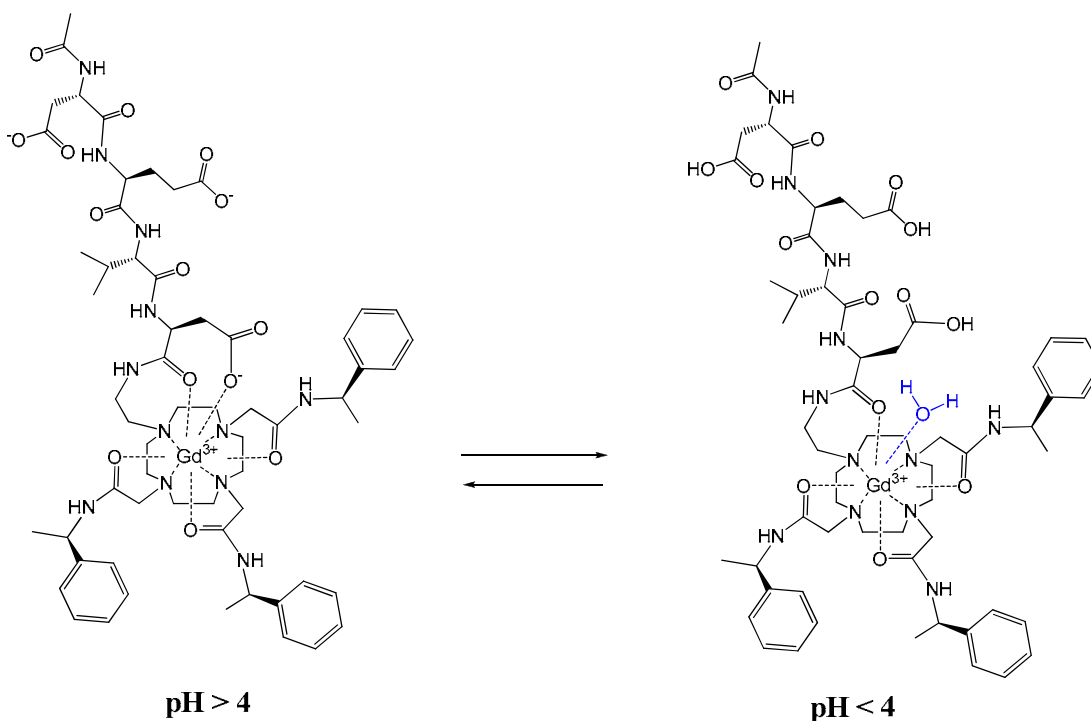
Figure 4.4 Hypothesized mechanism of pH dependent coordination geometry of 6. At pH > 4, the aspartic acid side-chain is deprotonated and coordinates to gadolinium(III), thus blocking inner-sphere water access. At pH < 4, the aspartic acid side-chain is protonated and dissociates from gadolinium(III), thus opening coordination sites for inner-sphere water.

Emission Spectra

Further support for **6** existing as a coordinatively saturated complex can be found in the luminescence emission spectra of the europium(III) analog, **7**. Upon excitation of europium(III) at 394 nm, the ratio of the intensity of the $^5D_0 \rightarrow {}^7F_2$ emission ($\Delta J = 2$ band) to the intensity of the $^5D_0 \rightarrow {}^7F_1$ emission ($\Delta J = 1$ band) reveals valuable information about the coordination geometry of the complex.[4] For coordinatively saturated complexes (termed "fully bound" in the literature), the $\Delta J = 2$ band at 614 nm is ~ 5 times as intense as the $\Delta J = 1$ band at 594 nm.[4] For

7, the ratio of the intensities of the $\Delta J = 2$ to $\Delta J = 1$ bands is ~3.5 (Figure 4.5). In contrast, if inner-sphere water is present, the $\Delta J = 2$ and $\Delta J = 1$ bands are approximately equal in intensity,[4] as is observed for **9** (Figure 4.6). Furthermore, a comparison of the relative intensities of the overall emission spectra of **7** and **9** in H_2O and D_2O reveals less efficient quenching of the europium luminescence of **7** due to a lack of inner-sphere water (Figures 4.5 and 4.6).
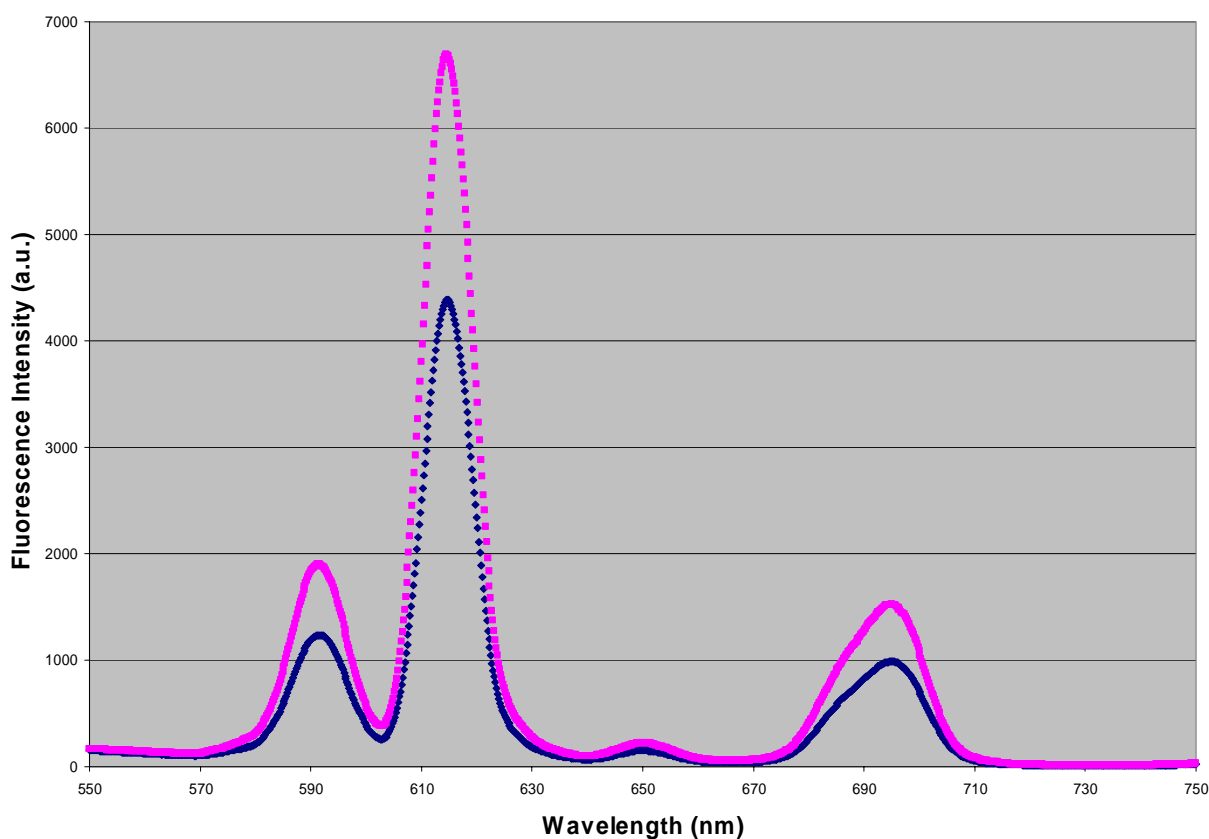
Figure 4.5 Emission spectra (λ_{ex} = 394 nm) of 7 in H_2O (blue) and D_2O (pink). The increased intensity of the $\Delta J = 2$ band (at 614 nm) relative to the $\Delta J = 1$ band (at 594 nm) is indicative of a coordinatively saturated complex.
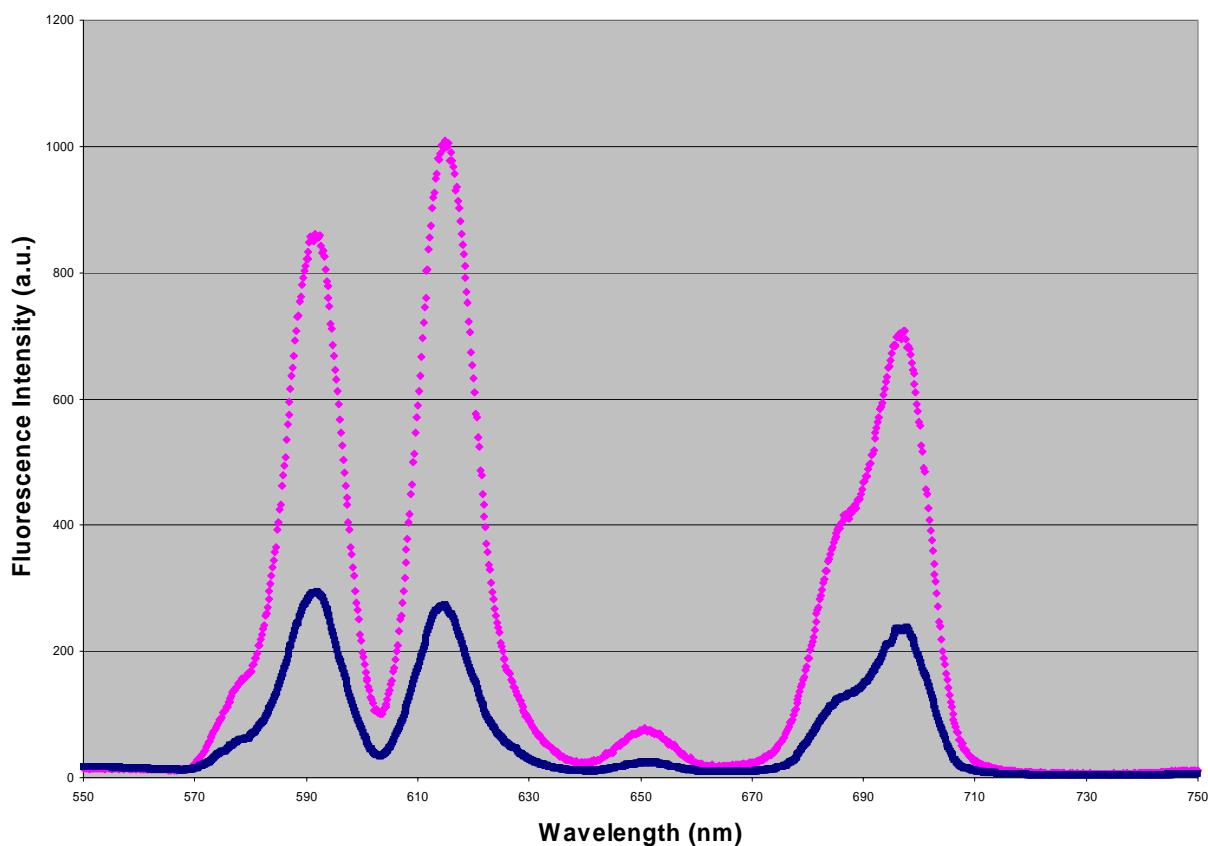
Figure 4.6 Emission spectra (λ_{ex} = 394 nm) of 9 in H_2O (blue) and D_2O (pink). The similar intensity of the ΔJ = 2 band (at 614 nm) relative to the ΔJ = 1 band (at 594 nm) is indicative of the presence of inner-sphere water. The overall difference in fluorescence intensity of 9 in H_2O and D_2O is due to inner-sphere water.

<u>Caspase-3 Assay</u>

The lack of inner-sphere water for **6** (q = 0.2) and the presence of inner-sphere water for

the expected enzymatic cleavage product, **8** (q = 1.7, Chapter III) suggests that **6** could be used

as a q-modulated MRI contrast agent for the detection of caspase-3. Upon enzymatic cleavage of

the Ac-DEVD peptide from the chelate, a change in the number of inner-sphere water molecules

would result in a significant change in the observed T_1, and hence, the MR image intensity

(Equation 1.8, Chapter I). Such a change would allow the monitoring of caspase-3 activity by MRI.

In order to test the ability of **6** to monitor caspase-3 activity by MRI, the T_1 of a solution of **6** with active caspase-3 was monitored as a function of time (using the procedure developed in Chapter III). Despite numerous attempts, the T_1 of the solution did not change over time. Longer reaction times (overnight) produced similar results. It was concluded that under the conditions of the experiment, caspase-3 does not cleave **6**.

It is hypothesized that intramolecular coordination of the C-terminal aspartic acid side-chain to gadolinium(III) (Figure 4.4) prevents caspase-3 from recognizing and cleaving the peptide from the chelate. A combinatorial study of the substrate specificity profile of caspase-3 revealed that recognition of the substrate C-terminal aspartic acid is absolutely required for substrate cleavage by caspase-3.[12] Since the aspartic acid side-chain of **6** is hypothesized to be coordinated to gadolinium(III), this key residue is not available for recognition by caspase-3, and, therefore, **6** is not cleaved by caspase-3.

SUMMARY AND FUTURE DIRECTIONS

The synthesis of **6** was accomplished in 15 steps with an overall yield of 3%. Luminescence lifetime measurements of the europium(III) analog, **7**, revealed 0.2 ± 0.1 inner-sphere water molecules. The lack of a temperature dependence for the transverse relaxation rate of **6** indicates a $q = 0$ complex. The absence of inner-sphere water was corroborated by a detailed analysis of the relative intensity of the $\Delta J = 2$ to $\Delta J = 1$ band found in the europium(III) emission spectrum of **7**.

The lack of inner-sphere water for **6** can be explained by intramolecular backbinding of the peptide to the lanthanide(III) complex. The C-terminal aspartic acid side-chain of **6** is hypothesized to coordinate to gadolinium(III), thus forming a coordinatively saturated complex. An investigation of the relaxivity of **6** as a function of pH supports the hypothesis and excludes the possibility of carbonate binding to **6** in a bidentate fashion. Efforts to grow single crystals of **6** for X-ray analysis are underway and such studies will help reveal further details concerning the coordination environment of gadolinium(III) in **6**.

The difference in q (0.2 vs. 1.7, respectively) between **6** and the corresponding enzymatic cleavage product, **8**, suggests that **6** could be utilized as a q-modulated MRI contrast agent for the detection of caspase-3. Incubation of **6** with active human caspase-3 did not yield a change in T_1. Since a C-terminal aspartic acid residue is required for recognition and cleavage by caspase-3, the inability of the enzyme to cleave **6** is in accord with the hypothesized intramolecular binding of the C-terminal aspartic acid side-chain to gadolinium(III). The coordination of the aspartic acid side-chain to gadolinium(III) prevents the recognition and cleavage of the DEVD substrate by caspase-3.

Previous studies of contrast agents appended to the N-terminus of peptide substrates revealed coordination to gadolinium(III) from the carbonyl oxygen located on the amide linkage between the peptide and the chelate (details in Appendix I). Further studies of contrast agents attached to the N-terminus of peptides revealed that the coordination geometry of the lanthanide(III) chelate was independent of the identity of the N-terminal amino acid.[13] In the present work, a contrast agent was attached to the C-terminus of a peptide. The coordination of the C-terminal aspartic acid side-chain to gadolinium(III) suggests a novel mechanism to control the relaxivity of MRI contrast agents. A study involving the variation of the C-terminal amino

acid of such systems would yield valuable information concerning the scope of this approach. For instance, a simple substitution from aspartic acid to glutamic acid would lengthen the side-chain by one methylene group, thus providing a simple method to study the distance dependence of side-chain coordination to gadolinium(III) chelates.

The synthesis of a coordinatively saturated gadolinium(III) chelate is a promising step towards highly effective q-modulated MRI contrast agents. In order to attain maximum change in signal intensity and avoid background artifacts, it is important to have a contrast agent with a very low initial relaxivity. The coordinatively saturated complex, **6,** is an example of a contrast agent which has achieved this goal and serves as a paradigm towards realizing the potential of q-modulated MRI contrast agents.

EXPERIMENTAL

General experimental details can be found in Chapter II.

Abbreviations:

THF = tetrahydrofuran, DMF = dimethylformamide, TEA = triethylamine, TFA = trifluoroacetic acid, MeCN = acetonitrile, TIS = triisopropylsilane, fmoc = 9-fluorenylmethoxycarbonyl, Boc = *tert*-butoxycarbonyl, HATU = *o*-(7-azabenzotriazol-1-yl)-N,N,N',N'-tetramethyluronium hexafluorophosphate, TSTU = N,N,N',N'-tetramethyl-*o*-(N-succinimidyl)uronium tetrafluoroborate, DIPEA = N,N-diisopropylethylamine, DCC = dicyclohexylcarbodiimide, DMAP = 4-(dimethylamino)pyridine, DOTA = 1,4,7,10-tetraazacyclododecane N,N',N'',N'''-

tetraacetic acid, HPLC = high performance liquid chromatography, RP-HPLC = reverse

phase high performance liquid chromatography, PDA = photodiode array, ESI-MS =

electrospray ionization mass spectrometry, cyclen = 1,4,7,10-tetraazacyclododecane

Ac-Asp(OBu-*t*)-Glu(OBu-*t*)-Val-Asp(OBu-*t*) (1)

Details in Chapter III.

(RRR)-1,4,7-tris[1-(1-phenyl)ethylcarbomoylmethyl]-(1,4,7,10-tetraazacyclododecane)

Details in Chapter III.

1-(2-*t*Boc-aminoethyl)-(RRR)-4,7,10-tris[1-(1-phenyl)ethylcarbomoylmethyl]-(1,4,7,10-tetraazacyclododecane) (2)

Details in Chapter III.

1-(2-aminoethyl)-(RRR)-4,7,10-tris[1-(1-phenyl)ethylcarbomoylmethyl]-(1,4,7,10-tetraazacyclododecane) (3)

Details in Chapter III.

***N*-[Ac-Asp(OBu-*t*)-Glu(OBu-*t*)-Val-Asp(OBu-*t*)]-2-(1-((RRR)-4,7,10-tris[1-(1-phenyl)ethylcarbomoylmethyl])-(1,4,7,10-tetraazacyclododecyl)))ethylamine (4)**

3 (150.47 mg, 0.21497 mmol, 1.0 equivalents), **1** (161.55 mg, 0.23571 mmol, 1.1 equivalents),

TSTU (98.84 mg, 0.3283 mmol, 1.5 equivalents), and TEA (60.0 μL, 0.430 mmol, 2.0

equivalents) were dissolved in 2 mL anhydrous DMF and reacted under nitrogen overnight. The reaction was determined complete after disappearance of **3** by TLC (10% MeOH/CH$_2$Cl$_2$, UV, Pt stain, product R$_f$ = 0.14) and ESI-MS. Solvent was removed by rotary evaporation under reduced pressure. The crude reaction mixture was dissolved in CH$_2$Cl$_2$ and extracted with 5% HCl (3 X 20 mL) and water (3 X 20 mL) followed by drying over Na$_2$SO$_4$. The crude product was dissolved in 10% MeOH/CH$_2$Cl$_2$ and purified on a silica gel column (4.5 cm diameter, 6 cm height, eluent = 10% MeOH/CH$_2$Cl$_2$). Solvent was removed by rotary evaporation under reduced pressure followed by drying under vacuum to afford 98.4 mg white solid (34% yield).

ESI-MS: Calc. 1366.83; Found positive mode 1366.60 (M$^+$), 1390.03 (M + Na$^+$); negative mode 1401.04 (M + Cl$^-$)

^{1}H NMR (CD$_3$OD): Note: fluxional on NMR timescale resulting in broad resonances and non-first order coupling δ = 0.9 (br, 6H, V$_\gamma$); 1.4 (s, 36H, *t*-Bu C*H$_3$* and CH$_2$CONHCHPhC*H$_3$*); 2.0-3.7 [br, 39H (Note – calculated integration is 38H; actual integration is higher due to solvent residual peak), acetyl C*H$_3$*, E$_\beta$, V$_\beta$, E$_\gamma$, D$_\beta$, cyclen, C*H$_2$*C*H$_2$*NH$_2$, and C*H$_2$*CONHCHPhCH$_3$]; 4.2-4.4 (br, 2H, E$_\alpha$, V$_\alpha$); 4.7 (br, 2H, D$_\alpha$); 4.7-5.2 (br, CH$_2$CONHC*H*PhCH$_3$, integration not available due to residual water peak); 7.2-7.4 (br, 15H, aromatics); 7.8, 7.9, 8.0, 8.1, 8.4 (br, N*H*)

^{13}C NMR (CD$_3$OD) : δ = 19.8, 19.9 (V$_\gamma$ and acetyl *C*H$_3$); 22.0-22.8 (br, V$_\beta$ and CH$_2$CONHCHPh*C*H$_3$); 26.5; 28.5 (*t*-Bu *C*H$_3$); 32.7, 35.4, 37.8 (E$_\beta$, E$_\gamma$,D$_\beta$); 50.2-52.6, 54.2, 55.4 (br, D$_\alpha$, E$_\alpha$, V$_\alpha$, cyclen, *C*H$_2$CH$_2$NH$_2$, and *C*H$_2$CONHCHPhCH$_3$); 62.1; 71.3; 82.0, 82.6, 82.8 (*t*-Bu); 127.3, 127.6, 127.8, 128.3, 128.5, 128.7, 129.8, 129.9, 130.1 (br, aromatic); 144.7, 144.8, 145.0 (aromatic ipso *C*); 171.4-171.7, 173.4-174.3 (br, peptide and CH$_2$*C*ONHCHPhCH$_3$ carbonyl)

N-(Ac-Asp-Glu-Val-Asp)-2-(1-((RRR)-4,7,10-tris[1-(1-phenyl)ethylcarbomoylmethyl])-

(1,4,7,10-

tetraazacyclododecyl)))ethylamine (5)

4 (90.4 mg, 0.0661 mmol) was dissolved in 10 mL of 95% TFA, 2.5% TIS, 2.5% H_2O and

reacted overnight. TFA was evaporated by passing N_2 over the reaction solution. Cold diethyl

ether (30 mL) was used to precipitate the crude product as a white solid. The suspension was

centrifuged and decanted. The diethyl ether extraction was repeated 4 times followed by

evaporation of residual diethyl ether by passing N_2 over the solid cake. The crude product was

dissolved in water (5 mL), frozen in liquid N_2, lyophilized, then purified using Solid-Phase

Extraction (details in Chapter 3) to yield 66.90 mg white powder (84% yield).

ESI-MS: Calc. 1198.64; Found positive mode 1198.73 (M^+), 1220.94 ($M + Na^+$); negative mode

1196.36 (M - H)

^1H NMR (CD$_3$OD): Note: fluxional on NMR timescale resulting in broad resonances and non-

first order coupling $\delta = 0.9$ (br, 6H, V$_\gamma$); 1.4 (s, 9H, CH$_2$CONHCHPhC*H$_3$*); 1.9-3.8 [br, 44H

(Note – calculated integration is 38H; actual integration is higher due to solvent residual peak),

acetyl C*H$_3$*, E$_\beta$, V$_\beta$, E$_\gamma$, D$_\beta$, cyclen, C*H$_2$*C*H$_2$*NH$_2$, and C*H$_2$*CONHCHPhCH$_3$]; 4.1-4.3 (br, 2H, E$_\alpha$,

V$_\alpha$); 4.6 (br, 2H, D$_\alpha$); 4.7-5.0 (br, CH$_2$CONHC*H*PhCH$_3$, integration not available due to residual

water peak); 7.1-7.2 (br, 15H, aromatics); 7.8, 7.9, 8.0, 8.3, 8.5 (br, N*H*)

^{13}C NMR (CD$_3$OD) : $\delta = 19.7$, 19.9 (V$_\gamma$ and acetyl C*H$_3$*); 22.8 (br, V$_\beta$ and

CH$_2$CONHCHPhC*H$_3$*); 31.0, 31.3, 36.6, 37.0 (E$_\beta$, E$_\gamma$,D$_\beta$); 50.4-52.3, 53.5, 56.0 (br, D$_\alpha$, E$_\alpha$, V$_\alpha$,

cyclen, C*H$_2$*C*H$_2$*NH$_2$, and C*H$_2$*CONH*C*HPhCH$_3$); 62.6; 71.6; 127.3, 128.4, 129.8 (br, aromatic);

144.9, 145.3 (aromatic ipso); 171.3 (br), 173.6, 173..7, 173.8, 174.1, 174.2, 174.3, 174.4, 174.5,

174.6, 174.7, 175.0, 176.8, 176.9 (carbonyl)

Gadolinium(III)-*N*-(Ac-Asp-Glu-Val-Asp)-2-(1-((RRR)-4,7,10-tris[1-(1-

phenyl)ethylcarbomoylmethyl])-(1,4,7,10-

tetraazacyclododecyl)))ethylamine (6)

5 (42.56 mg, 0.03548 mmol) was dissolved in 10 mL water and the pH was adjusted to 5.5 using

5% NaOH followed by addition of $Gd(OH)_3$ (12.70 mg, 0.04014 mmol, 1.1 equivalents). The

flask was capped with a rubber septum and placed in an 80 ^{o}C oilbath with stirring. The pH was

periodically monitored and adjusted to 5.5 using HCl vapor. The reaction was determined to be

complete when the pH ceased to change (typically 48-72 hours). The crude reaction mixture was

0.22 μm filtered, frozen in liquid nitrogen, and lyophilized. The crude product was purified

using preparative RP-HPLC (Solvent A = H_2O, Solvent B = MeCN; flow rate = 15 mL/min;

gradient starting at 0% B and ramping to 100% B over 30 minutes, hold isocratic 100% B for 5

minutes, ramp to 0% B over 5 minutes, hold isocratic 0% B for 5 minutes; fluorescence detection

of Gd^{3+} λ_{ex} = 274 nm, λ_{em} = 314 nm; UV/vis detection at 205 nm and 270 nm) by injecting crude

product dissolved in water (3 mL, 0.22 μm filtered) with the desired product eluting at 14

minutes. MeCN was removed by rotary evaporation under reduced pressure. The remaining

aqueous solution was frozen in liquid nitrogen and lyophilized to yield 25.90 mg white powder

(54 % yield). 86% metalated by mass as determined by Gd^{3+} ICP-MS.

ESI-MS: Calc. 1353.54; Found positive mode Gd^{3+} isotope pattern centered at 1355.26 (M +

H^+), negative mode Gd^{3+} isotope pattern centered at 1353.38 (M$^-$)

Europium(III)-*N*-(Ac-Asp-Glu-Val-Asp)-2-(1-((RRR)-4,7,10-tris[1-(1-phenyl)ethylcarbomoylmethyl])-(1,4,7,10-tetraazacyclododecyl)))ethylamine (7)

5 (10.83 mg, 0.009030 mmol) was metallated using Eu(OH)$_3$ (3.23 mg, 0.0104 mmol, 1.1 equivalents) and purified by RP-HPLC (product elutes at 14 minutes) using the same method as used for **6** to yield 7.28 mg white powder (61 % yield).

ESI-MS: Calc. 1348.54; Found positive mode Eu^{3+} isotope pattern centered at 1350.28 (M + H$^+$), negative mode Eu^{3+} isotope pattern centered at 1345.97 (M - H)

Gadolinium(III)-1-(2-aminoethyl)-(RRR)-4,7,10-tris[1-(1-phenyl)ethylcarbomoylmethyl]-(1,4,7,10-tetraazacyclododecane) (8)

Details in Chapter III.

Europium(III)-1-(2-aminoethyl)-(RRR)-4,7,10-tris[1-(1-phenyl)ethylcarbomoylmethyl]-(1,4,7,10-tetraazacyclododecane) (9)

Details in Chapter III.

Ac-Asp-Glu-Val-Asp (10)

Details in Chapter III.

Luminescence Emission Spectra and Decay Lifetimes:

1 mM solutions of **7** or **9** were prepared in either H$_2$O or D$_2$O. Emission spectra were recorded using excitation at 395 nm and plotted with Microsoft Excel. Time-resolved luminescence spectra were acquired with the following parameters: 395 nm excitation wavelength, 614 nm

emission wavelength, 10nm excitation slit width, 10nm emission slit width, 950 V PMT, 50

replicates. Data were fit to a single exponential decay using Origin version 7.0. The equation

from Supkowski and coworkers was used to determine q.[14]

Relaxivity

A stock solution consisting of 0.2 mM **6** in Caspase-3 assay buffer (50 mM HEPES, 100 mM

NaCl, 10 mM DTT, 1 mM EDTA, 10% sucrose, 0.1% CHAPS, 1 mg/mL BSA, pH 7.4) was

prepared. Serial dilutions of the stock solution produced concentrations of 0.100 mM, 0.050

mM, 0.025 mM. Twenty five microliters of each sample were used for determining Gd^{3+}

concentration using ICP-MS. Samples were equilibrated to 37 $^{\circ}$C in a water bath for 10 minutes

prior to T_1 measurement. The T_1 of each solution was determined using an inversion recovery

pulse sequence with appropriate recycle delays ($>5*T_1$). A plot of $1/T_1$ vs. concentration was fit

to a straight line yielding the relaxivity as the slope.

Relaxivity vs. pH

A 1 mM solution of **6** was prepared in 2 mL water. The solution was split into two 950 μL

aliquots: one was used for the acidic range and the other for the basic range. The pH was

adjusted into either the acidic range using HCl vapor (as to not change the concentration of the

solution) or the basic range using NaOH (using 0.5 μL additions of 5 mM, 50 mM, or 500 mM

NaOH; more concentrated NaOH solutions were used as the solution became increasingly basic).

For the basic range, the volume of NaOH added was recorded and used to correct the final

concentrations (the correction proved minimal as a total of only 38 μL of NaOH was added to

950 μL initial solution to effect a pH change from 5.00 to 12.46, a 4% increase in volume). Gd^{3+}

concentration was determined using ICP-MS. The samples were allowed to equilibrate at 37

^{o}C for 5 minutes before each T_1 measurement. The T_1 of each solution was determined using an

inversion recovery pulse sequence with appropriate recycle delays ($>5*T_1$). The difference in T_1

values vs. water were used to determine the relative relaxivity at each pH.

Mean Water Residence Lifetime

The transverse relaxation rate of **6** was measured as a function of temperature using the same

methods as described in Chapter III. The lack of temperature dependence for the transverse

relaxation rate of **6** precluded fitting of the data to determine the mean water residence lifetime.

Caspase-3 Enzyme activity

Details in Chapter III.

Caspase-3 T_1 Study

A time-dependent study of the T_1 of **6** in the presence of caspase-3 was performed using the

same methods as described in Chapter III.

CHAPTER V

TOWARDS MMP-7 CLEAVABLE T_1/T_2 MRI CONTRAST AGENTS

The text in this chapter is taken in part from:

INTRODUCTION

<u>T_1/T_2 Contrast Agents</u>

T_1/T_2 contrast agents, consisting of gadolinium(III)-diethylenetriaminepentaacetic acid (Gd-DTPA) T_1 contrast agents covalently attached to a cobalt ferrite nanoparticle T_2 contrast agent, have recently been developed in the Meade laboratory (in collaboration with the research group of Professor Vinayek Dravid, Northwestern University).[1] Since multiple T_1 contrast agents are attached to each T_2 nanoparticle contrast agent, these agents deliver high local concentrations of gadolinium(III) to enhance T_1 while exploiting the sensitivity of T_2 contrast agents. Therefore, T_1/T_2 agents have the potential to optimize MR imaging of both T_1 and T_2 processes. Preliminary investigations of T_1/T_2 agents show that covalent attachment of Gd-DTPA to cobalt ferrite nanoparticles has a substantial effect on the magnetic properties which differs from the magnetic properties of the constituent contrast agents. Furthermore, the magnetic properties of the T_1/T_2 agent are significantly different from a solution consisting of a mixture in which the T_1 agents are not covalently bound to the T_2 agents. The incorporation of an enzymatically cleavable linker between the T_1 contrast agent and the nanoparticle gives T_1/T_2 contrast agents the potential to monitor enzyme activity in vivo.

<u>Matrix Metalloproteinase-7</u>

An introduction to matrix metalloproteinase-7 (MMP-7) can be found in Chapter 2, Part II.

Design of a MMP-7 Cleavable T_1/T_2 MRI Contrast Agent

The integration of a MMP-7 substrate into a T_1/T_2 contrast agent is hypothesized to extend the utility of MRI to include in vivo detection of MMP-7 activity. The proposed change in relaxivity of the T_1/T_2 agent upon cleavage by MMP-7 presents a novel mechanism to detect enzyme activity. Such an agent would be useful in the detection and monitoring of cancer metastasis. The T_1/T_2 contrast agent consists of four parts: a T_1 contrast agent, a T_2 contrast agent, a polyethylene glycol (PEG) linker, and a peptidic substrate.

Gd-DTPA was chosen as the T_1 contrast agent due to cost and availability of starting reagents. Gd-DTPA is an F.D.A. approved clinical MRI contrast agent, therefore in vivo efficacy, pharmacokinetics, and stability have been well documented.[2] Moreover, Gd-DTPA was used by Schultz-Sikma and coworkers during the preliminary studies of T_1/T_2 agents and therefore the relaxivities obtained within the current work can be compared with previous results.[1]

The T_2 contrast agent consists of core-shell cobalt ferrite silica nanoparticles. The 7 nm cobalt ferrite core is uniformly isolated within a 10 nm silica shell. Further derivatization of the nanoparticles with 3-aminopropyl triethoxysilane (APTES) creates amine functionalities on the surface of the nanoparticle, which are amenable to coupling with the C-terminal carboxylic acid of the peptide.

A PEG linker was included in the target molecule for three reasons. First, the functionalized PEG linker used in the present work is commercially available in a variety of lengths from three to twenty eight glycol units, thus providing a facile method to study the effects of the relaxivity of the overall molecule as a function of distance between the T_1 and T_2 contrast agents. Second, the PEG linker aids water solubility of the peptide prior to conjugation

to the nanoparticle and is proposed to increase the aqueous stability of the peptide-nanoparticle conjugate. Third, the PEG linker between the peptide and the nanoparticle allows increased space for the enzyme to interact with the substrate. It is hypothesized that placement of the enzymatic cleavage site in close proximity to the nanoparticle could introduce unfavorable steric and/or electrostatic interactions between the enzyme and the nanoparticle, thus hindering recognition and cleavage of the substrate.

The peptidic substrate was designed to be cleaved by MMP-7. (Note: The overlapping substrate specificities within the family of MMP enzymes adds the potential for a substrate to be cleaved by multiple enzymes within this family.[3]) The ability of MMP-7 to cleave a broad range of substrates allowed for variation in the amino acid sequence of the specific peptidic substrate and provided some flexibility in the design of the target molecule. The substrate peptide sequence consists of PLA^LWA, where ^ denotes the expected MMP-7 cleavage site. To simplify the synthesis of the target molecule, amino acids with reactive side-chain functional groups (cysteine, aspartic acid, glutamic acid, lysine, arginine) were avoided. This reduced the need for amino acid side-chain protection strategy, leading to simplified starting materials and fewer reaction steps. The only amino acid side-chain protecting group required for the synthesis of the target molecule is the Boc protection of the tryptophan side-chain, which can be simultaneously removed during cleavage of the peptide from the resin. The addition of a tryptophan to the peptide provided a convenient chromophore for detection of the intermediate peptide by fluorescence during reverse-phase high performance liquid chromatography (RP-HPLC) purification. The remainder of the amino acids for the substrate were chosen based on the sequence specificities of MMP-7 as determined by Netzel-Arnett and coworkers.[4] An alanine residue was incorporated onto the N-terminus of the peptide (after the proline residue)

such that the coupling of DTPA-bis(anhydride) to the peptide could be monitored using the Kaiser test for free amines.[5] (Note: Alanine is a primary amine whereas proline is a secondary amine. The Kaiser test is based on the detection of primary amines; secondary amines result in a false negative Kaiser test.) An alanine reside was included on the C-terminal end of the PEG linker due to the commercial availability of starting materials. (Wang resin with preloaded alanine is commercially available, while Wang resin with preloaded PEG units is not commercially available. The Wang resin was purchased with the C-terminal alanine residue preloaded onto the resin because the addition of the first amino acid to the resin is notoriously laborious, low yielding, and can lead to enantiomerization of the amino acid residue.[6,7])

It is hypothesized that the relaxation properties of the T_1/T_2 conjugate will be sufficiently different than the relaxation properties of the individual T_1 or T_2 contrast agent components. The two different PEG linkers are hypothesized to have different relaxation properties due to the differing distance between the T_1 and T_2 contrast agents. It is hypothesized that cleavage of the substrate peptide by MMP-7 will result in a return of the overall relaxivity to that of a mixture of its components (Figure 5.1).
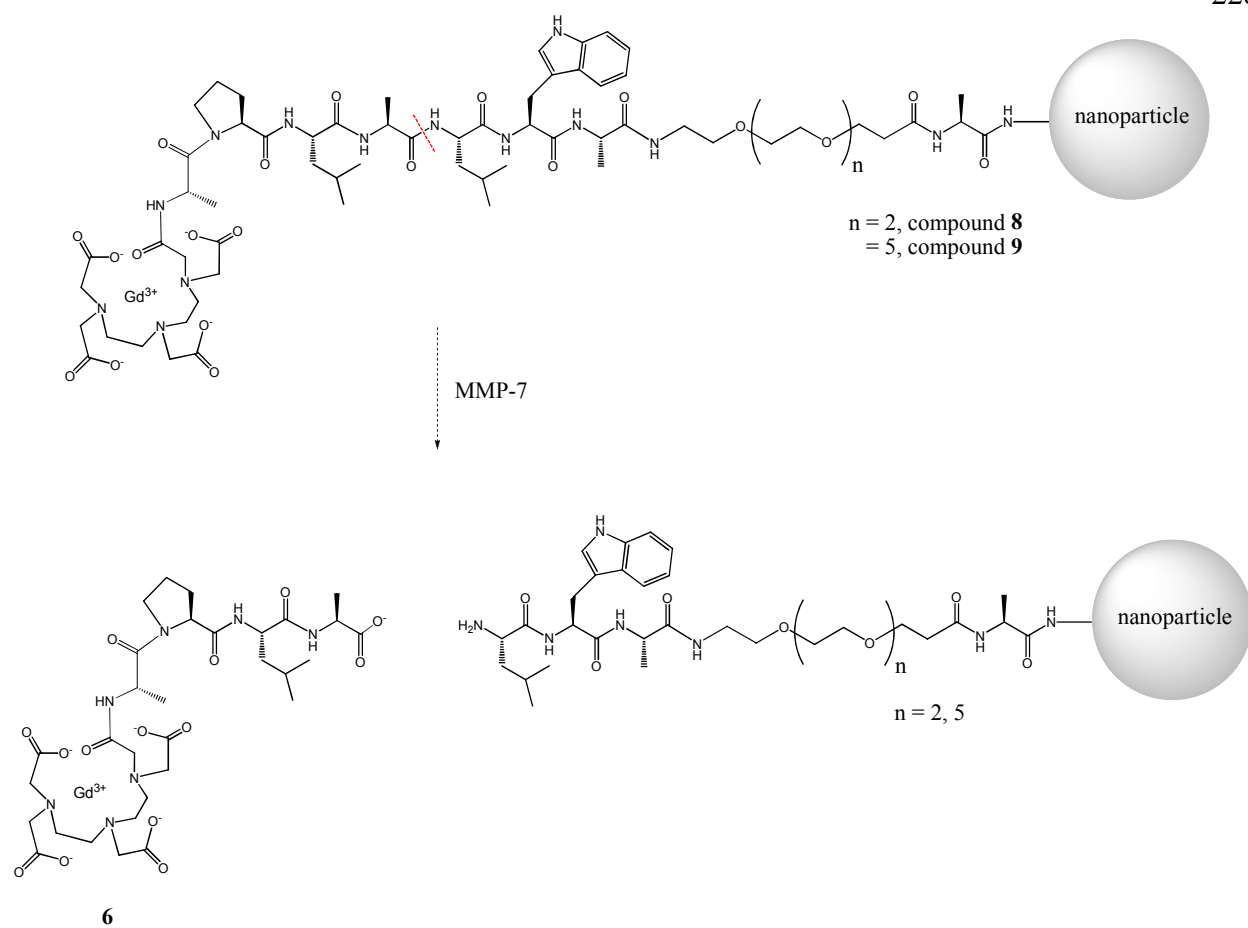
Figure 5.1 T_1/T_2 MRI contrast agents, 8 and 9, for the detection of MMP-7. The proposed cleavage of the substrate peptide by MMP-7 (at the cleavage site denoted with a red dashed line), separates the T_1 agent from the T_2 agent, leading to a hypothesized change in relaxivity.

RESULTS AND DISCUSSION

Synthesis of T_1 Contrast Agent with a Substrate Peptide and PEG Linker

Solid-phase peptide synthesis (SPPS) was used to synthesize the MMP-7 substrate peptide. The PEG linkers were added to the C-terminus of the peptide during SPPS through the use of commercially available PEG amino acids. The PEG amino acid consists of a 9-fluorenylmethoxycarbonyl (fmoc) protected amine with varying lengths of PEG units (3 and 6 used in the present study) and a carboxylic acid functionality. The use of fmoc protecting strategy allowed the PEG amino acids to be incorporated into SPPS in quantitative yields. After 16 SPPS steps, the substrate peptide with the PEG linker was completed (Scheme 5.1). Removal of the N-terminal fmoc group, coupling of DTPA-bis(anhydride), and hydrolysis of the remaining anhydride provided a facile means to covalently attach the T_1 chelate to the peptide (Scheme 5.2). Trifluoroacetic acid (TFA) was used to cleave the peptide from the solid support as well as remove the butyoxycarbonyl (Boc) protecting group from the tryptophan side-chain to afford **1** and **2** in an overall yield of 10% after 19 steps and purification by RP-HPLC (Scheme 5.3). Metalation with gadolinium(III) followed by RP-HPLC purification resulted in **3** and **4** in 86% yield (Scheme 5.4).

1. piperdine/DMF
2. fmoc-(PEG)$_n$-COOH
   HATU, DIPEA, DMF
3. piperidine/DMF
4. fmoc-ala-OH
   HATU, DIPEA, DMF
5. piperidine/DMF
6. fmoc-trp(Boc)-OH
   HATU, DIPEA, DMF
7. piperidine/DMF
8. fmoc-leu-OH
   HATU, DIPEA, DMF

9. piperidine/DMF
10. fmoc-ala-OH
    HATU, DIPEA, DMF
11. piperidine/DMF
12. fmoc-leu-OH
    HATU, DIPEA, DMF
13. piperidine/DMF
14. fmoc-pro-OH
    HATU, DIPEA, DMF
15. piperidine/DMF
16. fmoc-ala-OH
    HATU, DIPEA, DMF

(R) = Wang resin

n = 2, 5

Scheme 5.1 Solid-phase peptide synthesis of the MMP-7 substrate peptide with PEG linker. Two different lengths of PEG linkers were synthesized.

1. piperidine/DMF

2. i.

DIPEA, DMF

ii. H_2O, DMF

n = 2, 5

n = 2, 5
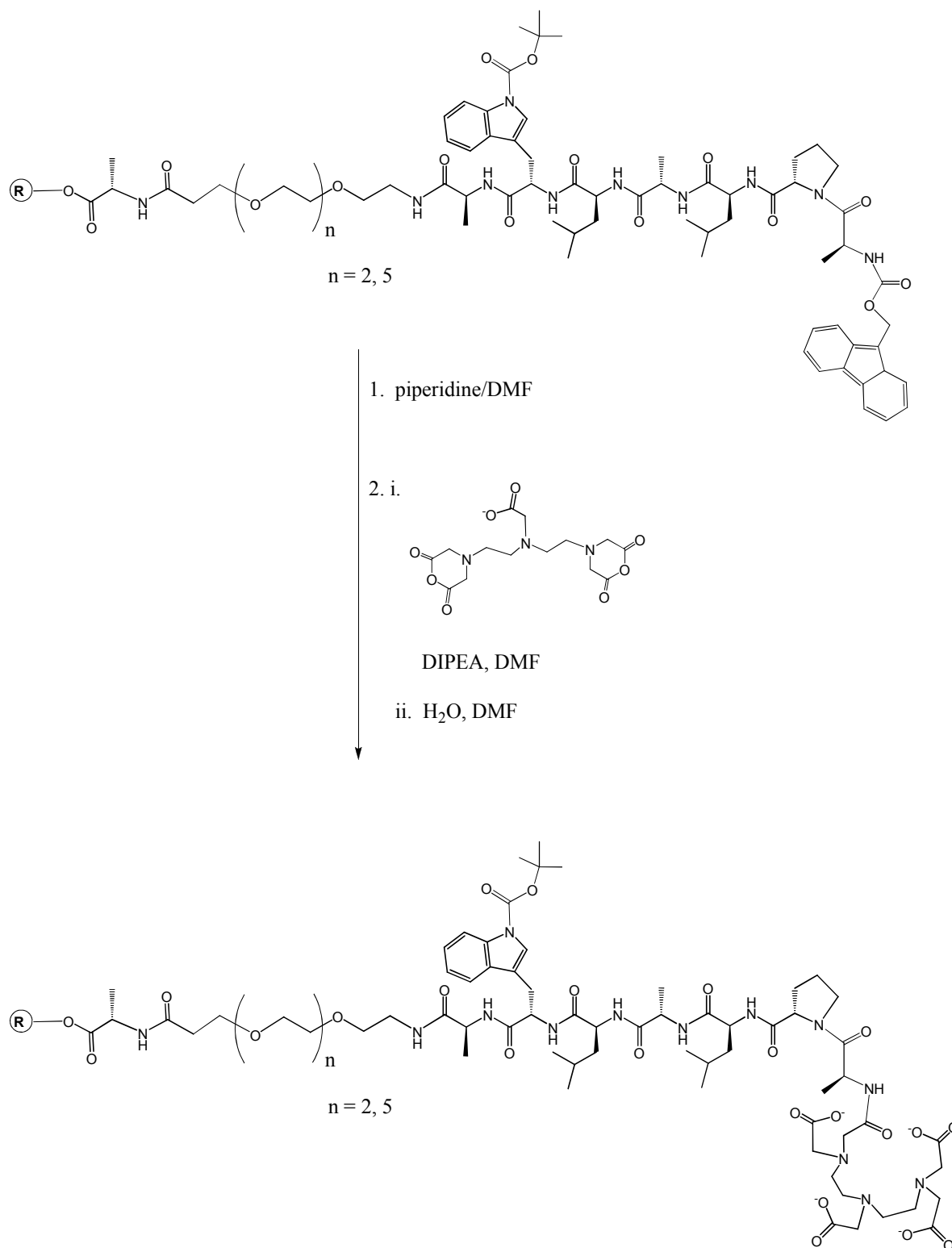
Scheme 5.2 Addition of DTPA (ligand for T_1 contrast agent) to the N-terminus of the substrate peptide containing a PEG linker.
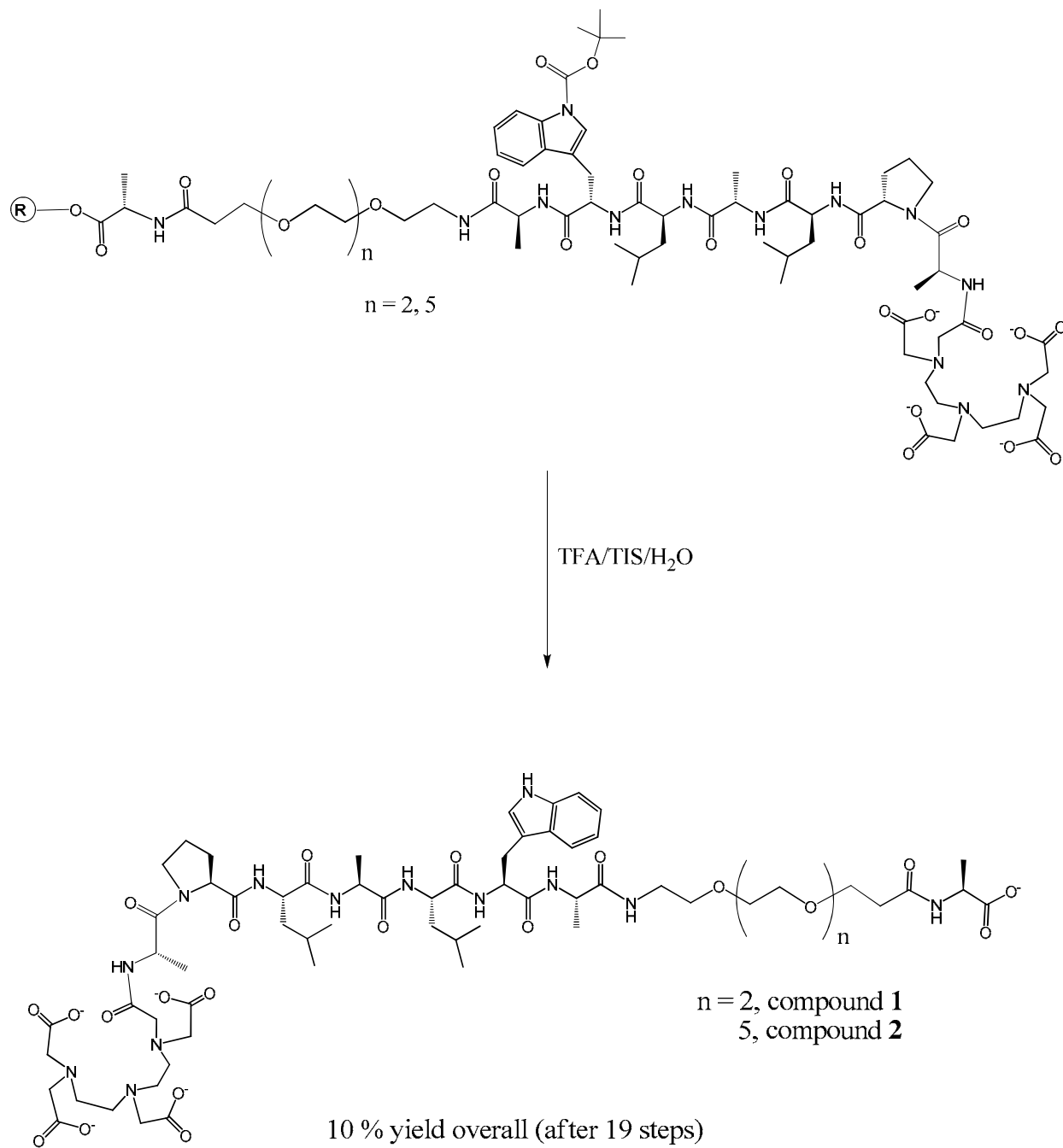
Scheme 5.3 Cleavage from the resin and deprotection to yield 1 and 2.

n = 2, 5

TFA/TIS/H₂O

n = 2, compound **1**
5, compound **2**

10 % yield overall (after 19 steps)

n = 2, compound **1**
5, compound **2**

Gd(OH)$_3$
H$_2$O

n = 2, compound **3**
5, compound **4**

86%
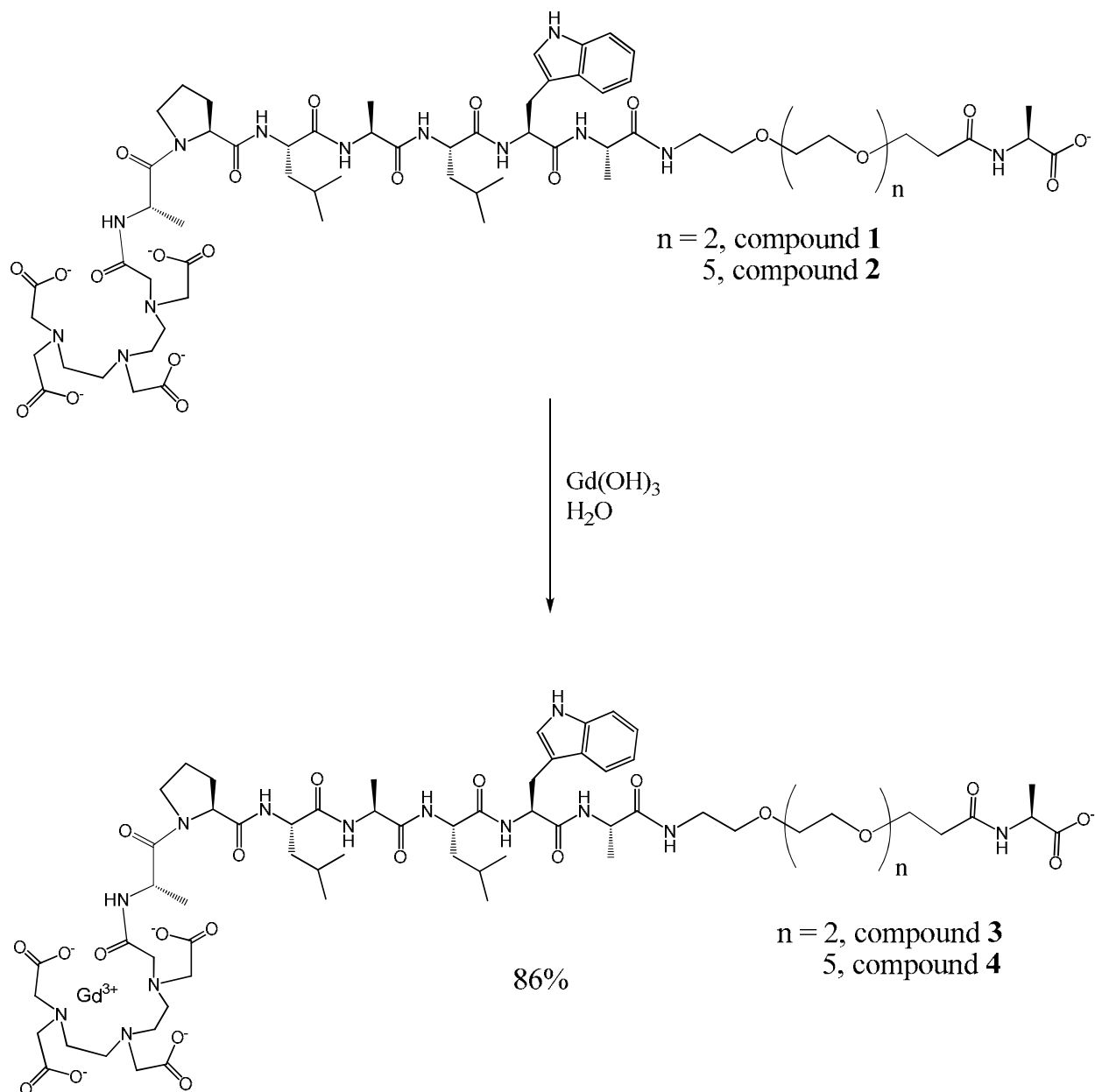
Scheme 5.4 Metalation of 1 and 2 with gadolinium(III) to afford 3 and 4, respectively.

Synthesis of Cleaved Agent

In order to simulate the effects of enzymatic cleavage of **8** and **9** and to provide an authentic standard for comparison, the cleaved contrast agent, **6**, was independently synthesized in 10 steps (Scheme 5.5). The synthesis of the cleaved ligand, **5**, was accomplished using SPPS and purified by RP-HPLC in a manner analogous to that used during the synthesis of **1** and **2**. Metalation of **5** with gadolinium(III), followed by RP-HPLC purification afforded **6**.

1. piperidine/DMF
2. fmoc-leu-OH
   HATU, DIPEA, DMF
3. piperidine/DMF
4. fmoc-pro-OH
   HATU, DIPEA, DMF

5. piperidine/DMF
6. fmoc-ala-OH
   HATU, DIPEA, DMF
7. piperidine/DMF
8. DTPA-dianhydride
   DIPEA, DMF
9. TFA/TIS/H$_2$O

R = Wang resin

5

5 $\xrightarrow[\text{H}_2\text{O}]{\text{Gd(OH)}_3}$ **6**
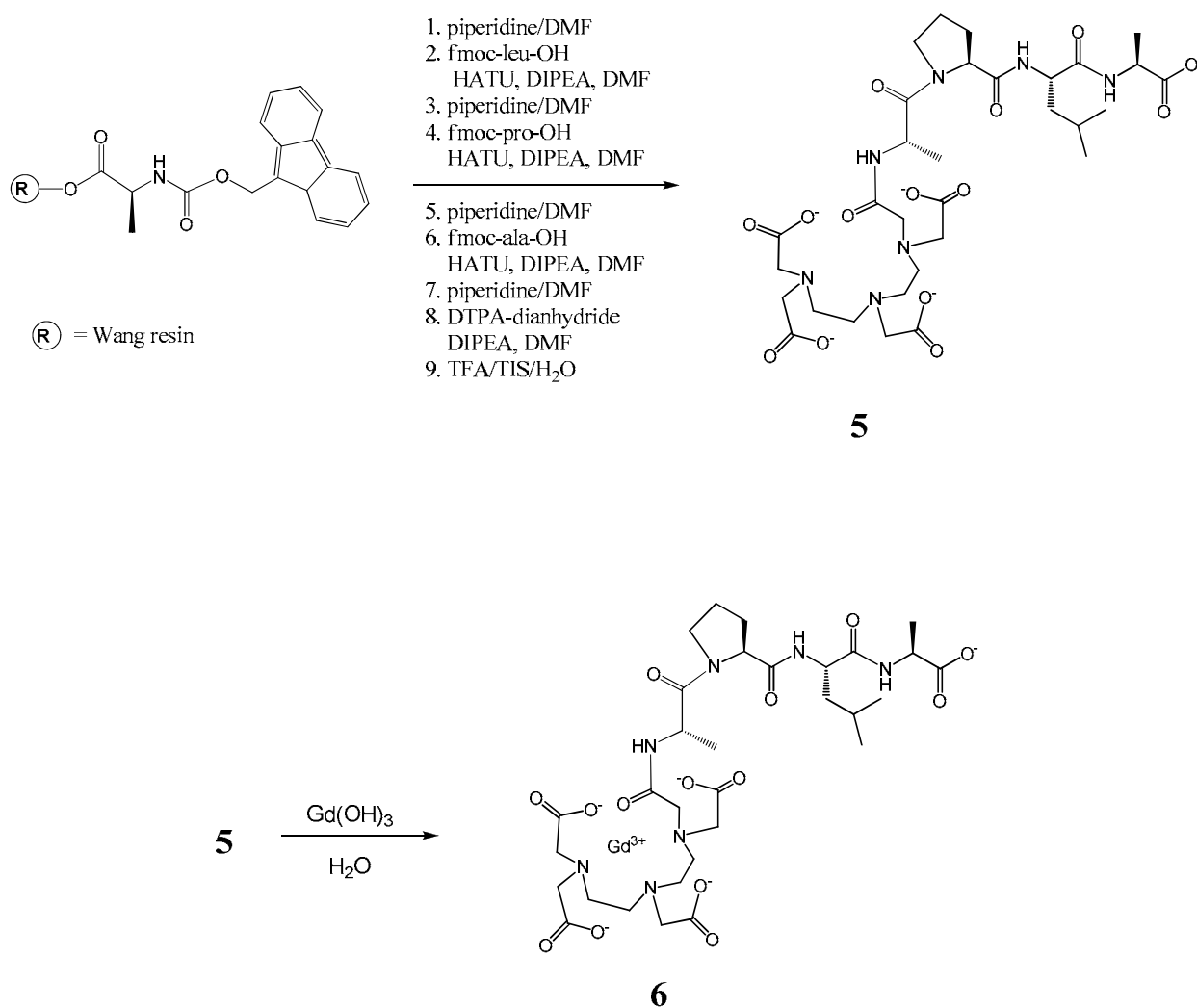
Scheme 5.5 Synthesis of 6, the contrast agent corresponding to enzymatic cleavage of 3, 4, 8, or 9 by MMP-7

Enzymatic Cleavage

As a proof of concept for the cleavage of the substrate peptide (prior to adding the nanoparticle), **3** was subjected to in vitro hydrolysis by human MMP-7 (Scheme 5.6). The enzymatic cleavage reaction was monitored by electrospray ionization mass spectrometry (ESI-MS). After 24 hour incubation with MMP-7, **3** was completely hydrolyzed at the expected cleavage site, resulting in **6** and **7**. ESI-MS of the enzymatic cleavage solution revealed the MMP-7 cleavage fragment **7** as the major peak in the spectrum. Uncleaved **3** could not be detected by ESI-MS after 24 hour exposure to active MMP-7. ESI-MS analysis of a control solution lacking MMP-7 revealed only the expected parent molecule, **3**.

Interestingly, the other cleavage fragment, **6**, could not be detected by ESI-MS. It is speculated that **6** is either associated with proteins or lacks sufficient solubility for detection by ESI-MS. The proteins in the enzymatic cleavage solution include MMP-7 and bovine serum albumin (BSA). MRI contrast agents have been reported to nonspecifically associate with serum albumin proteins.[8-10] The potential association of **6** with proteins would decrease the amount of **6** available in solution for detection by ESI-MS. Furthermore, the cleavage of **3** by MMP-7 to produce **6** may result in a change in solubility due to the removal of the PEG linker, which was originally used to help aid solubility of the peptide (which contains mostly hydrophobic side-chains). As a result, removal of the PEG linker by enzymatic cleavage can be expected to reduce aqueous solubility. The decreased solubility of **6** could hinder ionization and detection during ESI-MS, thus explaining the difficulty in observing **6** by ESI-MS.
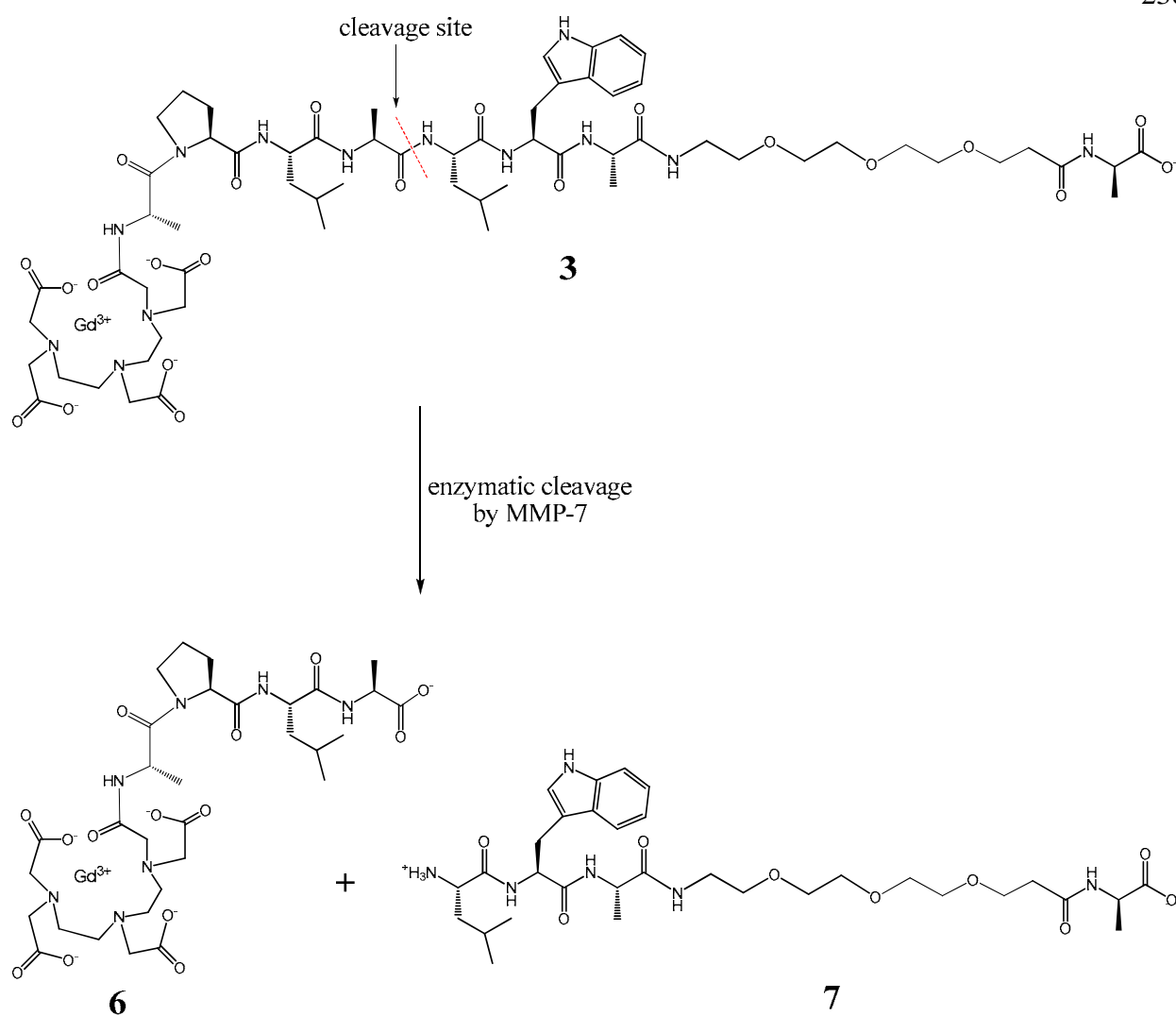
Scheme 5.6 Cleavage of 3 by MMP-7 produces 6 and 7. ESI-MS detected the disappearance of 3 and the appearance of 7 during in vitro cleavage by human MMP-7.

Synthesis of Amine-functionalized Core-shell $CoFe_2O_4@SiO_x$ Nanoparticles

(performed by Mohammed Aslam, research group of Professor Vinayek Dravid)

Cobalt ferrite ($CoFe_2O_4$) nanoparticles were synthesized using modified literature procedures.[8] Transmission electron microscopy (TEM) analysis of the $CoFe_2O_4$ nanoparticles showed uniformity in shape and size (7 nm, Std. deviation $\leq 10\%$) (Figure 5.2 A). X-ray diffraction (XRD) confirmed the cobalt ferrite phase formation (Figure 5.2 B). The Debye-Scherer equation was used to calculate particle size, which was in good agreement with TEM results.

The $CoFe_2O_4$ nanoparticles were coated with SiO_x by base-catalyzed silica formation from tetraethylorthosilicate in a water-in-oil microemulsion, using modified literature procedures.[9,10] $CoFe_2O_4@SiO_x$ nanoparticles were characterized by transmission electron microscopy (TEM), energy-dispersive spectroscopy, elemental mapping, FTIR, and x-ray photoelectron spectroscopy (XPS). TEM of the $CoFe_2O_4@SiO_x$ nanoparticles suggests that the 7 nm core is uniformly isolated in an individual shell with 10 nm thickness (Figure 5.2 C). FTIR of $CoFe_2O_4@SiO_x$ nanoparticles shows the presence of hydroxyl groups on the silica shell (peak at 940 cm^{-1}).

Surface modification of $CoFe_2O_4@SiO_x$ nanoparticles with amines was performed using 3-aminopropyl triethoxysilane (APTES). The presence of amines was confirmed by XPS (N 1s peak Binding Energy ~400 eV) (Figure 5.2 D).
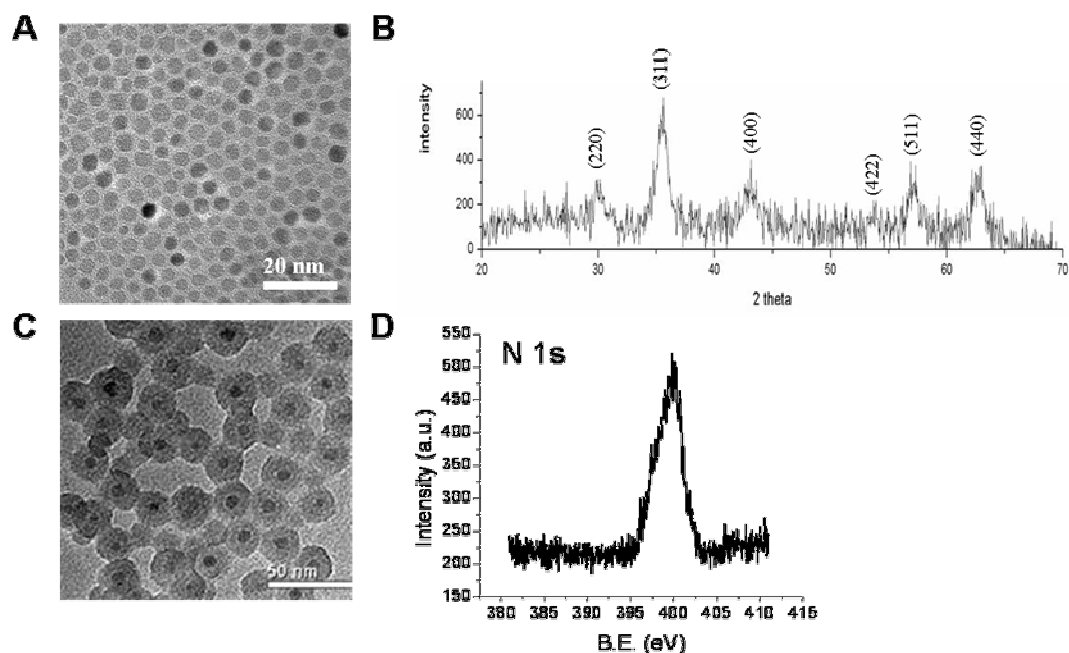
Figure 5.2 Characterization of nanoparticle synthesis
(A) TEM image of cobalt ferrite core formation
(B) confirmation of cobalt ferrite phase formation using XRD
(C) TEM image of silica-coated core-shell nanoparticles
(D) XPS spectrum showing N 1s peak at binding energy of ~400 eV indicating adsorption of APTES onto nanoparticle surface.

<u>Coupling of T_1 Contrast Agent with Peptide and PEG Linker to the Amine-functionalized Core-</u>

<u>shell T_2 Nanoparticle</u> *(performed by Elise Schultz-Sikma)*

The coupling of **3** to the amine-functionalized $CoFe_2O_4@SiO_x$ nanoparticles was

performed on a small-scale test reaction using standard peptide coupling techniques with 1-ethyl-

3-(3-dimethylaminopropyl)carbodiimide hydrochloride and N-hydroxysulfosuccinimide.

Dialysis was used to remove unconjugated **3**. ICP-MS of the nanoparticle solution revealed the

presence of gadolinium(III), albeit in low amounts. The conjugation conditions are currently being optimized prior to scaleup.

SUMMARY AND FUTURE DIRECTIONS

The synthesis of two Gd-DTPA T_1 contrast agents, each with a MMP-7 substrate peptide and a PEG linker, was accomplished in 20 steps with an overall yield of 9%. The two versions differ by the number of PEG groups incorporated into the linker (three PEG units for **3** and six PEG units for **4**). The different length PEG linkers for **3** and **4** will allow an investigation of the influence of distance between the T_1 and T_2 contrast agent components on the overall relaxivity of the conjugate.

The synthesis of **6**, which corresponds to the enzymatic cleavage product of **8** and **9**, was accomplished in 10 steps. This product will prove useful as a basis for comparison during the study of **8** and **9** as well as serve as a control molecule during relaxivity measurements.

Prior to coupling **3** and **4** to the core-shell nanoparticles, the in vitro cleavage of **3** by human MMP-7 was performed. The complete cleavage of **3** by MMP-7 at the expected cleavage site was confirmed by ESI-MS. These results proved feasibility of MMP-7 cleavage prior to the added complexity of being attached to a nanoparticle.

The amine-functionalized core-shell $CoFe_2O_4@SiO_x$ nanoparticles have been synthesized and characterized. Conjugation of **3** to the nanoparticles is currently underway. Future work involves optimizing the coupling conditions followed by scaleup. The optimized reaction conditions will be used as the initial conditions during the test reactions involving the

conjugation of **4** to the nanoparticles. A study of the T_1 and T_2 relaxivity of **8** and **9** both prior to and after cleavage by MMP-7 will follow.

The MMP-7 cleavable T_1/T_2 contrast agents presented in the present work will serve as a paradigm for future T_1/T_2 MRI contrast agents. The plethora of permutations to this system includes varying peptide length and composition, varying the length of the PEG spacer, varying the chelate for the T_1 contrast agent, and varying the size and composition of the T_2 nanoparticle. The optimization of each of these variables can then be applied to novel systems in which the substrate peptide sequence is changed such that other proteases can be detected using this novel method of MR contrast enhancement.

EXPERIMENTAL

General experimental details can be found in Chapter 2.

Abbreviations

DMF = dimethylformamide, TFA = trifluoroacetic acid, TIS = triisopropylsilane, fmoc = 9-fluorenylmethoxycarbonyl, Boc = *tert*-butoxycarbonyl, HATU = *o*-(7-azabenzotriazol-1-yl)-N,N,N',N'-tetramethyluronium hexafluorophosphate, DIPEA = N,N-diisopropylethylamine, DTPA = diethylenetriaminepentaacetic acid, HPLC = high performance liquid chromatography, RP-HPLC = reverse phase high performance liquid chromatography, ESI-MS = electrospray ionization mass spectrometry, MALDI-TOF MS = matrix assisted laser desorption ionization time of flight mass spectrometry, PEG = polyethylene glycol, BSA = bovine serum albumin, APMA = 4-aminophenylmercuric acetate, tris = 2-amino-2-hydroxymethylpropane-1,3-diol

MMP-7

Human recombinant MMP-7 was purchased from Anaspec (San Jose, CA). The enzyme solution was divided into 2 μL aliquots containing 10 μg/mL each [> 600 units/μg; one unit hydrolyzes 1 pmol of Mca-Pro-Leu-Gly-Leu-Dap(Dnp)-Ala-Arg-NH$_2$ per minute at pH 7.5 at 25 ^{o}C] and stored at -80 ^{o}C. MMP-7 assay buffer consists of 50 mM tris HCl, 150 mM NaCl, 10 mM CaCl$_2$, 1 mg/mL BSA, pH 7.5. MMP-7 was activated by incubation in 1mM APMA in assay buffer for 1 hour at 37 ^{o}C prior to use. Enzyme activity was confirmed using a SensoLyte 490 MMP-7 fluorescence assay kit (purchased from Anaspec; used according to manufacturer instructions).

N-[N-carbonylmethyl-ala-pro-leu-ala-leu-trp-ala-poly(ethylene glycol)$_3$-ala]-diethylenetriaminetetraacetic acid (1)

The peptide was synthesized according standard solid-phase peptide synthesis methods[6] using manual batch-type synthesis and fmoc protected amino acids.

A Wang resin consisting of 100-200 mesh 1% cross-linked polystyrene beads functionalized with p-benzyloxybenzyl alcohol handle was used as a solid support for the stepwise addition of amino acids. The Wang resin was purchased (NovaBiochem, San Diego, California) with the N-terminal amino acid, fmoc-alanine, preloaded onto the resin. The resin (1.09347 g, 0.68 mmol/g resin loading) was added to a fritted glass reactor vessel fitted with a 3-way valve for switching between N$_2$ (used to mix during all reactions and rinses) and vacuum (used to drain rinses and excess reactants). The dry Wang resin was pre-swelled with CH$_2$Cl$_2$ (1 X 10 minute rinse) followed by DMF (4 X 10 minute rinses). The N-terminal fmoc protecting group was removed using 20% piperidine in DMF (until determined >99% complete by the Kaiser test;[5] typically 4

X 10 minutes). The resin was rinsed with DMF (4 X 10 minutes). The next amino acid (2.5

equivalents relative to the N-terminal amine on the amino acid attached to the Wang resin) to be

added to the peptide was dissolved in a minimal amount of DMF. To this solution, HATU (2

equivalents) and DIPEA (5 equivalents) were added to form a yellow solution of the preactivated

fmoc-amino acid. This solution was added to the resin and allowed to react while gently

bubbling N_2 to mix the reactants until determined >99% complete (typically 2-12 hours) by the

Kaiser test. Upon completion, the resin was rinsed with DMF (4 X 10 minutes). Fmoc removal

and addition of the next amino acid was repeated for each amino acid until the desired sequence

was obtained. After fmoc removal, diethylenetriaminepentaacetic acid dianhydride (669.72 mg,

2.5 equivalents) was dissolved in a minimal amount of DMF using a few drops of anhydrous

DMSO to aid solubility followed by addition of DIPEA (650 µL, 5 equivalents). This solution

was added to the Wang resin and allowed to react until determined >99% complete (typically 2-4

hours) by the Kaiser test. After completion, the resin was rinsed with 1:1 DMF:H_2O (2 X 10

minutes) to hydrolyze the remaining anhydride of DTPA. The resin was rinsed with DMF (4 X

10 minutes), CH_2Cl_2 (4 X 10 minutes), methanol (4 X 10 minutes), then dried under vacuum

overnight. To the dried resin was added a cleavage cocktail (15 mL) consisting of 95% TFA,

2.5% TIS, 2.5% H_2O. The resin was allowed to react in the cleavage cocktail for one hour, after

which the solution was drained into a vial. Fresh cleavage cocktail (15 mL) was added to the

resin and allowed to react for 10 minutes, followed by draining into a vial. Fresh cleavage

cocktail (10 mL) was added to the resin and immediately drained into a vial. The cleavage

cocktail solutions were combined and TFA was evaporated by passing N_2 over the vial. The

volume was reduced to <1 mL followed by addition of cold (-20 ^{o}C) diethyl ether to precipitate

the crude product as a white solid. The suspension was centrifuged and decanted. The diethyl

ether extraction was repeated 4 times followed by evaporation of residual diethyl ether by

passing N_2 over the vial. The white solid cake was dissolved in water (25 mL), frozen in liquid

N_2, and lyophilized. Crude product was purified using preparative RP-HPLC (Solvent A =

0.05% TFA in H_2O, Solvent B = MeCN; flow rate = 15 mL/min; gradient starting at 0% B and

ramping to 30% B over 5 minutes, hold isocratic 30% B for 15 minutes, ramp to 100% B over 3

minutes, hold isocratic 100% B for 5 minutes, ramp to 0% B over 5 minutes, hold isocratic 0% B

for 7 minutes; fluorescence detection of tryptophan λ_{ex} = 250 nm, λ_{em} = 350 nm; UV/vis

detection at 205 nm and 270 nm) by injecting sample (typically ~60 mg per injection) dissolved

in water (3 mL, 0.22 μm filtered) with the desired product eluting at 13 minutes 45 seconds.

MeCN was removed by rotary evaporation under reduced pressure. The remaining aqueous

solution was frozen in liquid N_2 and lyophilized. Yield: 107.87 mg, 10% overall yield after 19

steps.

ESI-MS: calc. 1389.71; found positive mode 1390.68 (M + H), 1412.67 (M + Na^+); negative

mode 1388.76 (M^-).

_N_-[_N_-carbonylmethyl-ala-pro-leu-ala-leu-trp-ala-poly(ethylene glycol)$_6$-ala]-

diethylenetriaminetetraacetic acid (2)

2 was synthesized starting from 1.0001 g fmoc-ala-Wang resin (0.68 mmol/g resin loading) and

purified (RP-HPLC retention time = 14 minutes 30 seconds) using the same methods as

described for **1** by substituting the commercially available fmoc-PEG$_6$-COOH for fmoc-PEG$_3$-

COOH. Yield: 106.54 mg, 10% overall yield after 19 steps.

ESI-MS: calc. 1521.78; found positive mode 773.09 $(M + Na)^{2+}$, 784.83 $(M + 2Na)^{2+}$.

Gadolinium(III)-*N*-[*N*-carbonylmethyl-ala-pro-leu-ala-leu-trp-ala-poly(ethylene glycol)$_3$-ala]-diethylenetriaminetetraacetic acid (3)

1 (54.20 mg, 0.03912 mmol) was placed in a 50 mL round bottom flask with magnetic stirbar and dissolved in 25 mL H_2O. The pH was adjusted to 5.5 using 5% NaOH followed by addition of Gd(OH)$_3$ (9.31 mg, 0.0295 mmol, 0.8 equivalents). The flask was capped with a rubber septum and sonicated briefly to reduce the size of the Gd(OH)$_3$ particulates before placing in a 80 ^{o}C oilbath with stirring. Over the course of the reaction, the pH gradually increased due to the release of OH$^-$ and there was a visible decrease in the amount of Gd(OH)$_3$ solids. The pH was periodically monitored and adjusted to 5.5 using HCl vapor. The reaction was determined to be complete when the pH stabilized (usually 48-72 hours). The pH was raised to 10 using 20% NaOH (typically 2 μL) to precipitate any excess Gd^{3+} as Gd(OH)$_3$ and 0.22 μm filtered. The filtrate was then frozen in liquid nitrogen and lyophilized. The crude product was purified using preparative RP-HPLC (Solvent A = H_2O, Solvent B = MeCN; flow rate = 15 mL/min; same gradient as used above for **1**; fluorescence detection of tryptophan λ_{ex} = 250 nm, λ_{em} = 350 nm; UV/vis detection at 205 nm and 270 nm) by injecting sample dissolved in water (0.22 μm filtered) with the desired product eluting at 9 minutes 45 seconds (unreacted **1** elutes at 11 minutes under these conditions). MeCN was removed by rotary evaporation under reduced pressure. The remaining aqueous solution was frozen in liquid N_2 and lyophilized. Yield: 39.01 mg, 86%.

ESI-MS: calc. 1542.75, found positive mode 784.43 $(M + Na)^{2+}$

MALDI-TOF MS: found positive mode 1544.8 $(M + H^+)$, 1566.7 $(M + Na^+)$, 1588.6 $(M + 2Na)^+$, 1610.5 $(M + 3Na)^+$. MS showed characteristic Gd isotope ratios.

Gadolinium(III)-*N*-[*N*-carbonylmethyl-ala-pro-leu-ala-leu-trp-ala-poly(ethylene glycol)$_6$-ala]-diethylenetriaminetetraacetic acid (4)

2 (52.76 mg, 0.03476 mmol) was metallated using Gd(OH)$_3$ (12.69 mg, 0.04011 mmol, 1.2 equivalents) and purified using the same methods as described for **3**.

ESI-MS: calc. 1676.67; found positive mode 1743.65 (M + 3Na)$^+$, 885.99 (M + 4Na)$^{2+}$; negative mode 837.52 (m/2). MS showed characteristic Gd isotope ratios.

_N_-(_N_-carbonylmethyl-ala-pro-leu-ala)-diethylenetriaminetetraacetic acid (5)

5 was synthesized starting from 1.365 g fmoc-ala-Wang resin (0.68 mmol/g resin loading) and purified (RP-HPLC retention time = 9 minutes) using the same methods as described for **1**.

ESI-MS: calc. 745.35; found positive mode 746.80 (M + H)

^{1}H NMR (D$_2$O): δ = 0.8, 0.9 (two sets of doublets, 6H, L$_\delta$, J = 5.6 Hz); 1.4 (two sets of doublets, 6H, A$_\beta$, J = 7.2 Hz); 1.5-1.6 (m, 3H, L$_\beta$ and L$_\gamma$); 1.8-2.3 (m, 4H, P$_3$ and P$_4$); 3.1-3.8 (m, 12H, DTPA C*H$_2$*C*H$_2$*, DTPA C*H$_2$*CONH, and P$_5$); 4.0, 4.1 (s, 8H, DTPA C*H$_2$*COOH); 4.2 (t, 1H, P$_\alpha$ or L$_\alpha$, J = 6.4), 4.3 (q, 1H, A$_\alpha$, J = 7.2), 4.4 (t, 1H, P$_\alpha$ or L$_\alpha$, J = 7.2), 4.6 (q, 1H, A$_\alpha$, J = 7.2 Hz)

Gadolinium(III)-*N*-(*N*-carbonylmethyl-ala-pro-leu-ala)-diethylenetriaminetetraacetic acid (6)

5 (51.9 mg, 0.0696 mmol) was metallated using Gd(OH)$_3$ (24.2 mg, 0.766 mmol, 1.1 equivalents) and purified using the same methods as described for **3**.

ESI-MS: calc. 898.24; found positive mode Gd^{3+} isotope pattern centered at 896.66 (M$^+$), 918.69 (M + Na$^+$).

Enzymatic Cleavage

A 2 μL aliquot of human recombinant MMP-7 was thawed on ice, diluted to 50 μL with assay buffer containing 1 mM APMA, and incubated for 1 hour at 37 °C to activate the enzyme. To the activated enzyme solution was added 1 μL of a 20 mM solution of **3**. The solution was incubated at 37 °C for 24 hours after which 10 μL was dissolved in 50 μL MeOH for analysis by ESI-MS. The mass spectrum revealed a peak corresponding to the MMP-7 cleavage fragment Leu-Trp-Ala-PEG$_3$-Ala, **7**, [calc.:662.35, found: positive mode 685.89 ($M + Na^+$)]. ESI-MS of a control solution (prepared as above; 1 μL of 20 mM **3** in 50 μL assay buffer with 1mM APMA) lacking MMP-7 revealed only the expected uncleaved **3** [calc. 1542.75; found negative mode 771.60, (m/2)]

CoFe$_2$O$_4$ Nanoparticles

CoFe$_2$O$_4$ core particles were synthesized using modified literature methods.[8] A quantity of 40 mL of benzyl ether solution containing 2 mmol concentrated iron (III) tris(acetyl acetonate) and 2 mmol concentrated cobalt (III) tris(acetyl acetonate) was reduced by 10 mM hexadecanediol under N$_2$ atmosphere and heated at 275 °C to yield cobalt ferrite (CoFe$_2$O$_4$) nanoparticles. The solution was heated in presence of 6 mmol lauric acid and lauryl amine at 100 °C for 30 min. The solution was heated at 200 °C for 1 hour followed by heating at reflux (265-285 °C). The cobalt ferrite nanoparticle solution was subjected to magnetic separation by ethanol precipitation, and the resulting aggregate was washed with copious amounts of ethanol and acetone. The aggregate was dispersed in hexane for storage.

Core-shell CoFe$_2$O$_4$@SiO$_x$ Nanoparticles

CoFe$_2$O$_4$ nanoparticles were coated with SiO$_x$ using modified literature methods.[9,10] Igepal CO-520 [branched polyoxyethylene (5) nonylphenylether] (1 mL) was mixed with 20 ml of anhydrous cyclohexane and stirred for 10 minutes. Cobalt ferrite nanoparticles were dispersed in cyclohexane at a concentration of 1 mg/mL and poured slowly into the cyclohexane/Igepal solution. Aqueous 30% NH$_4$OH (120 µl) was added dropwise and stirred for 15 minutes, followed by the addition of tetraethylorthosilicate (190 µl). The mixture was stirred for 48 h before adding ethanol to precipitate the particles. The precipitate was collected by centrifugation at 10,000 rpm and particles were washed by redispersing in ethanol. CoFe$_2$O$_4$@SiO$_x$ nanoparticles were washed using this procedure at least three times to remove excess surfactant and stored as a toluene dispersion.

CoFe$_2$O$_4$@SiO$_x$ nanoparticles were characterized by transmission electron microscopy (TEM), energy-dispersive spectroscopy, elemental mapping, FTIR, and x-ray photoelectron spectroscopy (XPS).

Amine-functionalized Core-shell CoFe$_2$O$_4$@SiO$_x$ Nanoparticles

Surface modification of CoFe$_2$O$_4$@SiO$_x$ nanoparticles with 3-aminopropyl triethoxysilane (APTES) was carried out at room temperature by injecting 100 µl of APTES in a 1 mg/mL dispersion of CoFe$_2$O$_4$@SiO$_x$ nanoparticles in toluene followed by rigorous stirring for 2-4 days. The precipitated mixture was rinsed copiously with absolute alcohol and dispersed in water or DMSO for storage.

The presence of amines after reaction with APTES was confirmed by XPS (N 1s peak BE ~400 eV).

CHAPTER I REFERENCES

(1)   Moats, R. A.; Fraser, S. E.; Meade, T. J. *Angewandte Chemie, International Edition in English* **1997**, *36*, 726-728.

(2)   Louie, A. Y.; Huber, M. M.; Ahrens, E. T.; Rothbacher, U.; Moats, R.; Jacobs, R. E.; Fraser, S. E.; Meade, T. J. *Nature Biotechnology* **2000**, *18*, 321-325.

(3)   Lauffer, R. B.; McMurry, T. J.; Dunham, S. O.; Scott, D. M.; Parmelee, D. J.; Dumas, S. U.S. Patent, 2006.

(4)   Duimstra, J. A.; Femia, F. J.; Meade, T. J. *J. Am. Chem. Soc.* **2005**, *127*, 12847-12855.

(5)   Allen, M., California Institute of Technology, 2004.

(6)   Babine, R. E.; Bender, S. L. *Chemical Reviews* **1997**, *97*, 1359-1472.

(7)   Zhang, S.; Kovacs, Z.; Burgess, S.; Aime, S.; Terreno, E.; Sherry, A. D. *Chem. Eur. J.* **2001**, *7*, 288-296.

(8)   Vipond, J.; Woods, M.; Zhao, P.; Tirsco, G.; Ren, J.; Bott, S. G.; Ogrin, D.; Kiefer, G. E.; Kovacs, Z.; Sherry, A. D. *Inorg. Chem.* **2007**, *46*, 2584-2595.

(9)   Bruce, J. I.; Dickins, R. S.; Govenlock, L. J.; Gunnlaugsson, T.; Lopinski, S.; Lowe, M. P.; Parker, D.; Peacock, R. D.; Perry, J. J. B.; Aime, S.; Botta, M. *J. Am. Chem. Soc.* **2000**, *122*, 9674-9684.

(10)   Swift, T. J.; Connick, R. E. *J. Chem. Phys.* **1962**, *37*, 307-320.

(11)   Bianchi, A.; Garcia-Espana, E.; Micheloni, M.; Nardi, N.; Vizza, F. *Inorg. Chem.* **1986**, *25*, 4379-4381.

(12)   Bencini, A.; Bianchi, A.; Borselli, A.; Ciampolini, M.; Garcia-Espana, E.; Dapporto, P.; Micheloni, M.; Paoli, P.; Ramirez, J. A.; Valtancoli, B. *Inorg. Chem.* **1989**, *28*, 4279-4284.

(13)   Bencini, A.; Bianchi, A.; Chimichi, S.; Ciampolini, M.; Dapporto, P.; Garcia-Espana, E.; Micheloni, M.; Nardi, N.; Paoli, P.; Valtancoli, B. *Inorg. Chem.* **1991**, *30*, 3687-3691.

(14)   Ciampolini, M.; Micheloni, M.; Vizza, F.; Zanobini, F.; Chimichi, S.; Dapporto, P. *J. Chem. Soc., Dalton Trans.* **1986**, 505-510.

(15)   Wangler, B.; Beck, C.; Wagner-Utermann, U.; Schirrmacher, E.; Bauer, C.; Rosch, F.; Schirrmacher, R.; Eisenhut, M. *Tetrahedron Letters* **2006**, *47*, 5985-5988.

(16)   Hubin, T. J.; McCormick, J. M.; Alcock, N. W.; Busch, D. H. *Inorg. Chem.* **2001**, *40*, 435-444.

(17)   Springborg, J.; Glerup, J.; Sotofte, I. *Acta Chem. Scand.* **1997**, *51*, 357.

(18)   Urbanczyk-Pearson, L. M.; Femia, F. J.; Smith, J.; Parigi, G.; Duimstra, J. A.; Eckermann, A. L.; Luchinat, C.; Meade, T. J. *Inorg. Chem.* **2008**, *47*, 56-68.

(19)   Kovacs, Z.; Sherry, A. D. *Synthesis* **1997**, 759-763.

(20)   Wong, W.; Li, C.; Organization, W. I. P., Ed. Hong Kong, 2005.

(21)   Chan, W. C.; White, P. D. *Fmoc Solid Phase Peptide Synthesis*; Oxford University Press: New York, 2000.

(22)   Zhang, S.; Sherry, A. D. *J. Solid State Chem.* **2003**, *171*, 38-43.

(23)   Slichter, C. P. *Principles of Magnetic Resonance*; 3rd ed.; Springer-Verlag: New York, 1996.

(24)   Merbach, A. E.; Toth, E. *The Chemistry of Contrast Agents in Medical Magnetic Resonance Imaging*; John Wiley and Sons, Ltd.: Chichester, England, 2001.

(25)   Lide, D. *CRC Handbook of Chemistry and Physics*; 71st ed.; CRC Press: Boca Raton, 1990.

(26)   Bussi, S.; Fouillet, X.; Morisetti, A. *Experimental and Toxicologic Pathology* **2007**, *58*, 323-330.

(27)   Caravan, P.; Ellison, J. J.; McMurry, T. J.; Lauffer, R. B. *Chemical Reviews* **1999**, *99*, 2293-2352.

(28)   Kumar, K.; Chang, C. A.; Francesconi, L. C.; Dischino, D. D.; Malley, M. F.; Gougoutas, J. Z.; Tweedle, M. F. *Inorg. Chem.* **1994**, *33*, 3567-3575.

(29)   Smith, R. M.; Motekaitis, R. J.; Martell, A. E. *NIST Standard Reference Database#46*; 3.0 ed.; National Institute of Standards and Technology: Washington D.C. , 1997.

(30)   Aime, S.; Botta, M.; Panero, M.; Grandi, M.; Uggeri, F. *Magn. Reson. Chem.* **1991**, *29*, 923-927.

(31)   Brucher, E.; Cortes, S.; Chavez, F.; Sherry, A. D. *Inorg. Chem.* **1991**, *30*, 2092-2097.

(32)   Micskei, K.; Helm, L.; Brucher, E.; Merbach, A. E. *Inorg. Chem.* **1993**, *32*, 3844-3850.

(33)   Aime, S.; Barge, A.; Botta, M.; Parker, D.; De Sousa, A. S. *J. Am. Chem. Soc.* **1997**, *119*, 4767-4768.

(34)   Brasch, R. C. *Magnetic Resonance in Medicine* **1991**, *22*, 282-7.

(35)   Lauffer, R. B. *Magnetic Resonance in Medicine* **1991**, *22*, 339-346.

(36)   Kellar, K. E.; Henrichs, P. M.; Hollister, R.; Koenig, S. H.; Eck, J.; Wei, D. *Magn. Reson. Med.* **1997**, *38*, 712-716.

(37)   Wiener, E. C.; Brechbiel, M. W.; Brothers, H.; Magin, R. L.; Gansow, O. A.; Tomalia, D. A.; Lauterbur, P. C. *Magnetic Resonance in Medicine* **1994**, *31*, 1-8.

(38)   Grant, C. W. M.; Karlik, S.; Florio, E. *Magnetic Resonance in Medicine* **1989**, *11*, 236-43.

(39)   Allen, M.; Bulte, J. W. M.; Liepold, L.; Basu, G.; Zywicke, H. A.; Frank, J. A.; Young, M.; Douglas, T. *Magn. Reson. Med.* **2005**, *54*, 807-812.

(40)   Mikawa, M.; Kato, H.; Okumura, M.; Narazaki, M.; Kanazawa, Y.; Miwa, N.; Shinohara, H. *Bioconjugate Chemistry* **2001**, *12*, 510-514.

(41)   Zhang, S.; Merritt, M.; Woessner, D. E.; Lenkinski, R. E.; Sherry, A. D. *Acc. Chem. Res.* **2003**, *36*, 783-790.

(42)   Aime, S.; Carrera, C.; Castelli, D. D.; Crich, S. G.; Terreno, E. *Angewandte Chemie, International Edition* **2005**, *44*, 1813-1815.

CHAPTER II REFERENCES

(1)   Moats, R. A.; Fraser, S. E.; Meade, T. J. *Angewandte Chemie, International Edition in English* **1997**, *36*, 726-728.

(2)   Louie, A. Y.; Huber, M. M.; Ahrens, E. T.; Rothbacher, U.; Moats, R.; Jacobs, R. E.; Fraser, S. E.; Meade, T. J. *Nature Biotechnology* **2000**, *18*, 321-325.

(3)   Puente, X. S.; Sanchez, L. M.; Overall, C. M.; Lopez-Otin, C. *Nature Reviews Genetics* **2003**, *4*, 544-558.

(4)   Barrett, A. J.; Rawlings, N. D.; Woessner, J. F. *Handbook of Proteolytic Enzymes*; Academic Press: San Diego, 1998.

(5)   Meade, T.; Fraser, S.; Jacobs, R. In *PCT Int. Appl.*; (California Institute of Technology, USA; Meade, Thomas; Fraser, Scott; Jacobs, Russell). Wo, 1996, p 65 pp.

(6)   Allen, M., California Institute of Technology, 2004.

(7)   Liu, S.; Pietryka, J.; Ellars, C. E.; Edwards, D. S. *Bioconjugate Chemistry* **2002**, *13*, 902-913.

(8)   Babine, R. E.; Bender, S. L. *Chemical Reviews* **1997**, *97*, 1359-1472.

(9)   Cohen, G. M. *Biochem. J.* **1997**, *326*, 1-16.

(10)   Thornberry, N. A.; Rano, T. A.; Peterson, E. P.; Rasper, D. M.; Timkey, T.; Garcia-Calvo, M.; Houtzager, V. M.; Nordstrom, P. A.; Roy, S.; Vaillancourt, J. P.; Chapman, K. T.; Nicholson, D. W. *J. Biol. Chem.* **1997**, *272*, 17907-17911.

(11)   Zucker, S.; Cao, J. *Nature Medicine* **2001**, *7*, 655-656.

(12)   Kovacs, Z.; Sherry, A. D. *Synthesis* **1997**, 759-763.

(13)   Kaiser, E.; Colescott, R. L.; Bossinger, C. D.; Cook, P. I. *Analytical Biochemistry* **1970**, *34*, 595-598.

(14)   Barefield, E. K.; Wagner, F.; Hodges, K. D. *Inorg. Chem.* **1976**, *15*, 1370-1377.

(15)   Richman, J. E.; Atkins, T. J. *J. Am. Chem. Soc.* **1974**, *96*, 2268-2270.

(16)   Lambert, J.; Mazzola, E. P. *Nuclear Magnetic Resonance Spectroscopy. An Introduction to Principles, Applications, and Experimental Methods*; Pearson Education, Inc.: Upper Saddle River, NJ, 2004.

(17)   Supkowski, R. M.; Horrocks, W. D. *Inorganica Chimica Acta* **2002**, *340*, 44-48.

(18)   Lide, D. *CRC Handbook of Chemistry and Physics*; 71st ed.; CRC Press: Boca Raton, 1990.

(19)   Zhang, S.; Sherry, A. D. *J. Solid State Chem.* **2003**, *171*, 38-43.

(20)   Alpoim, M. C.; Urbano, A. M.; Geraldes, C. F. G. C.; Peters, J. A. *J. Chem. Soc., Dalton Trans.* **1992**, 463-467.

(21)   Powell, D. H.; Dhubhghaill, O. M. N.; Pubanz, D.; Helm, L.; Lebedev, Y. S.; Schlaepfer, W.; Merbach, A. E. *J. Am. Chem. Soc.* **1996**, *118*, 9333-9346.

(22)   Aime, S.; Barge, A.; Botta, M.; Howard, J. A. K.; Kataky, R.; Lowe, M. P.; Moloney, J. M.; Parker, D.; De Sousa, A. S. *Chem. Comm.* **1999**, 1047-1048.

(23)   Aime, S.; Botta, M.; Fasano, M.; Terreno, E. *Acc. Chem. Res.* **1999**, *32*, 941-949.

(24)   Aime, S.; Barge, A.; Botta, M.; Parker, D.; De Sousa, A. S. *J. Am. Chem. Soc.* **1997**, *119*, 4767-4768.

(25)   Swift, T. J.; Connick, R. E. *J. Chem. Phys.* **1962**, *37*, 307-320.

(26)   Micskei, K.; Helm, L.; Brucher, E.; Merbach, A. E. *Inorg. Chem.* **1993**, *32*, 3844-3850.

(27)   Zhang, S.; Kovacs, Z.; Burgess, S.; Aime, S.; Terreno, E.; Sherry, A. D. *Chem. Eur. J.* **2001**, *7*, 288-296.

(28)   Aime, S.; Botta, M.; Panero, M.; Grandi, M.; Uggeri, F. *Magn. Reson. Chem.* **1991**, *29*, 923-927.

(29)   Aime, S.; Botta, M.; Crich, S. G.; Giovenzana, G. B.; Pagliarin, R.; Piccinini, M.; Sisti, M.; Terreno, E. *Journal of Biological Inorganic Chemistry* **1997**, *2*, 470-479.

(30)   Aime, S.; Gianolio, E.; Morelli, G.; Pedone, C.; Tesauro, D.; Lattuada, L.; Visigalli, M.; Anelli, P. L. In *PCT Int. Appl.*; (Bracco Imaging S.P.A., Italy). Wo, 2003, p 44 pp.

(31)   Brasch, R. C. *Magnetic Resonance in Medicine* **1991**, *22*, 282-7.

(32)   Caravan, P.; Ellison, J. J.; McMurry, T. J.; Lauffer, R. B. *Chemical Reviews* **1999**, *99*, 2293-2352.

(33)   Merbach, A. E.; Toth, E. *The Chemistry of Contrast Agents in Medical Magnetic Resonance Imaging*; John Wiley and Sons, Ltd.: Chichester, England, 2001.

(34)   Anelli, P. L.; Calabi, L.; De Haen, C.; Fedeli, F.; Losi, P.; Murru, M.; Uggeri, F. *Gazz. Chim. It.* **1996**, *126*, 89-97.

(35)   Vipond, J.; Woods, M.; Zhao, P.; Tirsco, G.; Ren, J.; Bott, S. G.; Ogrin, D.; Kiefer, G. E.; Kovacs, Z.; Sherry, A. D. *Inorg. Chem.* **2007**, *46*, 2584-2595.

(36)   Whittaker, M.; Floyd, C. D.; Brown, P.; Gearing, A. J. H. *Chemical Reviews* **1999**, *99*, 2735-2776.

(37)   Mullins, D. E.; Rohrlich, S. T. *Biochimica et Biophysica Acta* **1983**, *695*, 177-214.

(38)   Coussens Lisa, M.; Fingleton, B.; Matrisian Lynn, M. *Science* **2002**, *295*, 2387-92.

(39)   Rosenberg, G. A.; Dencoff, J. E.; Correa, N., Jr.; Reiners, M.; Ford, C. C. *Neurology* **1996**, *46*, 1626-32.

(40)   Chandler, S.; Coates, R.; Gearing, A.; Lury, J.; Wells, G.; Bone, E. *Neuroscience Letters* **1995**, *201*, 223-6.

(41)   Proost, P.; Van Damme, J.; Opdenakker, G. *Biochemical and Biophysical Research Communications* **1993**, *192*, 1175-81.

(42)   Gijbels, K.; Steinman, L. *Journal of Cellular Biochemistry (Supplement)* **1994**, *18D*, 143.

(43)   Hook, R. M.; Hook, C. W.; Brown, S. I. *Investigative Ophthalmology* **1973**, *12*, 771-6.

(44)   Golub, L. M.; Wolff, M.; Roberts, S.; Lee, H. M.; Leung, M.; Payonk, G. S. *Journal of the American Dental Association* **1994**, *125*, 163-171.

(45)   Saarialho-Kere, U. K.; Vaalamo, M.; Puolakkainen, P.; Airola, K.; Parks, W. C.; Karjalainen-Lindsberg, M. L. *American Journal of Pathology* **1996**, *148*, 519-26.

(46)   Thompson, R. W.; Parks, W. C. *Annals of the New York Academy of Sciences* **1996**, *800*, 157-174.

(47)   Cawston, T. E. *Pharmacology & Therapeutics* **1996**, *70*, 163-182.

(48)   O'Byrne, E. M.; Parker, D. T.; Roberts, E. D.; Goldberg, R. L.; MacPherson, L. J.; Blancuzzi, V.; Wilson, D.; Singh, H. N.; Ludewig, R.; Ganu, V. S. *Inflammation Research* **1995**, *44*, S117-S118.

(49)   Edwards, D. R.; Murphy, G. *Nature* **1998**, *394*, 527-8.

(50)   Kataoka, H.; Uchino, H.; Iwamura, T.; Seiki, M.; Nabeshima, K.; Koono, M. *American Journal of Pathology* **1999**, *154*, 457-468.

(51)   Brabletz, T.; Jung, A.; Dag, S.; Hlubek, F.; Kirchner, T. *American Journal of Pathology* **1999**, *155*, 1033-1038.

(52)   Noe, V.; Fingleton, B.; Jacobs, K.; Crawford, H. C.; Vermeulen, S.; Steelant, W.; Bruyneel, E.; Matrisian, L. M.; Mareel, M. *Journal of Cell Science* **2001**, *114*, 111-118.

(53)   Aparicio, T.; Kermorgant, S.; Dessirier, V.; Lewin, M. J. M.; Lehy, T. *Carcinogenesis* **1999**, *20*, 1445-1451.

(54)   Lampert, K.; Machein, U.; Machein, M. R.; Conca, W.; Peter, H. H.; Volk, B. *American Journal of Pathology* **1998**, *153*, 429-437.

(55)   Zucker, S.; Hymowitz, M.; Rollo, E. E.; Mann, R.; Conner, C. E.; Cao, J.; Foda, H. D.; Tompkins, D. C.; Toole, B. P. *American Journal of Pathology* **2001**, *158*, 1921-1928.

(56)   Zeng, Z.-S.; Shu, W.-P.; Cohen, A. M.; Guillem, J. G. *Clinical Cancer Research* **2002**, *8*, 144-148.

(57)   Chambers, A. F.; Matrisian, L. M. *Journal of the National Cancer Institute* **1997**, *89*, 1260-1270.

(58)   Gersh, I.; Catchpole, H. R. *American Journal of Anatomy* **1949**, *85*, 457-521.

(59)   *American Cancer Society, Cancer Facts & Figures*, 2007.

(60)   Coussens, L. M.; Fingleton, B.; Matrisian, L. M. *Science* **2002**, *295*, 2387-2392.

(61)   Nelson, A. R.; Fingleton, B.; Rothenberg, M. L.; Matrisian, L. M. *Journal of Clinical Oncology* **2000**, *18*, 1135-1149.

(62)   Stack, M. S.; Gray, R. D. *Journal of Biological Chemistry* **1989**, *264*, 4277-81.

(63)   Netzel-Arnett, S.; Mallya, S. K.; Nagase, H.; Birkedal-Hansen, H.; Van Wart, H. E. *Analytical Biochemistry* **1991**, *195*, 86-92.

(64)   Netzel-Arnett, S.; Sang, Q. X.; Moore, W. G. I.; Navre, M.; Birkedal-Hansen, H.; Van Wart, H. E. *Biochemistry* **1993**, *32*, 6427-32.

(65)   Kates, S. A.; Albericio, F. *Solid-Phase Synthesis, A Practical Guide*; Marcel Dekker, Inc.: New York, New York, 2000.

(66)   Chan, K. W.-Y.; Wong, W.-T. *Coord. Chem. Rev.* **2007**, *251*, 2428-2451.

CHAPTER III REFERENCES

(1)   Thornberry, N. A.; Rano, T. A.; Peterson, E. P.; Rasper, D. M.; Timkey, T.; Garcia-Calvo, M.; Houtzager, V. M.; Nordstrom, P. A.; Roy, S.; Vaillancourt, J. P.; Chapman, K. T.; Nicholson, D. W. *J. Biol. Chem.* **1997**, *272*, 17907-17911.

(2)   Carl, P. L.; Chakravarty, P. K.; Katzenellenbogen, J. A. *J. Med. Chem.* **1981**, 479-480.

(3)   de Groot, F. M. H.; Albrecht, C.; Koekkoek, R.; Beusker, P. H.; Scheeren, H. W. *Angewandte Chemie, International Edition* **2003**, *42*, 4490-4494.

(4)   Amir, R. J.; Pessah, N.; Shamis, M.; Shabat, D. *Angewandte Chemie, International Edition* **2003**, *42*, 4494-4499.

(5)   Jones, G. B.; Crasto, C. F.; Mathews, J. E.; Xie, L.; Mitchell, M. O.; El-Shafey, A.; D'Amico, A. V.; Bubley, G. J. *Bioorganic & Medicinal Chemistry* **2006**, *14*, 418-425.

(6)   de Graaf, M.; Nevalainen, T. J.; Scheeren, H. W.; Pinedo, H. M.; Haisma, H. J.; Boven, E. *Biochemical Pharmacology* **2004**, *68*, 2273-2281.

(7)   Alaoui, A. E.; Schmidt, F.; Monneret, C.; Florent, J.-C. *J. Org. Chem.* **2006**, *71*, 9628-9636.

(8)   Alaoui, A. E.; Saha, N.; Schmidt, F.; Monneret, C.; Florent, J.-C. *Bioorganic & Medicinal Chemistry* **2006**, *14*, 5012-5019.

(9)   Abraham, S.; Guo, F.; Li, L.-S.; Rader, C.; Liu, C.; Barbas, C. F.; Lerner, R. A.; Sinha, S. C. *PNAS* **2007**, *104*, 5584-5589.

(10)   Duimstra, J. A.; Femia, F. J.; Meade, T. J. *J. Am. Chem. Soc.* **2005**, *127*, 12847-12855.

(11)   Bruce, J. I.; Dickins, R. S.; Govenlock, L. J.; Gunnlaugsson, T.; Lopinski, S.; Lowe, M. P.; Parker, D.; Peacock, R. D.; Perry, J. J. B.; Aime, S.; Botta, M. *J. Am. Chem. Soc.* **2000**, *122*, 9674-9684.

(12)   Wong, W.; Li, C.; Organization, W. I. P., Ed. Hong Kong, 2005.

(13)   Kaul, R.; Brouilette, Y.; Sajjadi, Z.; Hansford, K. A.; Lubell, W. D. *J. Org. Chem.* **2004**, *69*, 6131-6133.

(14)   Wu, Y.-Q.; Limburg, D. C.; Wilkinson, D. E.; Vaal, M. J.; Hamilton, G. S. *Tetrahedron Letters* **2000**, *41*, 2847-2849.

(15)   Caravan, P.; Ellison, J. J.; McMurry, T. J.; Lauffer, R. B. *Chemical Reviews* **1999**, *99*, 2293-2352.

(16)   Aime, S.; Botta, M.; Crich, S. G.; Giovenzana, G. B.; Pagliarin, R.; Piccinini, M.; Sisti, M.; Terreno, E. *Journal of Biological Inorganic Chemistry* **1997**, *2*, 470-479.

(17)   Aime, S.; Botta, M.; Fasano, M.; Crich, S. G.; Terreno, E. *Journal of Biological Inorganic Chemistry* **1996**, *1*, 312-319.

(18)   Toth, E.; Connac, F.; Helm, L.; Adzamli, K.; Merbach, A. E. *Journal of Biological Inorganic Chemistry* **1998**, *3*, 606-613.

(19)   Aime, S.; Barge, A.; Botta, M.; Howard, J. A. K.; Kataky, R.; Lowe, M. P.; Moloney, J. M.; Parker, D.; De Sousa, A. S. *Chem. Comm.* **1999**, 1047-1048.

(20)   Pasha, A.; Tircso, G.; Benyo, E. T.; Brucher, E.; Sherry, A. D. *Eur. J. Inorg. Chem.* **2007**, 4340-4349.

(21)   Supkowski, R. M.; Horrocks, W. D. *Inorganica Chimica Acta* **2002**, *340*, 44-48.

(22)   Micskei, K.; Helm, L.; Brucher, E.; Merbach, A. E. *Inorg. Chem.* **1993**, *32*, 3844-3850.

(23)   Aime, S.; Barge, A.; Botta, M.; Parker, D.; De Sousa, A. S. *J. Am. Chem. Soc.* **1997**, *119*, 4767-4768.

(24)   Aime, S.; Botta, M.; Fasano, M.; Terreno, E. *Chem. Soc. Rev.* **1998**, *27*, 19-29.

(25)   Swift, T. J.; Connick, R. E. *J. Chem. Phys.* **1962**, *37*, 307-320.

(26)   Michaelis, L.; Menten, M. *Biochem. Z.* **1913**, *49*, 333-369.

(27)   Briggs, G. E.; Haldane, J. B. S. *Biochem. J.* **1925**, *19*, 338-339.

(28)   Cohen, G. M. *Biochem. J.* **1997**, *326*, 1-16.

(29)   Allen, M.; Meade, T. J. *J. Biol. Inorg. Chem.* **2003**, *8*, 746-750.

(30)   Ratnakar, S. J.; Woods, M.; Lubag, A. J. M.; Kovacs, Z.; Sherry, A. D. *J. Am. Chem. Soc.* **2008**, *130*, 6-7.

(31)   Zhang, S.; Merritt, M.; Woessner, D. E.; Lenkinski, R. E.; Sherry, A. D. *Acc. Chem. Res.* **2003**, *36*, 783-790.

(32)   Yoo, B.; Pagel, M. D. *J. Am. Chem. Soc.* **2006**, *128*, 14032-14033.

(33)   Aime, S.; Carrera, C.; Castelli, D. D.; Crich, S. G.; Terreno, E. *Angewandte Chemie, International Edition* **2005**, *44*, 1813-1815.

(34)   Kates, S. A.; Albericio, F. *Solid-Phase Synthesis, A Practical Guide*; Marcel Dekker, Inc.: New York, New York, 2000.

(35)   Kaiser, E.; Colescott, R. L.; Bossinger, C. D.; Cook, P. I. *Analytical Biochemistry* **1970**, *34*, 595-598.

(36)   Chan, K. W.-Y.; Wong, W.-T. *Coord. Chem. Rev.* **2007**, *251*, 2428-2451.

CHAPTER IV REFERENCES

(1)   Wong, W.; Li, C.; Organization, W. I. P., Ed. Hong Kong, 2005.

(2)   Beeby, A.; Clarkson, I. M.; Dickins, R. S.; Faulkner, S.; Parker, D.; Royle, L.; De Sousa, A. S.; Williams, J. A. G.; Woods, M. *J. Chem. Soc., Perkin Trans.* **1999**, *2*, 493-504.

(3)   Vipond, J.; Woods, M.; Zhao, P.; Tirsco, G.; Ren, J.; Bott, S. G.; Ogrin, D.; Kiefer, G. E.; Kovacs, Z.; Sherry, A. D. *Inorg. Chem.* **2007**, *46*, 2584-2595.

(4)   Bruce, J. I.; Dickins, R. S.; Govenlock, L. J.; Gunnlaugsson, T.; Lopinski, S.; Lowe, M. P.; Parker, D.; Peacock, R. D.; Perry, J. J. B.; Aime, S.; Botta, M. *J. Am. Chem. Soc.* **2000**, *122*, 9674-9684.

(5)   Caravan, P.; Ellison, J. J.; McMurry, T. J.; Lauffer, R. B. *Chemical Reviews* **1999**, *99*, 2293-2352.

(6)   Merbach, A. E.; Toth, E. *The Chemistry of Contrast Agents in Medical Magnetic Resonance Imaging*; John Wiley and Sons, Ltd.: Chichester, England, 2001.

(7)   Aime, S.; Botta, M.; Fasano, M.; Terreno, E. *Chem. Soc. Rev.* **1998**, *27*, 19-29.

(8)   Aime, S.; Barge, A.; Botta, M.; Howard, J. A. K.; Kataky, R.; Lowe, M. P.; Moloney, J. M.; Parker, D.; De Sousa, A. S. *Chem. Comm.* **1999**, 1047-1048.

(9)   Aime, S.; Botta, M.; Fasano, M.; Terreno, E. *Acc. Chem. Res.* **1999**, *32*, 941-949.

(10)   Dawson, R. M. C.; Elliott, D. C.; Elliott, W. H.; Jones, K. M. *Data for Biochemical Research*; 3rd ed.; Oxford Science Publications, 1986.

(11)   Pasha, A.; Tircso, G.; Benyo, E. T.; Brucher, E.; Sherry, A. D. *Eur. J. Inorg. Chem.* **2007**, 4340-4349.

(12)   Thornberry, N. A.; Rano, T. A.; Peterson, E. P.; Rasper, D. M.; Timkey, T.; Garcia-Calvo, M.; Houtzager, V. M.; Nordstrom, P. A.; Roy, S.; Vaillancourt, J. P.; Chapman, K. T.; Nicholson, D. W. *J. Biol. Chem.* **1997**, *272*, 17907-17911.

(13)   Allen, M., California Institute of Technology, 2004.

(14)   Supkowski, R. M.; Horrocks, W. D. *Inorganica Chimica Acta* **2002**, *340*, 44-48.

CHAPTER V REFERENCES

(1)   Schultz-Sikma, E. A.; Aslam, M.; Endres, P. J.; Dravid, V. P.; Meade, T. J. *Unpublished results.*

(2)   Caravan, P.; Ellison, J. J.; McMurry, T. J.; Lauffer, R. B. *Chemical Reviews* **1999**, *99*, 2293-2352.

(3)   Whittaker, M.; Floyd, C. D.; Brown, P.; Gearing, A. J. H. *Chemical Reviews* **1999**, *99*, 2735-2776.

(4)   Netzel-Arnett, S.; Sang, Q. X.; Moore, W. G. I.; Navre, M.; Birkedal-Hansen, H.; Van Wart, H. E. *Biochemistry* **1993**, *32*, 6427-32.

(5)   Kaiser, E.; Colescott, R. L.; Bossinger, C. D.; Cook, P. I. *Analytical Biochemistry* **1970**, *34*, 595-598.

(6)   Kates, S. A.; Albericio, F. *Solid-Phase Synthesis, A Practical Guide*; Marcel Dekker, Inc.: New York, New York, 2000.

(7)   Chan, W. C.; White, P. D. *Fmoc Solid Phase Peptide Synthesis*; Oxford University Press: New York, 2000.

(8)   Sun, S.; Zeng, H.; Robinson, D. B.; Raoux, S.; Rice, P. M.; Wang, S. X.; Li, G. *J. Am. Chem. Soc.* **2004**, *126*, 273-279.

(9)   Lee, D. C.; Mikulec, F. V.; Pelaez, J. M.; Koo, B.; Korgel, B. A. *J. Phys. Chem. B* **2006**, *110*, 11160-11166.

(10)   Deng, Y. H.; Wang, C. C.; Hu, J. H.; Yang, W. L.; Fu, S. K. *Colloids Surf. A* **2005**, *262*, 87-93.

APPENDIX I

PEPTIDES WITH N-TERMINAL MRI CONTRAST AGENTS

INTRODUCTION

      This appendix details peptides with N-terminal MRI contrast agents as mentioned in the Introduction of Chapter II. These agents served as early examples of the covalent attachment of peptides to MRI contrast agents. The results of this study lead to insight into the coordination geometry of peptides with N-terminal contrast agents and prompted the evolution of peptide-based contrast agents into the bridged agents found in Chapter II.

Matrix Metalloproteinase-7

      Matrix metalloproteinases (MMPs) are a family of zinc containing enzymes that mediate the breakdown of connective tissues.[1] The enzymes are generally expressed at low levels, but these levels rise rapidly during inflammation, wound healing, and cancer.[2] Overexpression of MMPs is linked to tumor invasion and metastasis.[3-8]

      The detection of MMP activity is critical for identifying metastatic cancer and could be used to monitor the efficacy of MMPIs, leading to the optimization of anti-cancer therapeutic protocols.[9-11] The current method of monitoring MMP activity consists of *ex vivo* assays on excised tissues or fluid samples. In order to detect MMP activity *in vitro*, fluorescent probes have been developed.[12,13] The practical applications of fluorescence techniques are restricted to the observation of cells, small animals, and tumors near the surface of the skin due to the limited penetration of light (<10 mm).[9] MRI provides an alternative to light microscopy, allowing the imaging of opaque organisms in three dimensions at cellular resolution.[14]

      Of the twenty-four known MMPs, MMP-7 has been closely linked to events occurring during tumor metastasis and invasion.[2,3,7,8,15-17] Through the use of combinatorial peptide libraries, a heptapeptide consensus sequence consisting of pro-met-ala-leu-trp-met-arg was

designed to be cleaved by MMP-7 between the alanine and leucine residues.[18,19] This

consensus sequence served as the basis for the peptide-based MRI contrast agents described in

this Appendix.

RESULTS AND DISCUSSION

A series of peptides was synthesized using Solid-Phase Peptide Synthesis (SPPS)

(Scheme A1.1). The peptides feature varying lengths of the consensus sequence pro-met-ala-leu-

trp-met-arg. The number of amino acid residues on the N-terminus of the peptide was

systematically shortened to effectively bring the enzymatic cleavage site closer to the N-terminal

contrast agent.
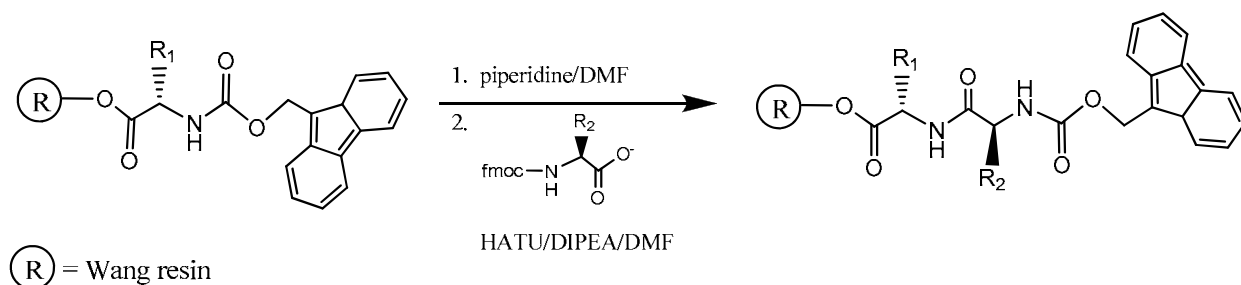
Scheme A1.1 General scheme for Solid-Phase Peptide Synthesis (SPPS)

After synthesizing the desired peptide sequences, 1,4,7-tris(*tert*-butoxycarbonylmethyl)-10-

(carboxymethyl)-1,4,7,10-tetraazacyclododecane was covalently attached to the N-terminus of

each peptide via an amide bond (Scheme A1.2). Cleavage of the peptide from the resin and

deprotection of the amino acid side-chains as well as the pendant acetate groups of DOTA

afforded ligands **1-3** (Figure A1.1). Metalation of **1-3** was performed using Gd(OH)$_3$ (Scheme

A1.2) to yield **7-9** which were hypothesized to be cleaved by MMP-7 between the alanine and

leucine residues (Figure A1.2).
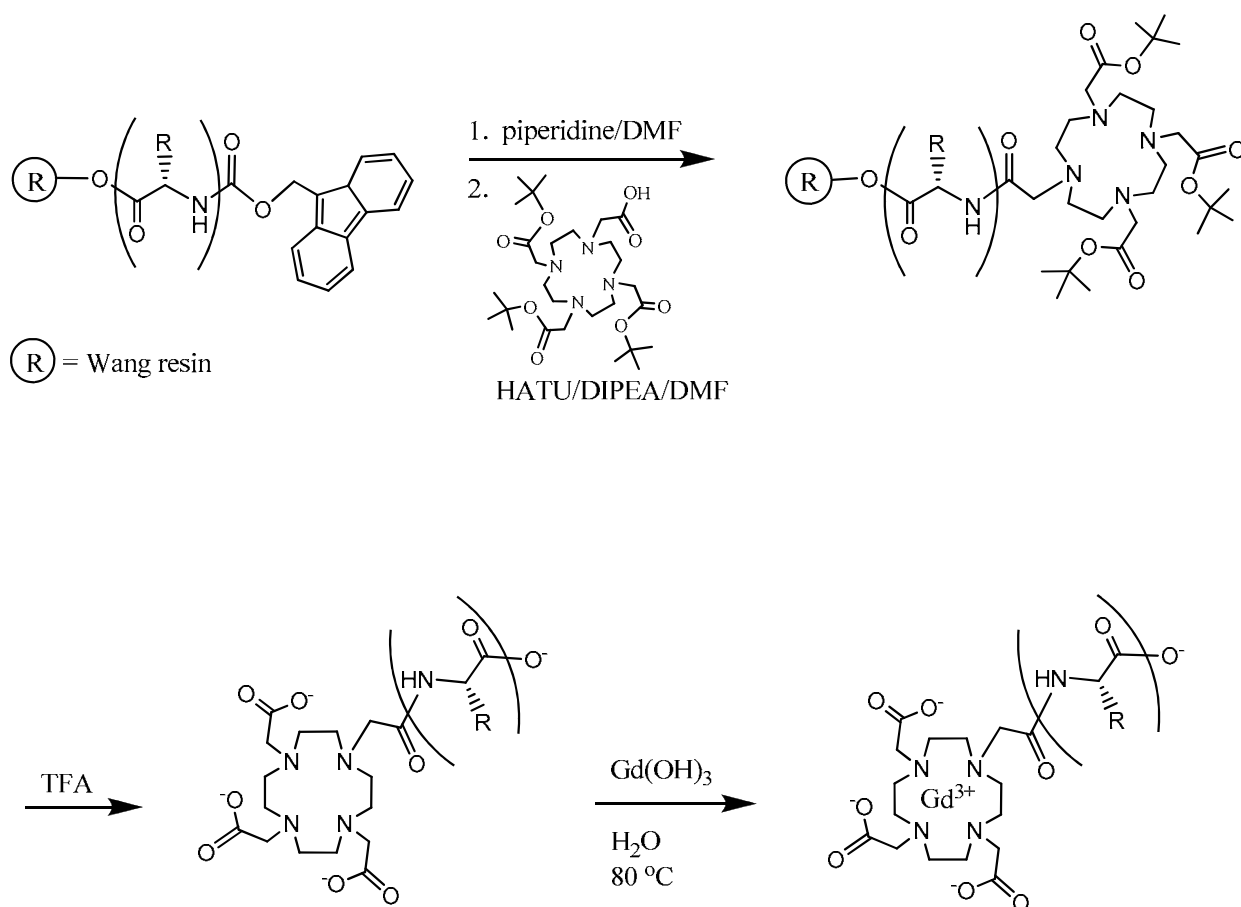
Scheme A1.2 General scheme for synthesis of peptides with N-terminal MRI contrast agents

DOTA-PMALWMR

1

DOTA-MALWMR

2

DOTA-ALWMR

3
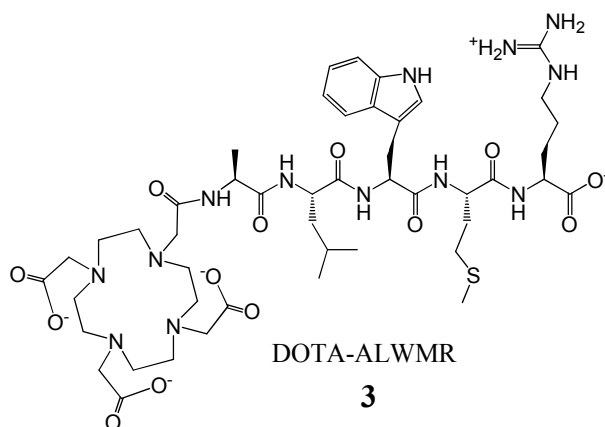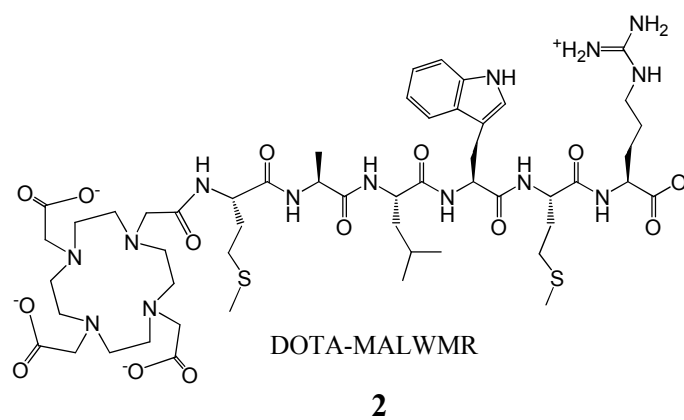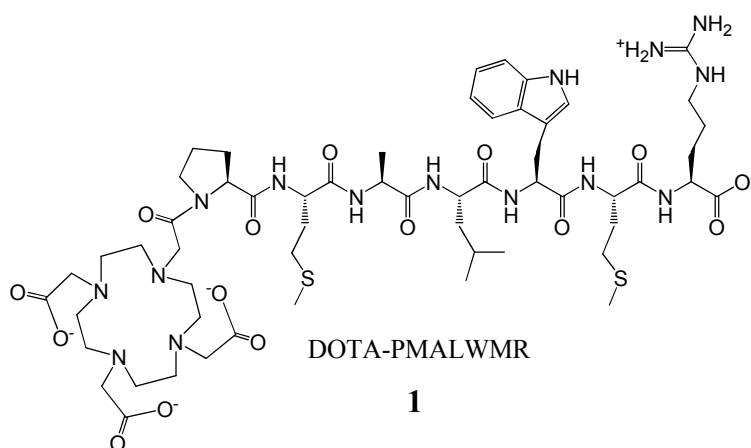
Figure A1.1 Ligands synthesized
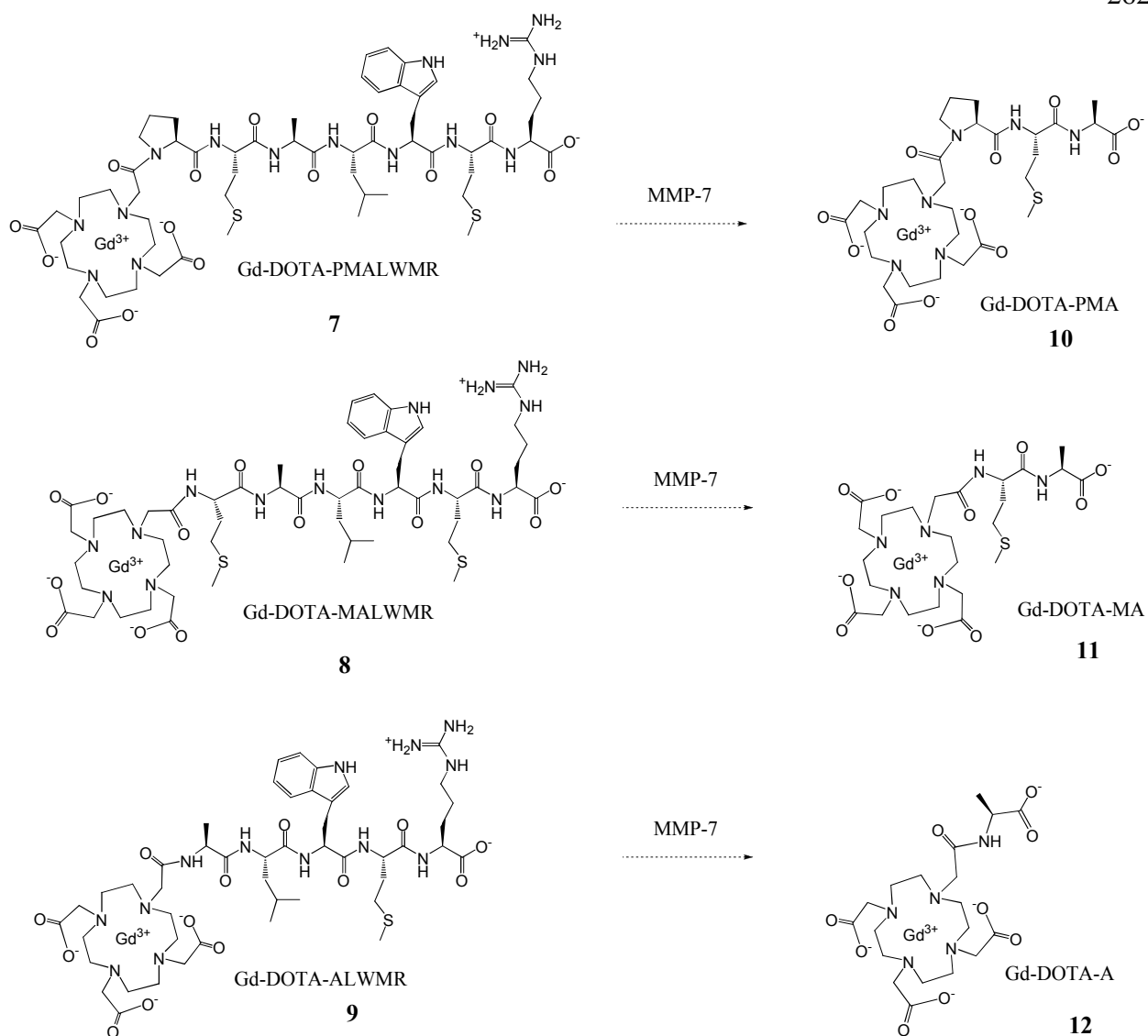
Figure A1.2 Proposed enzymatic cleavage of 7-9 to form 10-12

It was hypothesized that the peptide would block water in a method analogous to previous "smart" MRI contrast agents.[20] Subsequent cleavage by MMP-7 was hypothesized to lead to a change in the number of inner-sphere water molecules (q), thus leading to a change in

the relaxivity of the agent. The variation of the cleavage site distance to the N-terminal

contrast agent allowed an investigation of the influence of peptide length vs. q. As the peptide is

cleaved by the enzyme, it was hypothesized that the shorter peptides would be less efficient at

blocking inner-sphere water access to Gd^{3+}.

In order to determine the influence of peptide length vs. q, the corresponding "cleaved"

peptide" ligands **4-6** (Figure A1.3) and Gd^{3+} complexes **10-12** (Figure A1.2) were synthesized

according to Scheme A1.2. The comparison of **7-9** with **10-12** allows the effect of enzymatic

cleavage to be investigated before embarking on a complex study of enzyme activity with these

agents.
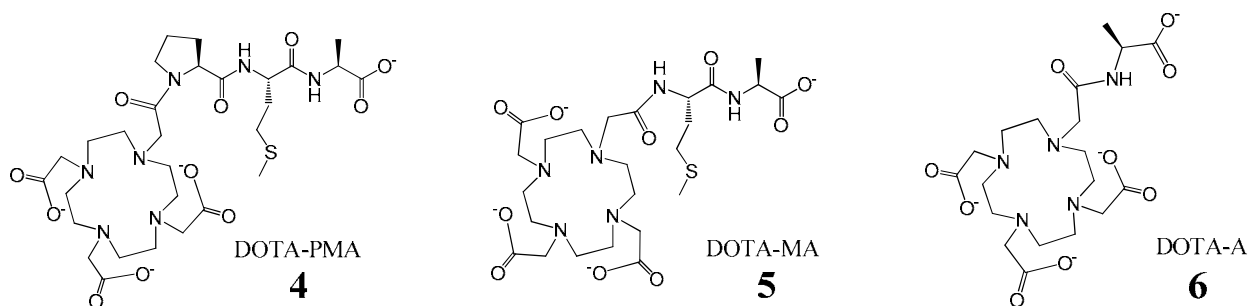
Figure A1.3 DOTA-peptides 4-6 synthesized - "cleaved" ligands

The relaxivities of **7-12** were measured in pH 7.41 buffer (10 mM MOPS, 100 mM NaCl,

20 mM $NaHCO_3$, 4 mM NaH_2PO_4). Unfortunately, **7-12** were not fully soluble when prepared

as 10 mM solutions in the buffer. The solutions were 0.2 μm filtered, however this lead to

uncertainties in the composition and concentration of the final solutions. The relaxivity results obtained were not consistent between multiple trials. Due to the uncertainty of the final composition of the solutions and inconsistencies of the measured values, the relaxivities of **7-12** cannot be reported with confidence. Further investigations involving the use of different buffer systems was not attempted due to the concurrent results obtained concerning the q values of the Eu^{3+} analogs of **7-12,** vida infra.

The number of inner-sphere water molecules, q, was determined using the method of Horrocks and coworkers.[21] The fluorescence lifetime decay of the Eu^{3+} analogs of **7-12** in water and deuterium oxide was measured by fellow graduate student Matthew Allen.[22] The results of the q studies indicate that the number of inner sphere water molecules of **7-12** will not change upon cleavage by MMP-7 (Figure A1.4). The Eu^{3+} analogs of **7-12** each exhibited one inner-sphere water molecule.[22] It is postulated that the N-terminal amide carbonyl oxygen coordinates to the lanthanide, creating a ligand with an overall coordination number of 8. The presence of one inner-sphere water molecule fills the 9th coordination site of the lanthanide ion. This coordination motif is supported by additional studies[22] with a series of model DOTA-peptide complexes as well as by literature examples[23] of amide carbonyl oxygen coordination. Therefore, the identity of the N-terminal amino acid does not have an effect on the number of inner-sphere water molecules for agents of this type.

Uncleaved Agents   Cleaved Agents

Eu-DOTA-PMALWMR

$q = 1.0 \pm 0.1$

Eu-DOTA-PMA

$q = 1.1 \pm 0.1$

Eu-DOTA-MALWMR

$q = 1.1 \pm 0.1$

Eu-DOTA-MA

$q = 1.0 \pm 0.1$

Eu-DOTA-ALWMR

$q = 1.0 \pm 0.1$

Eu-DOTA-A

$q = 1.0 \pm 0.1$
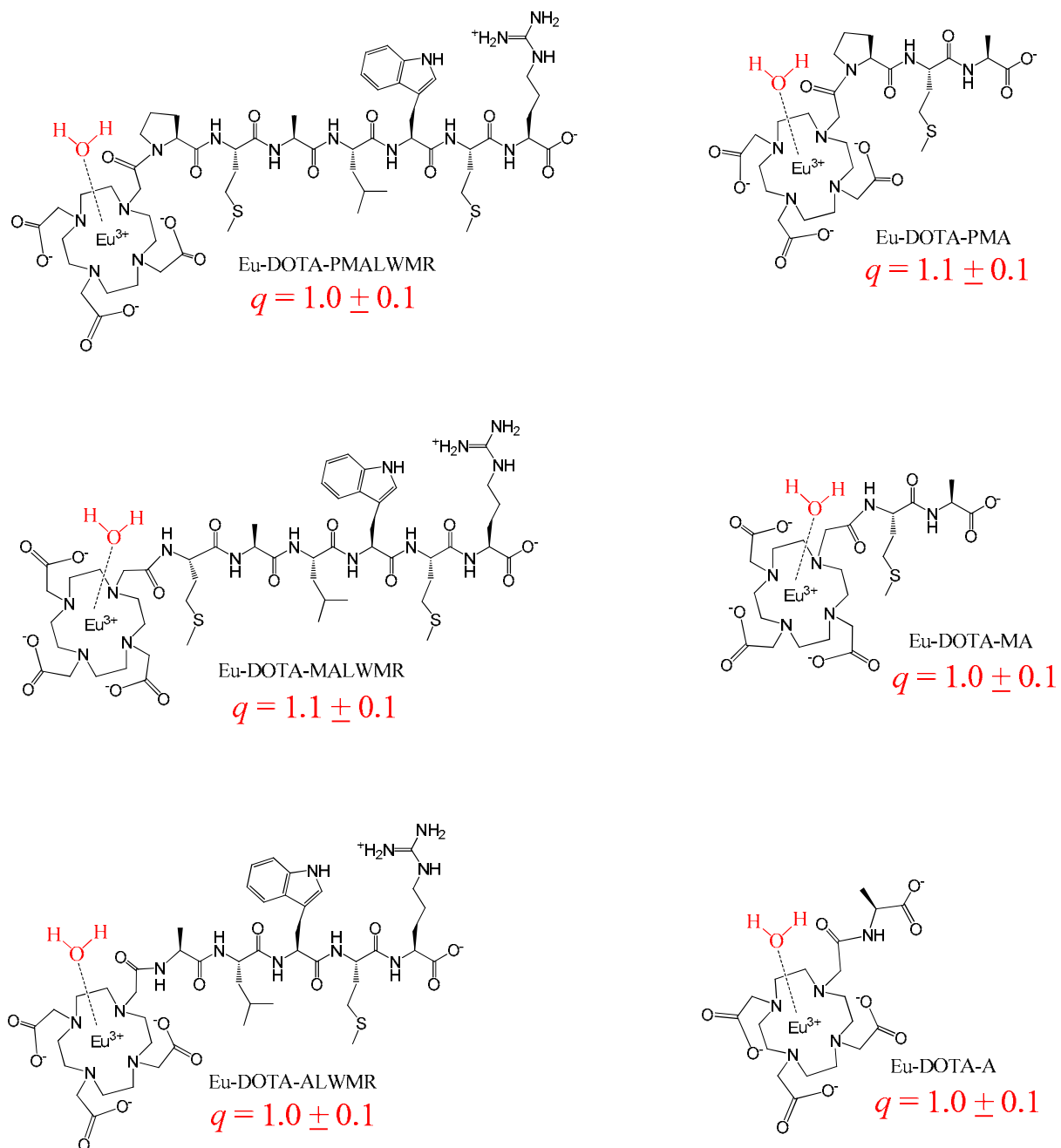
Figure A1.4 Number of inner-sphere water molecules (q) measured for the Eu^{3+} analogs of 7-12[22]

CONCLUSIONS

A series of peptides with N-terminal contrast agents were synthesized and characterized. The number of N-terminal amino acid residues was systematically varied to determine the effect of distance from the cleavage site to the N-terminal contrast agent. The appendage of a contrast agent to the N-terminus of a substrate peptide resulted in coordination of the amide carbonyl to the lanthanide. As a result, all of the complexes studied, **7-12**, exhibited eight coordinate ligands with one inner-sphere water. This coordination motif is independent of the individual amino acid side-chains and thus precludes a change in coordination geometry upon enzymatic cleavage of the substrate peptide.

The results of this study prompted the redesign of the peptide-based contrast agents. Instead of covalently attaching the MRI contrast agent on the N-terminus of the peptide, the new designs sought to bridge the peptide across a macrocyclic chelate in an attempt to modulate q. Agents of this type are the subject matter of Chapter II.

EXPERIMENTAL

General experimental details and abbreviations can be found in Chapter II.

General synthesis of peptides with N-terminal DOTA

Peptides were synthesized according standard solid-phase peptide synthesis methods[24] using manual batch-type synthesis and fmoc protected amino acids. Fmoc amino acids were purchased (NovaBiochem, San Diego, California) and used as received. Tryptophan was purchased with

Boc protection on the side-chain. Arginine was purchased with the guanidinium side-chain functionality protected by 2,2,4,6,7-pentamethyldihydrobenzofuran-5-sulfonyl (Pbf). A Wang resin consisting of 100-200 mesh 1% cross-linked polystyrene beads functionalized with p-benzyloxybenzyl alcohol handle was used as a solid support for the stepwise addition of amino acids. The Wang resin was purchased (NovaBiochem, San Diego, California) with the N-terminal amino acid pre-loaded onto the resin with the N-terminus protected by fmoc. The resin was added to a fritted glass reactor vessel fitted with a 3-way valve for switching between N_2 (used to mix during all reactions and rinses) and vacuum (used to drain rinses and excess reactants). The dry Wang resin was pre-swelled with CH_2Cl_2 (1 X 10 minute rinse) followed by DMF (4 X 10 minute rinses). The N-terminal fmoc protecting group was removed using 20% piperidine in DMF (until determined >99% complete by the Kaiser test[25]; typically 4 X 10 minutes), followed by rinsing with DMF (4 X 10 minutes). The next amino acid (2.5 equivalents relative to the N-terminal amino acid on the Wang resin) to be added to the peptide was dissolved in a minimal amount of DMF. To this solution, HATU (2.0 equivalents) and DIPEA (5.0 equivalents) were added to form a yellow solution of the pre-activated fmoc-amino acid. This solution was added to the resin and reacted while gently bubbling N_2 to mix the reactants until determined >99% complete (typically 2-12 hours) by the Kaiser test[25]. Upon completion, the resin was rinsed with DMF (4 X 10 minutes). This process of fmoc removal and addition of the next amino acid was repeated for each amino acid until the desired peptide sequence was obtained. Incorporation of the chelate, 1,4,7-tris(*tert*-butoxycarbonylmethyl)-10-(carbonylmethyl)-1,4,7,10-tetraazacyclododecane (purchased from Macrocyclics, Dallas, TX), onto the N-terminus of the peptide was accomplished in a manner analogous to the addition of amino acids.

General Cleavage of peptides with N-terminal DOTA from resin:

Resin was placed in a fritted reactor column and the N-terminal fmoc was removed with piperidine as described above. The resin was rinsed with DMF (4 X 10 minutes), CH_2Cl_2 (4 X 10 minutes), methanol (4 X 10 minutes); and dried under vacuum overnight. To the dried resin was added 35 mL of cleavage cocktail (specific for each amino acid sequence; see details for compounds **1-6**). The resin was reacted in the cleavage cocktail for one hour, after which the solution was drained into a vial. Fresh cleavage cocktail (10 mL) was added to the resin and reacted for 10 minutes, followed by draining into a vial. Fresh cleavage cocktail (5 mL) was added to the resin and immediately drained into a vial. The TFA filtrates were combined and stored in capped vials overnight to fully remove all tBu, Boc, and Pbf protecting groups. TFA was evaporated by passing N_2 over the vial. The volume was reduced to ~7.5 mL followed by addition of cold (-20 °C) diethyl ether to precipitate the crude product as an off-white solid. The suspension was centrifuged and decanted. The diethyl ether extraction was repeated 4 times followed by evaporation of residual diethyl ether by passing N_2 over the vial. The solid cake was dissolved in water (20 mL), frozen in liquid N_2 and lyophilized.

1-(*N*-carbonylmethyl-proline-methionine-alanine-leucine-tryptophan-methionine-arginine)-4,7,10-tris(carboxymethyl)-1,4,7,10-tetraazacyclododecane (1)

Cleavage cocktail: 81.5% TFA, 5% thioanisole, 5% phenol, 5% water, 2.5% 1,2-ethanedithiol, 1% TIS

Yield = 429.4 mg (55%)

^{1}H NMR (D_2O): δ = 0.8 (d, 6H, leucine δH, J = 16.4 Hz), 1.1-2.1 (br, 19H), 2.1-2.3 (m, 2H, proline), 2.4 (m, 4H, methionine γH), 2.8-4.0 (br, 34H), 4.2 (t, 1H, proline αH, J = 8.0 Hz), 4.3

(q, 1H, alanine αH), 4.6 (t, 1H, methionine αH), 6.8 (t, 1H, arginine αH), 7.1-7.7 (m, 5H, tryptophan aromatic)

MALDI-TOF MS: Calc. 1289.63; Found positive mode 1290.92 (M + H$^+$), 1313.06 (M + Na$^+$)

1-(*N*-carbonylmethyl-methionine-alanine-leucine-tryptophan-methionine-arginine)-4,7,10-tris(carboxymethyl)-1,4,7,10-tetraazacyclododecane (2)

Cleavage cocktail: 81.5% TFA, 5% thioanisole, 5% phenol, 5% water, 2.5% 1,2-ethanedithiol, 1% TIS

Yield = 751.32 mg (86%)

^{1}H NMR (D$_2$O): δ = 0.8 (d, 6H, leucine δH, *J* = 16.4 Hz), 1.1-2.1 (br, 17H), 2.4 (m, 4H, methionine γH), 2.8-4.0 (br, 32H), 4.3 (q, 1H, alanine αH), 4.6 (t, 1H, methionine αH), 6.8 (t, 1H, arginine αH), 7.1-7.7 (m, 5H, tryptophan aromatic)

MALDI-TOF MS: Calc. 1192.57; Found positive mode 1193.90 (M + H$^+$)

1-(*N*-carbonylmethyl-alanine-leucine-tryptophan-methionine-arginine)-4,7,10-tris(carboxymethyl)-1,4,7,10-tetraazacyclododecane (3)

Cleavage cocktail: 81.5% TFA, 5% thioanisole, 5% phenol, 5% water, 2.5% 1,2-ethanedithiol, 1% TIS

Yield = 25.2 mg (61%)

^{1}H NMR (D$_2$O): δ = 0.8 (d, 6H, leucine δH, *J* = 16.4 Hz), 1.1-2.1 (br, 12H), 2.3 (t, 2H, methionine γH, *J* = 7.2 Hz), 2.8-4.0 (br, 31H), 4.3 (q, 1H, alanine αH), 4.6 (t, 1H, methionine αH), 6.8 (t, 1H, arginine αH), 7.1-7.7 (m, 5H, tryptophan aromatic)

MALDI-TOF MS: Calc. 1061.53; Found positive mode 1062.57 (M + H$^+$)

1-(*N*-carbonylmethyl-proline-methionine-alanine)-4,7,10-tris(carboxymethyl)-1,4,7,10-tetraazacyclododecane (4)

Cleavage cocktail: 94% TFA, 2.5% water, 2.5% 1,2-ethanedithiol, 1% TIS

Yield = 248.4 mg (93%)

^{1}H NMR (D$_2$O): δ = 1.4 (d, 3H, alanine βH, J = 7.2 Hz), 1.8-2.4 (br, 9H, methionine βH, methionine SC*H*$_3$, proline H$_3$, proline H$_4$), 2.6 (t, 2H, methionine γH, J = 7.2 Hz), 2.8-4.0 (br, 26H, cyclen, C*H*$_2$COOH, proline H$_5$), 4.2 (t, 1H, proline αH J = 8.0 Hz), 4.3 (q, 1H, alanine αH), 4.5 (t, 1H, methionine αH)

MALDI-TOF MS: Calc. 703.32; Found positive mode 704.39 (M + H$^+$)

1-(*N*-carbonylmethyl-methionine-alanine)-4,7,10-tris(carboxymethyl)-1,4,7,10-tetraazacyclododecane (5)

Cleavage cocktail: 94% TFA, 2.5% water, 2.5% 1,2-ethanedithiol, 1% TIS

Yield = 316.8 mg (89%)

^{1}H NMR (D$_2$O): δ = 1.4 (d, 3H, alanine βH, J = 7.2 Hz), 2.0 (m, 2H, methionine βH), 2.1 (s, 3H, methionine SC*H*$_3$), 2.6 (t, 2H, methionine γH, J = 7.2 Hz), 3.2-4.2 (br, 24H, cyclen and C*H*$_2$COOH), 4.4 (q, 1H, alanine αH), 4.5 (t, 1H, methionine αH)

MALDI-TOF MS: Calc. 606.27; Found positive mode 606.71 (M$^+$), 628.66 (M + Na$^+$)

1-(*N*-carbonylmethyl-alanine)-4,7,10-tris(carboxymethyl)-1,4,7,10-tetraazacyclododecane (6)

Cleavage cocktail: 95% TFA, 2.5% water, 2.5% TIS

Yield = 379.6 mg (94%)

^{1}H NMR (D$_2$O): δ = 1.4 (d, 3H, alanine βH, *J* = 7.2 Hz), 3.0-4.1 (br, 24H, cyclen and

C*H*$_2$COOH), 4.4 (q, 1H, alanine αH)

MALDI-TOF MS: Calc. 475.23; Found positive mode 476.39 (M + H$^+$), 498.40 (M + Na$^+$)

General synthesis of peptides with N-terminal Gadolinium(III)-DOTA

Ligands (**1-6**) were dissolved in water (as 5-15 mM solutions) to which Gd(OH)$_3$ was added.

The pH was adjusted to 5.5, and the solution was stirred overnight at 80 ^{o}C then cooled to room

temperature. Concentrated NH$_4$OH was added (usually 8-12 drops) until the pH was raised to

10. The solution was 0.2 μm filtered and lyophilized. The crude product was purified using a

Sephadex G-25 (20-80 μm) gel filtration column with water as eluent. Product elution was

identified using TLC with Pt stain. Fractions containing the desired product were combined and

lyophilized. Purity of the Gd^{3+} complexes (**7-12**) was verified using analytical HPLC:

Ultrahydrogel column (Waters Corp, Milford, MA; DP 102Å, 7.8 mm X 300 mm) with guard

column (DP, 6 mm X 40 mm), isocratic water, flow rate = 0.6 mL/min, fluorescence detection of

Gd^{3+} λ_{ex} = 271 nm, λ_{em} = 314 nm. Metalation with Gd^{3+} was confirmed using ICP-MS.

MALDI-TOF MS of **7-12** was performed using CHCA matrix (as described in general

experimental section of Chapter II) and showed distinctive Gd^{3+} isotope patterns.

Gadolinium(III)-1-(*N*-carbonylmethyl-proline-methionine-alanine-leucine-tryptophan-

methionine-arginine)-4,7,10-tris(carboxymethyl)-1,4,7,10-tetraazacyclododecane (7)

Yield = 57.0 mg (47%)

HPLC: retention time = 23.7 min

MALDI-TOF MS: Calc. 1444.53; Found positive mode 1446.05 (M + H$^+$), 1468.08 (M + Na$^+$)

272

Gadolinium(III)-1-(*N*-carbonylmethyl-methionine-alanine-leucine-tryptophan-methionine-arginine)-4,7,10-tris(carboxymethyl)-1,4,7,10-tetraazacyclododecane (8)

Yield = 39.0 mg (45%)

HPLC: retention time = 26.0 min

MALDI-TOF MS: Calc. 1347.47; Found positive mode 1348.50 (M + H$^+$), 1370.55 (M + Na$^+$)

Gadolinium(III)-1-(*N*-carbonylmethyl-alanine-leucine-tryptophan-methionine-arginine)-4,7,10-tris(carboxymethyl)-1,4,7,10-tetraazacyclododecane (9)

Yield = 92.8 mg (54%)

HPLC: retention time = 23.1 min

MALDI-TOF MS: Calc. 1216.43; Found positive mode 1217.92 (M + H$^+$), 1239.68 (M + Na$^+$)

Gadolinium(III)-1-(*N*-carbonylmethyl-proline-methionine-alanine)-4,7,10-tris(carboxymethyl)-1,4,7,10-tetraazacyclododecane (10)

Yield = 96.3 mg (64%)

HPLC: retention time = 10.4 min

MALDI-TOF MS: Calc. 858.22; Found positive mode 859.37 (M + H$^+$), 881.31 (M + Na$^+$)

Gadolinium(III)-1-(*N*-carbonylmethyl-methionine-alanine)-4,7,10-tris(carboxymethyl)-1,4,7,10-tetraazacyclododecane (11)

Yield = 99.2 mg (64%)

HPLC: retention time = 10.3 min

MALDI-TOF MS: Calc. 761.17; Found positive mode 762.49 (M + H$^+$), 784.50 (M + Na$^+$),

806.38 (M + 2Na)$^+$

Gadolinium(III)-1-(*N*-carbonylmethyl-alanine)-4,7,10-tris(carboxymethyl)-1,4,7,10-

tetraazacyclododecane (12)

Yield = 165.5 mg (89%)

HPLC: retention time = 10.0 min

MALDI-TOF MS: Calc. 630.13; Found positive mode 630.06 (M$^+$), 652.03 (M + Na$^+$), 673.98

(M + 2Na)$^+$

APPENDIX II

DEVELOPMENT OF PEPTIDE-BRIDGED MACROBICYCLES

INTRODUCTION

This appendix details the development of peptide-bridged macrobicycles contained in Chapter II. These details provide insight into the design of such agents and present approaches which resulted in unexpected byproducts. In addition, this appendix is provided such that the novel compounds contained herein may be of use as ligands or synthons for future MRI contrast agents, positron emission (PET) agents, and/or lanthanide luminescence agents.

RETROSYNTHETIC ANALYSIS

The synthetic schemes described in this Appendix are the result of an iterative process. At the conception of this project there were very few polyaza macrobicyclic chelates in the literature, most of which were used as "proton sponges" and to chelate Li^+, Cu^{2+}, or Zn^{2+} (Figure A2.1).[1-4]

$$n = 1,2$$
$$D = O, S, NH, NCH_3$$
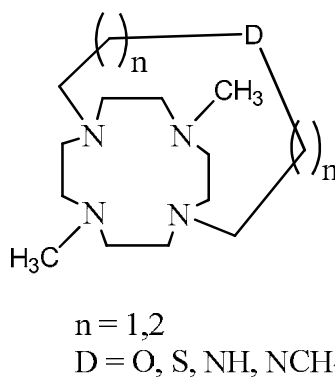
Figure A2.1 Literature examples of polyaza macrobicyclic chelates[1-4]

In order to form highly stable lanthanide chelates, the structures in Figure A2.1 must be augmented to incorporate additional donor atoms in order to effectively increase the coordination number of the ligand. A seminal paper by Kovacs and coworkers created novel lanthanide

chelates with extraordinary command over the functionalization of 1,4,7,10-tetraazacyclododecane (cyclen).[5] Through precise pH control, cyclen was selectively substituted at the 1 and 7 positions (pseudo-*trans*) with a number of functional groups. With the current work, it was envisioned that the use of protecting groups would allow this methodology to be extended to form a variety of chelates featuring functional groups which are orthogonal, both spatially and chemically. These bi-functional chelates could then be coupled to the side-chain residues of a peptide to form novel polyaza macrobicyclic lanthanide chelates. Figure A2.2 shows a retrosynthetic analysis of the target compound.
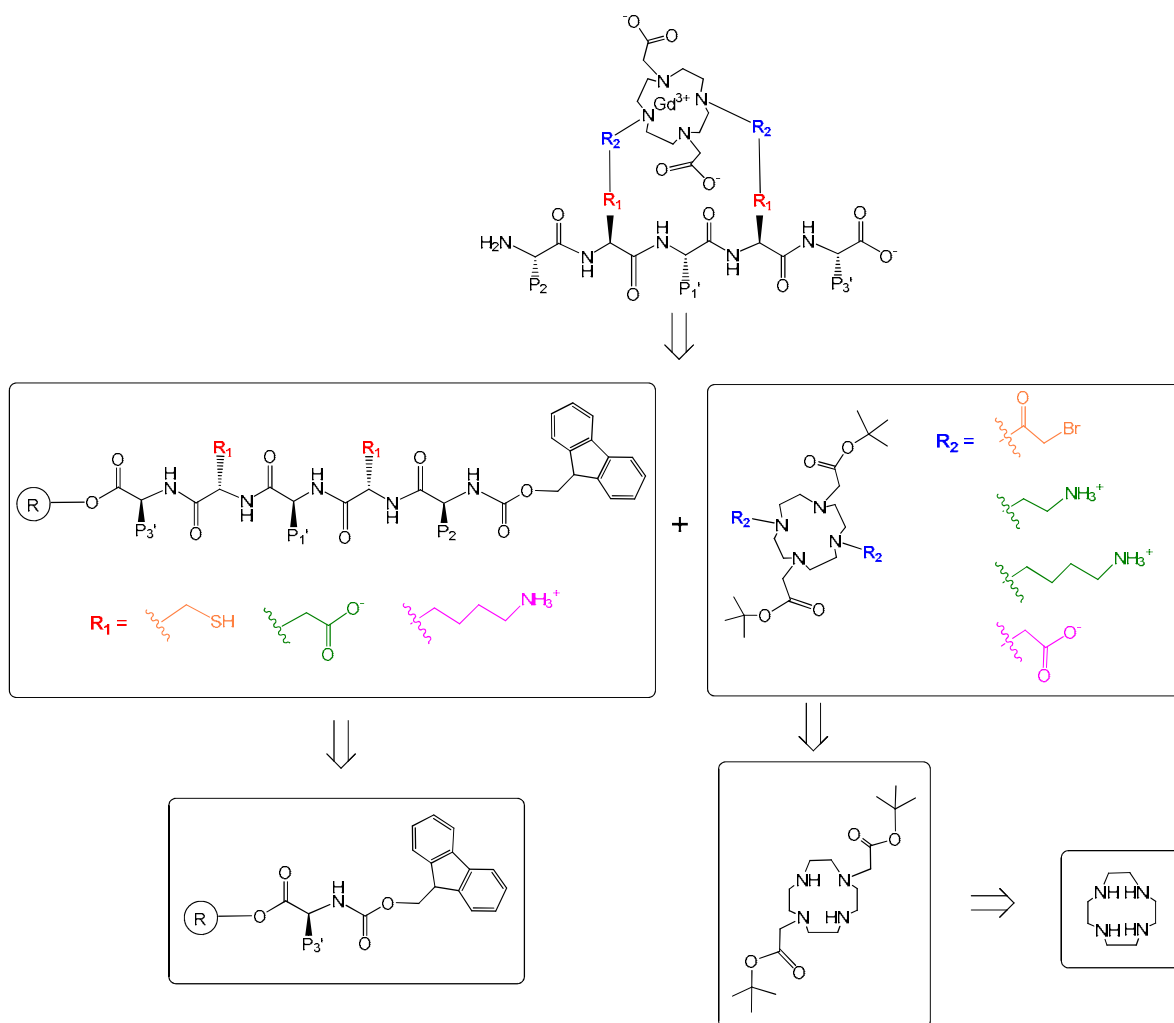
Figure A2.2 Retrosynthetic Analysis of Peptide-Bridged Macrobicycles

While examining the possibilities of covalent attachment between the bi-functional chelator and the peptide, a number of functional groups come to mind. Within in the realm of the 20 amino acids commonly used by nature, the available side chain functionalities include thiols, carboxylic acids, amines, amides, and alcohols. Of these, amino acids containing thiols, carboxylic acids, and amines were chosen for synthetic utility as well as commercial availability of suitably protected starting materials. In order to synthesize gram quantities of peptides in overall good yields and purity, the method of Solid-Phase Peptide Synthesis (SPPS) was utilized.

SOLID-PHASE PEPTIDE SYNTHESIS: General Considerations

Solid-phase peptide synthesis (SPPS) is routinely used for building short peptides in a stepwise manner.[6] Fmoc protecting strategy is based on orthogonal protecting groups, using 9-fluorenylmethoxycarbonyl (fmoc) to protect the N-terminal amine while acid-labile groups are used to protect amino acid side-chains as well as to link the C-terminus to the solid support (resin).[7] While SPPS is a convenient method for preparing peptides, there are limitations to the scope of reactions which can be performed on the solid support. These limitations include choice of solvent; chemical compatibility with commonly employed protecting groups such as fmoc, Boc, and tBu; and the necessity of very high-yielding reactions.

The use of solvents in SPPS is limited to those in which the resin has suitable swelling properties. For instance, the polystyrene-based Wang resin used in this study swells in DMF, THF, DMSO, CH_2Cl_2, whereas methanol and ethanol are known to shrink the resin. Swelling of the resin is preferred such that the functional groups on the resin are fully solvated and available for reaction with the reagents in solution.

Chemical compatibility is a concern when protecting amino acid side-chain functionalities. It is imperative for the protecting groups to have orthogonal reactivities such that premature deprotection does not occur. Orthogonal protecting groups allow precise control of functional group reactivity on various amino acid side-chains; this is the fundamental strategy utilized for the formation of the peptide-bridged macrobicycles described in this Appendix and Chapter II.

Finally, the use of SPPS requires very high yielding reactions. Due to the step-wise nature of building peptides by SPPS, any by-products arising from incomplete reactions or undesired side-reactions will accumulate on the resin and result in low yields and impure product. The impurities accumulated by incomplete reactions will be very similar to the desired product and thus very hard to remove. A simple calculation shows that a yield of 95% per reaction, while considered excellent by most standards, will result in only 60% overall yield of the desired product after a 10-step reaction scheme. Kinetic studies show that the reaction rate of a functional group bound to a copolymer bead is about half of the reaction rate of that functional group in solution.[8] Therefore, many reactions in SPPS use excess reagents and increased reaction times to drive the reaction towards quantitative yields. Another method to increase yields is to repeat coupling reactions until the yield for each step is >99%. A great advantage of SPPS over solution-based synthesis is that excess reagents can easily be washed away from the solid-supported peptide by rinsing the resin with solvent.

RESULTS AND DISCUSSION

APPROACH #1

The first approach for bridge formation involved the S_N2 reaction between a thiol and an alkyl bromide (orange colored R groups in Figure A2.2). The thiol functionality can be easily introduced into a substrate peptide by substituting cysteine into the peptide sequence. The alkyl bromide functionality was envisioned to be incorporated as pendant arms of the macrocyclic chelator, forming a bi-functional chelate. Due to the number of steps and associated cost of synthesizing significant quantities of the peptide, the synthesis of the bi-functional chelate was investigated prior to peptide synthesis.

The incorporation of an alkyl bromide onto cyclen using bromoacetyl bromide was based on literature examples involving the addition of cyclen to an N-terminal amine during SPPS[9] and the addition of bromoacetamidobenzyl-DOTA to a cysteine thiol within a peptide/protein.[10] Starting from commercially available cyclen, 1,7-bis(*tert*-butoxycarbonylmethyl)-1,4,7,10-tetraazacyclododecane was synthesized according to literature methods[5] (Scheme A2.1) and reacted with bromoacetyl bromide. This reaction resulted in an unexpected by-product (Scheme A2.2) [obtained as a white solid in 38% yield, purified by silica gel chromatography: 16:4:1 $CHCl_3$:MeOH:NH_4OH eluent; $R_f = 0.25$; ESI-MS calc 562.52, found 563.2 (M + H^+)]. Variation of reaction temperature, reaction time, amount of bromoacetyl bromide, amount of base, and type of base all resulted in formation of the undesired by-product.
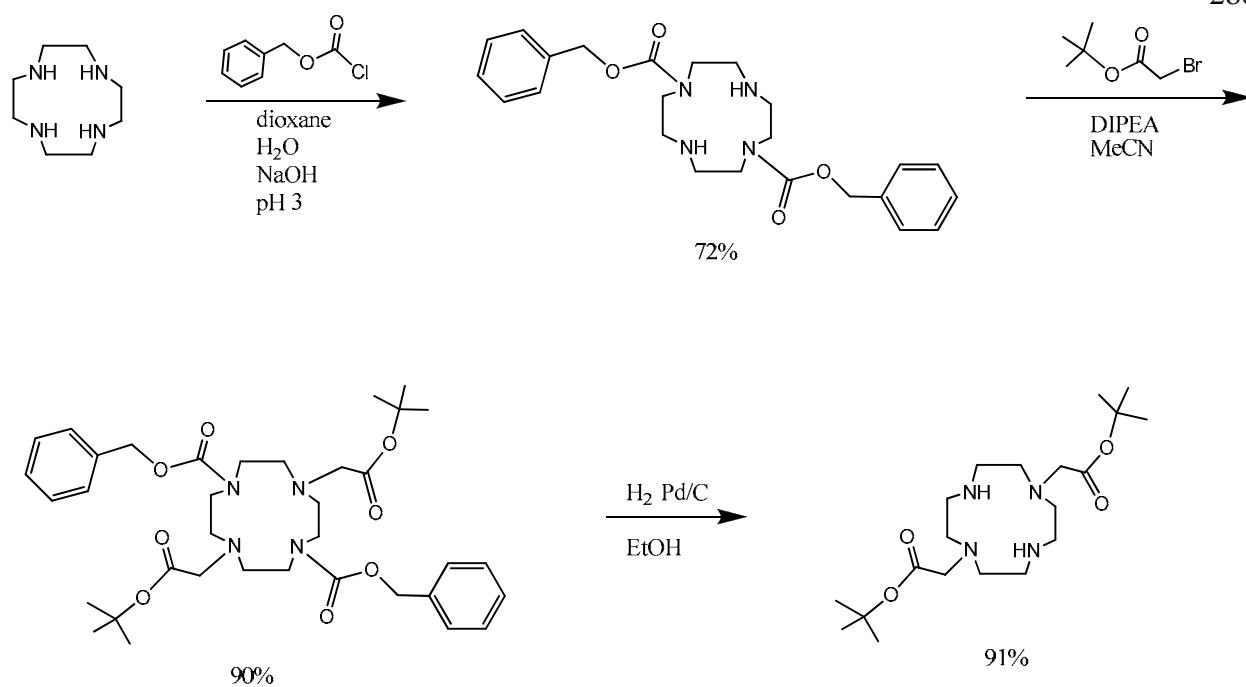
Scheme A2.1 Synthesis of 1,7-bis(*tert*-butoxycarbonylmethyl)-1,4,7,10-tetraazacyclododecane[5]
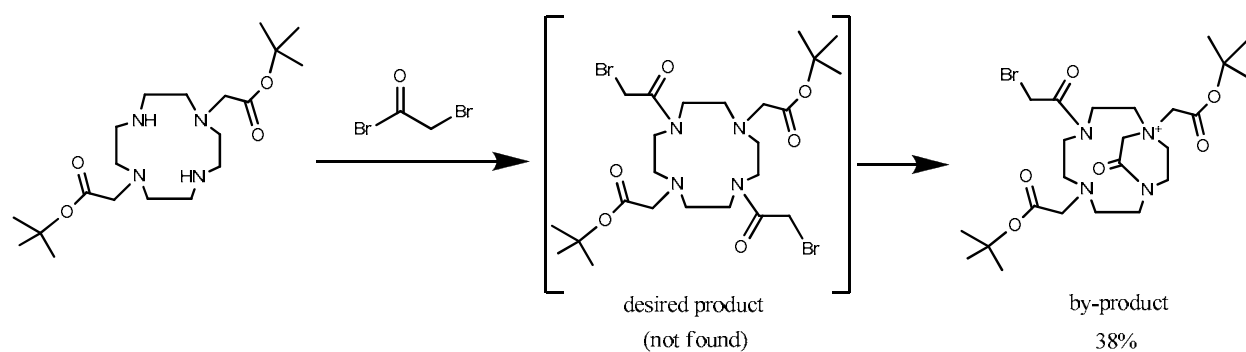
Scheme A2.2 Attempted synthesis of 1,7-bis(*tert*-butoxycarbonylmethyl)-4,10-bis(bromomethylcarbonyl)-1,4,7,10-tetraazacyclododecane and resultant by-product (*Note- the depicted isomer of the byproduct is not the only possible isomer)

Wangler and coworkers observed a similar side-reaction during the attempted

monoalkylation of cyclen at moderate temperatures (Figure A2.2). A search of the literature

revealed related complexes ("cross-bridged" tetraazamacrocycles) in which a two carbon

moiety[11] and a three carbon moiety[12] bridges across a cyclen based macrocycle (Figure A2.3).
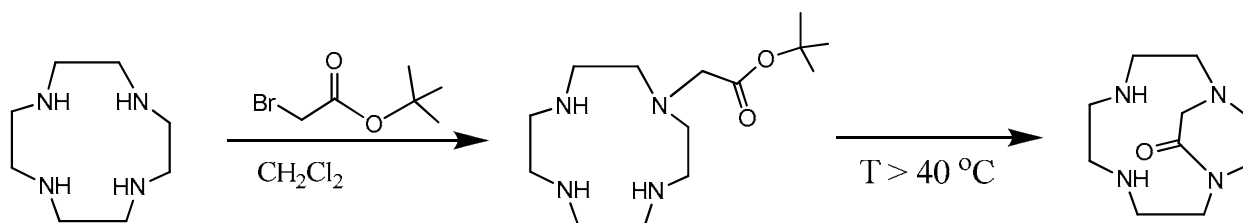
Figure A2.2 Side reaction observed by Wangler and coworkers.[13]
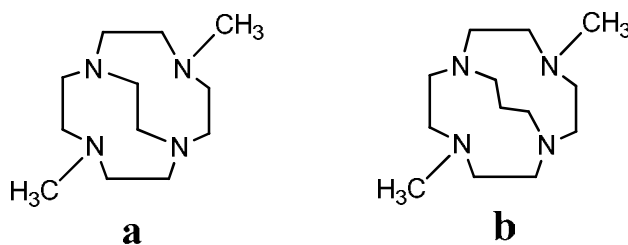
Figure A2.3 Cross-bridged macrocycles from (a) Hubin and coworkers[11] and (b) Springborg and coworkers[12]

Due to the instability/undesired reactivity of 1,7-bis(*tert*-butoxycarbonylmethyl)-4,10-

bis(bromomethylcarbonyl)-1,4,7,10-tetraazacyclododecane (Scheme A2.2), Approach #1 was

abandoned in favor of an alternate route (Approach #2).

APPROACH #2

The second approach was to employ amide bond formation between a carboxylic acid on the peptide side-chains and an amine on the macrocyclic chelate (green colored R groups in Figure A2.2). The carboxylic acid functionality can be easily introduced into a substrate peptide by substituting aspartic acid or glutamic acid into the peptide sequence. This choice of amino acids differing by a single methylene group in the side-chain allows precise control over the distance between the peptide backbone and the chelate. The amine functionality was envisioned to be incorporated as pendant arms of the macrocyclic chelator, forming a bi-functional chelate. Two versions of the chelate, differing by two methylene groups, allowed further control over the distance between the peptide backbone and the chelate.

Two versions of the bi-functional chelate, Compounds **2** and **4**, were synthesized according to Schemes A2.3 and A2.4, respectively. (See Appendix IV for a related intermediate.)
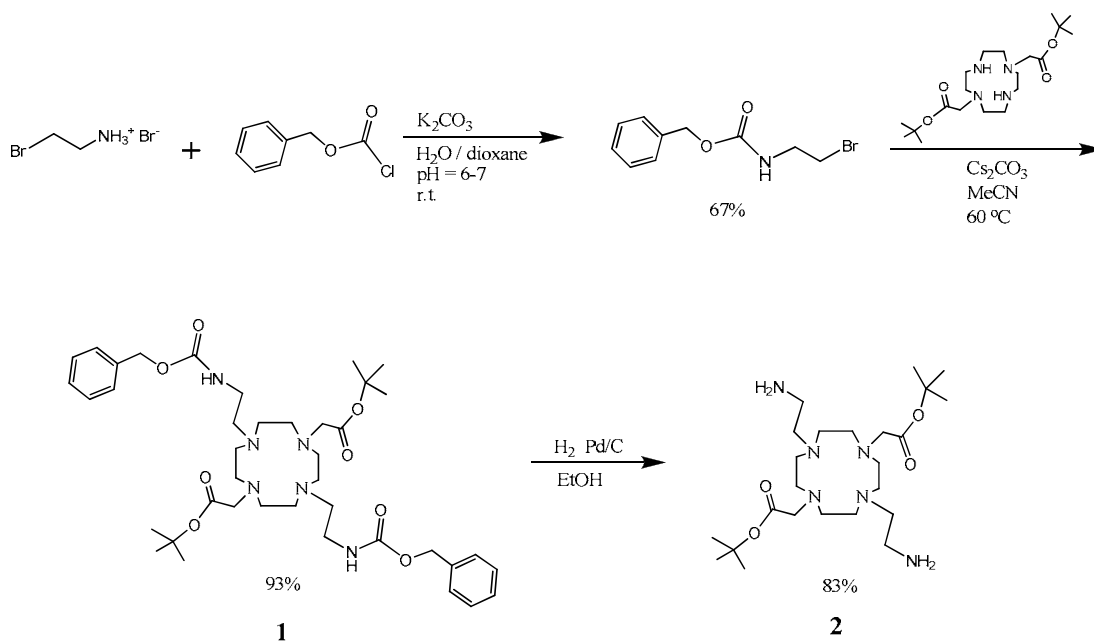
Scheme A2.3 Synthesis of bi-functional chelate 2
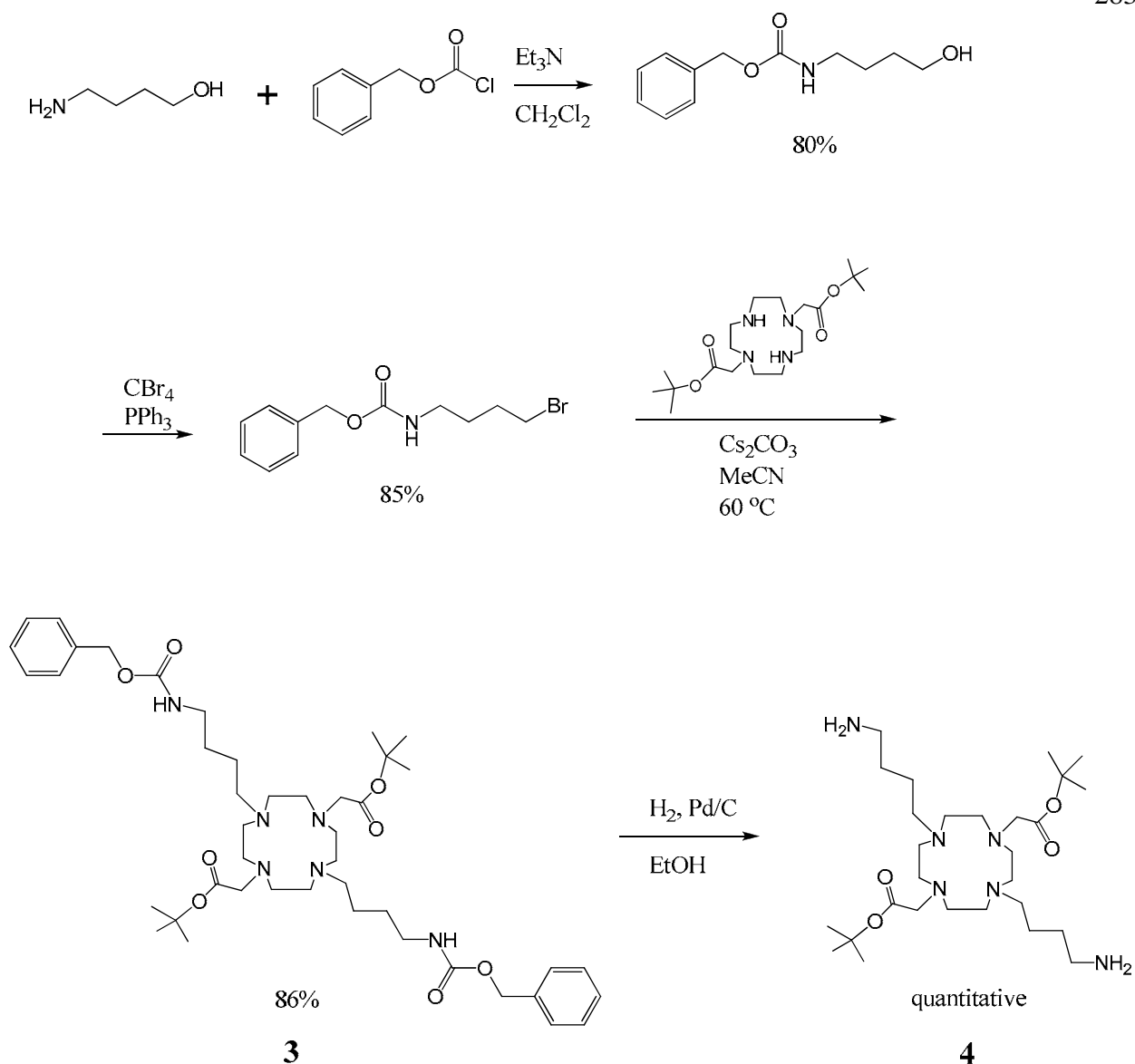
Scheme A2.4 Synthesis of bi-functional chelate 4

The protected peptide was prepared using SPPS according to Scheme A2.5. The peptide

sequence of WDEXDXG was chosen based upon the Caspase-3 substrate DEXD^X (where X

denotes amino acid variability and ^ denotes the cleavage site; described in further detail in

Chapter II, Part I). Due to tolerance of substitution in the P_2 and P_1' sites[14] (for nomenclature,

see Figure 2.5, Chapter II), these amino acids were chosen as the positions of attachment to the chelate. The C-terminal glycine was added for synthetic ease/cost of starting materials and the N-terminal tryptophan was added for fluorescence detection during HPLC purification.

The peptide required a 3-way orthogonal protecting strategy. Acid-labile protecting groups include the t-Bu groups found on the side chains of aspartic acids at P_1 and P_4 and glutamic acid at P_3 as well as the Boc group on tryptophan at P_5. The C-terminus was effectively protected through attachment to the solid support through the acid-labile Wang resin linker. All of these acid-labile groups prevent unwanted side reactions from occurring with these functionalities, yet are easily 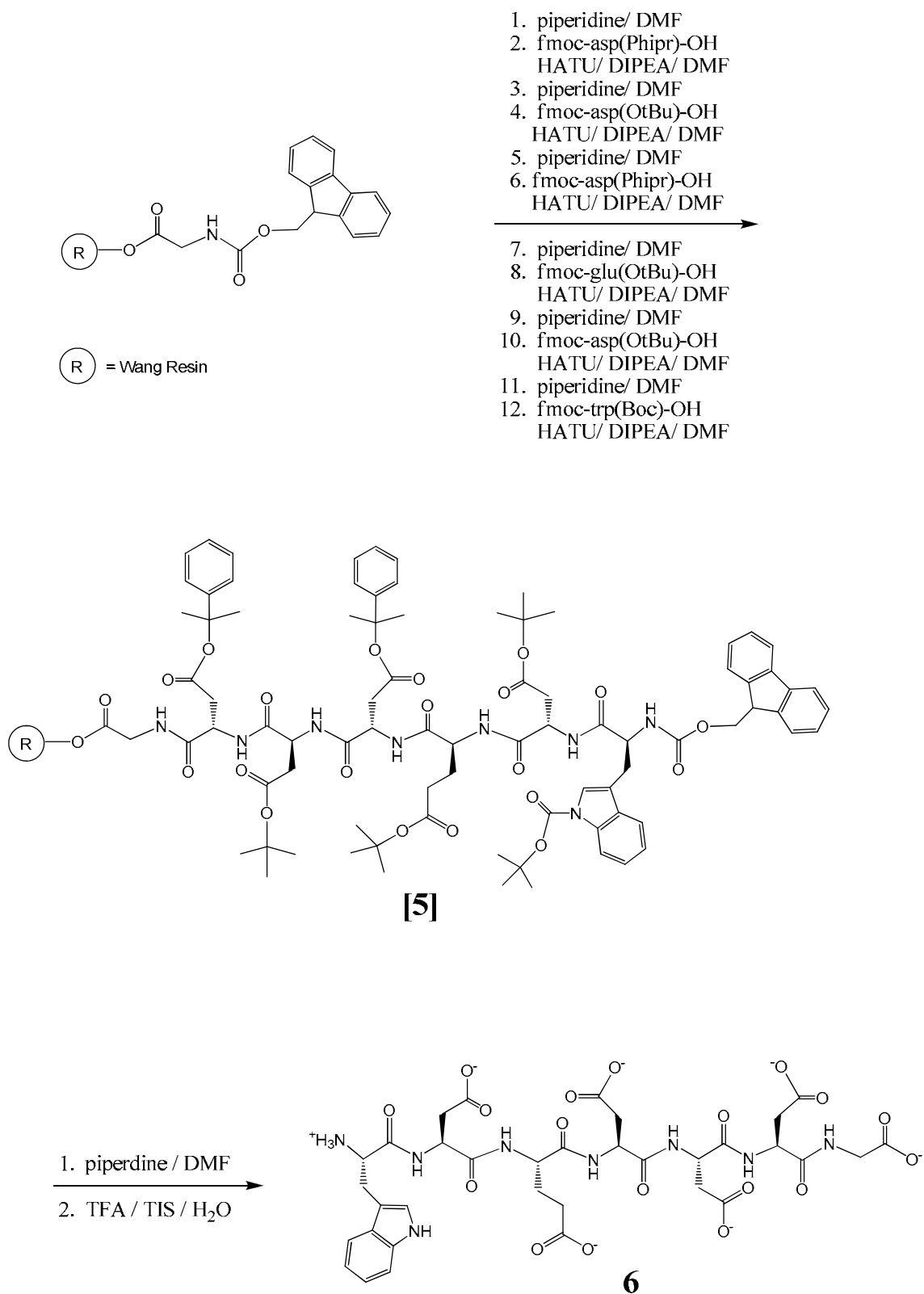removed during the cleavage of the peptide from the resin using 95% trifluoroacetic acid. The N-terminus was protected with fmoc, which is easily removed using a solution of 20% piperidine in DMF. The third level of orthogonality comes from the use of the phenylisopropyl (Phipr) protecting group on the aspartic acids at P_2 and P_1'. Phipr is removed using weakly acidic conditions (2% trifluoroacetic acid in CH_2Cl_2). This allows selective removal of Phipr without disturbing the other acid-labile groups.[15] Using this approach, the Phipr groups were used such that they can be selectively removed while the protected peptide is anchored to the solid support.

Unfortunately, during the synthesis of the protected peptide **[5]**, the desired product **6** was achieved in very low yields, and the major product could not be identified. Upon cleavage of **[5]** from the resin (Scheme A2.5), the major product was insoluble in water or other polar solvents which is inconsistent with the highly charged nature of **6**. The desired product **6** was detected by mass spectrometry but could not be isolated in appreciable quantities. Consequently, addition of chelate **2** or **4** after Phipr removal resulted in low yields of the desired macrobicycle (Scheme A2.6).

1. piperidine/ DMF
2. fmoc-asp(Phipr)-OH
   HATU/ DIPEA/ DMF
3. piperidine/ DMF
4. fmoc-asp(OtBu)-OH
   HATU/ DIPEA/ DMF
5. piperidine/ DMF
6. fmoc-asp(Phipr)-OH
   HATU/ DIPEA/ DMF

7. piperidine/ DMF
8. fmoc-glu(OtBu)-OH
   HATU/ DIPEA/ DMF
9. piperidine/ DMF
10. fmoc-asp(OtBu)-OH
    HATU/ DIPEA/ DMF
11. piperidine/ DMF
12. fmoc-trp(Boc)-OH
    HATU/ DIPEA/ DMF

R = Wang Resin

[5]

1. piperdine / DMF

2. TFA / TIS / H$_2$O

6

**Scheme A2.5 Synthesis of the protected peptide [5] and cleavage from resin to afford 6**
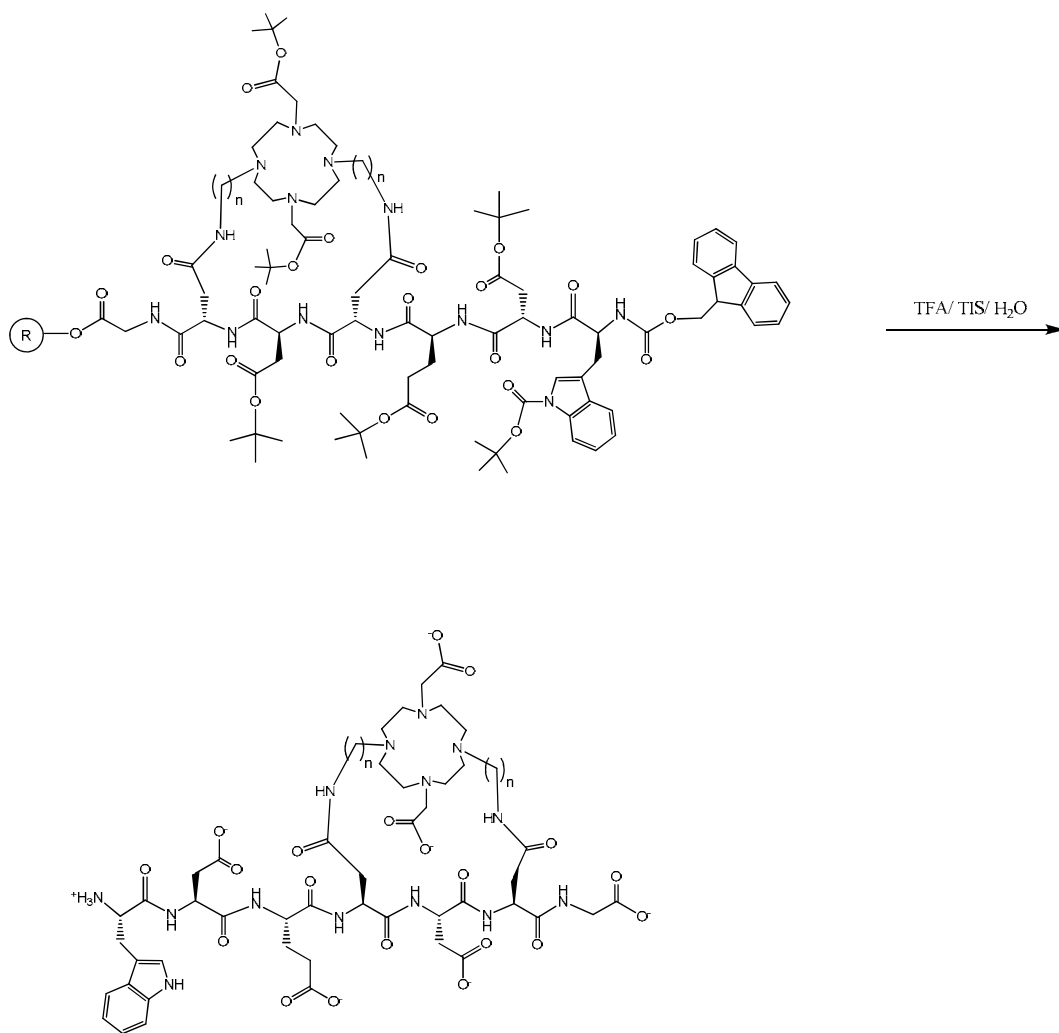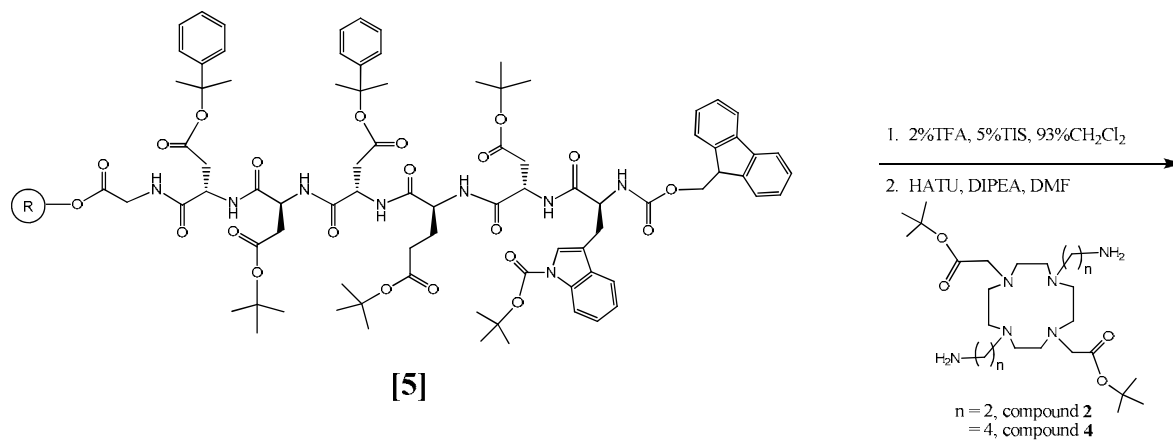
Scheme A2.6 Coupling of 2, 4 to the resin-bound peptide

A possible explanation for the low yields experienced in Schemes A2.5 and A2.6 is the competing side-reaction involving intramolecular cyclization of **[5]** at the aspartic acid residues to form an aspartimide (Scheme A2.7). Aspartimide formation is the side–reaction mostly likely to be encountered in routine SPPS[7] and occurs most frequently with peptides containing an asp(OtBu)-X motif, where X = gly, asn(Trt), ser, thr (Scheme A2.8).[16] Analysis of the ESI-MS of the crude product obtained from Scheme A2.6 shows evidence of the aspartimide by-product depicted in Scheme A2.7 [by-product m/z calc: 814.24, found: negative mode 813.2 (M – H), positive mode 815.1 (M + H$^+$)].

In order to further study the potential for aspartimide formation, a model system of reactions was devised (Scheme A2.9). The model system consists of a truncated version of **[5]** (less synthetic steps and simpler products for characterization) and was subjected to the same conditions as in Scheme A2.6. After the attempted coupling of **4** to the aspartic acid side-chain (Scheme A2.9), the Kaiser test[17] failed to detect primary amines. This result is inconsistent with successful coupling of **4** because the coupling of **4** to the aspartic acid side-chain should yield a positive Kaiser test for the pendant primary amine of **4**. To confirm the efficacy of the Kaiser test in detecting a pendant primary amine, **4** was subjected to the Kaiser test and resulted in the expected purple color observed for primary amines. This simple experiment confirmed the ability of the Kaiser test to detect the pendant primary amine of **4**. After cleavage of the model peptide from the resin (Scheme A2.10), aspartimide formation was detected by ESI-MS [m/z calc: 172.05, found: positive mode 172.9 (M + H$^+$)]. The reactions of the model system (Scheme A2.10) were repeated in triplicate, with each trial yielding a similar conclusion. Therefore, the results of the model system corroborate the formation of the aspartimide by-product observed in Scheme A2.7.
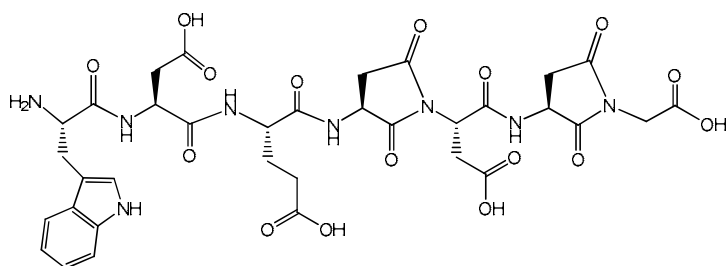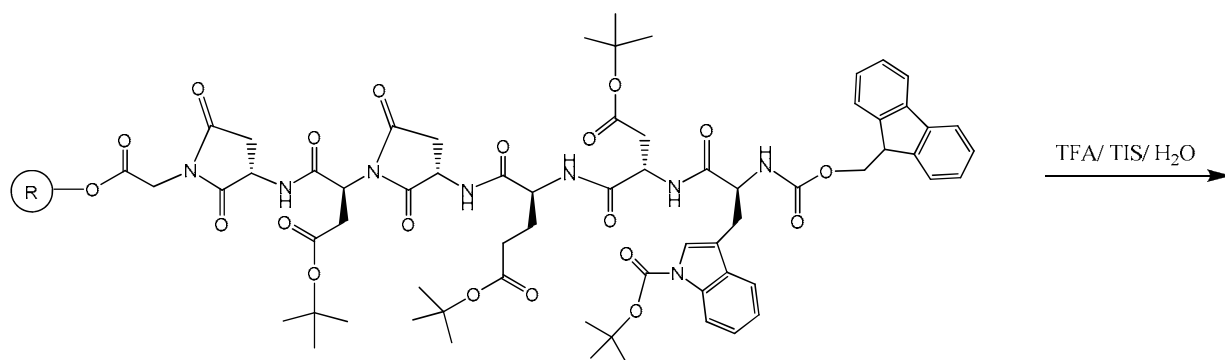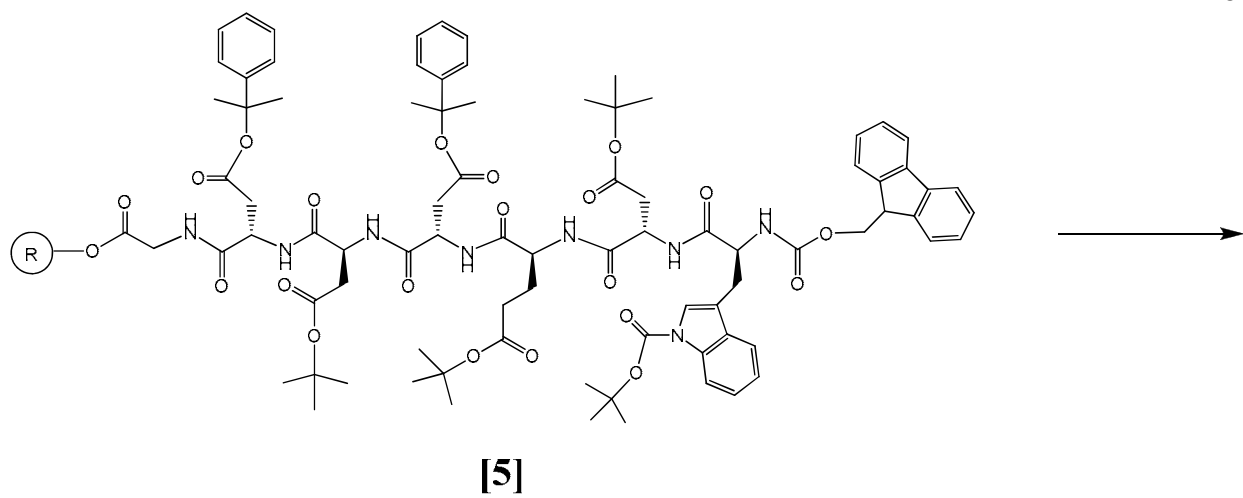
Scheme A2.7 Intramolecular cyclization of [5] to form aspartimide by-product
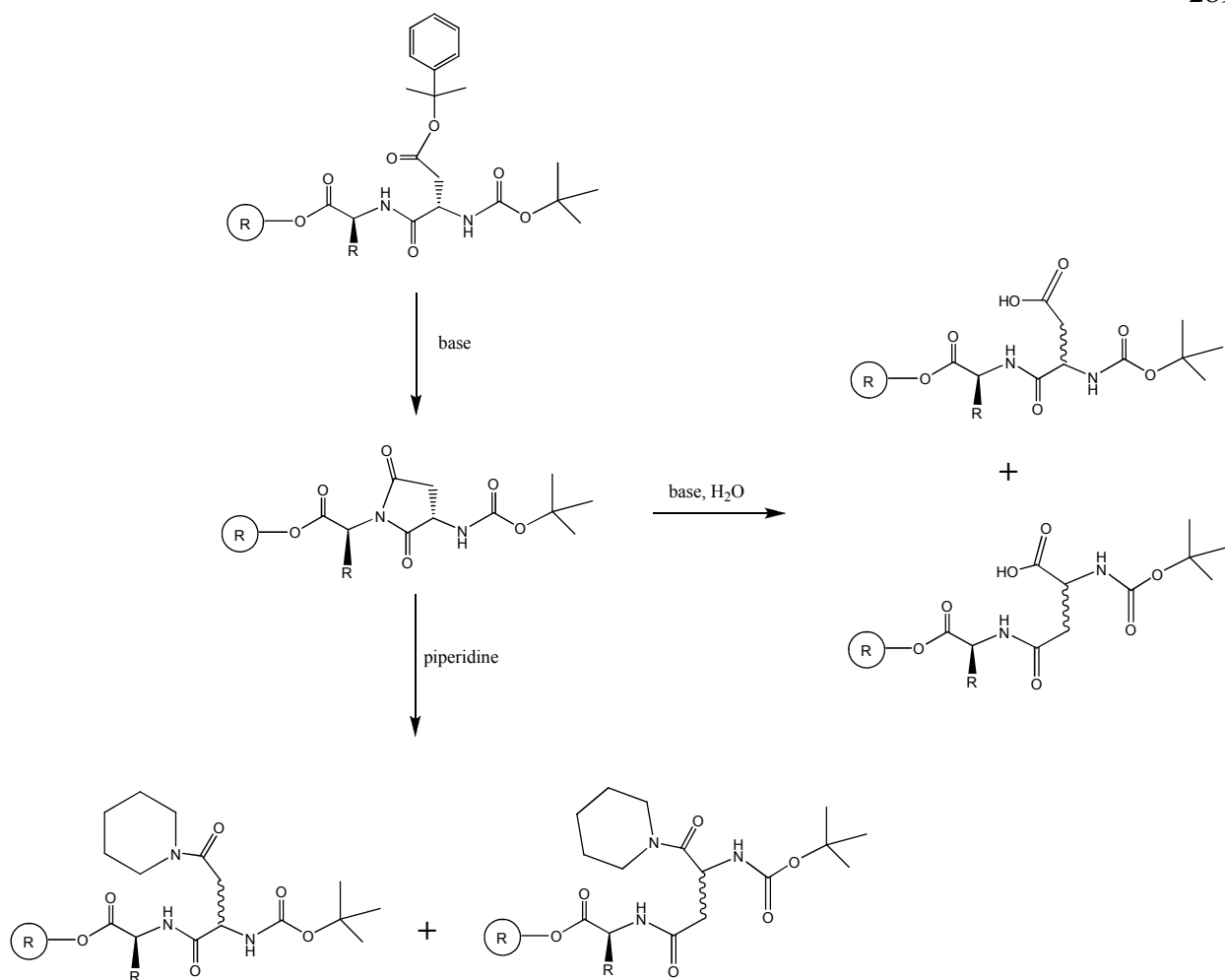
Scheme A2.8 Mechanism of aspartimide formation[7]
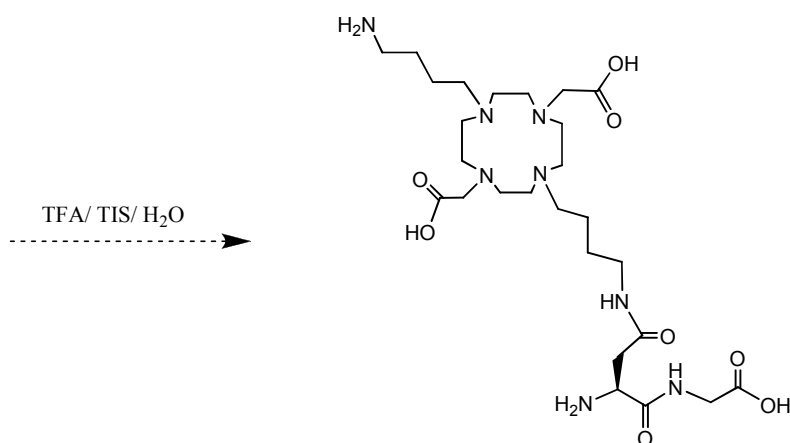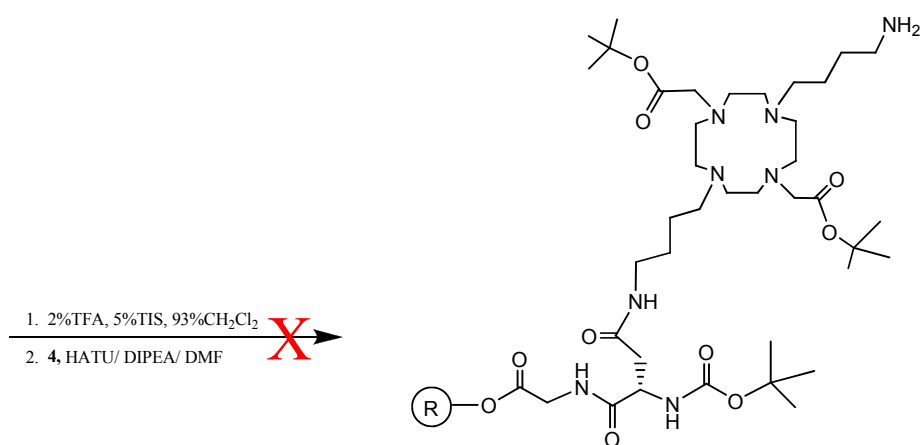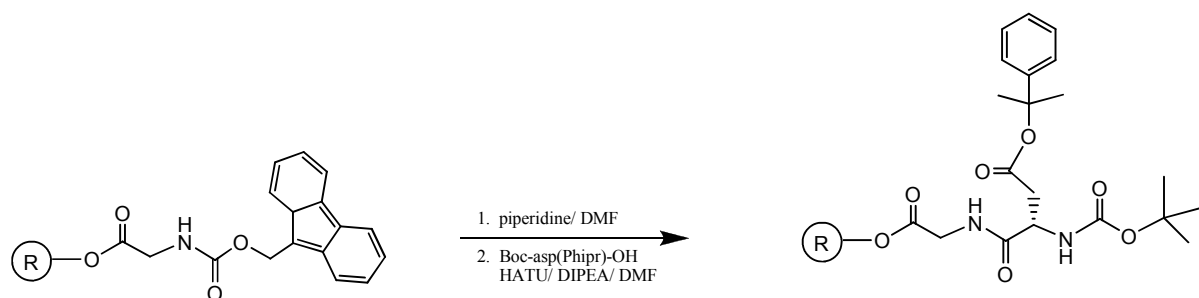
Scheme A2.9 Test reactions for aspartimide formation
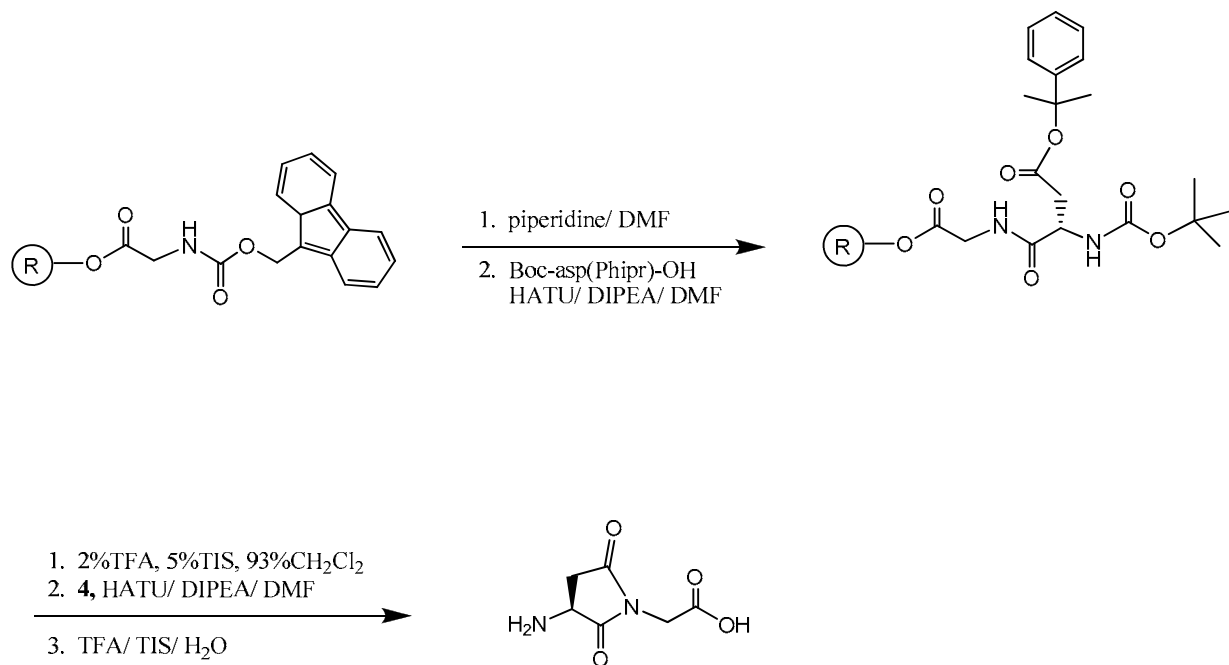
Scheme A2.10 Aspartimide formation detected during test reaction

Another possibility of the low yields observed in Scheme A2.6 could be due to incomplete removal of the Phipr protecting groups from the side-chains of the aspartic acid residues. In order to test Phipr removal under similar conditions, the protected amino acid starting material, fmoc-asp(Phipr)-OH, was dissolved in CH_2Cl_2 and subjected to conditions mimicking those performed during SPPS (2% trifluoroacetic acid for 10 minutes, Scheme A2.11). This afforded the expected complete removal of Phipr (as evidenced by ^{1}H-NMR and ESI-MS), therefore it was confirmed that Phipr is effectively removed under mild acidic conditions.
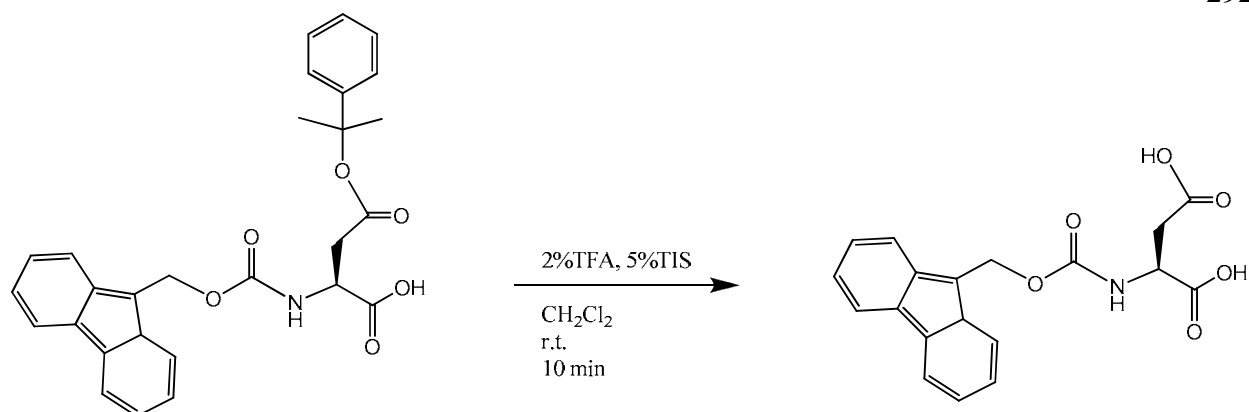
Scheme A2.11 Test reaction for Phipr removal

Due to low yields and aspartimide by-product formation, Approach #2 was abandoned in favor of an alternate route (Approach #3).

APPROACH #3

The third approach, similar to approach #2, employs amide bonds to form the linkage between the peptide and the chelate. However, the distinct difference is the reversed position of the functional groups. In approach #3, the acid functionality is located on the chelate, while the amine functionality is located on the peptide (pink colored R groups in Figure A2.2). This was performed in an attempt to avoid aspartimide formation as well as alleviate the difficulties in characterizing intermediates during the formation of the bridge. The incorporation of amine side-chain functionalities was easily accomplished through the inclusion of lysine residues in the P_2 and P_1' sites.

The protected peptide [7] was synthesized according to Scheme A2.12 and cleaved from the resin to afford **8** for characterization. The methyltrityl (Mtt) protecting group chosen for the side-chain amine of the lysine residues can be removed under mild acidic conditions (1% trifluoroacetic acid in CH_2Cl_2). This allows a 3-way orthogonal protection strategy (similar to the protecting strategy described for Approach #2).

The bi-functional chelate, **10**, was synthesized according to Scheme A2.13. During the addition of **10** to the lysine side-chains of the peptide (Scheme A2.14), several by-products were detected by ESI-MS (Figure A2.4). These products arise from incomplete coupling between the amines on the lysine side-chains of the peptide and the carboxylic acids of **10**. Since the peptide is attached to the resin, any unreacted **10** is washed away during the rinses following the reaction. A potential by-product is the bridging of **10** between two distinct peptides. This reaction, however, was not detected and is not likely to occur due to the pseudodilution effect[18] of SPPS when using low resin loading. The pseudodilution effect occurs due to the lack of proximity of the peptides when bound to the resin. Another potential by-product is the coupling of two molecules of **10** onto a single peptide, however this by-product was not observed by ESI-MS. The RP-HPLC chromatogram of the crude product displayed five distinct peaks which further supports the formation of multiple products. The reactions in Scheme A2.14 were repeated with varying rate of addition of **10** to the peptide, relative amount of **10**, and overall reaction time. Each time, the reaction resulted in a similar ratio of products as detected by RP-HPLC.

1. piperidine/ DMF
2. fmoc-lys(Mtt)-OH
   HATU/ DIPEA/ DMF
3. piperidine/ DMF
4. fmoc-asp(OtBu)-OH
   HATU/ DIPEA/ DMF
5. piperidine/ DMF
6. fmoc-lys(Mtt)-OH
   HATU/ DIPEA/ DMF

7. piperidine/ DMF
8. fmoc-glu(OtBu)-OH
   HATU/ DIPEA/ DMF
9. piperidine/ DMF
10. fmoc-asp(OtBu)-OH
    HATU/ DIPEA/ DMF
11. piperidine/ DMF
12. fmoc-trp(Boc)-OH
    HATU/ DIPEA/ DMF

R = Wang Resin

[7]

1. piperidine/ DMF
2. TFA/ TIS/ H₂O

8

Scheme A2.12 Synthesis of the protected peptide [7] and cleavage from resin to afford 8

Scheme A2.13 Synthesis of bi-functional chelate 10

[7]

1% TFA, 5% TIS

CH₂Cl₂

1. **10,** HATU/ DIPEA/ DMF

2. piperidine/ DMF
3. TFA/ TIS/ H₂O
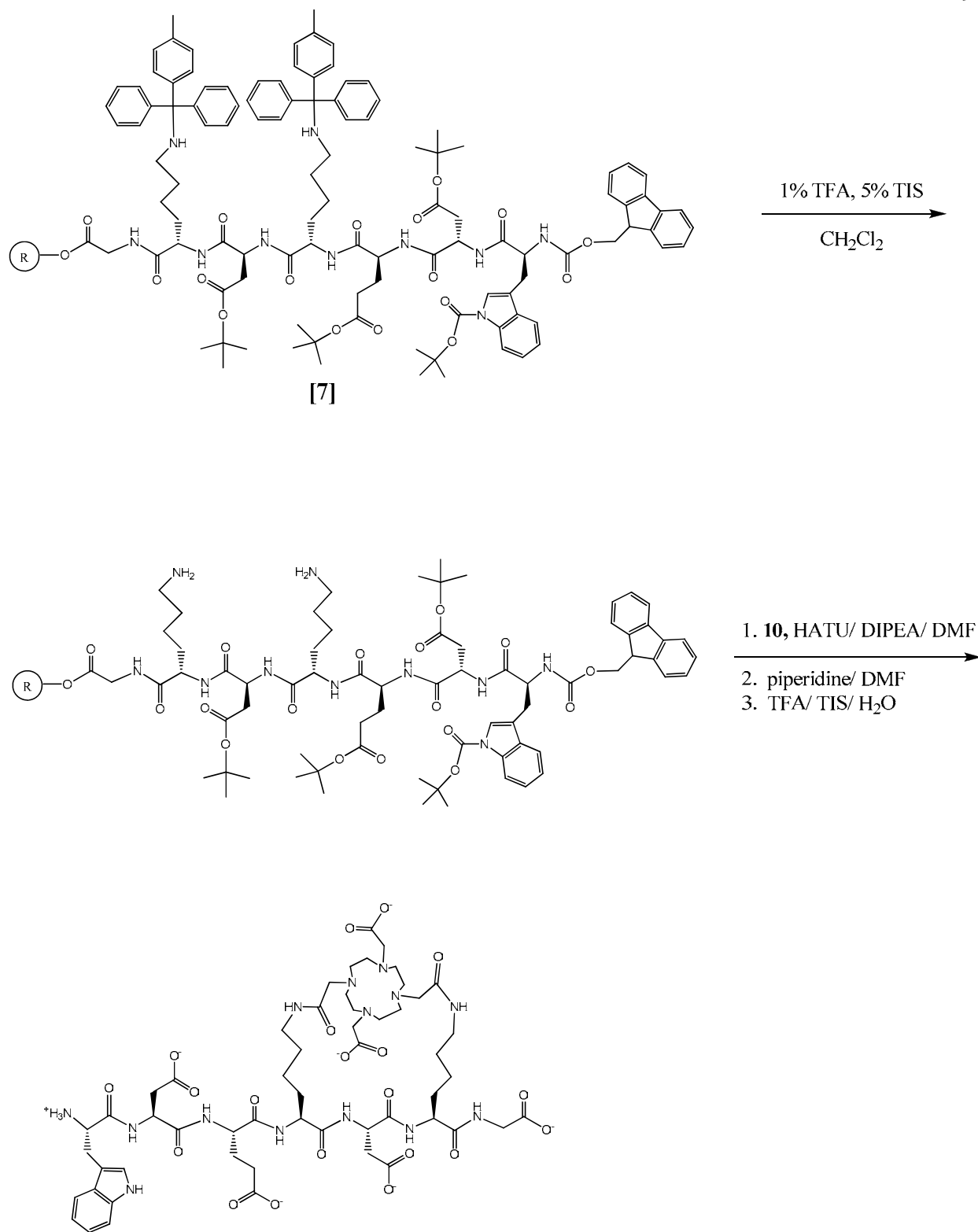
Scheme A2.14 Coupling of 10 to the resin-bound peptide
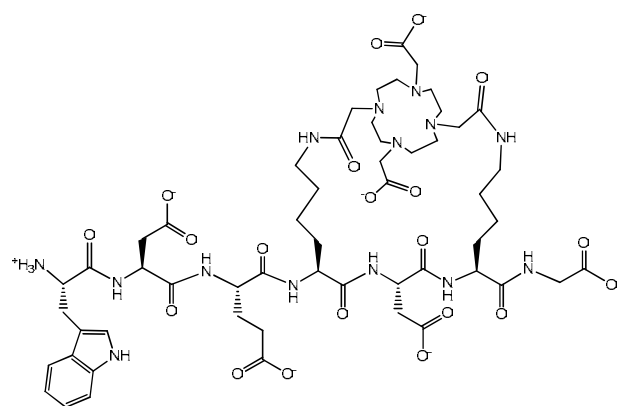
Desired Product
ESI-MS m/z Calc. 1244.57
Found 1245.5 (M + H$^+$)
1267.5 (M + Na$^+$)
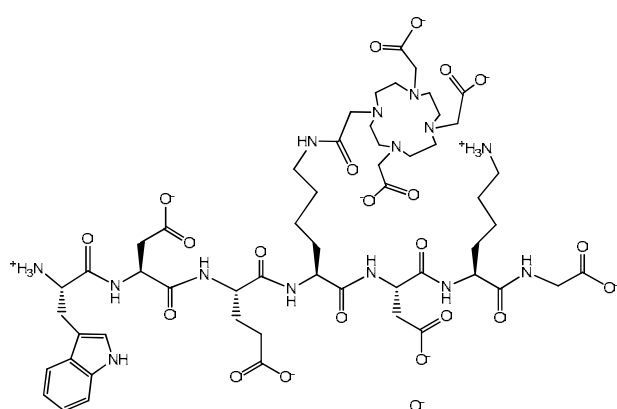
By-Products (incomplete coupling)
ESI-MS m/z Calc. 1262.58
Found 1263.4 (M + H$^+$)
1285.4 (M + Na$^+$)
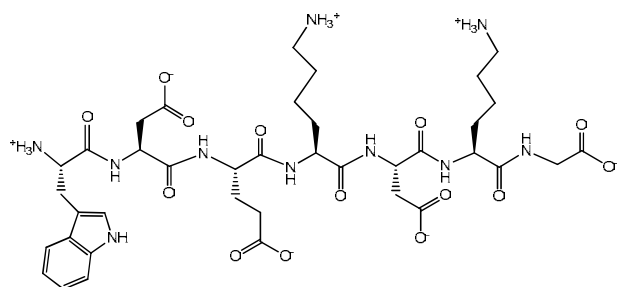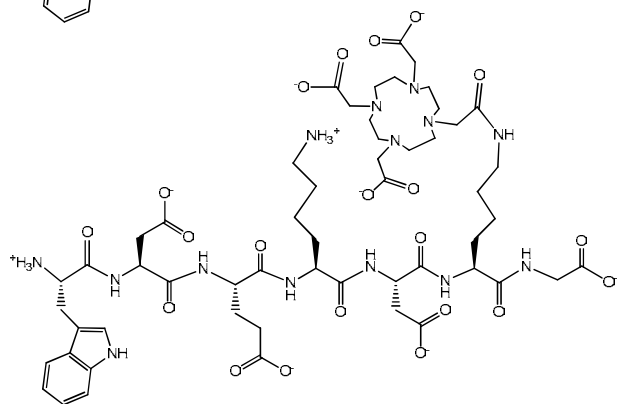
By-Product (unreacted peptide)
ESI-MS m/z Calc. 876.40
Found 877.3 (M + H$^+$)
899.3 (M + Na$^+$)

Figure A2.5 Crude products from Scheme A2.13 detected by ESI-MS

Due to the low yields resulting from multiple by-products, Approach #3 was abandoned in favor of an alternate route (Approach #4).

APPROACH #4

The fourth approach to form a peptide-bridged macrobicycle involved step-wise formation of the bridge using a novel 4-way orthogonal protecting strategy (details in Chapter II). This approach circumvented the problems of Approach #3 (low bridge yield formation due to multiple coupling products) and was ultimately scaled and used for the synthesis of the macrobicyclic agents described in Chapter II.

CONCLUSIONS

After several approaches were investigated, a robust and reproducible method was developed for the synthesis of peptide-bridged macrobicycles. The efforts contained in this appendix ultimately led to the novel 4-way orthogonal protection strategy presented in Chapter II. Through the course of the present work, several protecting strategies were utilized and a number of new macrocyclic chelates were synthesized. Several synthetic pathways resulted in unexpected byproducts; from these, much was learned about the unique chemistry of cyclen-based macrocycles. In addition, the aspartimide formation observed during Approach # 2 provides an example of potential side-reactions which must be considered when working with peptides containing aspartic acid residues. The novel macrocyclic chelates contained in this appendix have potential to be useful synthons in a myriad of applications including MRI contrast agents, positron emission tomography (PET) agents, and lanthanide-based luminescence agents.

EXPERIMENTAL

General details can be found in Chapter II.

1,7-bis(*tert*-butoxycarbonylmethyl)-4,10-bis(*N*-benzyloxycarbonylaminoethyl)-1,4,7,10-tetraazacyclododecane (1)

1,7-bis(*tert*-butoxycarbonylmethyl)-1,4,7,10-tetraazacyclododecane (synthesized according to literature methods[5]) (1.5881 g, 3.9647 mmol) was dissolved in 10 mL MeCN and placed in a 500 mL 3-neck roundbottom flask with magnetic stirbar and Cs_2CO_3 (3.0 equivalents, 3.8621 g, 11.853 mmol). *N*-benzyloxycarbonyl-2-bromo-1-ethylamine (synthesized according to literature methods[19]) (2.1 equivalents, 2.1588 g, 8.3639 mmol) was dissolved in 5 mL MeCN and added dropwise over 5 min while stirring. The flask was attached to a water-cooled reflux condenser equipped with a drying tube (Drierite) and placed in a 60 °C oilbath overnight. The reaction was determined complete by TLC (silica gel, 1:9:90 saturated KNO_3:H_2O:MeCN, Pt stain, product R_f = 0.57). The solution was cooled to room temperature and paper filtered to remove Cs_2CO_3. MeCN was removed by rotary evaporation under reduced pressure to afford the crude product as a yellow oil. The crude product was dissolved in CH_2Cl_2 and loaded onto a silica gel column. Excess *N*-benzyloxycarbonyl-2-bromo-1-ethylamine was eluted with CH_2Cl_2, followed by a gradient up to 10% MeOH in CH_2Cl_2 to elute the desired product. Solvents were removed by rotary evaporation under reduced pressure followed by pumping vacuum overnight to afford **1** as a white crystalline solid (2.7776 g, 93% yield). Recrystallization from MeOH was performed using seed crystals, however the crystals obtained were too small for X-ray diffraction.

ESI-MS: Calc. 754.46; Found positive mode 755.7 ($M + H^+$), 777.7 ($M + Na^+$)

^{1}H NMR (CDCl$_3$): δ = 1.4 (s, 18H, t-Bu), 2.3-2.8 (br, 20H, cyclen and CH_2CH$_2$NHCBz), 3.1-3.3 (br, 8H, CH_2COO-tBu and CH$_2$CH_2NH-CBz), 5.1 (s, 4H, CBz CH_2), 7.3-7.4 (br, CBz aromatic, Note: integration not available due to solvent residual peak at 7.26 ppm)

^{13}C NMR (CDCl$_3$): δ = 28.3, 39.0, 51.0, 52.4(br), 53.4(br), 56.1, 66.5, 81.1, 128.1, 128.4, 128.5, 137.0, 156.7, 170.7

1,7-bis(*tert*-butoxycarbonylmethyl)-4,10-bis(aminoethyl)-1,4,7,10-tetraazacyclododecane (2)

1 (67.7 mg, 0.0887 mmol) was dissolved in 5 mL absolute ethanol and transferred to a glass hydrogenation vessel with Pd/C catalyst (10% catalyst loading, 53.59 mg). The vessel was purged four times with H$_2$/vacuum then charged with H$_2$ (30 psi) and reacted for 48 hours with mechanical shaking. The mixture was 0.22μm filtered to remove the catalyst. Solvent was removed by rotary evaporation under reduced pressure, followed by high vacuum to afford **2** as a clear and colorless oil (36.5 mg, 83% yield).

ESI-MS: Calc. 486.39; Found positive mode 487.4 (M + H$^+$), 509.4 (M + Na$^+$)

^{1}H NMR (CDCl$_3$): δ = 1.5 (s, 18H, t-Bu), 2.4-2.9 (br, 24H, cyclen, CH_2CH$_2$NH$_2$, and CH$_2$CH_2NH$_2$), 3.2-3.3 (br, 4H, CH_2COO-tBu)

^{13}C NMR (CDCl$_3$): δ = 28.3, 37.6, 40.8, 50.1, 50.6(br), 51.0(br), 56.5, 57.0, 65.1, 82.2, 171.0

1,7-bis(*tert*-butoxycarbonylmethyl)-4,10-bis(*N*-benzyloxycarbonylaminobutyl)-1,4,7,10-tetraazacyclododecane (3)

1,7-bis(*tert*-butoxycarbonylmethyl)-1,4,7,10-tetraazacyclododecane (synthesized according to literature methods[5]) (255.65 mg, 0.63823 mmol) was dissolved in 1 mL MeCN and placed in a 10 mL roundbottom flask with magnetic stirbar and Cs$_2$CO$_3$ (3.0 equivalents, 637.10 mg, 1.9554

mmol). *N*-benzyloxycarbonyl-4-bromo-1-butylamine (synthesized according to literature

methods[20]) (2.1 eq., 394.9 mg, 1.380 mmol) was dissolved in 1 mL MeCN and added dropwise

while stirring. The flask was attached to a water-cooled reflux condenser equipped with a drying

tube (Drierite) and placed in a 60 °C oilbath overnight. The reaction was determined complete

by TLC (silica gel, 1:9:90 saturated KNO_3:H_2O:MeCN, Pt stain, product $R_f = 0.23$). The

solution was cooled to room temperature and paper filtered to remove Cs_2CO_3. MeCN was

removed by rotary evaporation under reduced pressure to afford the crude product as a yellow

oil. The crude product was dissolved in CH_2Cl_2 and loaded onto a silica gel column. Excess *N*-

benzyloxycarbonyl-4-bromo-1-butylamine was eluted with CH_2Cl_2, followed by a gradient up to

10% MeOH in CH_2Cl_2 to elute the desired product. Solvents were removed by rotary

evaporation under reduced pressure followed by pumping vacuum overnight to afford **3** as a

yellow solid (445.4 mg, 86% yield).

ESI-MS: Calc. 810.53; Found positive mode 811.6 $(M + H^+)$, 833.6 $(M + Na^+)$

^{1}H NMR (CDCl$_3$): δ = 1.2 (m, 4H, CH$_2$C*H*$_2$CH$_2$CH$_2$NHCBz) 1.4 (s, 18H, *t*-Bu), 1.5 (m, 4H,

CH$_2$CH$_2$C*H*$_2$CH$_2$NHCBz), 2.3-3.3 (br, 28H, cyclen, C*H*$_2$COO-tBu, and

C*H*$_2$CH$_2$CH$_2$C*H*$_2$NHCBz), 5.0 (s, 4H, CBz C*H*$_2$), 7.3 (br, CBz aromatic, Note: integration not

available due to solvent residual peak at 7.26 ppm)

^{13}C NMR (CDCl$_3$): δ = 28.0, 28.3, 41.0, 52.5(br), 52.8(br), 56.6, 66.5, 81.5, 128.0, 128.2, 128.5,

136.9, 156.7, 171.0

1,7-bis(*tert*-butoxycarbonylmethyl)-4,10-bis(aminobutyl)-1,4,7,10-

tetraazacyclododecane (4)

3 (676.5 mg, 0.8341 mmol) was dissolved in 75 mL absolute ethanol and transferred to a glass

hydrogenation vessel with Pd/C catalyst (10% catalyst loading, 562.75 mg). The vessel was

purged four times with H_2/vacuum then charged with H_2 (35 psi) and to reacted for 65 hours with

mechanical shaking. The mixture was paper filtered and 0.22μm filtered to remove the catalyst.

Solvent was removed by rotary evaporation under reduced pressure, followed by high vacuum to

afford **4** as a clear and colorless oil which crystallized upon storage at -20 ^{o}C (504.5 mg,

quantitative yield).

ESI-MS: Calc. 542.45; Found positive mode 543.6 (M + H^+), 565.5 (M + Na^+)

^{1}H NMR (CDCl$_3$): δ = 1.2 (q, 4H, CH$_2$C*H$_2$*CH$_2$CH$_2$NH$_2$, *J* = 4.5 Hz), 1.5 (s, 18H, *t*-Bu), 1.8 (m,

4H, CH$_2$CH$_2$C*H$_2$*CH$_2$NH$_2$), 2.4-3.0 (br, 24H, cyclen and C*H$_2$*CH$_2$CH$_2$C*H$_2$*NH$_2$), 3.2-3.4 (br, 4H,

C*H$_2$*COO-tBu), 7.1 (br, N*H$_2$*)

^{13}C NMR (CDCl$_3$): δ = 28.2, 39.8, 45.0, 50.0(br), 51.2(br), 54.1, 57.9(multiple), 81.9, 82.2,

171.1, 171.4

Trp-Asp-Glu-Asp-Asp-Asp-Gly (6)

The protected peptide **[5]** was synthesized according standard solid-phase peptide synthesis

methods[6] using manual batch-type synthesis and fmoc protected amino acids.

A Wang resin consisting of 100-200 mesh 1% cross-linked polystyrene beads functionalized

with p-benzyloxybenzyl alcohol handle was used as a solid support for the stepwise addition of

amino acids. The Wang resin was purchased (NovaBiochem, San Diego, California) with the N-

terminal amino acid, fmoc-glycine, preloaded onto the resin. The resin (4.9805 g, 0.63 mmol/g

resin loading, 3.1 mmol glycine) was added to a fritted glass reactor vessel fitted with a 3-way valve for switching between N_2 (used to mix during all reactions and rinses) and vacuum (used to drain rinses and excess reactants). The dry Wang resin was pre-swelled with CH_2Cl_2 (1 X 10 minute rinse) followed by DMF (4 X 10 minute rinses). The N-terminal fmoc protecting group was removed using 20% piperidine in DMF (until determined >99% complete by the Kaiser test[17]; typically 4 X 10 minutes). The resin was rinsed with DMF (4 X 10 minutes). The next amino acid (2.5 equivalents relative to the N-terminal glycine on the Wang resin) to be added to the peptide was dissolved in a minimal amount of DMF. To this solution, HATU (2.0 equivalents) and DIPEA (5.0 equivalents) were added to form a yellow solution of the preactivated fmoc-amino acid. This solution was added to the resin and reacted while gently bubbling N_2 to mix the reactants until determined >99% complete (typically 2-12 hours) by the Kaiser test[17]. Upon completion, the resin was rinsed with DMF (4 X 10 minutes). This process of fmoc removal and addition of the next amino acid was repeated for each amino acid until the desired sequence, Trp(Boc)-Asp(OtBu)-Glu(OtBu)-Asp(Phipr)-Asp(OtBu)-Asp(Phipr)-Gly-Wang resin **[5]**, was obtained. At this point, a small amount (10 mg) of resin was removed for cleavage (see "Cleavage of peptide from resin" below) to afford **6** (used for characterization) while the remainder of **[5]** was carried through to the next step of the synthesis.

ESI-MS: Calc. 850.25; Found positive mode 873.1 (M + Na$^+$) negative mode 849.2 (M$^-$)

Trp-Asp-Glu-Lys-Asp-Lys-Gly (8)

The protected peptide **[7]** was synthesized according standard solid-phase peptide synthesis methods[6] using manual batch-type synthesis and fmoc protected amino acids.

A Wang resin consisting of 100-200 mesh 1% cross-linked polystyrene beads functionalized with p-benzyloxybenzyl alcohol handle was used as a solid support for the stepwise addition of amino acids. The Wang resin was purchased (NovaBiochem, San Diego, California) with the N-terminal amino acid, fmoc-glycine, preloaded onto the resin. The resin (1.00371 g, 0.66 mmol/g resin loading, 0.66 mmol glycine) was added to a fritted glass reactor vessel fitted with a 3-way valve for switching between N_2 (used to mix during all reactions and rinses) and vacuum (used to drain rinses and excess reactants). The dry Wang resin was pre-swelled with CH_2Cl_2 (1 X 10 minute rinse) followed by DMF (4 X 10 minute rinses). The N-terminal fmoc protecting group was removed using 20% piperidine in DMF (until determined >99% complete by the Kaiser test[17]; typically 4 X 10 minutes). The resin was rinsed with DMF (4 X 10 minutes). The next amino acid (2.5 equivalents relative to the N-terminal glycine on the Wang resin) to be added to the peptide was dissolved in a minimal amount of DMF. To this solution, HATU (2.0 equivalents) and DIPEA (5.0 equivalents) were added to form a yellow solution of the preactivated fmoc-amino acid. This solution was added to the resin and reacted while gently bubbling N_2 to mix the reactants until determined >99% complete (typically 2-12 hours) by the Kaiser test[17]. Upon completion, the resin was rinsed with DMF (4 X 10 minutes). This process of fmoc removal and addition of the next amino acid was repeated for each amino acid until the desired sequence, Trp(Boc)-Asp(OtBu)-Glu(OtBu)-Lys(Mtt)-Asp(OtBu)-Lys(Mtt)-Gly-Wang resin **[7]**, was obtained. At this point, a small amount (10 mg) of resin was removed for cleavage (see "Cleavage of peptide from resin" below) to afford **8** (used for characterization) while the remainder of **[7]** was carried through to the next step of the synthesis.

ESI-MS: Calc. 876.39; Found positive mode 877.4 ($M + H^+$), 899.4 ($M + Na^+$), 439.4 (M^{2+}), negative mode 875.4 (M^-), 897.4 [$(M + Na)^-$], 919.4 [$(M + 2Na)^-$]

Note: ^{1}H NMR (D$_2$O) spectrum displays non-first order coupling, thus making unambiguous assignments difficult without the aid of a complete 2D NMR analysis.

^{13}C NMR (D$_2$O, with acetone added for reference): δ = 22.4, 22.6, 26.7, 27.3, 30.4, 30.7, 35.9, 36.3, 39.6, 39.7, 41.8, 50.4, 50.8, 54.1, 54.2, 54.4, 59.9, 106.7, 112.6, 115.8, 118.1, 118.6, 120.1, 120.4, 122.7, 125.7, 127.2, 136.8, 163.3, 163.6, 169.8, 171.9, 172.6, 173.7, 173.8, 174.2, 174.5, 174.6, 174.7, 177.4

1,7-bis(*tert*-butoxycarbonylmethyl)-4,10-bis(benzyloxycarbonylmethyl)-1,4,7,10-tetraazacyclododecane (9)

Experimental details for the synthesis and characterization of **9** are included in Chapter II.

1,7-bis(*tert*-butoxycarbonylmethyl)-4,10-bis(carboxymethyl)-1,4,7,10-tetraazacyclododecane (10)

Experimental details for the synthesis and characterization of **10** are included in Chapter II.

APPENDIX III

LUMINESCENCE AND NMR STUDIES OF α-EGadMe and β-EGadMe

INTRODUCTION

EGadMe

An introduction to EGad[1] and EGadMe[2] can be found in Chapter I.

α-EGadMe and β-EGadMe

The two MRI contrast agents discussed in the present work, α-EGadMe and β-EGadMe, differ in chemical structure by the location of a single methyl group. Despite this seemingly trivial difference, the two agents display differing relaxivitiy, q, and τ_m values.[3] An investigation of the relaxometric properties of these agents is in agreement with carbonate binding to strictly the α-isomer and not the β-isomer.[3] Urbanczyk-Pearson and coworkers proposed an explanation of these phenomena based on the purported positions of the galactopyranose sugar and the macrocyclic chelate (Figure A3.1). The present work extends the structural investigations of Urbanczyk-Pearson and coworkers[3] to include laser luminescence spectroscopy and nuclear magnetic resonance (NMR) spectroscopy of the europium(III) and yttrium(III) analogs of α-EGadMe and β-EGadMe (Figure A3.1).
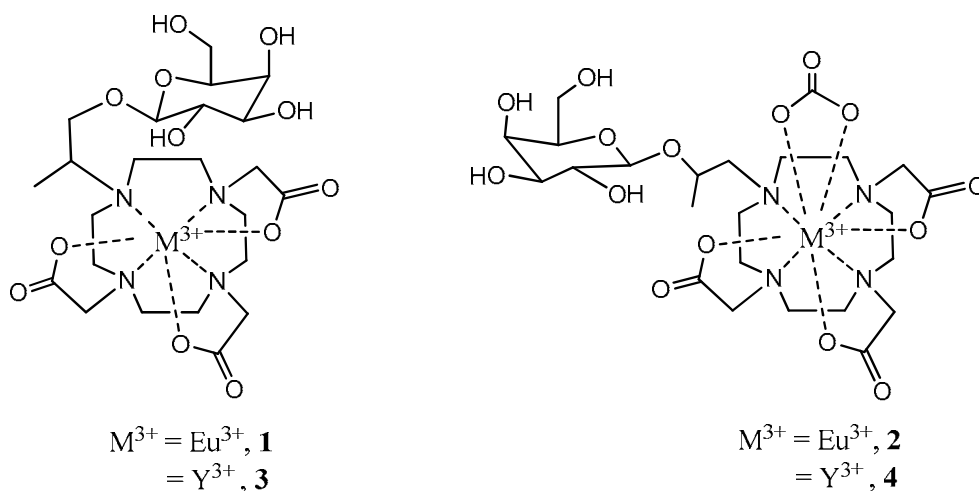
Figure A3.1 Hypothesized conformations of α-EGadMe (left) and β-EGadMe (right) in the presence of exogenous carbonate.[3] The numbering schemes for the europium(III) and yttrium(III) complexes refer to the current work.

Luminescence

The luminescence excitation spectra of europium(III) complexes is extremely sensitive to the coordination environment of the metal.[4] Therefore, an investigation of the excitation spectra of **1** and **2** upon titration of carbonate was hypothesized to yield valuable information concerning the potential for these complexes to bind carbonate.

Nuclear Magnetic Resonance

Nuclear magnetic resonance (NMR) is a powerful method commonly used to determine the structures of molecules in solution.[5] However, in the case of MRI contrast agents, the severe line broadening produced by gadolinium(III) limits the utility of NMR. Therefore, the substitution of diamagnetic yttrium(III) or paramagnetic europium(III) for gadolinium(III) in MRI contrast agents has been used to study these complexes by ^{1}H-NMR.[6] The substitution of europium(III) into the chelate causes the ^{1}H-NMR spectra to be dispersed over 70 ppm due to the

lanthanide induced shift (LIS). While an initial inspection of such a spectrum may lead one to render it useless, a closer look reveals a wealth of information. The distance dependence ($1/r^3$) of the LIS dictates that protons closest to the paramagnetic europium(III) experience the greatest amount of LIS.[7] For DOTA-based chelates, this phenomenon makes the identification of the protons located on the ethylene bridges of macrocyclic chelate (cyclen) straightforward due to their large chemical shifts. The axial protons of DOTA-based chelates are shifted downfield to approximately 10 to 40 ppm while the equatorial protons are shifted upfield to approximately -5 to -30 ppm.[8] Furthermore, the protons due to the square anti-prismatic (SAP) and twisted square anti-prismatic (TSAP) isomers of a chelate can be distinguished by their characteristic chemical shifts (see Figure 2.13, Chapter II for a diagram of the SAP and TSAP geometries). The axial protons of the SAP isomer are closer to the paramagnetic center and are thus shifted further downfield than the axial protons of the TSAP isomer.[8]

RESULTS AND DISCUSSION

Synthesis

The synthesis of **1**, **2**, **3**, and **4** was performed by Lauren Urbanczyk-Pearson and Dave Ballweg.

Laser Luminescence

The laser system developed by the laboratory of Professor Janet Morrow (University at Buffalo, SUNY) provided high resolution (0.01 nm) spectroscopy to probe the excitation spectra of **1** and **2**. The titration of **2** with carbonate resulted in a red shift of the excitation maximum

from 579.5 nm to 580.0 nm (Figure A3.2). The change in the excitation spectrum indicates a change in the coordination environment of europium(III). In contrast, the titration of **1** with carbonate did not result in a shift in the excitation maximum (Figure A3.3). Interestingly, the intensity of the europium(III) excitation of **1** increased upon titration with carbonate. It is hypothesized that carbonate is somehow interacting with the second coordination sphere of europium(III), yet not binding directly to europium(III).
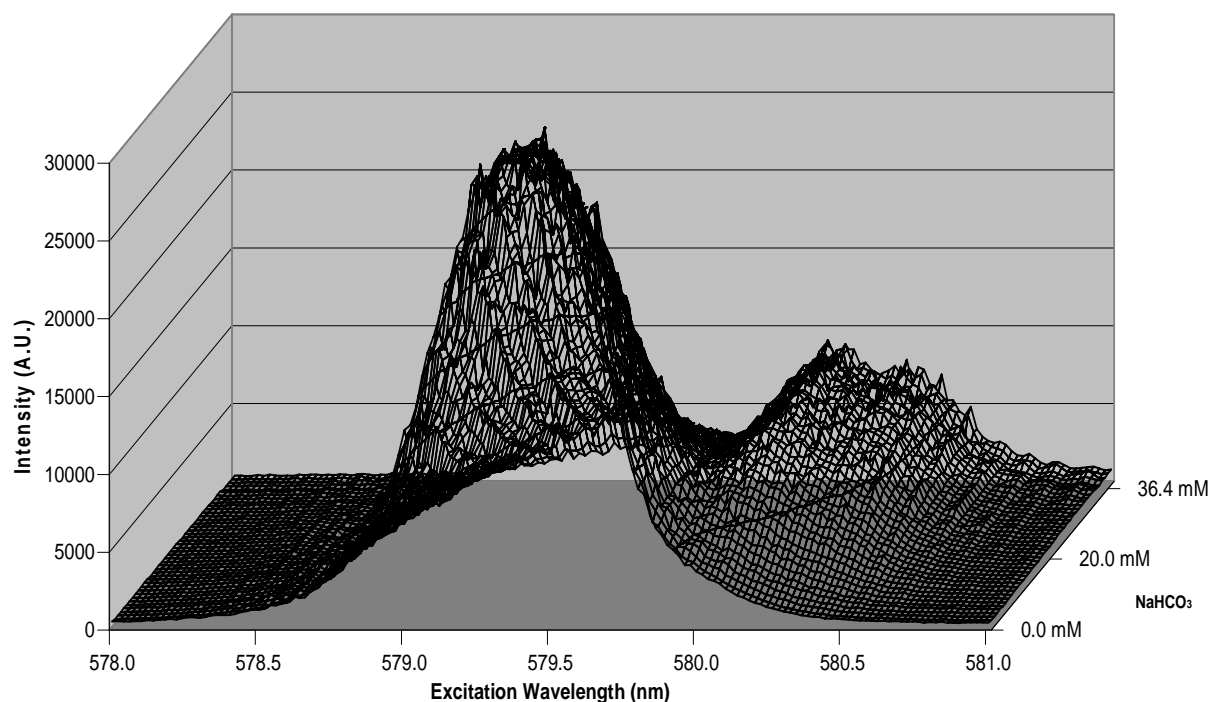
Figure A3.2 Excitation spectrum of 0.5 mM β-EGadMe (**2**) upon titration of NaHCO$_3$. With increasing concentrations of NaHCO$_3$, the excitation maximum at 579.5 nm decreases with a concomitant increase in two new maxima at 580.0 nm and 580.3 nm.
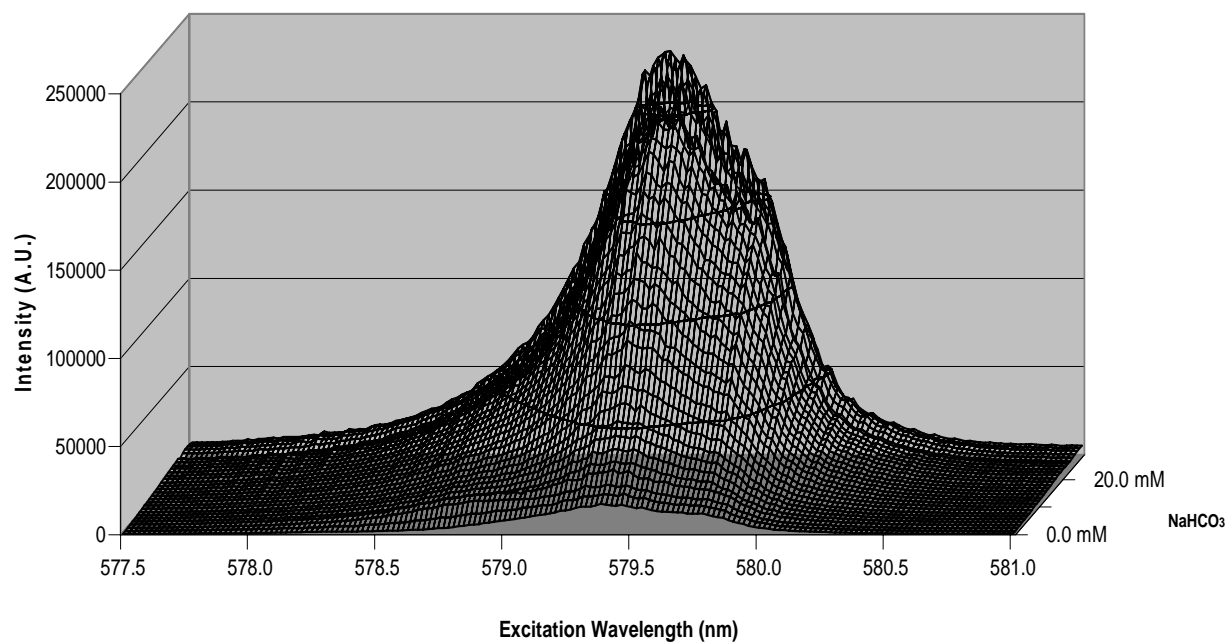
Figure A3.3 Excitation spectrum of 0.5 mM α-EGadMe (**1**) upon titration with NaHCO$_3$. The excitation intensity increases with increasing NaHCO$_3$, however there is no shift in the excitation maximum.

NMR

The ^{1}H-NMR spectra of the diamagnetic Y(III) complexes show an increased line broadening for the cyclen and sugar protons (at 2.5-3.5 ppm) for **4** relative to **3** (Figure A3.4). It is hypothesized that the broad ^{1}H-NMR spectrum of **4** is due to conformational fluxionality of the sugar and the macrocycle on the NMR timescale. This hypothesis is supported by the ^{1}H-NMR spectra of the europium(III) complexes, **1** and **2** (Figure A3.5). The presence of both the SAP and the TSAP isomers of the macrocycle can be detected for **1**. In contrast, the fluxionality of **2** precludes the resolution of the SAP and TSAP isomers.

In an effort to try to resolve the ^{1}H-NMR spectrum of **2** for future 2-dimensional (2D) NMR structural analysis, spectra were acquired at various temperatures between 0 ^{o}C and 80 ^{o}C. The variable temperature (VT) NMR studies indicated that **2** is in the intermediate fluxional regime throughout the entire temperature range studied. At low temperature (0 ^{o}C), the resolution improved slightly (Figure A3.6, top). At high temperature (80 ^{o}C), the resonances began to coalesce, further supporting the hypothesized fluxionality of **2** (Figure A3.6, bottom).

The binding of carbonate to **2,** as proposed by Urbanczyk-Pearson and coworkers,[3] lead to a new hypothesis that carbonate binding could be used to help resolve the ^{1}H-NMR spectra of **2**. The addition of 0.1 equivalents of Na_2CO_3 relative to **2** was insufficient to change the broadening of the ^{1}H-NMR spectrum. Once again, VT NMR showed slight improvements in resolution at low temperature (0 ^{o}C, Figure A3.7, top) and coalescence at high temperature (80 ^{o}C, Figure A3.7, bottom).

Higher concentrations of carbonate were used to successfully resolve the ^{1}H-NMR spectrum of **2**. The addition of a slight excess of Na_2CO_3 relative to **2** resulted in a well resolved ^{1}H-NMR spectum at ambient temperature (Figure A3.8). Interesting to note is the presence of

only the TSAP isomer. The lack of resonances for the SAP isomer suggests that the binding

of carbonate to **2** constrains the macrocycle to adopt only the TSAP structure. VT NMR of this

sample revealed insignificant changes upon cooling to 0 $^{\circ}$C and coalescence of the resonances at

80 $^{\circ}$C (Figure A3.9).
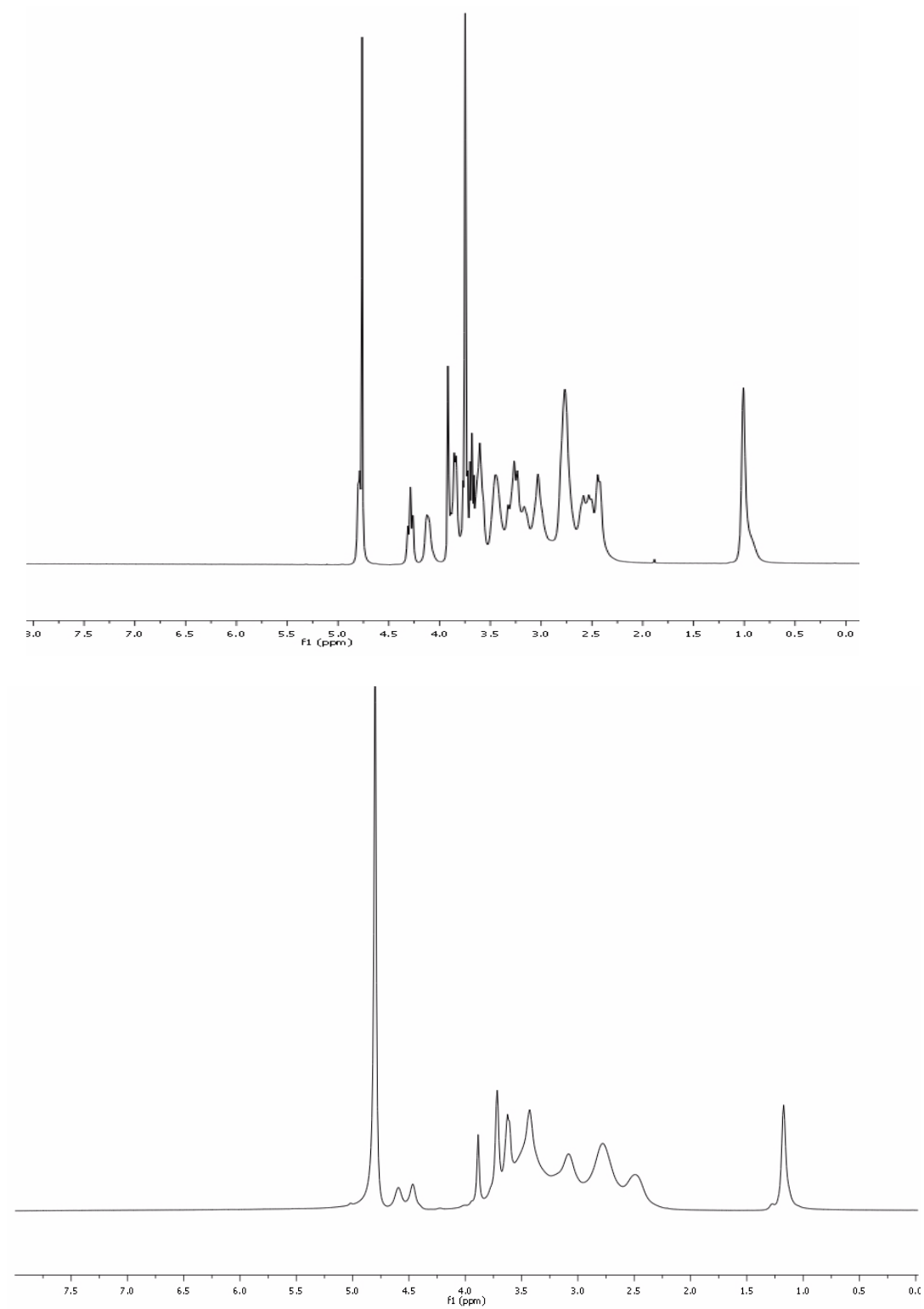
Figure A3.4 ^{1}H-NMR spectra of the diamagnetic Y(III) complexes of α-EGadMe (**3**, top) and β-EGadMe (**4**, bottom) in D$_2$O. The broad resonances of the cyclen and sugar protons of **4** (at 2.5-3.5 ppm) are indicative of conformational fluxionality.
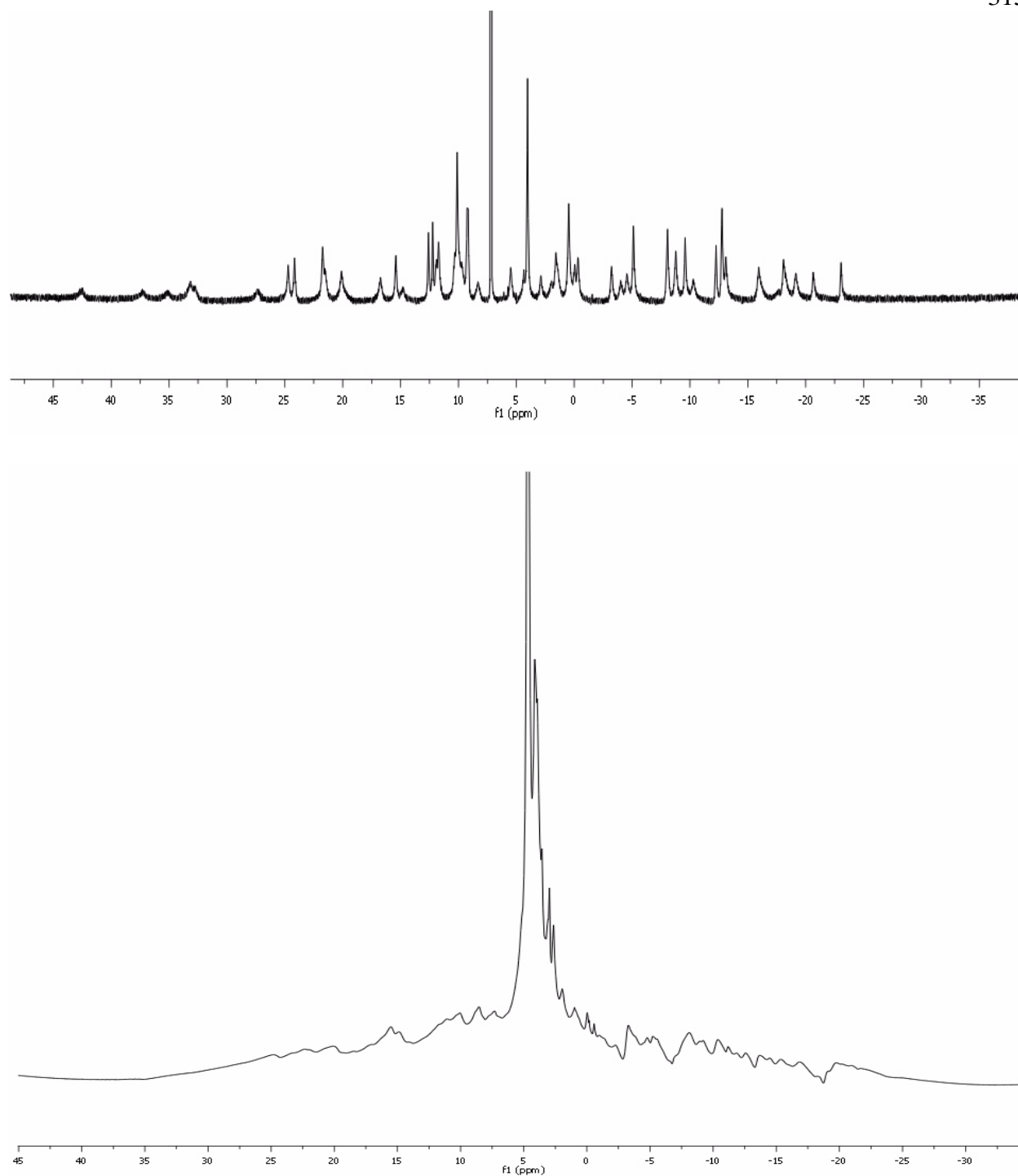
Figure A3.5 ^{1}H-NMR spectra of the paramagnetic Eu(III) complexes of α-EGadMe (**1**, top) and β-EGadMe (**2**, bottom) in D$_2$O. The cyclen axial protons due to the SAP isomer (at 32-43 ppm) and the TSAP isomer (at 15-27 ppm) are well-resolved for **1**. In contrast, the fluxionality of **2** results in broad proton resonances.
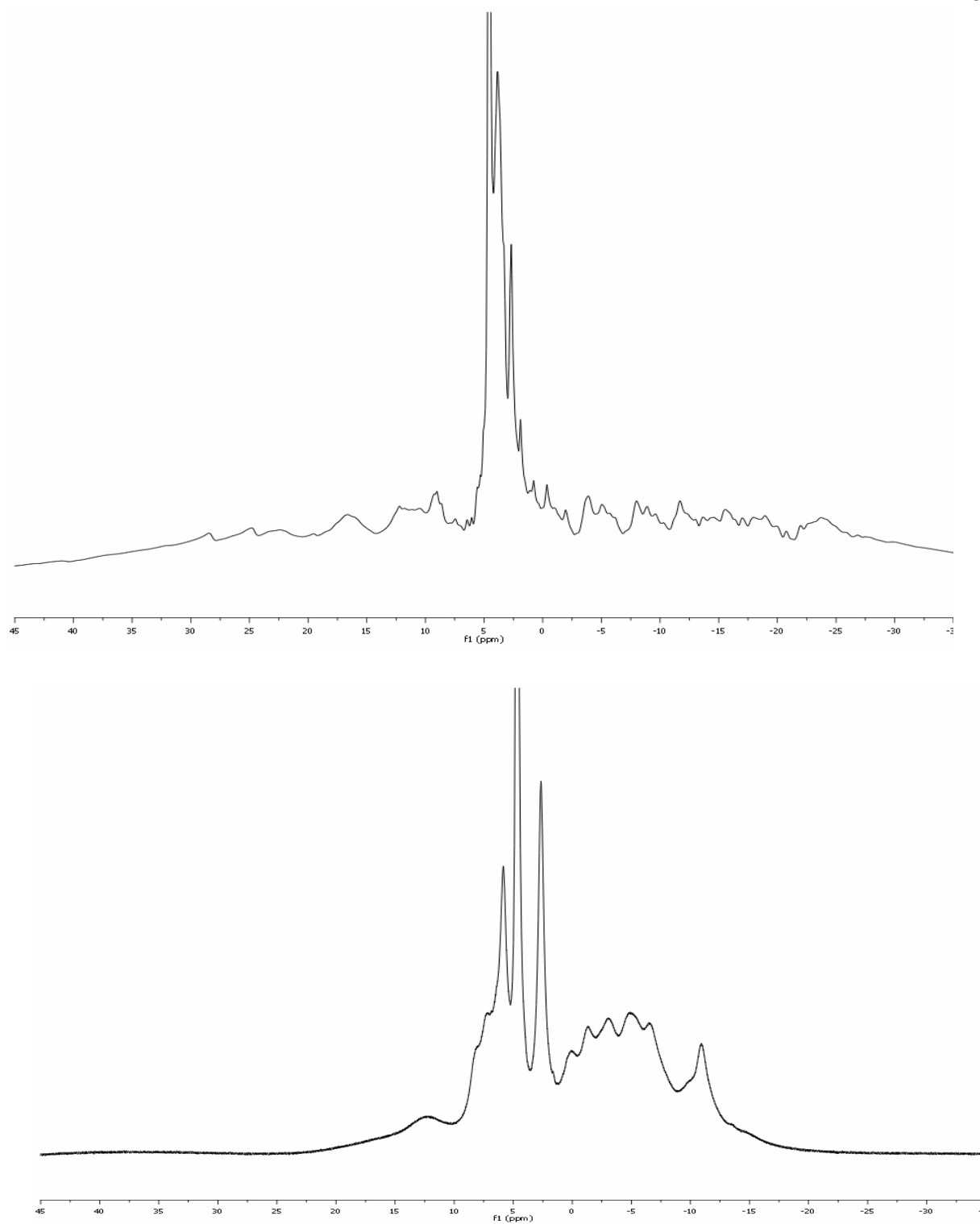
Figure A3.6 Low (0 °C, top) and high (80 °C, bottom) temperature ^{1}H-NMR spectra of Eu(III)-β-EGadMe (**2**) in D$_2$O. The paramagnetically shifted cyclen protons begin to coalesce at high temperature.

317
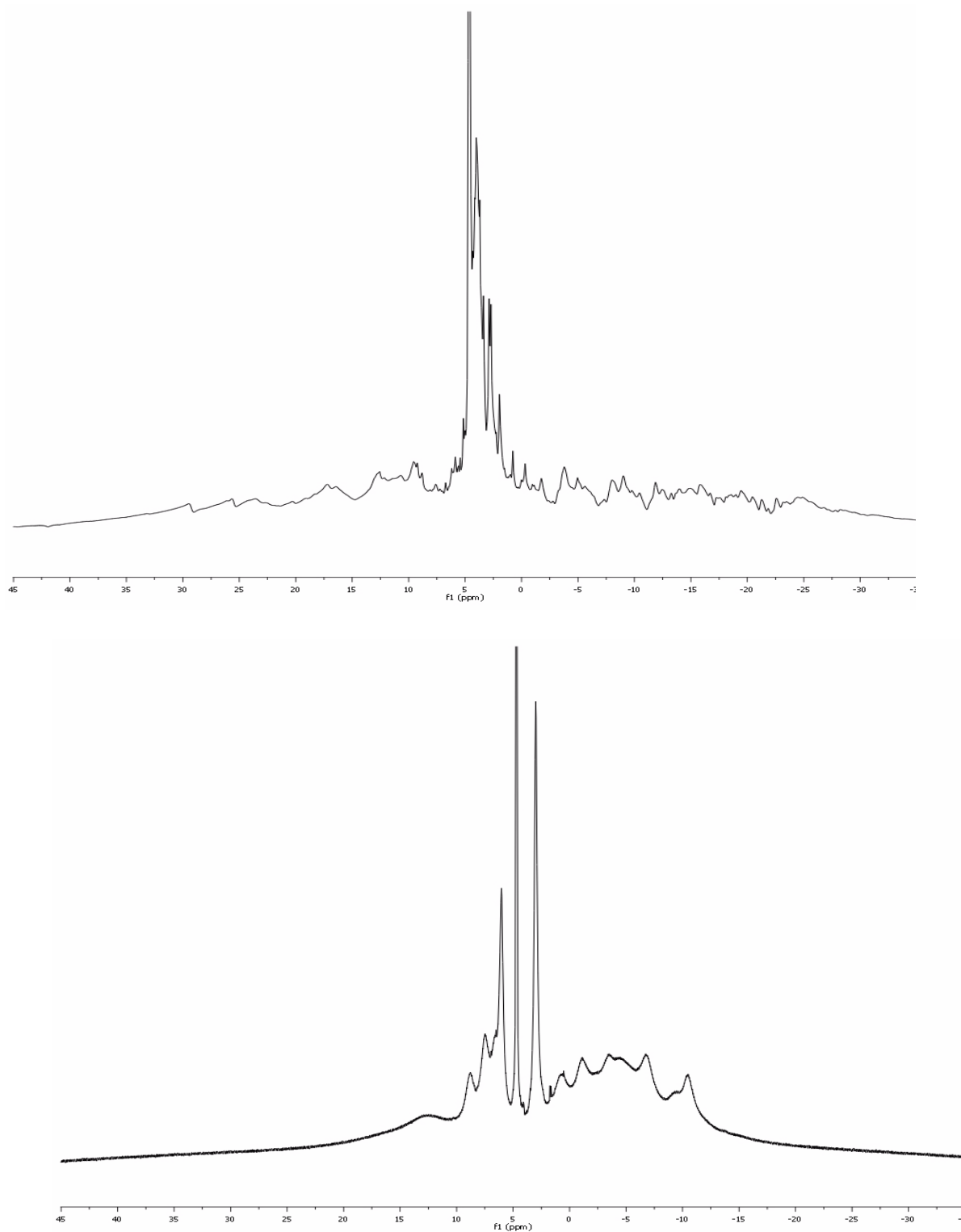
Figure A3.7 Low (0 $^{\circ}$C, top) and high (80 $^{\circ}$C, bottom) temperature ^{1}H-NMR spectra of 240 mM **2** in D$_2$O with 24 mM Na$_2$CO$_3$ added. The presence of 0.1 equivalents of carbonate has little effect on the ^{1}H-NMR spectra (compare to spectra in Figure A3.6).
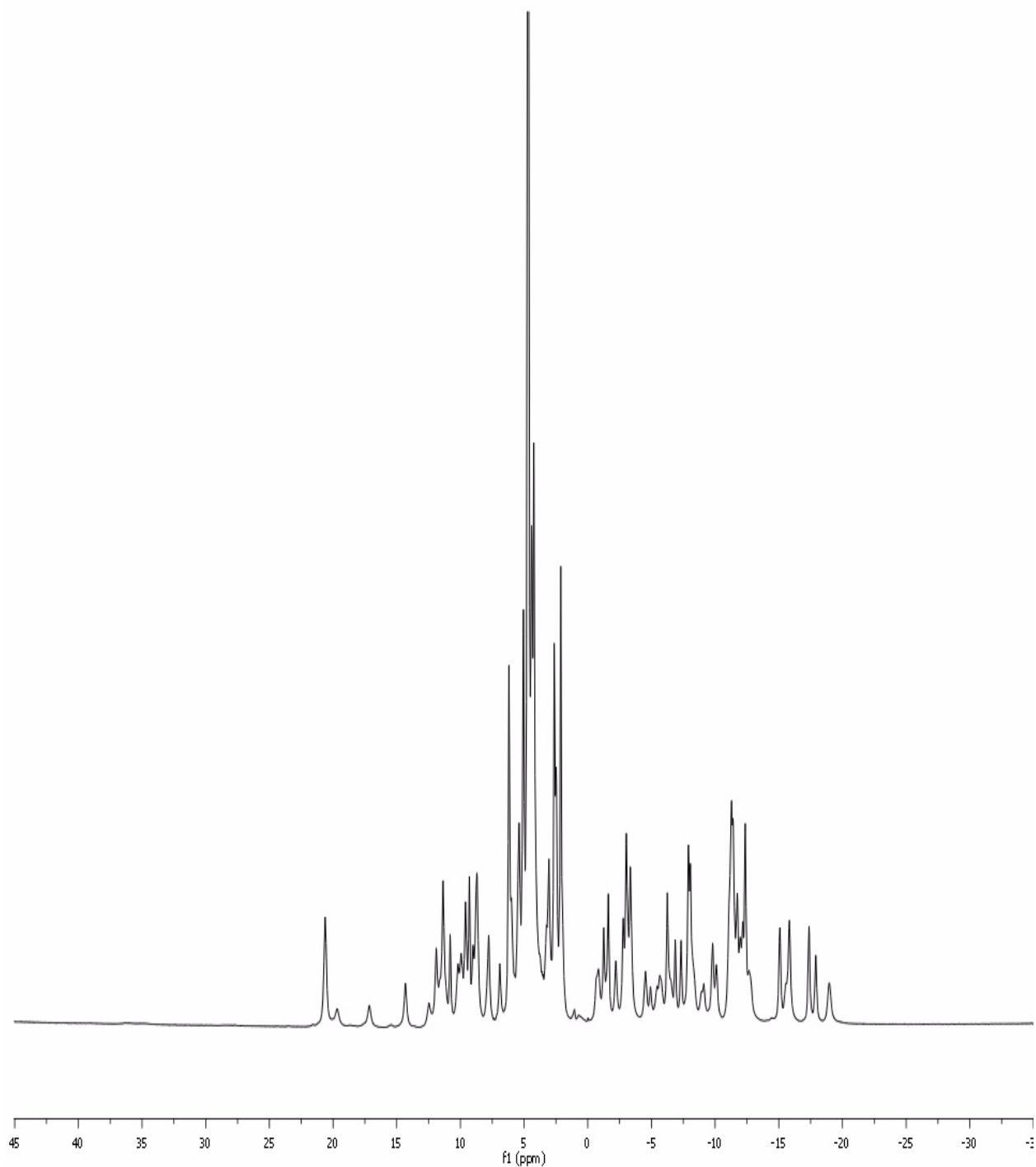
Figure A3.8 Ambient temperature(20 °C) ^{1}H-NMR spectrum of 240 mM **2** in D$_2$O with 250 mM Na$_2$CO$_3$. The addition of a slight stoichiometric excess of carbonate to **2** results in a sharpening of the proton resonances. The absence of resonances at 30-45 ppm and the presence of sharp resonances at 14-22 ppm suggest that only the TSAP isomer is present under these conditions.
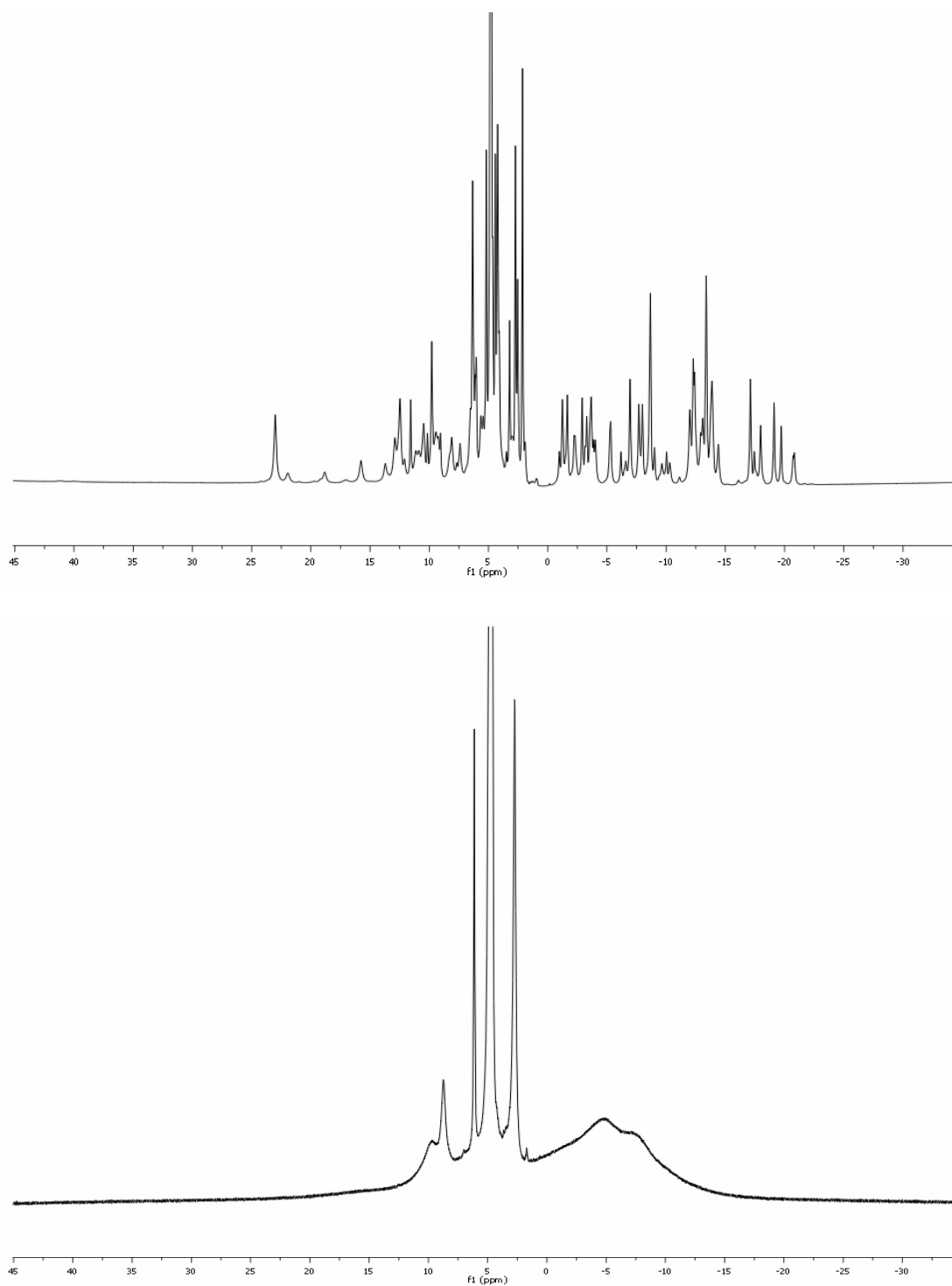
Figure A3.9 Low (0 ^{o}C, top) and high (80 ^{o}C, bottom) temperature ^{1}H-NMR spectra of 240 mM **2** in D$_2$O with 250 mM Na$_2$CO$_3$. The sharp resonances observed at low temperature coalesce at high temperature.

SUMMARY AND FUTURE DIRECTIONS

The hypothesis originally proposed by Urbanczyk-Pearson and coworkers[3] concerning the binding of carbonate to β-EGadMe and not to α-EGadMe has been supported by laser luminescence spectroscopy and ^{1}H-NMR spectroscopy. A titration of **2** with carbonate exhibited a distinctive red shift of the excitation maximum, which is indicative of a change in the coordination environment of europium(III). A similar titration of **1** did not result in a shift of the excitation maximum.

The ^{1}H-NMR spectra of the diamagnetic Y(III) complexes **3** and **4** show that **4** has greater fluxionality. The ^{1}H-NMR spectra of the paramagnetic europium(III) chelates shows a similar trend: **1** was well resolved at room temperature while **2** exhibited broad resonances due to conformational fluxionality on the NMR timescale. Variable temperature NMR revealed the coalescence of the paramagnetically shifted cyclen axial and equatorial protons at high temperature. Addition of a slight stoichiometric excess of carbonate to **2** resulted in a sharpening of the resonances in the ^{1}H-NMR spectrum. These effects support the hypothesis of carbonate binding to **2**. Interestingly, the addition of carbonate causes the macrocycle of **2** to be present only as the TSAP isomer. These results are particularly intriguing as the TSAP isomer is most often found to be present in lesser amounts than the SAP isomer.[9] Additionally, the TSAP isomer has been reported to exhibit a faster water exchange rate than the SAP isomer (discussed in Chapter II), leading to an increased relaxivity contribution from the TSAP isomer to the overall observed relaxivity of the contrast agent (discussed in Chapter I).[9]

Current efforts include a complete 2D NMR investigation of the structures of **1**, **2**, **3**, and **4,** both with and without the addition of carbonate. Analysis of the 2D NMR spectra will provide insight into the overall geometry of these chelates.

It is both astounding and intriguing that the position of a single methyl group can have such a profound impact on the overall conformation of EGadMe. Furthermore, the addition of carbonate had a dramatic influence on the conformational fluxionality of β-EGadMe. Clearly, similar studies are warranted for other chelates in order to understand the delicate mechanisms which can so greatly influence the relaxivity, and overall utility, of MRI contrast agents. A thorough investigation of the structures of individual chelates and the influence of exogenous coordinating anions (carbonate, lactate, citrate, acetate) is necessary for the progression of activatable MRI contrast agents towards clinically useful products.

EXPERIMENTAL

Synthesis

(R)-(+)-(2-(4,7,10-trismethylcarboxymethyl-(1,4,7,10-tetraazacyclododecyl))propan)-1-β-D-galactose tetraacetate and R-(+)-1-(4,7,10-trismethylcarboxymethyl-(1,4,7,10-tetraazacyclododecyl))propan-2-β-D-galactose tetraacetate and their Eu(III) complexes were prepared as described by Meade and coworkers.[3] Y(III) complexes were prepared in an analogous manner.

Laser Luminescence

Laser luminescence was performed in collaboration with the research group of Professor Janet Morrow at the University at Buffalo, SUNY. Aqueous samples were prepared consisting of 0.5 mM of Eu-complex; 100 mM $NaNO_3$ (to control ionic strength); and 20 mM HEPES buffer.

Titration solutions consisted of 0.5 mM Eu-complex with 1, 5, 10, or 100 μL additions of 200 mM $NaHCO_3$. Spectra were acquired on a Spectra-Physics Quanta Ray PRO-270-10 Q-switched Nd: YAG pump laser (10 Hz, 60-70 mJ $pulse^{-1}$) with a MOPO SL. Excitation spectra of the Eu^{3+} $^7F_o \rightarrow {}^5D_o$ transition were recorded at 0.01 nm increments between 578-581 nm for each complex. The $^5D_0 \rightarrow {}^7F_2$ emission was passed through a 628 nm band-pass filter (Semrock, model FF01-628/27-25) and focused onto a time-grated photomultiplier tube (Hamamatsu, model H 7680-01 MOD).

NMR

NMR spectra were acquired on a Varian Inova 500 MHz spectrometer using samples dissolved in D_2O.

APPENDIX IV

SINGLE CRYSTAL X-RAY DIFFRACTION STRUCTURE

OF A MACROCYCLIC SYNTHON

RESULTS AND DISCUSSION

Crystal Structure of 1,7-bis(*tert*-butoxycarbonylmethyl)-4,10-bis[*N*-(tert-butoxycarbonyl)aminoethyl]-1,4,7,10-tetraazacyclododecane

The compound presented in the current work is an intermediate synthesized during the development of the peptide-bridged macrobicyclic structures presented in Appendix II, Approach #2. The compound was intended to yield a bifunctional chelate (compound **2**, Appendix II) after selective removal of the Boc protecting groups from the pendant amines (Scheme A4.1). The selective removal of the Boc groups under acidic conditions could not be accomplished in appreciable yields due to concomitant removal of the *tert*-butyl protecting groups on the pendant acetates. Nevertheless, in an effort to purify the title compound by recrystallization, crystals of appreciable size were formed. Single crystal X-ray diffraction data supported formation of the expected product (Figure A4.1 and Table A4.1) and fulfilled the unofficial Meade laboratory rule which states, "you must have a crystal structure to graduate".

74 %

1,7-bis(tert-butoxycarbonylmethyl)-
4,10-bis[N-(tert-butoxycarbonyl)aminoethyl]-
1,4,7,10-tetraazacyclododecane
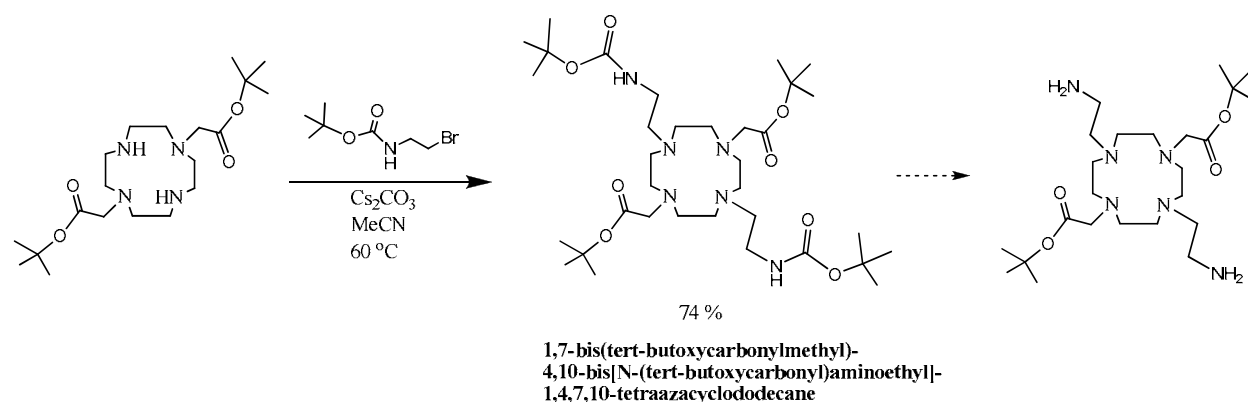
Scheme A4.1 Synthesis of 1,7-bis(*tert*-butoxycarbonylmethyl)-4,10-bis[*N*-(tert-butoxycarbonyl)aminoethyl]-1,4,7,10-tetraazacyclododecane

Figure A4.1 Crystal Structure of 1,7-bis(*tert*-butoxycarbonylmethyl)-4,10-bis[*N*-(tert-butoxycarbonyl)aminoethyl]-1,4,7,10-tetraazacyclododecane (Structure solved by Danielle L. Gray)

326

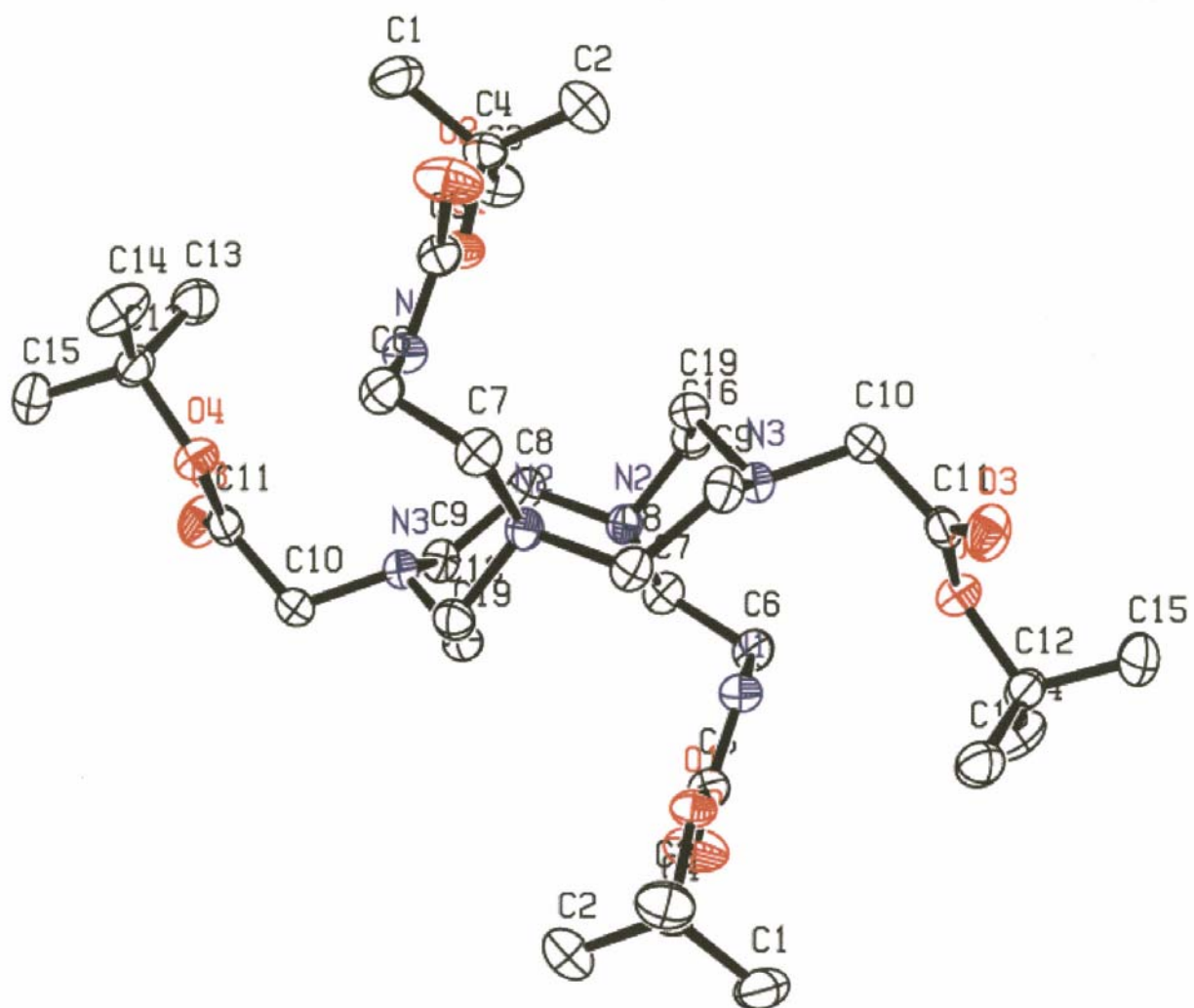|	
Empirical formula	C34 H66 N6 O8
Formula weight	686.93
Temperature	153(2) K
Wavelength	0.71073 A
Crystal system, space group	Orthorhombic, P
Unit cell dimensions	a = 17.7941(16) A alpha = 90 deg.
	b = 9.8056(9) A beta = 90 deg.
	c = 22.791(2) A gamma = 90 deg.
Volume	3976.6(6) A^3
Z, Calculated density	4, 1.147 Mg/m^3
Absorption coefficient	0.081 mm^-1
F(000)	1504
Crystal size	0.402 x 0.280 x 0.254 mm
Theta range for data collection	1.79 to 28.86 deg.
Limiting indices	-24<=h<=23, -12<=k<=13, -29<=l<=31
Reflections collected / unique	34942 / 4979 [R(int) = 0.0421]
Completeness to theta = 28.86	95.3 %
Absorption correction	Numerical
Max. and min. transmission	0.98366 and 0.97116
Refinement method	Full-matrix least-squares on F^2
Data / restraints / parameters	4979 / 0 / 217
Goodness-of-fit on F^2	1.206
Final R indices [I>2sigma(I)]	R1 = 0.0432, wR2 = 0.1072
R indices (all data)	R1 = 0.0691, wR2 = 0.1202
Largest diff. peak and hole	0.269 and -0.230 e.A^-3

Table A4.1 Crystallographic data and structure refinement for 1,7-bis(*tert*-butoxycarbonylmethyl)-4,10-bis[*N*-(tert-butoxycarbonyl)aminoethyl]-1,4,7,10-tetraazacyclododecane (Structure solved by Danielle L. Gray)

EXPERIMENTAL

General experimental details can be found in Chapter II.

Synthesis

1,7-bis(*tert*-butoxycarbonylmethyl)-4,10-bis[*N*-(tert-butoxycarbonyl)aminoethyl]-1,4,7,10-tetraazacyclododecane

1,7-bis(*tert*-butoxycarbonylmethyl)-1,4,7,10-tetraazacyclododecane (synthesized according to literature methods[1]) (1.0250 g, 2.5589 mmol) was dissolved in 15 mL MeCN and placed in a 500 mL 3-neck roundbottom flask with magnetic stirbar and Cs_2CO_3 (2.5104 g, 7.7049mmol, 3.0 equivalents). *N*-(*tert*-butoxycarbonyl)-2-bromo-1-ethylamine (1.2196 g, 5.4424 mmol, 2.1 equivalents) was dissolved in 10 mL MeCN and added dropwise over 5 min while stirring. The flask was attached to a water-cooled reflux condenser equipped with a drying tube (Drierite) and placed in a 60 ^{o}C oilbath. After each 24 hour period of the reaction, *N*-(*tert*-butoxycarbonyl)-2-bromo-1-ethylamine (0.2 equivalents) was added until the reaction was determined complete by TLC (silica gel, 1:9:90 saturated KNO_3:H_2O:MeCN, Pt stain, product $R_f = 0.47$). The solution was cooled to room temperature and paper filtered to remove Cs_2CO_3. MeCN was removed by rotary evaporation under reduced pressure to afford the crude product as a yellow oil. The crude product was dissolved in CH_2Cl_2 and loaded onto a silica gel column. Excess *N*-(*tert*-butoxycarbonyl)-2-bromo-1-ethylamine was eluted with CH_2Cl_2, followed by a gradient up to 10% MeOH in CH_2Cl_2 to elute the desired product. Solvents were removed by rotary evaporation under reduced pressure followed by pumping vacuum overnight to afford the title compound as a white crystalline solid which was further purified by recrystallization from CH_2Cl_2 (1.3071 g, 74% yield). Crystals for X-ray diffraction were grown by vapor diffusion from $CDCl_3$.

ESI-MS: Calc. 686.92; Found positive mode 687.6 (M + H$^+$), 709.6 (M + Na$^+$)

^{1}H NMR (CDCl$_3$): δ = 1.4 (s, 36H, *t*-Bu and N-Boc), 2.4 (t, 4H, CH$_2$C*H$_2$*NHBoc), 2.6 (br, 8H, cyclen), 2.8 (br, 8H, cyclen), 3.1 (br, 4H, C*H$_2$*CH$_2$NHBoc), 3.2 (s, 4H, C*H$_2$*COOtBu), 6.3 (br, NH)

^{13}C NMR (CDCl$_3$): δ = 28.4, 28.7, 38.8, 52.5, 53.8, 54.0, 56.2, 78.7, 81.0, 156.3, 170.8

APPENDIX I REFERENCES

(1)   Whittaker, M.; Floyd, C. D.; Brown, P.; Gearing, A. J. H. *Chemical Reviews* **1999**, *99*, 2735-2776.

(2)   Coussens Lisa, M.; Fingleton, B.; Matrisian Lynn, M. *Science* **2002**, *295*, 2387-92.

(3)   Brabletz, T.; Jung, A.; Dag, S.; Hlubek, F.; Kirchner, T. *American Journal of Pathology* **1999**, *155*, 1033-1038.

(4)   Aparicio, T.; Kermorgant, S.; Dessirier, V.; Lewin, M. J. M.; Lehy, T. *Carcinogenesis* **1999**, *20*, 1445-1451.

(5)   Lampert, K.; Machein, U.; Machein, M. R.; Conca, W.; Peter, H. H.; Volk, B. *American Journal of Pathology* **1998**, *153*, 429-437.

(6)   Zucker, S.; Hymowitz, M.; Rollo, E. E.; Mann, R.; Conner, C. E.; Cao, J.; Foda, H. D.; Tompkins, D. C.; Toole, B. P. *American Journal of Pathology* **2001**, *158*, 1921-1928.

(7)   Zeng, Z.-S.; Shu, W.-P.; Cohen, A. M.; Guillem, J. G. *Clinical Cancer Research* **2002**, *8*, 144-148.

(8)   Chambers, A. F.; Matrisian, L. M. *Journal of the National Cancer Institute* **1997**, *89*, 1260-1270.

(9)   Zucker, S.; Cao, J. *Nature Medicine* **2001**, *7*, 655-656.

(10)   Coussens, L. M.; Fingleton, B.; Matrisian, L. M. *Science* **2002**, *295*, 2387-2392.

(11)   Nelson, A. R.; Fingleton, B.; Rothenberg, M. L.; Matrisian, L. M. *Journal of Clinical Oncology* **2000**, *18*, 1135-1149.

(12)   Stack, M. S.; Gray, R. D. *Journal of Biological Chemistry* **1989**, *264*, 4277-81.

(13)   Netzel-Arnett, S.; Mallya, S. K.; Nagase, H.; Birkedal-Hansen, H.; Van Wart, H. E. *Analytical Biochemistry* **1991**, *195*, 86-92.

(14)   Louie, A. Y.; Huber, M. M.; Ahrens, E. T.; Rothbacher, U.; Moats, R.; Jacobs, R. E.; Fraser, S. E.; Meade, T. J. *Nature Biotechnology* **2000**, *18*, 321-325.

(15)   Edwards, D. R.; Murphy, G. *Nature* **1998**, *394*, 527-8.

(16)   Kataoka, H.; Uchino, H.; Iwamura, T.; Seiki, M.; Nabeshima, K.; Koono, M. *American Journal of Pathology* **1999**, *154*, 457-468.

(17)   Noe, V.; Fingleton, B.; Jacobs, K.; Crawford, H. C.; Vermeulen, S.; Steelant, W.; Bruyneel, E.; Matrisian, L. M.; Mareel, M. *Journal of Cell Science* **2001**, *114*, 111-118.

(18)   Netzel-Arnett, S.; Sang, Q. X.; Moore, W. G. I.; Navre, M.; Birkedal-Hansen, H.; Van Wart, H. E. *Biochemistry* **1993**, *32*, 6427-32.

(19)   Smith, M. M.; Shi, L.; Navre, M. *Journal of Biological Chemistry* **1995**, *270*, 6440-9.

(20)   Moats, R. A.; Fraser, S. E.; Meade, T. J. *Angewandte Chemie, International Edition in English* **1997**, *36*, 726-728.

(21)   Supkowski, R. M.; Horrocks, W. D. *Inorganica Chimica Acta* **2002**, *340*, 44-48.

(22)   Allen, M., California Institute of Technology, 2004.

(23)   Liu, S.; Pietryka, J.; Ellars, C. E.; Edwards, D. S. *Bioconjugate Chemistry* **2002**, *13*, 902-913.

(24)   Kates, S. A.; Albericio, F. *Solid-Phase Synthesis, A Practical Guide*; Marcel Dekker, Inc.: New York, New York, 2000.

(25)   Kaiser, E.; Colescott, R. L.; Bossinger, C. D.; Cook, P. I. *Analytical Biochemistry* **1970**, *34*, 595-598

APPENDIX II REFERENCES

(1)   Bianchi, A.; Garcia-Espana, E.; Micheloni, M.; Nardi, N.; Vizza, F. *Inorg. Chem.* **1986**, *25*, 4379-4381.

(2)   Bencini, A.; Bianchi, A.; Borselli, A.; Ciampolini, M.; Garcia-Espana, E.; Dapporto, P.; Micheloni, M.; Paoli, P.; Ramirez, J. A.; Valtancoli, B. *Inorg. Chem.* **1989**, *28*, 4279-4284.

(3)   Bencini, A.; Bianchi, A.; Chimichi, S.; Ciampolini, M.; Dapporto, P.; Garcia-Espana, E.; Micheloni, M.; Nardi, N.; Paoli, P.; Valtancoli, B. *Inorg. Chem.* **1991**, *30*, 3687-3691.

(4)   Ciampolini, M.; Micheloni, M.; Vizza, F.; Zanobini, F.; Chimichi, S.; Dapporto, P. *J. Chem. Soc., Dalton Trans.* **1986**, 505-510.

(5)   Kovacs, Z.; Sherry, A. D. *Synthesis* **1997**, 759-763.

(6)   Kates, S. A.; Albericio, F. *Solid-Phase Synthesis, A Practical Guide*; Marcel Dekker, Inc.: New York, New York, 2000.

(7)   Chan, W. C.; White, P. D. *Fmoc Solid Phase Peptide Synthesis*; Oxford University Press: New York, 2000.

(8)   Erickson, B. W.; Merrifield, R. B. *J. Am. Chem. Soc.* **1973**, *95*, 3750-3756.

(9)   Peterson, J. J.; Pak, R. H.; Meares, C. F. *Bioconjugate Chemistry* **1999**, *10*, 316-320.

(10)   Whetstone, P. A.; Butlin, N. G.; Corneillie, T. M.; Meares, C. F. *Bioconjugate Chemistry* **2004**, *15*, 3-6.

(11)   Hubin, T. J.; McCormick, J. M.; Alcock, N. W.; Busch, D. H. *Inorg. Chem.* **2001**, *40*, 435-444.

(12)   Springborg, J.; Glerup, J.; Sotofte, I. *Acta Chem. Scand.* **1997**, *51*, 357.

(13)   Wangler, B.; Beck, C.; Wagner-Utermann, U.; Schirrmacher, E.; Bauer, C.; Rosch, F.; Schirrmacher, R.; Eisenhut, M. *Tetrahedron Letters* **2006**, *47*, 5985-5988.

(14)   Cohen, G. M. *Biochem. J.* **1997**, *326*, 1-16.

(15)   Yue, C.; Thierry, J.; Potier, P. *Tetrahedron Letters* **1993**, *34*, 323-326.

(16)   Lauer, J. L.; Fields, C. G.; Fields, G. B. *Lett. Pept. Sci.* **1994**, *1*, 197.

(17)   Kaiser, E.; Colescott, R. L.; Bossinger, C. D.; Cook, P. I. *Analytical Biochemistry* **1970**, *34*, 595-598.

(18)   Mazur, S.; Jayalekshmy, P. *J. Am. Chem. Soc.* **1979**, *101*, 677-683.

(19)   Wei, W.-H.; Tomohiro, T.; Kodaka, M.; Okuno, H. *J. Org. Chem.* **2000**, *65*, 8979-8987.

(20)   Boseggia, E.; Gatos, M.; Lucatello, L.; Mancin, F.; Moro, S.; Palumbo, M.; Sissi, C.; Tecilla, P.; Tonellato, U.; Zagotto, G. *J. Am. Chem. Soc.* **2004**, *126*, 4543-4549.

APPENDIX III REFERENCES

(1)   Moats, R. A.; Fraser, S. E.; Meade, T. J. *Angewandte Chemie, International Edition in English* **1997**, *36*, 726-728.

(2)   Louie, A. Y.; Huber, M. M.; Ahrens, E. T.; Rothbacher, U.; Moats, R.; Jacobs, R. E.; Fraser, S. E.; Meade, T. J. *Nature Biotechnology* **2000**, *18*, 321-325.

(3)   Urbanczyk-Pearson, L. M.; Femia, F. J.; Smith, J.; Parigi, G.; Duimstra, J. A.; Eckermann, A. L.; Luchinat, C.; Meade, T. J. *Inorg. Chem.* **2008**, *47*, 56-68.

(4)   Supkowski, R. M.; Horrocks, W. D. *Inorganica Chimica Acta* **2002**, *340*, 44-48.

(5)   Lambert, J.; Mazzola, E. P. *Nuclear Magnetic Resonance Spectroscopy. An Introduction to Principles, Applications, and Experimental Methods*; Pearson Education, Inc.: Upper Saddle River, NJ, 2004.

(6)   Caravan, P.; Ellison, J. J.; McMurry, T. J.; Lauffer, R. B. *Chemical Reviews* **1999**, *99*, 2293-2352.

(7)   Peters, J. A.; Huskens, J.; Raber, D. J. *Prog. Nucl. Magn. Reson. Spect.* **1996**, *28*.

(8)   Woods, M.; Aime, S.; Botta, M.; Howard, J. A. K.; Moloney, J. M.; Navet, M.; Parker, D.; Port, M.; Rousseaux, O. *J. Am. Chem. Soc.* **2000**, *122*, 9781-9792.

(9)   Zhang, S.; Kovacs, Z.; Burgess, S.; Aime, S.; Terreno, E.; Sherry, A. D. *Chem. Eur. J.* **2001**, *7*, 288-296.

APPENDIX IV REFERENCES

(1)   Kovacs, Z.; Sherry, A. D. *Synthesis* **1997**, 759-763.

(2)   Wei, W.-H.; Tomohiro, T.; Kodaka, M.; Okuno, H. *J. Org. Chem.* **2000**, *65*, 8979-8987.

Bradley Ulrich
2614 N. Clybourn Ave., Apt. 213
Chicago, IL 60614
(847) 863-5840
e-mail: bdulrich79@yahoo.com

Education   PhD, Chemistry, Northwestern University, Evanston, IL
(GPA 3.8/4.0), 2008
Thesis: *Peptide-Based Magnetic Resonance Imaging Probes for Detection of Enzyme Activity*
Advisor: Professor Thomas J. Meade

BS, Chemistry, The Ohio State University, Columbus, OH
(GPA 3.4/4.0), 2001
Synthesis, Characterization, and Chemistry of Dimethyl Sulfide Derivatives of closo-$B_{10}H_{10}^{2-}$
Advisor: Professor Sheldon G. Shore

- University Scholarship, Ohio Academic Scholarship, Ruth E. Smith Scholarship, MacNevin Scholarship

Research Experience   Graduate Research Assistant, Northwestern University, 2001-2008
Advisor: Professor Thomas J. Meade

- Completed 15 to 24-step syntheses of five target compounds
- Experienced in characterization techniques including NMR (1D ^{1}H, ^{13}C, ^{17}O, ^{11}B and 2D), MALDI-MS, ESI-MS, ICP-MS, HPLC, and LC-MS
- Performed *in vitro* enzyme testing of MRI contrast agents
- Mentored an undergraduate student in honors thesis research and in writing of two successful grants to fund research
- Presented research at ACS Conference

Undergraduate Research, The Ohio State University, 1999-2001
Advisor: Professor Sheldon G. Shore

- Synthesized anti-tumor agents for Boron Neutron Capture Therapy
- Discovered a new isomer of a dimethyl sulfide derivative of *closo*-$B_{10}H_{10}^{2-}$
- Presented research at International *B.U.S.A.*.and *C.O.U.R.S. 2000* Conferences

Laboratory Assistant, Renite Company, 1999
Supervisor: Dr. John T. Golden
- Developed graphite-based, water-based, and petroleum-based lubricants for glass and forging industries

Patents   Sikma, E.S.; <u>Ulrich, B.D.</u>; Meade, T.J. "Contrast Agent Compositions and Methods" (*patent pending, filed September 14, 2007)*

<u>Ulrich, B. D.</u>; Lee, P.J.; Meade, T.J. "Bioactivated Magnetic Resonance Agents for the Detection of Proteases" (*in preparation)*

Publications   <u>Ulrich, B. D.</u>; Harney, A. S.; MacRenaris, K.; Meade, T. J. "A Bioactivated Magnetic Resonance Agent for the Detection of Caspase-3" *Bioconjugate Chemistry, submitted*

<u>Ulrich, B. D.</u>; Ballweg, D.; Urbanczyk-Pearson, L.; Morrow, J. R.; Meade, T. J. "Laser Luminescence and 2-D NMR Studies of α-EGadMe and β-EGadMe. The Effect of Hydrogencarbonate Binding to Lanthanide (III) Chelates" (*in preparation*)

<u>Ulrich, B. D.</u> and Meade, T. J. "Synthesis of Peptide-Bridged Macrocycles as Bioactivatable Magnetic Resonance Imaging Contrast Agents" Abstract of Papers, 233rd ACS National Meeting, 2007

Sikma, E. S.; <u>Ulrich, B. D.</u>; Aslam, M.; Dravid, V.; Meade, T. J. "A T_1/T_2 MRI Contrast Agent with Cleavable Linker for Detection of Matrix Metalloproteinase-7" (*in preparation*)

Hall, H. D.; <u>Ulrich, B. D.</u>; Kultyshev, R.; Liu, J.; Liu, S.; Meyers, E. D.; Greau, S.; and Shore, S.G. "Synthesis, Characterization, and Chemistry of Dimethyl Sulfide Derivatives of *closo*-$B_{10}H_{10}^{2-}$" *Collect. Czech. Chem. Commun.* **2002**, *67*, 1007-1024

Activities   Phi Lambda Upsilon, Honorary Chemical Society, 2003-present
- Alpha Gamma Chapter President, 2004-2005 academic year
  - Championed a new scholarship for senior graduate students with unused department funds
  - Increased student awareness of available Travel Grants, resulting in a 540% increase in funding for graduate student travel to scientific conferences
- Teaching Assistant Awards Chair, 2003-2004 academic year

Volunteer   Science in the Classroom, Program Teacher, 2005-2006 academic year
- Developed curriculum for 4th grade students to increase interest in science
- Led a 5 person team to teach hands-on science experiments to underprivileged students

Chicago Serve-A-Thon, 2006

H.A.N.D.S. Science Outreach, Chicago, IL, 2002

Wonders of Our World (W.O.W.) Science Outreach, Columbus, OH, 2000-2001

Affiliations   American Chemical Society member, 2006-present